# THE PHYSICAL REVIEW

VOLUME 47 Second Series NUMBER 2

JANUARY 15, 1935

Published for the

AMERICAN PHYSICAL SOCIETY

by the

AMERICAN INSTITUTE OF PHYSICS

LANCASTER, PA., AND NEW YORK, N. Y.

## American Physical Society

OFFICERS OF THE SOCIETY

..., *President*
...s Hopkins University
..., Maryland

..., *Secretary*
... University
..., New York

..., *Editor*
... of Minnesota
..., Minnesota

F. K. Richtmyer, *Vice-President*
Cornell University
Ithaca, New York

G. B. Pegram, *Treasurer*
Columbia University
New York, New York

L. B. Loeb, *Local Secretary for the Pacific Coast*
University of California
Berkeley, California


# The Physical Review


BOARD OF EDITORS

...T. Tate, *Editor* — J. W. Buchta, *Assistant Editor*

*Associate Editors*

...arrow — A. Ellett — W. V. Houston
...rand — L. A. Turner — R. S. Mulliken
...ark — G. E. Uhlenbeck — I. I. Rabi


...Review, which was established ... journal of experimental and ... It is published for the American Physical Society by the American Institute of Physics Incorporated. There are two volumes annually with twelve issues in each volume.

...publication should be submitted to ... of Minnesota, Minneapolis, ...

...correspondence concerning papers in the ... should be addressed to the Editorial ... Institute of Physics, 11 East 38th ..., New York City, New York.

...prices: United States and Possessions and ... Foreign, $16.00. Subscriptions and orders ... should be addressed to Prince and ..., Pennsylvania, or to the American ..., 11 East 38th Street, New York, ...

...arranged for the *Physical Review* but ... the *Review of Scientific Instruments* ... Plates, a companion publication of ... medium through which the field of physics can be reached most effectively. Rates and other information will be furnished on request to the Editorial Secretary.

Changes of address and complaints of failure to receive the *Physical Review*, in the case of members of the American Physical Society, should be addressed to the Treasurer; in the case of other subscribers, to the Editorial Secretary. New copies can be sent free in response to complaints of non-delivery only if notice of non-delivery is received within three months of date of issue.


The Physical Review is published semi-monthly at Prince and Lemon Streets, Lancaster, Pennsylvania.

Entered at the Post Office at Lancaster, Pennsylvania, as second class matter.

Acceptance for mailing at special rate of postage provided for in section 1103, Act of October 3, 1917, authorized September 6, 1924.

THE
PHYSICAL REVIEW
A Journal of Experimental and Theoretical Physics
VOL. 47, NO. 2 JANUARY 15, 1935 SECOND SERIES

# The Disintegration of Nitrogen by Neutrons

FRANZ N. D. KURIE,* *Radiation Laboratory, Department of Physics, University of California*
(Received November 20, 1934)

Measurements made on 29 Wilson cloud chamber photographs of the disintegration of nitrogen by artificially produced neutrons (beryllium+deutons) are presented and discussed. It is shown that the loss in kinetic energy can be satisfactorily accounted for by postulating the momentary production of a radioactive nitrogen $N^{15}$ by a radiative capture of the neutron. This nitrogen disintegrates with the emission of $\alpha$-particles so that the half-life on the Gamow theory is around $10^{-20}$ sec. A distinction is thus made between nuclear transformations in which the energy absorbed is a constant (such as in the case of the disintegration of nitrogen by $\alpha$-particles) and those in which the proper disintegration energy $E$ is a constant. Disintegrations caused by neutrons are, as far as the data from cloud chamber measurements go, all of this latter type. For nitrogen $E$ is found to be 3.1 MV. The scatter of the values of $E$ is probably all to be attributed to experimental error but may in part be due to the short life of the radioactive $N^{15}$. The energy level from which the $\alpha$-particle leaves the $N^{15}$ nucleus is roughly identified with the resonance level through which an $\alpha$-particle may enter a $B^{11}$ nucleus in the reverse reaction. A mass for the radioactive $N^{15}$ of 15.0166 is proposed on the basis of the mechanism here discussed. The data of other workers on the transmutation of oxygen, fluorine and neon are reviewed in the light of these considerations and lend support to them. The values found for $E$ are nearly the same for all of the four elements on which data exist.

THE ability of neutrons to cause the disintegration of light nuclei was first noted by N. Feather[1] who showed that the occasional bent tracks found in a cloud chamber which is being traversed by neutrons could be interpreted as being the traces left by the two bodies resulting from a nuclear disruption brought about by the capture of a neutron, which of course leaves no track in the chamber. Thus Feather established the reactions:

$$_7N^{14}+{}_0n^1={}_7N^{15}={}_5B^{11}+{}_2He^4, \quad (1)$$

$$_8O^{16}+{}_0n^1={}_8O^{17}={}_6C^{13}+{}_2He^4, \quad (2)$$

with considerable certainty. Further and more extensive work has been done by Harkins, Gans and Newson[2, 3, 4] who studied nitrogen, neon and fluorine, suggesting two further reactions

$$_{10}Ne^{20}+{}_0n^1={}_{10}Ne^{21}={}_8O^{17}+{}_2He^4, \quad (3)$$

$$_9F^{19}+{}_0n^1={}_9F^{20}={}_7N^{16}+{}_2He^4. \quad (4)$$

Both Feather and Harkins, Gans and Newson have examined the disintegration of carbon, with discouraging results. Feather found only one fork which could be attributed to

$$_6C^{12}+{}_0n^1={}_6C^{13}={}_4Be^9+{}_2He^4, \quad (5)$$

while the others found none which could not be explained as disintegrations of oxygen, which was present in the chamber. Chadwick, Feather and

* National Research Fellow

[1] N. Feather, Proc. Roy. Soc. **A136**, 709 (1932); Nature **130**, 257 (1932); Proc. Roy. Soc. **A142**, 689 (1933).

[2] W. D. Harkins, D. M. Gans and H. W. Newson, Phys. Rev. **44**, 945 (1933).

[3] W. D. Harkins, D. M. Gans and H. W. Newson, Phys. Rev. **44**, 236 (1933).

[4] W. D. Harkins, D. M. Gans and H. W. Newson, Phys. Rev. **44**, 945 (1933).

Davies[5] have recently described a trident which may be assigned to either

$$_6C^{12}+{}_0n^1=2{}_2He^4+{}_2He^5 \quad (6a)$$

or

$$_6C^{12}=3{}_2He^4. \quad (6b)$$

Meitner and Philipp[6] have reported several nitrogen and oxygen disintegrations. The sum total of the data already published may be summarized as follows: for nitrogen there are data on 31 forks; for oxygen, 7 forks; for fluorine, 7 forks; for neon, 4 forks; for carbon, one fork, one trident.

Feather[1] has described the method of computing the energy and direction of motion of the neutron before it precipitated the disintegration, together with the energies of the disintegration particles. Briefly, this consists in assigning to the two particles velocities appropriate to their ranges and natures. The latter requires a guess as to the probable nuclear reaction which has occurred; if one's guess has been right one finds the direction of the resultant momentum of the fork passing through or very close to the source of the neutrons. The reactions (1), (2), (3), (4) above have, in a decreasing degree of certainty, stood this test. Of course, due to the ease with which a neutron may be scattered a fraction of the forks will be due to a scattered neutron—this depends to a great extent on the geometry of the cloud chamber and associated apparatus. One must rigorously reject any fork whose resultant momentum does not pass through the source in spite of this effect of scattering, because one can never be certain that the right reaction has been chosen to represent the fork.

From the data already known two characteristics of disintegrations incited by neutrons have been noted. Firstly, one of the particles is, in most cases, an $\alpha$-particle. This is not generally true; for Feather[1] considers that in one of his nitrogen disintegrations a deuton was emitted, and Kurie[7] has suggested that either nitrogen or oxygen may break up with the emission of a proton. The evidence for the latter is based on the appearance of several forks observed in a cloud chamber filled with air. Secondly, kinetic energy is not conserved in the disintegration; nor is the energy change found to be a constant. This disappearance of kinetic energy has been attributed to the excitation of one of the new nuclei. Harkins[2] has proposed a set of energy levels in the $B^{11}$ formed in the transmutation of nitrogen to represent this loss. His arguments in favor of this interpretation, considering the scarcity and the treatment of the data, are not very persuasive.

It is the purpose of this paper to present some further measurements of the disintegration of nitrogen. An interpretation of the process will be proposed which will attempt to account reasonably for the anomalous behavior of these disintegrations.[8]

## Experimental Details

The neutrons were derived from the bombardment of beryllium with 2 MV deutons in accordance with the reaction:

$$_4Be^9+{}_1H^2={}_5B^{10}+{}_0n^1, \quad (7)$$

which has been discussed by Lawrence and Livingston.[9] With the apparatus described by Lawrence and Livingston[10] it is possible to direct a stream of 2 MV deutons against a thick beryllium target. At this voltage the yield of neutrons is very great, amounting to several per $(10)^5$ incident deutons. Currents of the order of one microampere, being readily obtainable, will then produce about $10^9$ neutrons per second. A cloud chamber placed 50 cm from such a source subtends a solid angle of about $10^{-3}$ and will therefore be traversed by roughly a million neutrons per second. An equivalent Po+Be source would require a strength of several thousand millicuries of polonium, if placed in the center of the cloud chamber.

Such an intensity is obtained however at a loss of knowledge of the direction of motion of the neutrons, since the large masses of iron and

[5] J. Chadwick, N. Feather and W. T. Davies, Proc. Camb. Phil. Soc. **30**, 357 (1934).
[6] L. Meitner and K. Philipp, Naturwiss. **20**, 929 (1932); Zeits. f. Physik **87**, 484 (1933).
[7] F. N. D. Kurie, Phys. Rev. **45**, 904 (1934).
[8] A preliminary account of this work was given at the Berkeley meeting of the American Physical Society in June 1934. See reference 14.
[9] E. O. Lawrence and M. S. Livingston, Phys. Rev. **45**, 220 (1934).
[10] E. O. Lawrence and M. S. Livingston, Phys. Rev. **45**, 608 (1934).

copper which make up the magnet forming part of the ion accelerator are very efficient scatterers. It was found in a separate series of experiments that one neutron in ten came from some other point than the source. In considering the disintegration forks all those whose resultant momentum did not pass through the source were rejected.

The cloud chamber to be used near the large accelerator was designed with the following considerations in mind: 1st, it must be portable; 2nd, it must be compact in a vertical direction in order to fit between the coils of the magnet of the ion accelerator where the clearance is only 24 inches; 3rd, it must be possible to operate it in a magnetic field of 1000 gauss, since the stray field of the magnet is of this order.

The pressure operated sylphon chamber described by Dahl, Hafstad and Tuve[11] was copied except that the device permitting an auxiliary expansion was omitted, and a wire gauze was stretched across the junction of the sylphon and the cloud chamber proper. This gauze contributed greatly to the removal of the turbulence arising from the convolutions of the sylphon. The chamber is 2 cm deep and 16 cm in diameter. By using ethyl or propyl alcohol instead of water to supply the vapor the expansion ratio necessary to produce good tracks was reduced to around 1.15 and so less motion of the sylphons was required. They are now being used within the limits of stretch advised by their makers.

Some difficulty was experienced at first in getting the chamber to "clean up." After fresh air had been introduced into the chamber it required several hundred expansions before the general fog, which is mainly due to dust, disappeared. This seems to be a general characteristic of "dry" chambers. Provision of a moist pad (black velvet soaked in alcohol) at the base of the chamber greatly accelerated the "clean up." Propyl alcohol is much less troublesome in this regard than ethyl alcohol, using it the chamber cleans up to be sensitive to $\beta$-rays in about 10 expansions.

Tracks are illuminated by a condensed discharge (1 $\mu f$ at 30,000 volts) through two Pyrex capillaries connected in series. The switch for the discharge is operated by a contact made by the expansion ratio adjusting nut on the chamber and the timing is done by varying the resistance in series with this switch.

The camera is in principle the same as that described earlier by the author.[12] It has been rebuilt into a much more compact and serviceable structure than the first model. The principle difficulty with the first one was the frequent tarnishing of the front silvered mirrors employed. Mirrors of evaporated aluminum[13] are now being used and apparently will last indefinitely.

All the operations in taking the pictures and in working the cloud chamber are automatic and with the exception of the timing of the illumination all are accomplished by means of a series of relays driven from contacts attached to the second hand of an electric clock. The period of a complete cycle is 15 seconds. All the control circuits and the high tension set for the illumination are mounted on a small truck.

The forks are measured by the now common reprojection practice.[11] No attempt is made completely to recombine a fork; each tine is combined separately and its angular altitude and azimuth together with its length are measured. From these data and a knowledge of the stopping power of the gas in the chamber the energies of the neutron and of the disintegration particles may be computed.

## Experimental Results

The data with the neutrons from the Be +deuton source are divisible into two batches. The first comprises 34 forks photographed in the cloud chamber when it contained mostly air, some oxygen from a tank having been added to bring the pressure up to the required amount. The stopping power of the gas in the chamber was about 1.3 relative to standard air. When the forks were measured and computed as nitrogen disintegrations without any selective measures being taken, a number of peculiarities were noticed. Firstly, many of the forks had resultant momenta which did not pass through the source. One would expect this in view of the large masses of iron and copper in the immediate neighbor-

[11] Dahl, Hafstad and Tuve, Rev. Sci. Inst. **4**, 373 (1933).

[12] F. N. D. Kurie, Rev. Sci. Inst. **3**, 655 (1932).

[13] I am greatly indebted to Dr. O. E. Anderson and Dr. K. R. More for making these mirrors for me.

hood of the cloud chamber, which by scattering the neutrons would throw great chaos into the directions from which the neutrons reach the chamber. Secondly, the momenta pertaining to the tines of the forks indicated neutron energies ranging up to 20 MV. Now the maximum energy to be expected in the neutrons from Be+deuton is 10.1 MV. Most of the forks of these high energies (above 10 MV) were poor in quality. Thirdly, in common with the experience of other observers there was found to be a disappearance of kinetic energy in most cases, though a few examples showed a gain. This loss in kinetic energy, we shall call $\Delta$ and define it by

$$\Delta = E_n - (E_\alpha + E_\beta), \tag{8}$$

where $E_n$ is the energy of the impinging neutron and $E_\alpha$ and $E_\beta$ are, respectively, the kinetic energies of the light and heavy disintegration products. Values of $\Delta$ were found to be distributed over a very wide range; and, moreover, it was pointed out at that time[14] that a definite (linear) relation exists between $\Delta$ and the energy of the incident neutron. In an attempt to establish this relation more definitely a new series of photographs was taken in which the cloud chamber contained nitrogen greatly diluted with helium, so that the stopping power relative to standard air was 0.53. The photographs yielded 18 new forks which constitute the second batch of data. These forks exhibited the same peculiarities as the first batch except that there were no neutrons found with energies above 10 MV. Points from this second batch fell on the same line in the $\Delta$ against $E_n$ plot as had those from the first batch, with about the same deviations from it.

When all forks having their resultant momenta not passing close to the neutron source were rejected all the high energy neutrons were by this act also cast out, with the exception of three cases. Two of these do not exceed the upper limit by more than the upper limit of error to be expected. The third indicates a neutron energy of 20.4 MV. This fork is poor technically; by the broadness of the track it must have been formed before the chamber was fully expanded. Great caution must be exercised in passing judgment on any but the sharpest tracks in this type of work. A group of ions which has lived through an expansion finds itself distorted by the strain of the gas due to the sudden increase in volume of the chamber. The more the plane of the fork is inclined to the plane of the chamber the greater this distortion will be. It is of such a character that the lengths of the tines are increased and in most cases the angle between the tines is decreased. The magnitude of these effects over the decrease in the stopping power accompanying an expansion (which acts in the other direction, tending to cause one to underestimate energies) is in general small but because of the dependence of one's estimate of the neutron's energy on the angle between the tines of the fork it can be responsible for appreciable errors. Among the photographs of the forks indicating high energy neutrons none can with certainty be classed as being of tracks which were formed when the chamber was fully expanded.

In deriving the neutron's energy from the lengths of the tines and the angle between them one can only hope to get the true value if the measured quantities have not been disturbed. We have mentioned a small and unsymmetrical effect due to distortions produced by the expansion. There are two symmetrical effects which must be given careful consideration. The first of these is that the angle between the tines of the fork which one measures will not be the true angle at which the particles separated from each other if one or the other has been scattered in the first tenth-millimeter or so of its course. Such a deflection would pass unnoticed at the pressures usually used in cloud chambers for this work. The recent work of Joliot[15] on the recoil of radioactive atoms has drawn attention to the likelihood of deflections amounting to occasionally as much as 20° in the first few encounters such a heavy atom makes with other atoms. It is very probable that this is an extra-nuclear effect and that the cross sections responsible for such scattering are large compared with nuclear cross sections. Even if it were purely a nuclear effect one can see that the chance of a deflection greater than say 5° in the first 0.2 mm of the path of the heavy nucleus resulting from the disintegration

[14] F. N. D. Kurie, Phys. Rev. **46**, 324 (1934).

[15] F. Joliot, J. de Physique **5**, 219 (1934).

of nitrogen by neutrons is around 1 percent for the energies usually found in this case. Additional information should be obtainable from the data on elastic collisions of $\alpha$-particles with nuclei in the first row of the periodic table. If such scattering plays an appreciable role in the motion of particles of this order of mass it should reveal itself in an apparent failure of the laws of conservation of energy or momentum or both for such collisions. The work of Auger and Perrin and of Akiyama[16] seems to indicate that such scattering is important, while that of Blackett[17] gives no evidence that energy and momentum are not apparently conserved. It is reasonable then to regard such scattering as possible and indeed likely, since the data on elastic $\alpha$-particle collisions are not at all unequivocal on this point. It will perhaps partially relieve this situation to photograph neutron stimulated disintegrations at low pressures (of the order of 1/5 to 1/10 of an atmosphere) and rejecting all tracks in which any hint of a deflection near the point of their origin can be discerned.

There remains yet one further intrinsic source of symmetrical errors in the fact that the energies of the two disintegration particles are obtained from the lengths of their tracks from empirical range-energy curves. These curves give the energy of a particle of a certain *mean* range. Straggling is so great for a particle as heavy as say boron that for any *individual* track length there is considerable spread in the energy which may be assigned to it. In extreme cases this amounts to around 0.20 MV for a 1 MV $B^{11}$ nucleus.

Considering all the unfortunate uncertainties which attend the evaluating of the energy of the incident neutron from one of these disintegration forks one feels safe in saying that from the experimental data now on hand on neutron stimulated disintegrations there is no good indication of neutron energies greater than the theoretical limit of 10.1 MV in the case of beryllium bombarded by deutons. A similar remark can be made with reference to the high energies reported by various authors when the neutrons arose from Be+Po sources.

[16] P. Auger and F. Perrin, C. R. **175**, 340 (1922); M. Akiyama, Jap. J. Phys. **2**, 279, 287 (1923).
[17] P. M. S. Blackett, Proc. Roy. Soc. **A103**, 62 (1923).

TABLE I. *Data on 29 cases of the disintegration of nitrogen by neutrons from beryllium+deutons.* $E_n$ = energy of incident neutron in MV; $\Delta$ = kinetic energy lost in the reaction in MV; $E_\alpha+E_\beta$ = kinetic energy of particles resulting from the disintegration in MV; $E$ = proper disintegration energy in MV; $v$ = deviations of individual values of $E$ from the mean.

| No. | $E_n$ | $\Delta$ | $E_\alpha$ | $E_\beta$ | $E$ | $v$ | No. | $E_n$ | $\Delta$ | $E_\alpha$ | $E_\beta$ | $E$ | $v$ |
|---|---|---|---|---|---|---|---|---|---|---|---|---|---|
| 1. | 2.4 | −1.1 | 3.5 | 3.3 | | +0.2 | 16. | 5.6 | 2.6 | 3.0 | 2.7 | | −0.4 |
| 2. | 2.5 | −0.6 | 3.1 | 2.9 | | −0.2 | 17. | 5.7 | 2.5 | 3.3 | 2.1 | | −1.0 |
| 3. | 3.4 | 1.5 | 1.6 | 1.1 | | −2.0 | 18. | 5.8 | 2.3 | 3.5 | 3.1 | | 0.0 |
| 4. | 3.6 | −0.4 | 3.2 | 3.0 | | −0.1 | 19. | 6.7 | 4.2 | 3.4 | 2.9 | | −0.2 |
| 5. | 3.8 | 1.1 | 2.7 | 2.4 | | −0.7 | 20. | 7.7 | 3.2 | 4.5 | 3.9 | | +0.8 |
| 6. | 3.9 | 0.7 | 3.2 | 3.0 | | −0.1 | 21. | 8.0 | 3.8 | 4.2 | 3.7 | | +0.6 |
| 7. | 3.9 | 1.7 | 2.2 | 1.9 | | −1.2 | 22.*Y* | 8.6 | 4.1 | 4.6 | 3.9 | | +0.8 |
| 8. | 4.0 | 0.4 | 3.6 | 3.3 | | +0.2 | 23. | 9.1 | 4.4 | 4.7 | 4.1 | | +0.9 |
| 9. | 4.0 | 1.3 | 2.8 | 2.4 | | −0.7 | 24. | 9.6 | 5.8 | 3.9 | 3.2 | | +0.1 |
| 10. | 4.7 | 3.3 | 1.4 | 1.1 | | −2.0 | 25.*Y* | 11.0 | 8.6 | 2.4 | 1.6 | | −1.5 |
| 11. | 4.8 | −0.0 | 4.8 | 4.4 | | +1.3 | 26. | 12.1 | 8.0 | 5.1 | 4.2 | | +1.1 |
| 12.*Y* | 5.2 | 1.8 | 3.5 | 3.1 | | 0.0 | 27. | 13.2 | 7.2 | 6.0 | 5.1 | | +2.0 |
| 13. | 5.2 | 1.0 | 3.6 | 3.4 | | +0.3 | 28.*Y* | 17.1 | 13.6 | 3.4 | 2.4 | | −0.7 |
| 14. | 5.2 | 1.0 | 4.2 | 3.9 | | +0.8 | 29. | 20.4 | 14.5 | 5.9 | 4.5 | | +1.4 |
| 15. | 5.6 | 2.4 | 3.6 | 3.2 | | +0.1 | Mean $E$ = 3.1 MV, $v^2$ = 27.1; standard deviation = 0.97 MV | | | | | | |

All the data which remained after forks whose resultant momenta did not pass through the source were rejected are collected in Table I without distinction as to whether they belong to the first or to the second batch. They are there arranged in the order of their neutron energies. The table includes four forks, marked *Y*, which the author measured at Yale in the spring of 1933, the neutrons being obtained from a Be+Po source. Except for the one at 17 MV[18] they have not as yet been published.

## THE ENERGY OF THE NEUTRONS FROM BERYLLIUM+DEUTONS

It will be noticed from Table I that neutrons are indicated by the forks as having energies from about 2 MV to at least 10 MV. In order to be sure these energies are not entirely fictitious a study of the energy spectrum of the neutrons was made by measuring the length of track made by helium atoms recoiling from collisions with the neutrons, together with their angle of projection from the most probable neutron path. This angle was in all cases the smaller of the two possible angles, since the beginning and end of the helium trajectory could not be distinguished. Evidence was thus exposed for the existence of neutron energies ranging from 1 MV up to 10–11 MV. There seem to be a great number of neutrons with energies below 3 MV and a falling off in numbers above this value. The data

[18] F. N. D. Kurie, Phys. Rev. **43**, 771 (1933).

constitute very strong corroborative evidence that the energies represented by the forks of Table I, below around 11 MV, are not greatly in error.

### The Energy Loss in Nitrogen

Many authors have consigned the loss of kinetic energy to the role of an excitation energy of the heavy nucleus ($B^{11}$). The evidence for this is very poor. One may examine critically all the data now at hand for nitrogen, some 60 tracks, by plotting a frequency distribution curve of the number of cases where the energy loss lies between $\Delta$ and $\Delta+\alpha$. In a case where the abscissae are subject to error it is unwise to group them into classes where the interval $\alpha$ is smaller than the probable error, for so doing causes serious distortion of the distribution curve. Eddington has shown that this distortion is proportional to the square of the ratio of the probable error to the class interval and also to a factor which depends on the curvature of the distribution curve. The effect is not serious when the class interval is taken equal to the probable error. All the data available are shown in Fig. 1. The histogram is quite smooth, as also is the integral curve which is the more sensitive of the two to any evidence of grouping. It is impossible to affirm on the basis of this curve that either of the following do not represent the conditions obtaining here: Firstly, there may be two or more excited states in the $B^{11}$ nucleus and the groups representing them in the frequency diagram are two or three MV broad and so remain concealed; secondly, there may be many groups, very narrow and close together with a spacing of the order of or less than the class interval $\alpha$, so that their detection is impossible with the present errors.

On the basis of the masses involved in the transmutation here considered (1) we expect the reaction to be exothermic to the extent of 1.5 MV (using $n^1=1.0067$). If the disintegration were of the usual type we should expect the $\Delta$ frequency diagram to be more or less symmetrical about the point marked $\delta m$ in Fig. 1.

It is more difficult to understand the above mentioned linear relation between $\Delta$ and $E_n$ as exhibited in Fig. 2. This is a poor way to plot the data because errors in the fork measurements which are traceable to errors in the determination of the angle between the tines of the fork effect both $\Delta$ and $E_n$ equally and would cause points for which $E_\alpha+E_\beta$ is constant to range along a line equally inclined to the two axes. One might

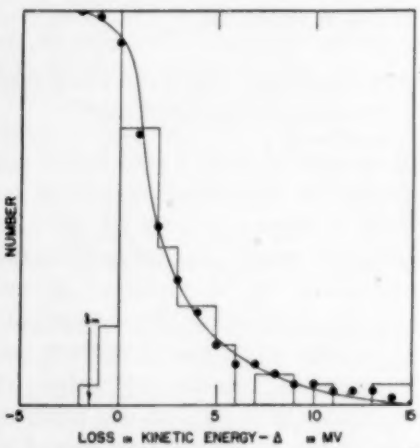


Fig. 1. Integral distribution curve of the loss in energy in the disintegration of nitrogen by neutrons, showing the number of cases in which the loss is greater than $\Delta$. In outline is shown the distribution histogram for the same data, giving the number of cases in which the loss is between $\Delta$ and $\Delta+1$. The curves were plotted from all the published data (60 cases) and have been taken from the work of Feather, Meitner and Philipp, Harkins, Gans and Newson, and Kurie. The point marked $\delta m$ is the energy lost in the mass change of the (exothermic) reaction (hence it corresponds to a negative $\Delta$). If the disintegration were of the usual type (constant energy change) we should expect the histogram to cluster about this point.

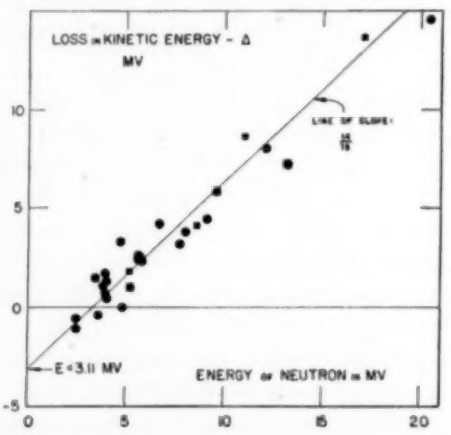


Fig. 2. The relation between the energy of the incident neutron and the energy it looses when it causes the disintegration of a nitrogen nucleus. The line of slope 14/15 has been fitted to the observed points and indicates by its intercept on the axis of ordinates a proper disintegration energy of 3.1 MV.

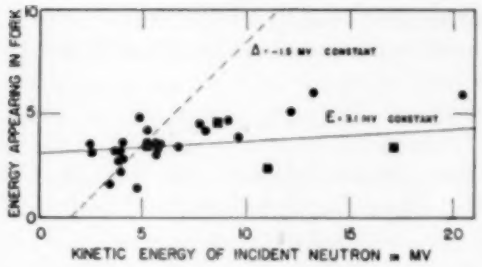


FIG. 3. The relation between the energy of the incident neutron and the energy appearing as kinetic energy in the products of disintegration. The dotted line of slope unity is the line on which the points should fall if the energy change were constant in the process ($\Delta = -1.5$ MV), while the heavy line describes a transmutation in which the energy released is constant ($=3.1$ MV).

regard this relation *per se* as being derivable from disintegrations in which the neutrons responsible have a small range of energies (giving the spread on both sides of the line) and in which the errors in measuring the angles are large. It seems unlikely that such a pronounced trend can be accounted for simply on the basis of experimental error, particularly since we know from recoil data that neutrons are emitted from beryllium when struck by deutons with a very wide range of energies, and since a similar plot of $\Delta$ against $E_n$ can be made from the data obtained with Be+Po sources where conservation of momentum can be much better checked than it could in the present experiments.

However it is more satisfactory to plot the data in a way in which errors in measurements of angles and of lengths can be separated better. This is done in Fig. 3 where $E_\alpha + E_\beta$ is plotted against $E_n$. Here errors in the ordinates are solely due to errors in measurements in lengths, while both lengths and angles contribute to the errors involved in the abscissae. If the disintegrations are of the more usual type in which $\Delta$ is a constant the points are to be expected to fall along a line at 45° to either axis as indicated by the dotted line having an intercept on the axis of abscissae at $E_n = -\Delta$, here taken for the purpose of the drawing at 1.5 MV (the energy available from the masses in the change here being considered—Eq. (1)). The observed points are seen to fall, not on this line, but on a line much less steeply inclined. This suggests that the energies of the disintegration particles are very nearly constant; and the fact that the increase of their energies with the energy of the incident neutron is considerably slower than in the usual case where $\Delta$ is constant suggests that a different mechanism is at work. Indeed we find that the energy which an observer at rest relative to the center of mass would measure, namely the *proper disintegration energy*, is constant in the sense that it shows no increase as $E_n$ is increased. This disintegration energy we shall designate by $E$, where $E = E_\alpha + E_\beta - E_n/15$. Individual values of $E$ are given in Table I. The mean of these observations is $E = 3.11$ MV.

It is clear from what has been said about the types of errors which are encountered in these measurements that it is possible to analyze a fork and obtain the disintegration energy without serious error while making a large error in $E_r$ (and hence in $\Delta$). Such a condition is met for example when the heavy nucleus suffers a deflection shortly after beginning its flight. To a first approximation our evaluation of the disintegration energy depends on the lengths of the tines alone while that of the neutron's energy involves the angle between the tines. From this point of view it is not surprising that the points at 17 and 20 MV fit well on the curve of Fig. 2, since the only condition demanded of a point that it fall on the line is that it represent a disintegration energy of approximately 3.1 MV.

Deviations $v$ from the mean value of $E$ are given in the last column. From these residuals one may compute in the usual way the standard deviation (S. D.) of the values of $E$ which is a measure of the scatter of the observations about the mean. We thus obtain S. D. $= 0.97$ MV.

From repeated measurements on several tracks, it was found that the length of the tines could be repeated to about $\pm 0.25$ mm (in standard air and that the angle between the tines could be got to within 3°. These are liberal estimates, from which we find that for neutron energies around 5 MV this leads to probable errors in $E_n$ of 1.3 MV and in $E$ of 0.43 MV. It follows that the distribution in $E$ is expected to have a S. D. of 0.63 MV on the basis of errors of measurements alone. We have mentioned a further source of error which will probably account for the remainder of this S. D., namely that the ranges measured pertain to single particles, whereas the range energy curves are

constructed for the mean ranges of many particles.

The fact that the proper disintegration energy is constant is made reasonable by postulating that the intermediate nucleus $N^{15}$ is radioactive with the emission of $\alpha$-particles in the strict sense of the word. We learn from Gamow's theory that the half-life of such a radioactive nucleus is roughly of the order of $10^{-20}$ sec.; consequently there is no chance of observing the track of the intermediate radioactive nucleus in cloud chamber photographs of such a disintegration. Furthermore, so short a lifetime imposes an uncertainty on the energy of disintegration of about a half million volts so that the observed values of $E$ should have a S. D. of this order. With experimental errors as large as they are it is impossible to say whether such an effect is observed.

### Digression on Capture Collisions

It is well that we pause to examine in detail the differences between the type of disintegration herein proposed as accounting for the neutron precipitated disintegrations and the more usual type such as is found in the case of the transmutation of nitrogen by $\alpha$-particles.

Let us consider a particle $A$ (of mass $A$) impinging with energy $E_A$ on a nucleus $B$ at rest. The intermediate nucleus $AB$ will, if momentum is conserved, move off with energy $E_{AB}$ given by

$$E_{AB}=[A/(A+B)]E_A. \tag{9}$$

The remainder of the energy will either contribute to the mass of $AB$ or be radiated in some form, perhaps as a $\gamma$-ray. The energy radiated is then

$$E_R=[B/(A+B)]E_A-[AB-(A+B)]. \tag{10}$$

where the second term represents the energy required to create the mass of $AB$ from $A$ and $B$. If now $AB$ disintegrates into two new bodies $C$ and $D$, they will be observed to have a total energy

$$E_C+E_D=E+E_{AB}, \tag{11}$$

where $E$ is what we have called the proper disintegration energy and is simply the energy which $C$ and $D$ would seem to have to an observer at rest relative to $AB$; it is entirely derived from the mass change occasioned by the disintegration. Thus

$$E=AB-(C+D). \tag{12}$$

We have already defined the loss in energy $\Delta=E_A-(E_C+E_D)$. It follows then that

$$E=[B/(A+B)]E_A-\Delta. \tag{13}$$

We may now distinguish two cases:

**Case 1. $\Delta$ = constant**

We see from the definition of $\Delta$ that a plot of $E_C+E_D$ against $E_A$ is a straight line of slope unity cutting the $E_A$ axis at $\Delta$. In a disintegration of this type then the particles $C$ and $D$ take all of the incident kinetic energy which remains after the mass change and the radiated energy have been accounted for—these last quantities being always the same amount. The data of Blackett and Lees[19] on the disintegration of nitrogen by $\alpha$-particles with the formation of $O^{17}$ and the emission of a proton, provide a good example of this sort of inelastic collision. If their data are plotted in the form of Fig. 2 they fit the 45° line very well. The sequence of events in such a transmutation may be thought of as follows: An $\alpha$-particle of energy $E_\alpha$ on penetrating the nuclear barrier is captured in some level $E_\alpha^0$, conveys the entire energy difference $(E_\alpha-E_\alpha^0)$ to a proton residing on a level $E_p^0$ which now emerges from the nucleus with a kinetic energy $E_p=E_\alpha-(E_\alpha^0-E_p^0)$. The thing that particularizes this case, $\Delta$ = constant, means that the proton may be elevated by means of the $\alpha$-particle's excess energy into a continuous band of energy levels perhaps all higher than the top of the barrier so that it has a high probability of escaping.

From the considerations above we find

$$E_R=\Delta+(A+B)-(C+D). \tag{14}$$

In the particular case of nitrogen bombarded by $\alpha$-particles Bothe and Becker[20] were unable to find any $\gamma$ radiation accompanying the proton emission so all the energy loss is probably taken up by a mass change.

---

[19] P. M. S. Blackett and D. S. Lees, Proc. Roy. Soc. **A136**, 325 (1932).

[20] W. Bothe and H. Becker, Zeits. f. Physik **66**, 289 (1930).

**Case 2. $E$ = constant**

This case amounts to the creation of a radioactive nucleus by the absorption by $B$ of $A$ and $E_A$ with a large radiative loss of energy at the moment of capture. It may be recognized by the fact that a plot of $E_C+E_D$ against $E_A$ is a line of very much smaller slope than in the previous case. The slope as can be seen from the above considerations (9) and (11) is $A/(A+B)$, and the intercept on the $E_C+E_D$ axis is $E$. The line drawn in Fig. 2 through the observed data pertaining to the disintegration of nitrogen by neutrons has been drawn with a slope of 1/15 and an intercept at $E=3.1$ MV. The data of other authors on the disintegration of nitrogen, oxygen, fluorine and neon indicate that in all the known cases the transmutations produced by neutrons are probably of this type.

This process of disintegration is thus different from any so far encountered and may be described as follows: $A$ neutron of energy $E_n$ on entering a nucleus is captured in its ground state $E_n^0$. If the energy made available by this change is sufficient it will elevate an $\alpha$-particle from its ground state $E_\alpha^0$ to some excited state $E_\alpha$ from which it escapes—in a purely radioactive fashion. The difference between $E_n$ and $E_\alpha$ is $\Delta$ (we are neglecting recoil for simplicity here), and this of course varies linearly with $E_n$ since $E_\alpha$ is constant in this system. Clearly, if the neutron has less energy than is required to raise the $\alpha$-particle from its ground state to the excited state it will not be able to cause the transmutation; we shall speak of this lower limit at which disintegrations begin as the *threshold energy*, $E_t$ and note that $E_t=AB-(A+B)$. This case is characterized by the existence of a level in the radioactive quasi-nucleus from which the $\alpha$-particle has a relatively large probability of escaping through the barrier. The height of the $N^{15}$ barrier to $\alpha$-particles is in the neighborhood of 4 MV and as we have seen this level to be around 3 MV the escape is necessarily through the barrier and not over it.

In this case we see from (14) that if the nuclei $A$, $B$, $C$, and $D$ are definite nuclei, $E_R$ may take on any value from zero up to that appropriate to the highest energy neutron. The maximum $E_R$, when a 10 MV neutron disintegrates nitrogen is about 5.5 MV. If this energy is in the form of $\gamma$-rays, their energy spectrum for a given set of neutrons disintegrating a given element is then derivable from the neutron's energy spectrum by foreshortening it along the energy axis in accordance with (13) and (14) in an amount depending upon the element being disintegrated.

Beside these two cases there is of course the possibility of many intercombinations of them occurring in the same disintegration. It is particularly likely that the disintegrations will not concern themselves solely with one particular set of energy levels, but with many; in this event the pattern of the transmutation becomes very complicated and more precise measurements on the disintegration forks will have to be made before we can obtain any of the information about the finer details of the processes.

## Discussion

It is interesting to examine further the implications of the proposed mode of disintegration of nitrogen under neutron bombardment. Essentially the existence of a virtual $\alpha$-particle level in the $N^{15}$ nucleus has been assumed and its energy has been found to be around 3 MV. If Eq. (1) be now read from left to right it describes the production of neutrons when boron is battered by $\alpha$-particles. The virtual $\alpha$-particle level should make itself felt as a resonance level for entrance of the $\alpha$-particle. The excitation curve for this reaction has been explored by Chadwick.[21] There is clear evidence of a resonance level beginning at 2.4 MV and having, as nearly as one can judge, a mean value of about 2.8 MV, which does not compare unfavorably with the value of 3.1 MV deduced from the present work. This agreement is very satisfactory, considering the data on which the two figures depend.

There are only two other methods of creating $N^{15}$ with the projectiles and targets which seem to be now available. The first is the bombardment of $C^{13}$ (which constitutes about 1 percent of ordinary carbon) with deutons. The second is to direct a stream of fast $Li^6$ ions against beryllium. In the first case it would be very difficult to detect any short range $\alpha$-particles among the large yield of longer range protons arising from

[21] J. Chadwick, Proc. Roy. Soc. **A142**, 1 (1933).

$C^{12}$. The second method is probably quite feasible if sufficiently intense beams can be obtained, despite the strongly repulsive forces which will exist between the lithium and beryllium nuclei. It is difficult to predict what may be observed in either of these two cases but it seems very likely that either neutrons or $\alpha$-particles will be found and that, since the neutronic spectrum depends on the energy characteristics of the body stimulating its emission, nothing can be said about it; the $\alpha$-particles, however, if the views expressed in this paper are in the main part correct, should appear with the same energy of about 3 MV.

Let us now enquire as to the mass of $N^{15}$. Thus, $N^{15} = B^{11} + He^4 + E = 11.0110 + 4.002 + 0.0033 = 15.0165$. By including the threshold energy we may equally well compute this figure from the left hand side of Eq. (1). The lowest energy neutron which has been capable of disintegrating nitrogen is one at 1.86 MV reported by Harkins, Gans and Newson.[2] As the energy of the neutron approaches zero the change expected in the character of the fork is not a diminishing of the length of the tines, if $E$ is to remain constant, but a spreading of the angle between them. At as low an energy as 2 MV this angle is still no larger than 150°, so forks of lower energies would still be perfectly recognizable. Furthermore we have noted above that there are abundant quantities of neutrons with energies below 2 MV, so this lower limit of 1.86 MV seems reasonably real, and no observational difficulties stand in the way of detecting forks due to lower energy neutrons. We have then, since 1.86 MV = 0.0020 mass units $N^{15} = N^{14} + n^1 + E_i = 14.0080 + 1.0067 + 0.0020 = 15.0167$. The agreement of these two figures is most satisfactory.

A nitrogen of mass 15 is known to spectroscopists,[22] who give as its mass $15.0028 \pm 0.0038$. In view of the fact that the nitrogen which we are considering has a half life comparable to the natural period of such a nucleus, its production may be compared to the state of predissociation which is found in band spectra, and consequently its mass cannot be compared to that of such a stable nucleus as the spectroscopists have measured.

The data of other authors are most conveniently treated by plotting $\Delta$ against $E_n$ and fitting a line of the proper slope to them, so obtaining $E$ from an intercept. Thus for nitrogen the data of Harkins, Gans and Newson[2] give $E = 3.2$ MV; Feather's[1] give $E = 3.4$ MV; Meitner and Philipp's[6] give $E = 3.3$ MV.

For oxygen only seven forks have been measured[1, 6] and lead to $E = 3.8$ MV, none are found for $E_n$ below 7.0 MV. The mass of the intermediate quasi-nucleus ${}_8O^{17}$ is 17.0102 from the left hand side of equation (2), including $E$ of course; and from the right hand side, including the threshold energy (7 MV), 17.0142. The data are not sufficiently abundant to establish the threshold with anything approaching certainty, so one may conclude that disintegrations will be found due to neutrons with energies as low as 3 MV.

From (4) it is clear in the case of fluorine that whatever is said of the mass of $F^{20}$ must be viewed with caution since we know nothing of the mass of $N^{16}$. However if one regards the numerical coincidences in the case of nitrogen as significant we may evaluate the masses of both the heavy fluorine and the heavy nitrogen in terms of the mass of ordinary fluorine (using that recently given by Henderson, Livingston and Lawrence)[23] and the energy data of Harkins, Gans and Newson.[4] They find no disintegrations for which $E_n < 3.5$ MV, so $F^{20} = 19.0031 + 1.0067 + 0.0037 = 20.0135$. From their data one gets $E = 4.2$ MV, and therefore, $N^{16} = 20.0135 - 4.0022 - 0.0045 = 16.0068$. In this connection it may be remarked that Fermi and his co-workers[24] have found that fluorine when bombarded with neutrons becomes radioactive, with the emission of $\beta$-particles. The decay period is found to be 9 sec. and the mean energy of the $\beta$-rays is given as 2 MV; $\gamma$-rays are also emitted in the process. There is thus ample energy available in $N^{16}$ to account for the energy of the $\beta$-spectrum.

Finally, Harkins, Gans and Newson[3] have

[22] G. Herzberg, Zeits. f. physik. Chemie **9**, 43 (1930); R. T. Birge, Phys. Rev. **37**, 841 (1931).

[23] M. C. Henderson, M. S. Livingston and E. O. Lawrence, Phys. Rev. **46**, 38 (1934).

[24] E. Fermi, E. Amaldi, O. D'Agostino, F. Rasetti and E. Segré, Proc. Roy. Soc. **A146**, 483 (1934).

reported four disintegrations of neon in accordance with (3) for which $E=3.9$ MV, $E_t=7.8$ MV. The mass of $_{10}Ne^{21}$ is 21.0093 from the right hand side of (3), and 21.0099 from the left hand side. The first of these masses is based on the value 17.0029 for $_8O^{17}$. This agreement is very good, but here again the lack of data by its influence on $E_t$ makes it uncertain how much weight to give this agreement.

The following facts concerning neutron-stimulated disintegration of the Feather type (emission of an $\alpha$-particle) seem to be well established by the information now at hand:

(1) At least in the case of nitrogen, oxygen, fluorine, and neon they are all examples of case 2 disintegrations ($E$=constant).

(2) The disintegration energies ($E\sim 3-4$ MV) do not vary greatly from element to element.

(3) A large fraction of the neutron's energy is radiated, perhaps as a $\gamma$-ray, the remainder going into excitation, mass building and kinetic energy of the temporary radioactive element. The mass of this radioactive element can be estimated from the threshold energy, which is only well determined in the case of nitrogen, for which there are now data on 60 forks.

(4) In the case of $N^{15}$ the level in its nucleus from which $\alpha$-particles escape has been identified with the resonance level for entry of the $\alpha$-particles in the disintegration of boron with the emission of neutrons.

(5) Values of E show considerable spread. This is slightly in excess of that expected from experimental errors and it is suggested that it may in part be a consequence of the very short half-life expected for the radioactive intermediate nucleus.

I am very grateful to Professor E. O. Lawrence for the provision of material aids to this work. Discussion with him and Professor Robert Oppenheimer has been extremely valuable. Thanks are also due to Mr. J. R. Richardson who has checked all the calculations involved in this work. This work has been aided by grants from the Josiah Macy Jr. Foundation, the Chemical Foundation and the Research Corporation.

---

JANUARY 15, 1935 PHYSICAL REVIEW VOLUME 47

# X-Ray Levels of Radioactive Elements with Applications to Beta and Gamma-Ray Spectra

ARTHUR EDWARD RUARK* AND FREDERICK A. MAXFIELD,** *Department of Physics, University of Pittsburgh*

(Received July 6, 1934)

A table of x-ray levels of radioactive elements is presented. The levels for Tl, Pb, Bi, Th and U were computed by adding term-differences from x-ray emission spectra to some outer level obtainable from optical spectra; those for other elements were carefully interpolated. The energies of certain gamma-rays of Th B·C, Th C″·D, Ra C·C′, Ac B·C and Ac C·C″ are recomputed from the new levels and known beta-ray energies. In the case of Ellis' data, gamma-ray energies obtained from beta-rays ejected from the $K$-shell are brought into excellent agreement with those based on beta-rays from other shells. Energies of secondary electrons of Bi 83 and Po 84, arising in Auger processes and studied by Ellis, agree with those computed from the new levels within the limits of experimental error. This justifies the use of the new levels in computing the energies of Auger lines of other radioactive elements; those of Rd Ac·Ac X, Ac X·An, and Ms $Th_2$·Rd Th are discussed. The transition Pa·Ac gives gamma-rays of energy 347,400 and 359,300 electron volts, hitherto unknown. The beta-ray spectrum of this transition, so far as it is known, is now completely classified, except for one line. The beta-ray spectra of Rd Th·Th X and $UX_1$·$UX_2$ are produced by nuclear gamma-rays, not by the $K\alpha$-lines of the daughter elements. Evidence is presented for the view that the band at $Hr=2450$ gauss cm in the spectrum of $UX_2$·U II represents the disintegration electrons of $UX_2$, and that the group at 1,300,000 electron volts probably represents the secondary electrons. Attention is directed to the frequent occurrence of an energy difference of the order 84,000 to 90,000 electron volts, in gamma-ray spectra and nuclear energy diagrams.

* Now at the University of North Carolina.

** Now at the University of Wisconsin.

## I. X-Ray Terms of Radioactive Elements

GAMMA-RAY energies are derived from those of secondary beta-rays by the equation $h\nu = E_\beta + X$, where $X$ represents the binding energy of an x-ray level of the daughter atom, from which a secondary electron, of energy $E_\beta$, is ejected. The present situation in regard to gamma-ray energies is unsatisfactory, because different authors employ different term values, and in most cases do not state how they were derived. To classify beta-rays with certainty, and to get accurate values of gamma-ray energies, it is necessary to have a list of x-ray terms for the radioactive elements, in which the error is negligible compared to that of the best beta-ray measurements. We shall obtain x-ray terms for these elements which are believed to be more reliable than those employed in most papers on beta-ray spectra.

We have reasonably complete information on the x-ray spectra of all heavy elements which have both radioactive and stable isotopes, namely: Tl, Pb, Bi, Th and U.[1] Term and line values for other radioactive elements must be obtained by interpolation, with three exceptions. Siegbahn and Friman measured one line of the radium $L$-series, de Broglie determined $L_{II}$ and $L_{III}$ of radium, and Beuthe and von Grosse[2] measured the protactinium $L$-series. It has been customary to obtain x-ray terms by combining the $L_{III}$ limit with term differences from emission spectra. Since the breadth of the $L_{III}$ limit has introduced difficulties of measurement, and since the interpretation of absorption limits has been a matter for discussion, one of us[3] has described a more satisfactory procedure. An x-ray level of small magnitude is obtained from the optical spectra of the isolated atom,[4] and to this level one adds term differences, accurately known from x-ray line spectra, to get deeper levels. This method is satisfactory for all levels of Tl, Pb, Bi, Th and U, except the $K$-level, where existing measurements are less accurate than those of the more favorably situated $L$-series. For Tl, Pb and Bi we used the $K$-lines of Stephenson and Cork, and for Th and U the $K$ absorption limits of Mack and Cork.[5]

Knowing the levels of these elements, we interpolated values for intervening ones by plotting $\nu/R$ values of terms and term differences against the atomic number $Z$. Small term differences were used as far as possible, to reduce plotting errors, and a semi-graphical method devised by Idei was adopted in dealing with larger ones.[6] Table I shows the results in international electron volts, computed by the formula

$$V = \frac{300Rc}{b}\,\frac{h}{e}\,\frac{d_c}{d_a}\left(\frac{\nu}{R}\right)_c = (13.545 \pm .0131)\left(\frac{\nu}{R}\right)_c . \quad (1)$$

$R$, $c$, $h$ and $e$ have their customary meanings; $h/e = (1.3723 \pm 0.0008)10^{-17}$ erg sec./e.s.u.; $b$ is the ratio of the international to the absolute volt; $d_c/d_a$ is the ratio of the conventional to the actual calcite spacing at 18°C; namely, 3029.45/3027.85; and the subscript $c$ on $(\nu/R)$ indicates that this quantity is based on the conventional calcite spacing. The data are recorded to a greater accuracy than the *absolute* values possess so that small differences between energy levels, accurately known, may not be falsely rendered; for in many cases the corresponding $\nu/R$ values are known to 0.1 unit.

Our values for Pa agree with the $L$-series data of Beuthe and von Grosse within 6 electron volts. Values for the radium $L_{II}$ and $L_{III}$ limits are, respectively, 32 and 42 electron volts higher than those of de Broglie, whose measurements were made in the infancy of x-ray spectroscopy. The $L$, $M$, etc., levels of Tl, Pb, Bi and U agree with those in the second edition of Siegbahn's treatise within one $\nu/R$ unit. On the other hand, the values quoted by Siegbahn for Th are in error, for if they are used in conjunction with line-spectrum data, a negative value is obtained for $P_{II, III}$. We have compared our $L$ and $M$ levels for Tl, Pb, Bi, Th and U with absorption-edge

[1] For bibliography see Siegbahn, *Spektroskopie der Röntgenstrahlen*, 1931 edition.
[2] Siegbahn and Friman, Phys. Zeits. **17**, 61 (1916); de Broglie, Comptes rendus **168**, 854, **169**, 134 (1919); Beuthe and von Grosse, Zeits. f. Physik **61**, 170 (1930).
[3] Ruark, Phys. Rev. **45**, 827 (1934).
[4] Bacher and Goudsmit, *Atomic Energy States;* Beutler, Zeits. f. Physik **86**, 495, 710 (1933); Rasmussen, Zeits. f. Physik **87**, 607 (1934).
[5] Stephenson and Cork, Phys. Rev. **27**, 138 (1926); Mack and Cork, Phys. Rev. **30**, 741 (1927).
[6] Idei, Tohoku Science Reports **19**, 651 (1930).

TABLE I. *X-ray energy levels of radioactive elements in international electron volts.*

| | Tl 81 | Pb 82 | Bi 83 | Po 84 | 85 | Rn 86 | 87 | Ra 88 | Ac 89 | Th 90 | Pa 91 | U 92 |
|---|---|---|---|---|---|---|---|---|---|---|---|---|
| $K$ | 85320 | 87780 | 90280 | 92850 | 95490 | 98180 | 100920 | 103700 | 106550 | 109510 | 112590 | 115790 |
| $L_{\text{I}}$ | 15320 | 15827 | 16352 | 16902 | 17468 | 18039 | 18622 | 19213 | 19810 | 20429 | 21067 | 21711 |
| $L_{\text{II}}$ | 14672 | 15167 | 15676 | 16213 | 16766 | 17322 | 17890 | 18466 | 19048 | 19651 | 20272 | 20900 |
| $L_{\text{III}}$ | 12635 | 13006 | 13390 | 13787 | 14196 | 14604 | 15019 | 15432 | 15844 | 16264 | 16694 | 17128 |
| $M_{\text{I}}$ | 3702 | 3843 | 3991 | 4151 | 4319 | 4485 | 4655 | 4829 | 4998 | 5173 | 5353 | 5537 |
| $M_{\text{II}}$ | 3418 | 3554 | 3691 | 3843 | 4005 | 4163 | 4326 | 4492 | 4655 | 4822 | 4995 | 5172 |
| $M_{\text{III}}$ | 2956 | 3064 | 3174 | 3293 | 3421 | 3545 | 3671 | 3798 | 3919 | 4041 | 4167 | 4296 |
| $M_{\text{IV}}$ | 2487 | 2583 | 2685 | 2795 | 2914 | 3028 | 3144 | 3262 | 3373 | 3486 | 3602 | 3721 |
| $M_{\text{V}}$ | 2392 | 2480 | 2576 | 2681 | 2793 | 2900 | 3010 | 3120 | 3224 | 3328 | 3436 | 3546 |
| $N_{\text{I}}$ | 851 | 894 | 940 | 997 | 1062 | 1122 | 1181 | 1234 | 1280 | 1327 | 1382 | 1439 |
| $N_{\text{II}}$ | 727 | 763 | 807 | 861 | 921 | 978 | 1033 | 1082 | 1124 | 1168 | 1218 | 1271 |
| $N_{\text{III}}$ | 617 | 645 | 679 | 725 | 775 | 822 | 867 | 904 | 934 | 967 | 1003 | 1042 |
| $N_{\text{IV}}$ | 415 | 438 | 466 | 507 | 552 | 593 | 632 | 664 | 689 | 715 | 748 | 783 |
| $N_{\text{V}}$ | 393 | 419 | 442 | 480 | 524 | 563 | 601 | 631 | 654 | 679 | 708 | 739 |
| $N_{\text{VI}}$ | 131 | 146 | 165 | 194 | 230 | 261 | 292 | 314 | 330 | 347 | 368 | 391 |
| $N_{\text{VII}}$ | 127 | 140 | 159 | 190 | 225 | 256 | 286 | 308 | 322 | 338 | 359 | 382 |
| $O_{\text{I}}$ | 142 | 151 | 160 | 180 | 199 | 218 | 237 | 256 | 274 | 292 | 311 | 328 |
| $O_{\text{II}}$ | 83 | 88 | 121 | 140 | 159 | 177 | 194 | 210 | 224 | 237 | 248 | 258 |
| $O_{\text{III}}$ | | | 96 | 110 | 125 | 138 | 151 | 161 | 171 | 179 | 187 | 193 |
| $O_{\text{IV, V}}$ | 20 | 25 | 28 | 38 | 49 | 60 | 68 | 76 | 84 | 91 | 97 | 102 |
| $P_{\text{I}}$ | — | — | — | — | — | — | — | — | — | — | — | — |
| $P_{\text{II, III}}$ | 6 | 7 | 8 | 9 | 10 | 11 | 12 | 13 | 14 | 14 | 16 | 17 |
| $Q_{\text{I}}$ | — | — | — | — | — | — | — | 5 | — | — | — | — |
| Possible Errors: | | | | | | | | | | | | |
| $K$-level | 80 | 80 | 80 | 150 | 150 | 150 | 150 | 150 | 150 | 150 | 150 | 150 |
| Other levels | 11 | 11 | 11 | 13 | 13 | 13 | 13 | 13 | 13 | 11 | 13 | 11 |

data of Sandström and of Lindberg.[7] The results are such as to support the terms and limits of error in Table I.

In conclusion, the accuracy of Table I is more than sufficient for our present purpose, the calculation of gamma-ray energies from beta-ray energies; the controlling error is in the beta-ray measurements.

## 2. Application of the New Terms to the Beta-Rays of Th (B+C), Ra (B+C) and Ac (B+C)

All published data on beta-ray spectra have been reviewed to determine what changes are necessary in the light of the data in Table I. In the compilation by Rutherford, Chadwick and Ellis,[8] the data on Ra B, Ra C, Th B, Th C and Th C″ are superseded by Ellis' later and more accurate work, and those on Ac (B+C) by the work of Graf and Sze.[9] For all other elements listed, no x-ray term requires a change greater than 200 electron volts.

Ellis estimates that his energy values for the beta-rays of Ra(B+C) and Th(B+C) are correct to about one part in five hundred, and that relative values may be relied on to one part in two thousand. In his paper on Th(B+C), he used x-ray levels which agree well with ours, except that the $K$-levels for atomic numbers 82 and 83 are both low by 280 volts. Therefore, the gamma-ray energies which he computed from beta-rays ejected from the $K$-level are appreciably lower than those obtained from beta-rays arising in other levels. In a later paper on Ra(B+C) and Th(C+C′), Ellis adopted values for the levels of element 83 which agree excellently with ours. For element 84 (transition Ra C·C′), there is good agreement except that Ellis' $K$-level is 160 volts higher than ours. Graf's data on beta-rays of Ac B·C and Ac C·C″ arising from the $K$-shell are also in need of slight revision. Table I yields the revised gamma-ray energies in Table II, some values from $L_{\text{I}}$-conversion being included for comparison.

[7] Sandström, Zeits. f. Physik **65**, 632, **66**, 784 (1930); Lindberg, Nova Acta Regiae Soc. Sci. Upsaliensis, Series IV, **7**, No. 7 (1931).

[8] Rutherford, Chadwick and Ellis, *Radiations from Radioactive Substances*, p. 359 ff.

[9] Th (B+C): Ellis, Proc. Roy. Soc. **A138**, 318 (1932); Ra (B+C) and Th (C+C′): Ellis, Proc. Roy. Soc. **A143**, 350 (1934); Ac (B+C): Graf, Comptes rendus **197**, 238 (1933); Th (B+C), Ac (B+C): Sze, Ann. de Physique **19**, 59 (1933).

TABLE II. *Gamma-ray energies in electron volts,* $\times 10^{-5}$.

| Author | Source | Level in which gamma-ray is converted: $K$ | $L_I$ |
|---|---|---|---|
| Ellis | Th B·C | 2.3794 | 2.3805 |
| | " | 2.9920 | 2.9915 |
| | Th C″·D | 2.7646 | 2.7669 |
| | " | 5.0976 | 5.1000 |
| | " | 5.8195 | 5.8241 |
| | Ra C·C′ | 6.0662 | 6.0679 |
| | " | 7.6629 | —— |
| | " | 9.3333 | —— |
| Graf | Ac B·C | 4.0255 | 4.0233 |
| | " | 4.2453 | 4.2457 |
| | " | 8.2699 | —— |
| | Ac C·C″ | 3.4907 | 3.4875 |

### 3. Composite Photoelectric Effect in Ra(B+C), Th(B+C), Rd Ac and Ac X

Ellis[10] has shown that certain beta-ray lines having energies lying in the region 57,000 to 74,000 electron volts are common to the spectra of Ra(B+C) and Th(B+C) and that all of these arise from processes occurring in the planetary shells of atoms of atomic number 83. Thus, if a gamma-ray ejects a $K$-electron from an atom of Ra C(83), this atom may undergo an Auger process, in which, for example, an $L_I$-electron falls into the vacant place in the $K$-shell, and a second electron is ejected from the $L$-shell. The kinetic energy, $T$, of the latter electron will be given by

$$T=(K-L_I)-L^*, \qquad (1)$$

where $L^*$ is the energy required to remove it from an atom which already lacks an $L_I$ electron.

Hahn and Meitner have suggested that certain lines in the beta-ray spectra of Rd Ac and Ac X arise from Auger processes, and in Black's[11] measurements for Ms $Th_2$ there are unclassified lines lying in the region where Auger lines may be expected. To test Hahn and Meitner's classifications, and to come to some conclusion regarding Black's lines, it is necessary to know what values to use for the energy levels of an atom which lacks two $L$ electrons, or an $L$ and an $M$ electron. We shall now obtain this information empirically from Ellis' data on Auger lines of the elements 83 and 84.

Altogether, there are 10 terms arising from the configurations $2p^6$, $2s2p^5$ and $2s^22p^4$ of the doubly ionized $L$-shell. We could not find any computations of the positions of these terms, or of the transition probabilities for Auger processes involving them. However, as a working hypothesis, it is reasonable to assume the energies of all these final states are such, that for an atom of atomic number $Z$ the values of $L^*$ lie close to the $L$-levels of the atom of number $Z+1$. Let us call the latter levels $L_I'$, $L_{II}'$, $L_{III}'$. On this simple view, we expect beta-rays having the energies:

$$\begin{aligned} &K-L_{III}-L_{III}', \quad K-L_{III}-L_{II}', \quad K-L_{III}-L_I', \\ &K-L_{II}-L_{III}', \quad K-L_{II}-L_{II}', \quad K-L_{II}-L_I', \\ &K-L_I-L_{III}', \quad K-L_I-L_{II}', \quad K-L_I-L_I'. \end{aligned} \qquad (2)$$

As a matter of fact, Ellis found that the group consists of five lines in the case of the elements 83 and 84. He recognized that the removal of an $L$-electron increases the ionization energy of the others, but in his computations he did not use the above assumption concerning the energies. Instead, he compared the observed energies of Auger-process electrons with those given by the

TABLE III. *Energies of Auger beta-rays in volts.*

| Transition | Atomic Number 83 Calc. | Atomic Number 83 Obs. | Atomic Number 84 Calc. | Atomic Number 84 Obs. |
|---|---|---|---|---|
| $K-L_{III}-L_{III}'$ | 63100 | 62960 | 64860 | 64890 |
| $K-L_{II}-L_{III}'$ | 60820 | | 62440 | |
| $K-L_{III}-L_{II}'$ | 60680 | 60660 | 62300 | 62370 |
| $K-L_I-L_{III}'$ | 60140 | | 61750 | |
| $K-L_{III}-L_I'$ | 59990 | 59980 | 61590 | 61630 |
| $K-L_{II}-L_{II}'$ | 58390 | —— | 59870 | —— |
| $K-L_I-L_{II}'$ | 57710 | 57700 | 59180 | 59250 |
| $K-L_{II}-L_I'$ | 57700 | | 59170 | |
| $K-L_I-L_I'$ | 57030 | 56950 | 58480 | 58490 |
| $K-L_{III}-M_{III}'$ | 73600 | 73470 | | |
| $K-L_I-N_I'$ | 72930 | 72850 | | |
| $K-L_{II}-M_{III}'$ | 71310 | 71080 | | |
| $K-L_I-M_{III}'$ | 70640 | 70250 | | |
| $K-L_I-M_{II}'$ | 70080 | 69850 | | |

[10] Ellis, Proc. Roy. Soc. **A139**, 336 (1933).
[11] Hahn and Meitner, Zeits. f. Physik **34**, 795, 807 (1925); Black, Proc. Roy. Soc. **A106**, 632 (1924).

expressions $(K-L_1)-L_1$, etc. Naturally there were systematic deviations of considerable magnitude between calculated and observed values. It is now of interest to see how the energies given in the list (2) compare with the observed energies of his lines. The upper portion of Table III shows the results.

The discrepancies between the observed values and the calculated values opposite them are within the combined error of the $K$-levels in Table I and of Ellis' measurements. As an empirical regularity, this is interesting, but the absence of a line having the energy $K-L_{II}-L_{II}'$ reveals the weakness of this simple correlation of lines and calculated energies. It is quite probable that the coupling in the doubly ionized $L$-shell is such that all the possible lines lie in the neighborhoods of the five observed lines.

The lower portion of Table III shows similar regularities for lines of element 83, of the type $(K-L)-M'$. The transitions listed are those employed by Ellis. It is possible to achieve better agreement by choosing other levels, but, since a theory of these levels is not available, discussion of such details is not profitable.

It is fair to conclude that the positions of the Auger lines $K-L-L'$ in other beta-ray spectra can be computed within about 100 volts from the transitions written opposite the observed values in Table III. Thus *the Auger lines may serve as convenient standards in determining the energies of neighboring beta-ray lines.*

We may now consider the Auger lines of Rd Ac, Ac X, and Ms $Th_2$. Hahn and Meitner classified four lines of Rd Ac·Ac X, and two of Ac X·An, as due to Auger processes. There are unclassified lines near by, and so we have reexamined the matter. The question of reference lines must first be considered. Ellis has given the value $Hr = 1385.8$ gauss cm for the strongest line of Th B, used as a reference line by Hahn and Meitner, and has remeasured the lines of Ra(B+C) which Black employed as standards. Throughout this paper, $Hr$- and energy-values have been slightly changed to take advantage of Ellis' new values for the reference lines. Table IV shows the recomputed data for all lines of Rd Ac, Ac X and Ms $Th_2$ lying in the region of interest. The limits of the expected $K-L-L'$ and $K-L-M'$ groups are indicated, and the interpretations of Hahn and Meitner and of Black are indicated. The uncertainty in the energies may be estimated as one percent, and on this basis, we may draw the following conclusions:

TABLE IV. *Portions of the beta-ray spectra of Rd Ac, Ac X and Ms $Th_2$.*

| Substance | Number of line | Intensity | $Hr$, (gauss cm) | Energy of $\beta$-ray, (e.v.) | Original interpretation | Limits of Auger groups, (e.v.) |
|---|---|---|---|---|---|---|
| Rd Ac | 22 | 20 | 876 | 63600 | $K-L_{II}-L_I'$, | 64700–72400 |
| | 23 | 20 | 913 | 68700 | $K-L_{III}-L_I'$ | |
| | 24 | 20 | 952 | 74300 | | |
| | 25 | 15 | 983 | 78900 | $K-L_{II}-M_I'$ | |
| | 26 | 40 | 997 | 81100 | $h\nu-L_I$ | 79500–85000 |
| | 27 | 20 | 1011 | 83100 | $K-L_{III}-M_I'$ | |
| | 28 | 50 | 1076 | 93300 | $h\nu-K$ | |
| Ac X | 5 | 40 | 846 | 59500 | $h\nu-K$ | |
| Hahn-Meitner | 6 | 15 | 901 | 67000 | $K-L_{III}-L_I'$ | 61500–68600 |
| | 7 | 10 | 984 | 79000 | $K-L_{III}-M_I'$ | 75500–80600 |
| | 8 | 10 | 1001 | 81600 | | |
| Ms $Th_1$ | 7 | 16 | 901 | 67000 | | 68000–76500 |
| Black | 8 | 50 | 947 | 73600 | $h\nu-K$ | |
| | 9 | 35 | 976 | 77800 | | 83700–89800 |
| | 10 | 16 | 1070 | 92400 | | |

(1) The Auger groups are not completely resolved in the spectra of Rd Ac and Ac X. The lines assigned to such processes by Hahn and Meitner may indeed be Auger lines, but the possibility still exists that beta-rays ejected by nuclear gamma-rays practically coincide with them.

(2) The following unclassified beta-rays lying near the Auger groups are produced by nuclear gamma-rays:

Rd Ac 74,300 electron volts
Ms $Th_2$ 92,400 and possibly 77,800 electron volts.

## 4. THE BETA AND GAMMA-RAYS OF PROTACTINIUM

In the beta-ray spectrum of protactinium, Meitner[12] measured twelve rays, noted the existence of many others too faint to measure, and showed that nine of the twelve are due to conversion of three gamma-rays in the $K$, $L$ and $M$-shells. In Table V we give corrected energies,[13] based on the value $Hr = 1385.8$ gauss cm for the strong Th B line, instead of the value 1398 employed by Meitner.

The three lines which Meitner left unclassified are 92,030, 240,800 and 252,700 electron volts. Of these, the first can be explained as due to conversion of the gamma-ray 93,500 electron

[12] Meitner, Zeits. f. Physik **50**, 15 (1928).
[13] These data supersede slightly different ones in a preliminary note, Bull. Am. Phys. Soc. **9**, No. 1, 1934.

TABLE V. *Beta-ray spectrum of protactinium.*

| Number of line | Intensity | Origin | $Hr$, (gauss cm) | Energy of $\beta$-ray, e.v. | X-ray level, e.v. | Energy of $\gamma$-ray, e.v. |
|---|---|---|---|---|---|---|
| 1 | 60 | $L_1$ | 948 | 73720 | 19810 | 93530 |
| 2 | 40 | $L_{III}$? | 971 | 77220 | 15840 | 93060? |
| 3 | 40 | $M_1$ | 1046 | 88580 | 5000 | 93580 |
| 4 | 30 | $N_1$ | 1068 | 92030 | 1280 | 93310 |
| 5 | 100 | $K$ | 1581 | 186100 | 106600 | 292700 |
| 6 | 70 | $K$ | 1721 | 215300 | 106600 | 321900 |
| 7 | 30 | $K$ | 1839 | 240800 | 106600 | 347400 |
| 8 | 30 | $K$ | 1892 | 252700 | 106600 | 359300 |
| 9 | 60 | $L_1$ | 1968 | 269600 | 19810 | 289400 |
| 10 | 30 | $M_1$ | 2021 | 281900 | 5000 | 286900 |
| 11 | 40 | $L_1$ | 2085 | 296500 | 19810 | 316300 |
| 12 | 20 | $M_1$ | 2154 | 312700 | 5000 | 317700 |

volts in the $N_I$ shell, the intensity being of the right order of magnitude. The beta-ray 77,220 electron volts is stronger relative to the ray 73,720 electron volts than it should be if its classification is correct, and it is probable that this line is due, at least partially, to $K$ or $L_I$ conversion of a gamma-ray hitherto unknown.

The beta-rays 7 and 8 are due to conversion in the $K$-level, for if they came from any other shell, the corresponding $K$-conversion lines would lie in a large gap in the spectrum and would be so strong they could not have escaped notice. On this basis, we have two new gamma-rays at 347,400 and 359,300 electron volts. Beta-rays due to their conversion in the $L$, $M$, etc., shells would be weak, and inspection of a photograph published by Meitner encourages the belief that they would be too faint to measure. Thus, the measured lines are completely accounted for, with the possible exception of line 2, and the gamma-ray spectrum contains the following lines: 93,500, 289,700, 318,600, 347,400, 359,300 electron volts.

## 5. Beta-Ray Spectrum of Rd Th

Aided by the considerations in Section 3, we can decide between two alternative interpretations of the beta-ray spectra of Rd Th and $UX_1$. The beta-ray spectrum of Rd Th, measured by Meitner[14] and corrected for change of the Th B standard, is shown in Table VI, the uncertainty in energy associated with error in measuring line positions being less than one percent.

The lines 1 and 2 represent $K$ or $L_I$ conversion of two weak nuclear gamma-rays. The lines 3–6 are produced by two radiations of energies

[14] Meitner, Zeits. f. Physik **52**, 637, 645 (1928).

TABLE VI. *Rd Th beta-ray spectrum.*

| Number of line | Intensity | Origin | $Hr$ | Energy of $\beta$-ray, e.v. | X-ray level, e.v. | Energy of $\gamma$-ray, e.v. |
|---|---|---|---|---|---|---|
| 1 | w | — | 799 | 53390 | 103700, or 19210 | 157100, or 72600 |
| 2 | w | — | 820 | 56070 | 103700, or 19210 | 159800, or 75280 |
| 3 | s | $L_1$ | 883 | 64580 | 19210 | 83790 |
| 4 | m.s. | $L_1$ | 903 | 67340 | 19210 | 86550 |
| 5 | m.s. | $M_1$ | 979 | 78410 | 4830 | 83240 |
| 6 | m | $M_1$ | 1001 | 81690 | 4830 | 86520 |

83,520 and 86,530 electron volts, which lie in the neighborhood of $K\alpha_2$ and $K\alpha_1$ of the daughter element, 88, at 85,240 and 88,270 electron volts. This led Meitner to the hypothesis that these lines are produced in Auger processes, but she recognized that this interpretation leads to difficulties as follows.

She obtained a microphotometer record of a plate which contained both the lines of Rd Th and the strongest line of Th B. The number of electrons in the latter line, per 100 disintegrations, was determined by Gurney. Meitner compared the blackening due to this line with that due to the lines 3, 4, 5 and 6 of Rd Th, and assuming that the photographic effect of these beta-rays varies inversely as their energy, she found that the four lines together contain 0.072 electron per disintegration. She then assumed that the efficiency of internal conversion of the $K$-radiation is at the most 10 to 15 percent and concluded that in a very large percentage of the disintegrations the alpha-particles eject a $K$-electron from the planetary shells. This appeared very improbable to Meitner and she left the question open, but later, Rosenblum and Chamié[15] studied the alpha-particle spectrum of Rd Th and found by visual estimate that about 17 percent of the alpha-particles are emitted with an energy 88 electron kilovolts less than that of the normal group. This observation means that in 17 percent of the disintegrations the daughter nucleus is left in an excited state of 88 electron kilovolts energy, for this energy is not sufficient to ionize the $K$-shell of the daughter element. Accordingly, Meitner and Philipp[16] concluded that the lines 3–6 are due to nuclear gamma-rays. We shall

[15] Rosenblum and Chamié, Comptes rendus **196**, 1663 (1933).

[16] Meitner and Philipp, Zeits. f. Physik **80**, 277 (1933).

present other evidence in support of this interpretation.

(1) Other alpha-disintegrations are known in which the alpha-particles do not appreciably excite the $K$-radiation. Radium, for example, emits 0.35 quanta of $K$-radiation per 100 decomposing atoms,[17] and Bothe and Fränz[18] showed that alpha-particles entering heavy atoms from the *outside* produce less than one x-ray photon per 100 incident particles.

(2) The intensities of the lines 3 and 4 can be roughly accounted for on the assumption they are due to internal conversion of the two gamma-rays in the $L_{\mathrm{I}}$-shell. (The contribution of the $L_{\mathrm{II}}$ and $L_{\mathrm{III}}$ shells is of no importance.) It appears that Meitner's figures for the number of electrons in these lines should be revised. We find from her microphotometer curve and from a curve of Ellis,[19] giving the relative photographic efficiency of beta-rays as a function of velocity, that lines 3 and 4 contain about 11 electrons per hundred disintegrations, whereas in 17 percent of the disintegrations the nucleus is left in an excited state. Thus the efficiency of $L_1$ conversion is 65 percent, which may be compared with approximate theoretical values[20] of 35 percent for quadripole radiation and 23 percent for dipole radiation. The discrepancy can easily be due to inaccuracies in Ellis' photographic efficiency curve; in Rosenblum and Chamié's estimate of the relative intensities of the alpha-ray groups; and in Fisk's values.

(3) If Meitner's lines were due to Auger processes involving an excited $K$-shell, we should expect Auger groups of five lines each, similar to those found by Ellis. In Fig. 1A, the predicted positions of these groups are compared with those of the observed beta-rays, and the gamma-rays and $K$-lines are shown. There is no agreement; Meitner's published photograph of the spectrum and her microphotometer curve show clearly that the five-line Auger groups are not present. Further, Wentzel's[21] theory gives only 2 percent for the efficiency of internal conversion of the $K$-radiation of heavy elements, and this agrees roughly with the intensity found for Th B·C, which is about three percent.[22] Even if the $K$-shell of every disintegrating Rd Th atom were ionized, the Auger groups as a whole would have an intensity several times smaller than the lines 3 and 4 alone in Meitner's spectrum.

## 6. Beta and Gamma-Rays of $UX_1$ and $UX_2$

Meitner[23] found only three lines in the secondary beta-ray spectrum of $UX_1$, and interpreted them as $L$, $M$ and $N$ conversion of the $K\alpha$-lines of the daughter element, excited by the primary electrons. Ellis and Skinner[24] questioned this interpretation on the basis that the numerical agreement is not satisfactory, and stated that the beta-rays in question are produced by conversion of a nuclear gamma-ray of energy 91,900 electron volts, but, in the treatise of Rutherford, Chadwick and Ellis,[25] Meitner's interpretation is the only one mentioned, so the matter must be reexamined. Fig 1B shows the observed beta-

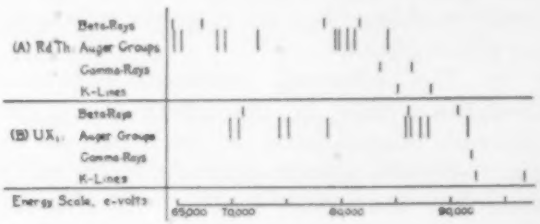


FIG. 1.

rays, the gamma-ray to which they lead, the $K$-lines, and the Auger groups to be expected. The following comments may be made.

(1) Meitner's published photograph of the spectrum and her energy values do not support the view that we are dealing with typical Auger groups containing five lines, like those found by Ellis.

(2) Meitner describes photographs obtained with the Rutherford (non-focussing) arrange-

[17] Stahel and Johner, J. de Physique **5**, 97 (1934).
[18] Bothe and Fränz, Zeits. f. Physik **52**, 466 (1928).
[19] Ellis, Proc. Roy. Soc. **A138**, 318 (1932).
[20] Fisk, Proc. Roy. Soc. **A143**, 674 (1934).
[21] Wentzel, Zeits. f. Physik **43**, 524 (1927).

[22] To obtain this figure, we added the measured photographic intensities of the Auger lines of Th B·C, and divided by the sum of the measured intensities of beta-rays ejected from the $K$-shell by nuclear gamma-rays. The quotient thus obtained is a rough measure of the ratio of the number of Auger processes to the number of atoms in which the $K$-shell is ionized. The failure to observe Auger lines in the Pa spectrum is easily explained by the smallness of the internal conversion coefficient for $K$-radiation.
[23] Meitner, Zeits. f. Physik **17**, 54 (1923).
[24] Ellis and Skinner, Proc. Roy. Soc. **A105**, 185 (1924).
[25] Reference 8, p. 360.

ment. The secondary beta-ray lines appear with considerable strength on plates which show the neighboring band of primary electrons, with its center of gravity at $Hr$ 1163 gauss cm. These lines, however, should be very weak if they are due to Auger processes. We know from experiments of Soddy and Russell[26] that the ratio of gamma-ray and beta-ray activities is about 18 times smaller for $UX_1+UX_2$ than for Ra(B+C), the measurements being made in such a way as to include all the soft rays possible. (The "gamma-ray activity" includes any x-rays which are emitted.) Kovarik[27] found that about two gamma-ray quanta are emitted by a source of Ra(B+C), for each disintegrating atom of Ra B. Roughly then, the efficiency of gamma-ray emission by $UX_1$ is less than 2/18 ray per disintegration; that is, if all its "gamma-rays" were really $K$-series x-rays, there would be about 0.1 quantum of $K$-radiation per disintegration, and since the efficiency of internal conversion of this radiation is about three percent (Section 5), there would be only 0.003 Auger-type beta-rays per disintegration.

(3) The following independent evidence strengthens that in the above paragraphs. Meitner's interpretation required that the primary electrons should copiously ionize the $K$-shell, but Bramson,[28] working with Meitner, found later that the primary electrons of Ra E excite only 0.01 quantum of $K$-radiation per disintegration. The much slower primaries of $UX_1$ should be less efficient in this respect, and so it appears there could not be more than $3\times10^{-4}$ Auger-type electrons per disintegration.

These facts show clearly that the *beta-ray lines of $UX_1$ are produced by internal conversion of a nuclear gamma-ray of energy about 91,900 electron volts.*

It is worth noting that an energy difference of about this magnitude appears rather frequently in connection with nuclear spectra. One of us (A.E.R.) has made a series of diagrams showing all known nuclear energy levels and gamma-rays of the heavy radioactive elements, and the energy difference 84 to 90 ekv is often encountered. This may be mere coincidence, or it may be that this energy difference will be found to possess a universal significance in the theory of nuclear energy levels, like that played by the spin-relativity doublet in the theory of x-ray spectra.

The beta and gamma-rays of $UX_2$ remain to be considered. It has been shown[29] that within the limits set by experimental difficulties, $UX_2$ is responsible for the hard beta and gamma-rays of $UX_1+UX_2$ in equilibrium. Von Baeyer, Hahn and Meitner[30] found the following beta-ray spectrum: Band, maximum at $Hr=2450$ gauss cm, or about 350 ekv. Band or group at $Hr=5800$ gauss cm, or about 1300 ekv. Sargent [31] presented indirect evidence, based on ionization measurements, that the energy distribution curve of the primaries has its maximum at $Hr=3600$ gauss cm, or slightly less than 700,000 electron volts, but did not discuss the discrepancy between this value and that for the above-mentioned bands. The lack of agreement is partially explained by the fact that the photographic efficiency of beta-rays falls off with increasing velocity. Using Ellis' curve of relative photographic efficiency and Sargent's energy distribution, it appears that the maximum photographic effect should lie at $Hr=3100$ gauss cm. Considering the difficulties involved, it is practically certain that Meitner's band at $Hr=2450$ gauss cm. represents the disintegration electrons of $UX_2$. If so, the group at 1300 ekv probably represents the secondary beta-rays.

This investigation is auxiliary to an experimental study of gamma-ray spectra, part of the facilities for which have been provided by the National Research Council. We wish to thank the Council for this aid.

[26] Soddy and Russell, Phil. Mag. **18**, 620 (1909).
[27] Kovarik, Phys. Rev. **23**, 559 (1924).
[28] Bramson, Zeits. f. Physik **66**, 721 (1930).
[29] Fajans and Göhring, Phys. Zeits. **14**, 877 (1913); Hahn and Meitner, Zeits. f. Physik **17**, 157 (1923).
[30] Von Baeyer, Hahn and Meitner, Phys. Zeits. **14**, 873 (1913).
[31] Sargent, Proc. Camb. Phil. Soc. **28**, 538 (1932).

# The Classification of the First Spark Spectrum of Lead: Pb II

LESTER T. EARLS AND RALPH A. SAWYER, *University of Michigan*

(Received November 22, 1934)

The spectrum of Pb II as excited in a Schüler hollow cathode discharge in helium has been photographed in the region from 800A to 10,000A. With these data the classification given by Fraülein H. Gieseler (Zeits. f. Physik **42**, 265 (1927)) has been corrected and extended. 247 lines have been classified, which locate 89 levels below the ionization level of the ion. These include the *s*, *p*, *d*, *f* and *g* series based on $6s^2$, extending to values of $n$ of from 14 to 19, and all levels of the other configurations which are expected below ionization. The assignment of these levels is checked by series considerations, by Zeeman effect data, by hyperfine structure data, by comparison with the similar spectra Ge II and Sn II, and by the agreement with the regular and irregular doublet laws in the isoelectronic sequence with Tl I and Bi III. The observed anomalous location of a number of the levels is shown to be explained qualitatively by the perturbations expected between the even levels.

MEASUREMENTS of the lead spectrum have been obtained by various experimenters, notably Eder and Valenta,[1] Exner and Haschek,[2] Thalén,[3] and Klein[4] in the visible and ultraviolet, Randall[5] in the infrared, and Carroll,[6] Lang,[7] and Arvidsson[8] in the vacuum region. The sources used in these investigations included arc in air and vacuum, spark in air and vacuum, and electrodeless discharge. The only important work on the classification of the Pb II spectrum was done by Fraülein H. Gieseler.[9] She photographed the ultraviolet and visible region of the emission from a Schüler hollow cathode tube and supplemented these data with vacuum region measurements by various workers. 72 lines were used to establish 36 levels, several of which appear to be erroneous in the light of the present investigation.

Theory predicts the level $6s^26p\ ^2P_{\frac{1}{2}}$ as the lowest state of singly ionized lead. Predicted excited states include the several series *ms*, *mp*, *md*, *mf*, ··· when both *6s* electrons remain unexcited; and, when one of these is raised to an excited state, configurations of the types $6s6p^2$, $6s6p6d$, $6s6d^2$, etc. By a consideration of the energy values in Pb III[11] corresponding to the excitation of a *6s* electron to *6p*, *6d*, etc., states, it becomes apparent that the levels from $6s6p6d$, $6s6d^2$, etc., lie considerably above the ionization potential of Pb II. The same is true of the possible configurations $6s6p7s$, etc., on the basis of a Ritzian formula calculation. This leaves only the $6s^2mx$ series and the $6s6p^2$ levels to be expected below ionization. The $6s6p^2$ configuration gives rise to the eight levels $^4P_{\frac{1}{2},\,1\frac{1}{2},\,2\frac{1}{2}}$, $^2D_{1\frac{1}{2},\,2\frac{1}{2}}$, $^2P_{\frac{1}{2},\,1\frac{1}{2}}$, and $^2S_{\frac{1}{2}}$ in Russell-Saunders notation, and of course to an equal number of levels in any coupling.

## EXPERIMENTAL

The excitation produced in a Schüler hollow cathode discharge in a rare gas atmosphere tends to be limited by the energy of the reactions between metal ions and metastable rare gas atoms, or between metal atoms and rare gas ions.[10] Since the ionization energy of Pb I is about 60,000 $cm^{-1}$ and that of Pb II about 120,000 $cm^{-1}$, it is evident that a discharge in helium (metastable state 160,000 $cm^{-1}$; ionization energy 198,000 $cm^{-1}$) should excite all levels of Pb II, but none of Pb III. Hence this arrangement was chosen as a source in the present investigation. Two mercury vapor pumps in series circulated helium through the discharge tube and suitable liquid air and charcoal traps. A high voltage direct-current generator served as a source of potential (700 to 1000 volts), but the ballast resistance in series with the discharge decreased considerably the effective voltage at the terminals of the tube. The current used was approximately 125 m.a. Cathodes of molybdenum and of iron

[1] Eder and Valenta, Wellenlängenmessungen, Wien, Ber. **119**, 519 (1910).
[2] Exner and Haschek, Wellenlängentabellen, Leipzig, 1904.
[3] Thalén, Nova acta reg. soc sc. Upsal. **3**, 6 (1868).
[4] Klein, Zeits. f. Wiss. Phot. **12**, 16 (1913).
[5] Randall, Astrophys. J. **34**, 1 (1911).
[6] Carroll, Trans. Roy. Soc. **A225**, 357 (1925).
[7] Lang, Trans. Roy. Soc. **A224**, 371 (1924).
[8] Arvidsson, Ann. d. Physik **12**, 787 (1932).
[9] Gieseler, Zeits. f. Physik **42**, 265 (1927).
[10] Sawyer, Phys. Rev. **36**, 44 (1930).

were used at different times. In each case a few of the strongest lines due to the cathode material showed in the emission. The lead (chemically pure) was laid within the cylindrical cathode in small pieces which promptly melted in the heat of the discharge. Photographs were taken under two conditions of discharge. In the first the discharge was started in the normal helium pressure. The inflow of helium was then almost completely shut off, and within a few seconds the pumps removed the helium to a point at which the discharge changed from a yellowish appearance to a deep blue. Under these conditions it appeared that the discharge was carried primarily by the lead vapor; the helium lines remained, but were considerably weakened. This method of operation gave a number of lines which are classified by Smith[11] as Pb III and Pb IV. The second condition of discharge involved the continued circulation of the helium throughout the time of the photograph; in this case the lines due to higher ionization were much weaker or entirely absent.

The spectrum was photographed from 800A to 10,000A. From 800A to 2400A a normal incidence concave grating vacuum spectrograph was used. This instrument[12] (1 m radius, 14,400 lines per inch) had a dispersion of about 17A/mm. Between 2100A and 5500A two Hilger quartz instruments were used (types E–1 and E–3), and from 5100A to 10,000A a spectrograph of design similar to the E–1, with glass optical system, was utilized. In the vacuum photographs He, Hg and H lines appeared as impurity lines and were used as standards. Iron arc comparison spectra were applied to all other photographs except those in the infrared, where a neon tube was used. In addition, plates from the first order of a 21-foot concave grating, covering the region 2200A to 10,000A, were kindly loaned by Dr. J. L. Rose, of New York University. The excitation for these photographs was also a hollow cathode discharge in helium. All plates were measured on a Gaertner comparator. The calculated wavelengths in air were reduced to wave numbers by means of Kayser's table. For wavelengths greater than 2100A the wave number values are probably correct to about one wave per centimeter; for shorter wavelengths the error may be as high as 10 or 15 $cm^{-1}$, especially for weak lines.

[11] Smith, Phys. Rev. **34**, 393 (1926); **36**, 1 (1930).
[12] Sawyer, J. O. S. A. **15**, 307 (1927).

## Data and Classification

The above experimental work provided 340 lines in the vacuum region ($\nu$185,000 to $\nu$47,000) and about 730 lines in the region from $\nu$47,000 to $\nu$10,000. About 60 of the strongest of these lines have been classified by Gieseler and Grotrian[13] in Pb I, and a smaller number by Smith[11] and others in Pb III or Pb IV. The 247 lines now classified in Pb II are listed in Table I. Fourteen of these lines, lying in the vacuum region, were also observed by Arvidsson.[8] His measurements, which are more accurate than is claimed for the vacuum data of the present work, are included in Table I and used for the location of the $6p\,^2P$ levels. The classified lines determine 89 levels; these are tabulated in Table II, with their effective quantum numbers in the case of series members. It will be noted that the effective quantum numbers of the two odd series $6s^2mp\,^2P$ and $6s^2mf\,^2F$ are very regular as they approach a limiting value for large $m$, though all $^2F$ members are inverted. The even series $6s^2mg\,^2G$ is also regular; its doublets are unresolved. The other two even series $6s^2ms\,^2S$ and $6s^2md\,^2D$ show pronounced irregularities in the lower members; these irregularities are explained below in terms of perturbations from the intermingling levels from the $6s6p^2$ configuration.

In determining the ionization potential of Pb II, use has been made of the series limits of the $^2F$ and $^2G$ series; these limits are located to within less than 1 $cm^{-1}$. Thus the value of the ionization potential (121,243 $cm^{-1}$) is determined within the error involved in the vacuum data on transitions to the lowest term $6s^26p\,^2P_{\frac{1}{2}}$. By using Arvidsson's data[8] for these lines (for which his estimate of probable error is 2 or 3 $cm^{-1}$), the ionization potential is correct to 2 or 3 $cm^{-1}$. The location of the next series, $6s^2mh\,^2H$, could be predicted very closely, but transitions from the low members were out of experimental range, and those from the higher members were not observed.

Comparison of the Pb II spectrum with the similar spectra of Ge II[14] and Sn II[14] has been

[13] Gieseler and Grotrian, Zeits. f. Physik **39**, 377 (1926).
[14] Bacher and Goudsmit, *Atomic Energy States* (1932).

TABLE I. *Classified lines in Pb II.*

| Classification | λ(A) | ν(cm⁻¹) | Intensity | Δν | Notes |
|---|---|---|---|---|---|
| $7D_{1\frac{1}{2}} - 9P_{\frac{1}{2}}$ | 9864.2 | 10139 | 00 | −1 | |
| $5G \quad - 9F_{2\frac{1}{2}}$ | 9440.1 | 10593 | 1 | −2 | |
| $5F_{2\frac{1}{2}} - 5G$ | 9063.7 | 11030 | 10 | 0 | $x\,h_0$ |
| $5F_{3\frac{1}{2}} - 5G$ | 9050.7 | 11045 | 10 | 0 | $x\,h_0$ |
| $8D_{3\frac{1}{2}} - 10F_{3\frac{1}{2}}$ | 8723.1 | 11461 | 3 | 2 | |
| $9P_{1\frac{1}{2}} - 12D_{1\frac{1}{2}}$ | 8721.3 | 11463 | 0 | 0 | |
| $6F_{2\frac{1}{2}} - 8G$ | 8719.7 | 11465 | 5 | 0 | $h_0$ |
| $6F_{3\frac{1}{2}} - 8G$ | 8710.1 | 11478 | 7 | 0 | $h_0$ |
| $8P_{1\frac{1}{2}} - 10S_{\frac{1}{2}}$ | 8550.6 | 11692 | 2 | 0 | |
| $7P_{1\frac{1}{2}} - p^2\,{}^2D_{2\frac{1}{2}}$ | 8545.0 | 11699 | 7 | 1 | $h_6$ |
| $7P_{1\frac{1}{2}} - 8S_{\frac{1}{2}}$ | 8395.6 | 11908 | 10 | 0 | $h_{12}$ |
| $p^2\,{}^2D_{1\frac{1}{2}} - 8P_{\frac{1}{2}}$ | 8335.0 | 11994 | 6 | 1 | $h_7$ |
| $8D_{1\frac{1}{2}} - 10F_{2\frac{1}{2}}$ | 8152.0 | 12263 | 0 | 0 | |
| $9P_{\frac{1}{2}} - 13D_{1\frac{1}{2}}$ | 8013.0 | 12476 | 00 | 1 | |
| $8D_{2\frac{1}{2}} - 11F_{3\frac{1}{2}}$ | 7973.2 | 12538 | 00 | 0 | |
| $9P_{1\frac{1}{2}} - 14D_{2\frac{1}{2}}$ | 7906.8 | 12644 | 0 | 2 | |
| $8P_{\frac{1}{2}} - 10S_{\frac{1}{2}}$ | 7777.8 | 12853 | 2 | 0 | |
| $6F_{2\frac{1}{2}} - 9G$ | 7739.8 | 12916 | 2 | 0 | $h_0$ |
| $6F_{3\frac{1}{2}} - 9G$ | 7732.3 | 12930 | 4 | −1 | $h_0$ |
| $8P_{1\frac{1}{2}} - 9D_{1\frac{1}{2}}$ | 7679.4 | 13018 | 1 | 1 | |
| $6F_{3\frac{1}{2}} - 12D_{3\frac{1}{2}}$ | 7664.8 | 13043 | 0 | 1 | |
| $8P_{1\frac{1}{2}} - 9D_{2\frac{1}{2}}$ | 7632.2 | 13098 | 10 | 0 | $h_0$ |
| $7D_{2\frac{1}{2}} - 7F_{3\frac{1}{2}}$ | 7558.7 | 13226 | 10 | −1 | $h_{12}$ |
| $7D_{3\frac{1}{2}} - 7F_{2\frac{1}{2}}$ | 7553.7 | 13234 | 1 | 0 | |
| $8D_{3\frac{1}{2}} - 12F_{3\frac{1}{2}}$ | 7499.6 | 13330 | 00 | 0 | |
| $p^2\,{}^2D_{2\frac{1}{2}} - 6F_{3\frac{1}{2}}$ | 7193.6 | 13897 | 20 | −1 | $h_6$ |
| $p^2\,{}^2D_{3\frac{1}{2}} - 6F_{3\frac{1}{2}}$ | 7187.1 | 13910 | 2 | −1 | |
| $6F_{3\frac{1}{2}} - 10G$ | 7165.1 | 13953 | 2 | −1 | $h_0$ |
| $6F_{2\frac{1}{2}} - 10G$ | 7158.7 | 13965 | 2 | 0 | $h_0$ |
| $6F_{3\frac{1}{2}} - 13D_{2\frac{1}{2}}$ | 7114.7 | 14051 | 0 | 1 | |
| $8P_{\frac{1}{2}} - 9D_{1\frac{1}{2}}$ | 7050.7 | 14179 | 9 | 1 | $h_0$ |
| $7D_{1\frac{1}{2}} - 7F_{2\frac{1}{2}}$ | 7013.2 | 14255 | 10 | −1 | $xxx\,h_0$ |
| $7D_{2\frac{1}{2}} - 10P_{1\frac{1}{2}}$ | 6872.0 | 14548 | 0 | −1 | |
| $6F_{2\frac{1}{2}} - 11G$ | 6791.7 | 14720 | 2 | −1 | $h_0$ |
| $7P_{\frac{1}{2}} - 8S_{\frac{1}{2}}$ | 6790.8 | 14722 | 10 | −1 | $h_{12}$ |
| $6F_{3\frac{1}{2}} - 11G$ | 6785.9 | 14732 | 3 | 0 | $h_0$ |
| $7S_{\frac{1}{2}} - 7P_{\frac{1}{2}}$ | 6660.0 | 15011 | 30 | 0 | $x\,h_0\,Z$ |
| $7D_{1\frac{1}{2}} - 10P_{\frac{1}{2}}$ | 6569.4 | 15218 | 5 | −2 | |
| $8S_{\frac{1}{2}} - 9P_{\frac{1}{2}}$ | 6558.7 | 15243 | 3 | −1 | |
| $6F_{2\frac{1}{2}} - 12G$ | 6533.1 | 15302 | 4 | 0 | $h_0$ |
| $6F_{3\frac{1}{2}} - 12G$ | 6527.8 | 15315 | 5 | 0 | $h_0$ |
| $8P_{1\frac{1}{2}} - 11S_{\frac{1}{2}}$ | 6518.2 | 15337 | 8 | −1 | $h_0$ |
| $7D_{1\frac{1}{2}} - 10P_{1\frac{1}{2}}$ | 6422.9 | 15565 | 0 | 2 | |
| $6F_{2\frac{1}{2}} - 13G$ | 6345.0 | 15756 | 5 | 0 | $h_0$ |
| $6F_{3\frac{1}{2}} - 13G$ | 6339.8 | 15769 | 3 | 0 | $h_0$ |
| $8S_{\frac{1}{2}} - 9P_{1\frac{1}{2}}$ | 6311.5 | 15840 | 9 | 0 | |
| $p^2\,{}^2D_{2\frac{1}{2}} - 9P_{1\frac{1}{2}}$ | 6229.7 | 16048 | 10 | 0 | $h_6$ |
| $6F_{2\frac{1}{2}} - 14G$ | 6203.7 | 16115 | 1*d* | 0 | $h_0$ |
| $6F_{3\frac{1}{2}} - 14G$ | 6198.8 | 16128 | 1*d* | 0 | $h_0$ |
| $8P_{1\frac{1}{2}} - 10D_{1\frac{1}{2}}$ | 6181.9 | 16172 | 7 | −1 | $h_0$ (*a*) |
| $8P_{1\frac{1}{2}} - 10D_{2\frac{1}{2}}$ | 6160.0 | 16229 | 10 | 0 | $h_0$ |
| $6F_{2\frac{1}{2}} - 15G$ | 6094.0 | 16405 | 0*d* | 0 | $h_0$ |
| $6F_{3\frac{1}{2}} - 15G$ | 6089.4 | 16418 | 1 | 0 | $h_0$ |
| $5F_{2\frac{1}{2}} - 6G$ | 6081.5 | 16439 | 40 | 0 | $x\,h_0$ |
| $5F_{3\frac{1}{2}} - 6G$ | 6075.8 | 16454 | 40 | 0 | $x\,h_0$ |
| $8P_{\frac{1}{2}} - 11S_{\frac{1}{2}}$ | | 16497 (calc.) | | | (*b*) |
| $p^2\,{}^4P_{\frac{1}{2}} - 7P_{\frac{1}{2}}$ | 6041.4 | 16548 | 8*d* | 0 | $h_7'$ |
| $7D_{3\frac{1}{2}} - 8F_{3\frac{1}{2}}$ | 6009.7 | 16635 | 9 | 1 | $h_{11}$ |
| $7D_{3\frac{1}{2}} - 8F_{2\frac{1}{2}}$ | 6007.5 | 16641 | 2 | 1 | |
| $7P_{1\frac{1}{2}} - 7D_{1\frac{1}{2}}$ | 5876.7 | 17011 | 10 | 1 | $xxx\,h_0\,Z$ (*c*) |
| $8P_{\frac{1}{2}} - 10D_{1\frac{1}{2}}$ | 5767.9 | 17333 | 10 | −1 | $h_0$ |
| $7D_{2\frac{1}{2}} - 11P_{1\frac{1}{2}}$ | 5713.8 | 17496 | 4 | 0 | |
| $7D_{1\frac{1}{2}} - 8F_{2\frac{1}{2}}$ | 5660.1 | 17663 | 2 | −1 | |
| $7S_{\frac{1}{2}} - 7P_{1\frac{1}{2}}$ | 5608.8 | 17824 | 10 | 0 | $x\,h_0\,Z$ |
| $7P_{1\frac{1}{2}} - 7D_{2\frac{1}{2}}$ | 5544.6 | 18031 | 10 | 1 | $h_{14}\,Z$ (*d*) |
| $8P_{1\frac{1}{2}} - 11D_{1\frac{1}{2}}$ | 5483 ? | 18230? | 000 | | |
| $8P_{1\frac{1}{2}} - 11D_{2\frac{1}{2}}$ | 5472.4 | 18268 | 7 | 1 | $xxx\,h_0$ |
| $p^2\,{}^4P_{2\frac{1}{2}} - 5F_{3\frac{1}{2}}$ | 5372.1 | 18608 | 10 | 1 | $xx\,h_1\,Z$ |
| $p^2\,{}^4P_{3\frac{1}{2}} - 5F_{2\frac{1}{2}}$ | 5367.3 | 18624 | 10 | 0 | $xx\,h_1$ |
| $8P_{\frac{1}{2}} - 12S_{\frac{1}{2}}$ | 5308.2 | 18834 | 3 | 1 | $h_0$ |
| $7D_{3\frac{1}{2}} - 9F_{3\frac{1}{2}}$ | 5306.8 | 18839 | 6 | 2 | $h_{12}$ |
| $8P_{1\frac{1}{2}} - 13S_{\frac{1}{2}}$ | 5191.4 | 19257 | 1 | 1 | |
| $p^2\,{}^4P_{\frac{1}{2}} - 7P_{1\frac{1}{2}}$ | 5163.8 | 19360 | 7 | 1 | $h_7'$ (*e*) |
| $8P_{\frac{1}{2}} - 11D_{1\frac{1}{2}}$ | 5155.8 | 19390 | 7 | −1 | $h_0$ |
| $p^2\,{}^2D_{3\frac{1}{2}} - 7F_{3\frac{1}{2}}$ | 5111.9 | 19557 | 10 | 0 | $h_6$ |
| $p^2\,{}^2D_{2\frac{1}{2}} - 7F_{3\frac{1}{2}}$ | 5109.6 | 19566 | 3 | 0 | $h_6$ |
| $8P_{1\frac{1}{2}} - 12D_{1\frac{1}{2}}$ | | 19647 (calc.) | | | (*f*) |
| $8P_{1\frac{1}{2}} - 12D_{2\frac{1}{2}}$ | 5081.2 | 19675 | 3 | −1 | $h_0$ |
| $5F_{2\frac{1}{2}} - 7G$ | 5074.6 | 19700 | 10 | 1 | $x\,h_0$ |
| $5F_{3\frac{1}{2}} - 7G$ | 5070.7 | 19716 | 10 | 0 | $x\,h_0$ |
| $p^2\,{}^2D_{1\frac{1}{2}} - 6F_{2\frac{1}{2}}$ | 5049.3 | 19799 | 9 | −1 | $h_7$ |
| $7P_{\frac{1}{2}} - 7D_{1\frac{1}{2}}$ | 5042.5 | 19825 | 50 | 0 | $xxx\,h_0\,Z$ |
| $7D_{1\frac{1}{2}} - 9F_{2\frac{1}{2}}$ | 5032.2 | 19866 | 6 | 0 | |
| $7D_{1\frac{1}{2}} - 12P_{\frac{1}{2}}$ | 4924.9 | 20299 | 1 | 2 | |
| $8S_{\frac{1}{2}} - 10P_{\frac{1}{2}}$ | 4920.4 | 20318 | 1 | 2 | |
| $7D_{2\frac{1}{2}} - 10F_{3\frac{1}{2}}$ | 4912.7 | 20350 | 3 | −1 | $h_{12}$ |
| $8P_{\frac{1}{2}} - 13S_{\frac{1}{2}}$ | 4895.6 | 20421 | 2 | −2 | |
| $8P_{1\frac{1}{2}} - 13D_{1\frac{1}{2}}$ | 4838.6 | 20661 | 0 | 0 | |
| $8S_{\frac{1}{2}} - 10P_{1\frac{1}{2}}$ | 4836.3 | 20671 | 6 | 0 | |
| $8P_{1\frac{1}{2}} - 13D_{2\frac{1}{2}}$ | 4833.7 | 20682 | 5 | 0 | $h_0$ |
| $8P_{\frac{1}{2}} - 12D_{1\frac{1}{2}}$ | 4804.5 | 20808 | 8 | 0 | $h_0$ |

| Classification | λ(A) | ν(cm⁻¹) | Intensity | Δν | Notes |
|---|---|---|---|---|---|
| $p^2\,{}^2D_{2\frac{1}{2}} - 10P_{1\frac{1}{2}}$ | 4788.1 | 20879 | 6 | 0 | $h_0$ |
| $p^2\,{}^2D_{3\frac{1}{2}} - 9P_{\frac{1}{2}}$ | 4684.9 | 21339 | 5 | 0 | $h_7$ |
| $7D_{1\frac{1}{2}} - 10F_{2\frac{1}{2}}$ | 4677.8 | 21372 | 7 | 1 | |
| $8P_{1\frac{1}{2}} - 14D_{1\frac{1}{2}}$ | 4668.9 | 21412 | 0 | 0 | |
| $7D_{2\frac{1}{2}} - 11F_{3\frac{1}{2}}$ | 4666.5 | 21423 | 1 | 1 | |
| $8P_{1\frac{1}{2}} - 14D_{2\frac{1}{2}}$ | 4665.5 | 21428 | 5 | 0 | $h_0$ |
| $5F_{2\frac{1}{2}} - 8G$ | 4582.3 | 21817 | 10 | 0 | $x\,h_0$ |
| $8P_{\frac{1}{2}} - 13D_{1\frac{1}{2}}$ | 4581.3 | 21822 | 4 | 0 | $h_0$ |
| $5F_{3\frac{1}{2}} - 8G$ | 4579.1 | 21832 | 10 | 0 | $x\,h_0$ |
| $p^2\,{}^2D_{1\frac{1}{2}} - 9P_{1\frac{1}{2}}$ | 4557.2 | 21937 | 2 | 0 | $h_7$ |
| $8P_{1\frac{1}{2}} - 15D_{2\frac{1}{2}}$ | 4544.8 | 21997 | 4 | 0 | $h_0$ |
| $7D_{2\frac{1}{2}} - 12F_{3\frac{1}{2}}$ | 4499.6 | 22218 | 0 | −2 | |
| $p^2\,{}^4P_{2\frac{1}{2}} - 8P_{1\frac{1}{2}}$ | 4476.3 | 22334 | 3 | −1 | $h_{11}$ |
| $8P_{1\frac{1}{2}} - 16D_{2\frac{1}{2}}$ | 4454.9 | 22441 | 1 | 0 | $h_0$ |
| $7D_{1\frac{1}{2}} - 11F_{2\frac{1}{2}}$ | 4453.8 | 22446 | 3 | 0 | |
| $8P_{\frac{1}{2}} - 14D_{1\frac{1}{2}}$ | 4428.7 | 22574 | 2 | −1 | $h_0$ |
| $6D_{1\frac{1}{2}} - 5F_{2\frac{1}{2}}$ | 4386.4 | 22791 | 20 | −2 | $x\,h_4\,Z$ |
| $8P_{1\frac{1}{2}} - 17D_{2\frac{1}{2}}$ | 4386.0 | 22793 | 2 | 0 | |
| $p^2\,{}^2D_{2\frac{1}{2}} - 8F_{3\frac{1}{2}}$ | 4352.7 | 22968 | 10 | 0 | $h_6$ |
| $p^2\,{}^2D_{3\frac{1}{2}} - 8F_{2\frac{1}{2}}$ | 4351.5 | 22974 | 3 | 0 | |
| $8P_{1\frac{1}{2}} - 18D_{2\frac{1}{2}}$ | 4332.2 | 23077 | 0 | 0 | |
| $8P_{\frac{1}{2}} - 15D_{1\frac{1}{2}}$ | 4319.2 | 23146 | 1 | 0 | $h_0$ |
| $7D_{1\frac{1}{2}} - 12F_{2\frac{1}{2}}$ | 4302.1 | 23238 | 1 | 0 | |
| $5F_{2\frac{1}{2}} - 9G$ | 4296.6 | 23268 | 6 | 0 | $x\,h_0$ |
| $5F_{3\frac{1}{2}} - 9G$ | 4293.8 | 23283 | 7 | 0 | $x\,h_0$ |
| $8P_{1\frac{1}{2}} - 19D_{2\frac{1}{2}}$ | 4288.9 | 23310 | 00 | 0 | |
| $8S_{\frac{1}{2}} - 11P_{\frac{1}{2}}$ | 4272.5 | 23399 | 3 | −1 | (*g*) |
| $6D_{2\frac{1}{2}} - 5F_{3\frac{1}{2}}$ | 4245.1 | 23550 | 20 | 0 | $x\,h_2\,Z$ |
| $6D_{3\frac{1}{2}} - 5F_{2\frac{1}{2}}$ | 4242.5 | 23565 | 9 | 0 | $x\,h_2\,Z$ |
| $8P_{\frac{1}{2}} - 16D_{1\frac{1}{2}}$ | 4237.6 | 23591 | 0 | 0 | $h_0$ |
| $8S_{\frac{1}{2}} - 11P_{1\frac{1}{2}}$ | 4232.4 | 23620 | 2 | 0 | |
| $p^2\,{}^2D_{2\frac{1}{2}} - 11P_{1\frac{1}{2}}$ | 4195.5 | 23828 | 3 | 0 | $h_6$ |
| $7D_{1\frac{1}{2}} - 13F_{2\frac{1}{2}}$ | 4193.7 | 23838 | 00 | 0 | |
| $8P_{\frac{1}{2}} - 17D_{1\frac{1}{2}}$ | 4175.0 | 23945 | 00 | 0 | |
| $7P_{1\frac{1}{2}} - 9S_{\frac{1}{2}}$ | 4152.8 | 24073 | 10 | 1 | $x\,h_0\,Z$ |
| $5F_{2\frac{1}{2}} - 10G$ | 4113.4 | 24304 | 4 | 0 | $x\,h_0$ |
| $5F_{3\frac{1}{2}} - 10G$ | 4110.8 | 24319 | 5 | 0 | $x\,h_0$ |
| $5F_{2\frac{1}{2}} - 11G$ | 3987.6 | 25070 | 2 | 1 | $x\,h_0$ |
| $5F_{3\frac{1}{2}} - 11G$ | 3985.2 | 25086 | 2 | 0 | $x\,h_0$ |
| $p^2\,{}^2D_{2\frac{1}{2}} - 9F_{3\frac{1}{2}}$ | 3971.3 | 25174 | 4 | −1 | $h_6$ |
| $p^2\,{}^2D_{1\frac{1}{2}} - 7F_{2\frac{1}{2}}$ | 3927.3 | 25456 | 6 | −1 | $h_7$ |
| $5F_{2\frac{1}{2}} - 12G$ | 3896.9 | 25654 | 0 | 0 | |
| $5F_{3\frac{1}{2}} - 12G$ | 3894.6 | 25669 | 1 | 0 | |
| $p^2\,{}^2D_{3\frac{1}{2}} - 12P_{1\frac{1}{2}}$ | 3880.5 | 25763 | 0 | 0 | |
| $5F_{2\frac{1}{2}} - 13G$ | 3829.2 | 26108 | 0 | 0 | |
| $7P_{1\frac{1}{2}} - 8D_{1\frac{1}{2}}$ | 3827.2 | 26121 | 3 | 1 | $h_{10}\,Z$ |
| $p^2\,{}^4P_{1\frac{1}{2}} - 5F_{2\frac{1}{2}}$ | 3785.9 | 26406 | 10 | −1 | $xx\,h_3\,Z$ |
| $p^2\,{}^2D_{1\frac{1}{2}} - 10P_{\frac{1}{2}}$ | 3784.0 | 26419 | 2 | −2 | |
| $6D_{1\frac{1}{2}} - 8P_{1\frac{1}{2}}$ | 3772.9 | 26497 | 00 | 1 | |
| $p^2\,{}^2D_{2\frac{1}{2}} - 10F_{3\frac{1}{2}}$ | 3746.9 | 26681 | 4 | 0 | $h_6$ |
| $p^2\,{}^2D_{1\frac{1}{2}} - 10P_{1\frac{1}{2}}$ | 3734.8 | 26767 | 2 | 1 | |
| $7P_{\frac{1}{2}} - 9S_{\frac{1}{2}}$ | 3718.2 | 26887 | 7 | 0 | $x\,h_0\,Z$ |
| $7P_{1\frac{1}{2}} - 8D_{2\frac{1}{2}}$ | 3714.0 | 26918 | 10 | 0 | $h_0\,Z$ |
| $7P_{1\frac{1}{2}} - p^2\,{}^2S_{\frac{1}{2}}$ | 3699.2 | 27025 | 2 | 0 | $h_{21}$ |
| $p^2\,{}^2D_{2\frac{1}{2}} - 13P_{1\frac{1}{2}}$ | 3689.0 | 27100 | 0 | 0 | (*i*) |
| $6D_{2\frac{1}{2}} - 8P_{1\frac{1}{2}}$ | 3665.6 | 27273 | 4 | 1 | $h_7$ |
| $7P_{1\frac{1}{2}} - p^2\,{}^2P_{1\frac{1}{2}}$ | 3649.0 | 27397 | 3 | 0 | $h_{11}$ |
| $p^2\,{}^2D_{2\frac{1}{2}} - 11F_{3\frac{1}{2}}$ | 3601.8 | 27756 | 3 | 0 | $h_6$ |
| $p^2\,{}^2D_{3\frac{1}{2}} - 12F_{3\frac{1}{2}}$ | 3501.9 | 28548 | 2 | 0 | $h_6$ |
| $p^2\,{}^2D_{1\frac{1}{2}} - 8F_{2\frac{1}{2}}$ | 3463.6 | 28863 | 6 | 0 | $h_7$ |
| $7P_{\frac{1}{2}} - 8D_{1\frac{1}{2}}$ | 3455.0 | 28935 | 8 | 0 | $h_{10}\,Z$ |
| $p^2\,{}^4P_{1\frac{1}{2}} - 8P_{\frac{1}{2}}$ | 3453.0 | 28952 | 0 | 1 | |
| $p^2\,{}^4P_{2\frac{1}{2}} - 6F_{3\frac{1}{2}}$ | 3451.7 | 28963 | 9 | 0 | $xx\,h_1\,Z$ |
| $p^2\,{}^4P_{3\frac{1}{2}} - 6F_{2\frac{1}{2}}$ | 3450.0 | 28976 | 2 | 0 | $xx\,h_1$ |
| $p^2\,{}^2D_{2\frac{1}{2}} - 13F_{3\frac{1}{2}}$ | 3429.6 | 29149 | 1 | 0 | |
| $p^2\,{}^2D_{1\frac{1}{2}} - 11P_{\frac{1}{2}}$ | 3389.4 | 29495 | 2 | 0 | $h_7$ |
| $p^2\,{}^2D_{2\frac{1}{2}} - 14F_{3\frac{1}{2}}$ | 3375.6 | 29616 | 00 | 0 | |
| $7P_{\frac{1}{2}} - p^2\,{}^2S_{\frac{1}{2}}$ | 3350.5 | 29838 | 00 | 0 | |
| $7P_{\frac{1}{2}} - p^2\,{}^2P_{1\frac{1}{2}}$ | 3309.2 | 30210 | 6 | 0 | $h_{11}$ |
| $7P_{1\frac{1}{2}} - 10S_{\frac{1}{2}}$ | 3261.0 | 30656 | 6 | 2 | $h_0$ |
| $p^2\,{}^2D_{1\frac{1}{2}} - 9F_{2\frac{1}{2}}$ | 3217.9 | 31067 | 3 | 0 | $h_7$ |
| $p^2\,{}^4P_{2\frac{1}{2}} - 9P_{1\frac{1}{2}}$ | 3213.0 | 31114 | 00 | 1 | |
| $p^2\,{}^2D_{1\frac{1}{2}} - 12P_{\frac{1}{2}}$ | 3173.5 | 31502 | 0 | 0 | |
| $7P_{1\frac{1}{2}} - 9D_{1\frac{1}{2}}$ | 3125.6 | 31985 | 6 | 0 | $h_0$ |
| $7P_{1\frac{1}{2}} - 9D_{2\frac{1}{2}}$ | 3117.7 | 32064 | 10 | 0 | $h_0$ |
| $p^2\,{}^2D_{1\frac{1}{2}} - 10F_{2\frac{1}{2}}$ | 3068.5? | 32574? | 2 | | $h_7$ (*j*) |
| $p^2\,{}^2D_{1\frac{1}{2}} - 13P_{\frac{1}{2}}$ | 3039.9 | 32886 | 00 | −2 | |
| $6D_{1\frac{1}{2}} - 6F_{2\frac{1}{2}}$ | 3016.4 | 33142 | 10 | −1 | $x\,h_4\,Z$ |
| $7P_{\frac{1}{2}} - 10S_{\frac{1}{2}}$ | 2986.9 | 33470 | 4 | 1 | $h_0$ |
| $p^2\,{}^2D_{1\frac{1}{2}} - 11F_{2\frac{1}{2}}$ | 2971.1 | 33647 | 0 | 0 | |
| $p^2\,{}^2D_{1\frac{1}{2}} - 14P_{\frac{1}{2}}$ | 2951.3 | 33873 | 00 | 2 | |
| $6D_{2\frac{1}{2}} - 6F_{3\frac{1}{2}}$ | 2948.5 | 33905 | 10 | −1 | $x\,h_2\,Z$ |
| $6D_{3\frac{1}{2}} - 6F_{2\frac{1}{2}}$ | 2947.5 | 33918 | 2 | −1 | $x\,h_2$ |
| $7P_{1\frac{1}{2}} - 11S_{\frac{1}{2}}$ | 2914.5 | 34302 | 3 | 0 | $h_0$ |
| $p^2\,{}^4P_{2\frac{1}{2}} - 7F_{3\frac{1}{2}}$ | 2887.3 | 34624 | 3 | 0 | $xx\,h_1$ |
| $7P_{\frac{1}{2}} - 9D_{1\frac{1}{2}}$ | 2873.0 | 34797 | 4 | 1 | $h_0$ |
| $7P_{1\frac{1}{2}} - 10D_{1\frac{1}{2}}$ | 2845.2 | 35136 | 1 | 1 | $h_0$ |
| $7P_{1\frac{1}{2}} - 10D_{2\frac{1}{2}}$ | 2840.6 | 35194 | 6 | 1 | $h_0$ |
| $7S_{\frac{1}{2}} - 8P_{\frac{1}{2}}$ | 2805.9 | 35628 | 00 | 1 | |
| $6D_{2\frac{1}{2}} - 9P_{1\frac{1}{2}}$ | 2772.7 | 36055 | 1 | 1 | $h_7$ |
| $7P_{1\frac{1}{2}} - 12S_{\frac{1}{2}}$ | 2728.4 | 36641 | 00 | −1 | $xxx$ |

TABLE I.—*Continued.*

| Classification | λ(A) | ν(cm⁻¹) | Intensity | Δν | Notes |
|---|---|---|---|---|---|
| $p^2\,{}^4P_{1\frac{1}{2}} - 6F_{2\frac{1}{2}}$ | 2719.8 | 36758 | 4 | −1 | *xx* $h_2$ *Z* |
| $7S_{\frac{1}{2}} - 8P_{1\frac{1}{2}}$ | 2717.5 | 36789 | 4 | 1 | $h_{10}$ *Z* |
| $7P_{\frac{1}{2}} - 11S_{\frac{1}{2}}$ | 2693.6 | 37114 | 0 | 1 | |
| $7P_{1\frac{1}{2}} - 11D_{2\frac{1}{2}}$ | 2684.9 | 37235 | 2 | 0 | $h_0$ |
| $7P_{\frac{1}{2}} - 10D_{1\frac{1}{2}}$ | 2634.3 | 37950 | 4 | 0 | $h_0$ |
| $p^2\,{}^4P_{2\frac{1}{2}} - 8F_{3\frac{1}{2}}$ | 2628.3 | 38036 | 3 | −1 | |
| $p^2\,{}^4P_{1\frac{1}{2}} - 8P_{1\frac{1}{2}}$ | 2608.4 | 38326 | 2 | 1 | |
| $7P_{1\frac{1}{2}} - 12D_{2\frac{1}{2}}$ | 2587.2 | 38640 | 0 | 0 | *xxx* $h_0$ |
| $6D_{1\frac{1}{2}} - 7F_{2\frac{1}{2}}$ | 2576.6 | 38799 | 8 | −1 | *x* $h_1$ |
| $6D_{2\frac{1}{2}} - 7F_{3\frac{1}{2}}$ | 2526.7 | 39566 | 8 | −1 | *x* $h_2$ *Z* |
| $7P_{1\frac{1}{2}} - 13D_{2\frac{1}{2}}$ | 2521.1 | 39653 | 0 | −5 | $h_0$ |
| $7P_{\frac{1}{2}} - 11D_{1\frac{1}{2}}$ | 2498.9 | 40005 | 2 | 2 | $h_0$ |
| $6D_{2\frac{1}{2}} - 10P_{1\frac{1}{2}}$ | 2445.1 | 40885 | 1 | 2 | |
| $p^2\,{}^4P_{1\frac{1}{2}} - 7F_{2\frac{1}{2}}$ | 2356.9 | 42414 | 1 | 0 | *xx* $h_2$ |
| $7P_{\frac{1}{2}} - 13D_{1\frac{1}{2}}$ | 2355.3 | 42444 | 0 | −4 | |
| $6D_{2\frac{1}{2}} - 8F_{3\frac{1}{2}}$ | 2326.2 | 42976 | 1 | 0 | *x* $h_2$ |
| $6D_{\frac{1}{2}} - 11P_{1\frac{1}{2}}$ | 2280.8 | 43831 | 0 | 5 | |
| $6P_{1\frac{1}{2}} - 7S_{\frac{1}{2}}$ | 2203.5 | 45368 | 2 | −1 | *x Z* |

From here on λ vac is given.

| Classification | Wave-length ($A_{vac}$) | Wave No. (cm⁻¹) | Intensity | Δν | Notes | ν Arvid. | Inten. Arv. | Δν Arv. |
|---|---|---|---|---|---|---|---|---|
| $6P_{1\frac{1}{2}} - p^2\,{}^4P_{1\frac{1}{2}}$ | 1921.66 | 52038 | 7 | 5 | | | | |
| $6P_{1\frac{1}{2}} - 6D_{2\frac{1}{2}}$ | 1822.03 | 54884 | 10 | −1 | | | | |
| $6P_{1\frac{1}{2}} - 6D_{1\frac{1}{2}}$ | 1796.68 | 55658 | 10 | 1 | *x* | | | |
| $6P_{\frac{1}{2}} - p^2\,{}^4P_{\frac{1}{2}}$ | 1726.75 | 57912 | 20 | −1 | | | | |
| $6P_{\frac{1}{2}} - 7S_{\frac{1}{2}}$ | 1682.15 | 59447 | 10 | 1 | *x* | | | |
| $6P_{1\frac{1}{2}} - p^2\,{}^4P_{2\frac{1}{2}}$ | 1671.53 | 59825 | 10 | −1 | *xx* | | | |
| $6P_{\frac{1}{2}} - p^2\,{}^4P_{1\frac{1}{2}}$ | 1512.42 | 66119 | 10 | 5 | | | | |
| $6P_{1\frac{1}{2}} - p^2\,{}^2D_{1\frac{1}{2}}$ | 1449.35 | 68996 | 3 | 6 | | | | |
| $6P_{\frac{1}{2}} - 6D_{1\frac{1}{2}}$ | 1433.96 | 69737 | 10 | 3 | *x* | 69740 | 8 | 0 |
| $6P_{1\frac{1}{2}} - p^2\,{}^2P_{\frac{1}{2}}$ | 1348.37 | 74164 | 10 | 3 | | 74168 | 4 | −1 |
| $6P_{1\frac{1}{2}} - p^2\,{}^2D_{2\frac{1}{2}}$ | 1335.20 | 74895 | 10 | −4 | C? | 74890 | 8 | 1 |
| $6P_{1\frac{1}{2}} - 8S_{\frac{1}{2}}$ | 1331.65 | 75095 | 10 | 4 | Hg? | 75097 | 1 | 2 |
| $6P_{1\frac{1}{2}} - 7D_{2\frac{1}{2}}$ | 1231.20 | 81222 | 10 | 1 | | 81223 | 9 | 0 |
| $6P_{\frac{1}{2}} - p^2\,{}^2D_{1\frac{1}{2}}$ | 1203.63 | 83082 | 10 | 1 | | 83083 | 4 | 0 |
| $6P_{1\frac{1}{2}} - 9S_{\frac{1}{2}}$ | 1145.91 | 87267 | 4 | −2 | | | | |
| $6P_{\frac{1}{2}} - p^2\,{}^2P_{\frac{1}{2}}$ | 1133.14 | 88250 | 10 | −2 | | 88248 | 7 | 0 |
| $6P_{\frac{1}{2}} - 8S_{\frac{1}{2}}$ | 1121.36 | 89177 | 10 | 3 | | 89180 | 0 | 0 |
| $6P_{1\frac{1}{2}} - 8D_{1\frac{1}{2}}$ | 1119.57 | 89320 | 10 | −7 | | 89314 | 4*d* | −1 |
| $6P_{1\frac{1}{2}} - 8D_{2\frac{1}{2}}$ | 1109.84 | 90103 | 10 | 6 | | 90110 | 1 | −1 |
| $6P_{1\frac{1}{2}} - p^2\,{}^2S_{\frac{1}{2}}$ | 1108.43 | 90218 | 10 | −2 | | 90217 | 4 | −1 |
| $6P_{\frac{1}{2}} - p^2\,{}^2P_{1\frac{1}{2}}$ | 1103.94 | 90585 | 10 | 3 | | 90590 | 5*d* | −2 |
| $6P_{1\frac{1}{2}} - 10S_{\frac{1}{2}}$ | 1065.58 | 93846 | 9 | 3 | | | | |
| $6P_{\frac{1}{2}} - 7D_{1\frac{1}{2}}$ | 1060.66 | 94281 | 10 | 3 | | 94285 | 4 | −1 |
| $6P_{1\frac{1}{2}} - 9D_{1\frac{1}{2}}$ | 1050.77 | 95168 | 10 | 8 | | | | |
| $6P_{1\frac{1}{2}} - 9D_{2\frac{1}{2}}$ | 1049.82 | 95254 | 10 | 1 | | | | |
| $6P_{1\frac{1}{2}} - 11S_{\frac{1}{2}}$ | | 97489 | (calc.) | | *k* | | | |
| $6P_{1\frac{1}{2}} - 10D$ | 1016.61 | 98366 | 10 | | *m* | | | |
| $6P_{1\frac{1}{2}} - 12S_{\frac{1}{2}}$ | 1001.81 | 99819 | 6 | 12 | | | | |
| $6P_{1\frac{1}{2}} - 11D$ | 995.89 | 100413 | 10 | | *m* | | | |
| $6P_{\frac{1}{2}} - 9S_{\frac{1}{2}}$ | 986.71 | 101347 | 10 | −1 | *x* | | | |
| $6P_{1\frac{1}{2}} - 12D$ | 982.17 | 101815 | 8 | | *m* | | | |
| $6P_{1\frac{1}{2}} - 14S_{\frac{1}{2}}$ | 975.35 | 102527 | 1 | 7 | | | | |
| $6P_{1\frac{1}{2}} - 13D$ | 972.56 | 102823 | 9 | | *m* H? | | | |
| $6P_{\frac{1}{2}} - 8D_{1\frac{1}{2}}$ | 967.23 | 103388 | 10 | 6 | | 103389 | 0 | 5 |
| $6P_{1\frac{1}{2}} - 14D$ | 965.36 | 103588 | 3 | | *m* | | | |
| $6P_{1\frac{1}{2}} - 15D$ | 960.21 | 104144 | 2 | | *m* | | | |
| $6P_{\frac{1}{2}} - p^2\,{}^2S_{\frac{1}{2}}$ | 958.76 | 104301 | 2 | −4 | | | | |
| $6P_{1\frac{1}{2}} - 16D$ | 955.91 | 104612 | 1 | | *m* | | | |
| $6P_{1\frac{1}{2}} - 17D$ | 952.92 | 104941 | 1 | | *m* | | | |
| $6P_{\frac{1}{2}} - 10S_{\frac{1}{2}}$ | 926.44 | 107940 | 5 | −10 | | | | |
| $6P_{\frac{1}{2}} - 9D_{1\frac{1}{2}}$ | | 109257 | (calc.) | | *n* | | | |
| $6P_{\frac{1}{2}} - 11S_{\frac{1}{2}}$ | 896.30 | 111570 | 3 | 4 | | | | |
| $6P_{\frac{1}{2}} - 10D_{1\frac{1}{2}}$ | 889.68 | 112400 | 8 | 9 | | | | |
| $6P_{\frac{1}{2}} - 12S_{\frac{1}{2}}$ | 877.96 | 113900 | 2 | 12 | | | | |
| $6P_{\frac{1}{2}} - 11D_{1\frac{1}{2}}$ | 873.71 | 114455 | 6 | 11 | | | | |
| $6P_{\frac{1}{2}} - 13S_{\frac{1}{2}}$ | 865.97 | 115477 | 1 | 19 | | | | |
| $6P_{\frac{1}{2}} - 12D_{1\frac{1}{2}}$ | 863.00 | 115875 | 3 | 10 | | | | |
| $6P_{\frac{1}{2}} - 13D_{1\frac{1}{2}}$ | 855.57 | 116881 | 3 | 18 | | | | |
| $6P_{\frac{1}{2}} - 14D_{1\frac{1}{2}}$ | 849.88 | 117664 | 2*d* | −14 | | | | |
| $6P_{\frac{1}{2}} - 15D_{1\frac{1}{2}}$ | 846.04 | 118198 | 2 | 25 | | | | |
| $6P_{\frac{1}{2}} - 16D_{1\frac{1}{2}}$ | 842.81 | 118651 | 1 | 17 | | | | |
| $6P_{\frac{1}{2}} - 17D_{1\frac{1}{2}}$ | 840.25 | 119012 | 00 | 12 | | | | |

*Notes and notation, Table I:*

$\Delta\nu = \nu_{\text{Predicted}} - \nu_{\text{Experimental}}$.

*x*—line classified previously by Gieseler.[9]

*xx*—line classified by Gieseler, but with different assignment of the levels involved.

*xxx*—line classified erroneously by Gieseler.

$h_0$—hyperfine structure observed by Rose: line single.

$h_{1,\ 2,\ \ldots}$—hyperfine structure observed by Rose, similar to other lines marked $h_{1,\ 2,\ \ldots}$.

(a) This line may cover the line $sp^2\,{}^2P_{\frac{1}{2}} - 9p\,{}^2P_{\frac{1}{2}}$.

(b) This line may be covered by a Pb I line.

(c) The absence of hyperfine structure in this line is inconsistent with its previous classification by Gieseler as $sp^2\,{}^4P_{\frac{1}{2}} - 7p\,{}^2P_{1\frac{1}{2}}$, since the level from $sp^2$ would be expected to show structure.

(d) Murakawa suggested on the basis of hyperfine structure that this line was a transition from $6s^27p\,{}^2P_{1\frac{1}{2}}$ to an unknown level with $J=2\frac{1}{2}$ which he called $6s6p^2\,{}^4P_{2\frac{1}{2}}$; this level was located independently in the present work, and is differently assigned.

(e) This line was classified by Gieseler as Pb I; its hyperfine structure is definitely inconsistent with that classification, but agrees with the present one.

(f) This line may be covered by a Pb I line.

(g) Smith[11] classified a line at 4272.63A with intensity 5 as Pb III ($6s7s\,{}^1S_0 - 6s7p\,{}^1P_1$).

(i) Smith[11] classified a line at 3689.32A, intensity 5, as Pb III ($6s7s\,{}^3S_1 - 6s7p\,{}^1P_1$).

(j) This value of ν is questionable; however, Rose observed a line at this point which had the correct hyperfine structure for the transition here ascribed to it.

(k) This line may be covered by a H line (λ1025.78).

(m) Unresolved doublet.

(n) This line may be covered by a Hg line (λ915.83).

made, with satisfactory general agreement. Comparison with the isoelectronic spectra Tl I and Bi III may be made by use of the regular and irregular doublet laws, as well as the similarity of relative positions of the $sp^2$ levels. The values of the screening constant *s* in the regular doublet law formula

$$\Delta\nu = f(l)(Z-s)^4/n^3$$

are given in Table III, where the agreement is as satisfactory as could be expected for heavy atoms and in view of the existing perturbations. The agreement of the observed levels with the irregular doublet law is shown in Fig. 1. The principal deviations occur in differences involving the $6d\,{}^2D$ terms, which are shown below to be considerably perturbed by neighboring $sp^2$ levels. In Fig. 2 the $sp^2$ levels of Pb II and Bi III are plotted together, with scales so adjusted that the separation of the extreme levels is equal. The

TABLE II. *Term values and effective quantum numbers in Pb II*—(Terms underlined are those previously found by Gieseler.[5])

| | $n=5$ | 6 | 7 | 8 | 9 | 10 | 11 | 12 | 13 | 14 | 15 | 16 | 17 | 18 | 19 |
|---|---|---|---|---|---|---|---|---|---|---|---|---|---|---|---|
| $^2S_{\frac{1}{2}}$ | | | 61795 | 32063 | 19897 | 13313 | 9669 | 7331 | 5747 | 4628 | | | | | |
| | | | 2.665 | 3.700 | 4.697 | 5.742 | 6.738 | 7.738 | 8.740 | 9.739 | | | | | |
| $^2P_{\frac{1}{2}}$ | | 121243 | 46784 | 26166 | 16821 | 11743 | 8665 | 6658 | 3276 | 4285 | | | | | |
| | | 1.903 | 3.063 | 4.096 | 5.108 | 6.114 | 7.118 | 8.120 | 9.121 | 10.121 | | | | | |
| $\Delta\nu$ | | 14081 | 2813 | 1161 | 598 | 351 | 222 | 150 | 105 | | | | | | |
| $^2P_{1\frac{1}{2}}$ | | 107162 | 43971 | 25005 | 16223 | 11392 | 8443 | 6508 | 5171 | | | | | | |
| | | 2.024 | 3.160 | 4.190 | 5.201 | 6.207 | 7.211 | 8.213 | 9.214 | | | | | | |
| $^2D_{1\frac{1}{2}}$ | | 51503 | 26959 | 17849 | 11986 | 8834 | 6777 | 5358 | 4344 | 3593 | 3020 | 2575 | 2221 | | |
| | | 2.920 | 4.035 | 4.959 | 6.051 | 7.049 | 8.048 | 9.051 | 10.052 | 11.053 | 12.056 | 13.056 | 14.057 | | |
| $\Delta\nu$ | | −776 | 1020 | 796 | 79 | 58 | 41 | 27 | 21 | 16 | 12 | 11 | 9 | | |
| $^2D_{2\frac{1}{2}}$ | | 52279 | 25939 | 17053 | 11907 | 8776 | 6736 | 5331 | 4323 | 3577 | 3008 | 2564 | 2212 | 1928 | 1695 |
| | | 2.898 | 4.114 | 5.074 | 6.072 | 7.072 | 8.073 | 9.074 | 10.077 | 11.078 | 12.080 | 13.084 | 14.087 | 15.089 | 16.092 |
| $^2F_{2\frac{1}{2}}$ | 28714 | 18362 | 12705 | 9297 | 7093 | 5586 | 4513 | 3721 | 3121 | | | | | | |
| | 3.910 | 4.890 | 5.878 | 6.871 | 7.867 | 8.864 | 9.862 | 10.86 | 11.86 | | | | | | |
| $\Delta\nu$ | −15 | −13 | −9 | −6 | −5 | −4 | −2 | −2 | −1 | | | | | | |
| $^2F_{3\frac{1}{2}}$ | 28729 | 18375 | 12714 | 9303 | 7098 | 5590 | 4515 | 3723 | 3122 | 2655 | | | | | |
| | 3.909 | 4.888 | 5.876 | 6.869 | 7.864 | 8.862 | 9.860 | 10.858 | 11.858 | 12.858 | | | | | |
| $^2G_{3\frac{1}{2},4\frac{1}{2}}$ | 17684 | 12275 | 9013 | 6897 | 5446 | 4410 | 3643 | 3060 | 2606 | 2247 | 1957 | | | | |
| | 4.982 | 5.980 | 6.979 | 7.978 | 8.978 | 9.98 | 10.98 | 11.98 | 12.98 | 13.98 | 14.98 | | | | |

| | | | | | | | | | | | | |
|---|---|---|---|---|---|---|---|---|---|---|---|---|
| | $6s6p^3$ | $^4P_{\frac{1}{2}}$ | 63332 | $^2D_{1\frac{1}{2}}$ | 38160 | $^2P_{\frac{1}{2}}$ | 32995 | $^2S_{\frac{1}{2}}$ | 16946 | | | |
| | | $^4P_{1\frac{1}{2}}$ | 55119 | $^2D_{2\frac{1}{2}}$ | 32271 | $^2P_{1\frac{1}{2}}$ | 16574 | | | | | |
| | | $^4P_{2\frac{1}{2}}$ | 47338 | | | | | | | | | |

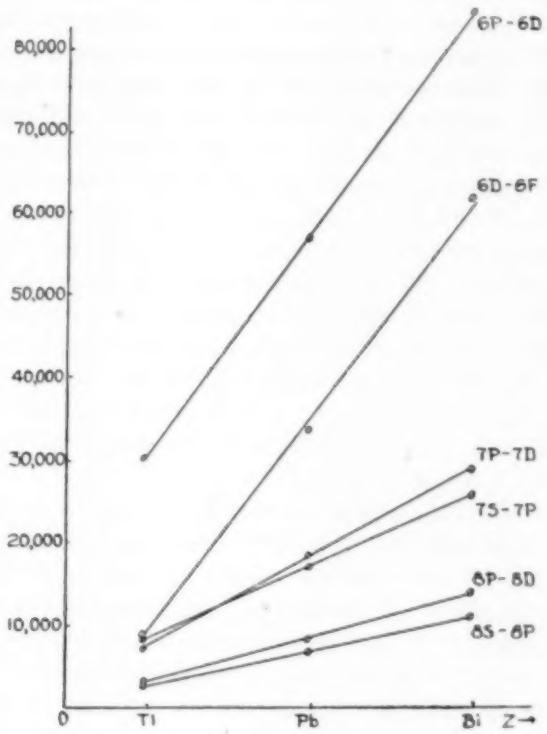


FIG. 1. Irregular doublet law.

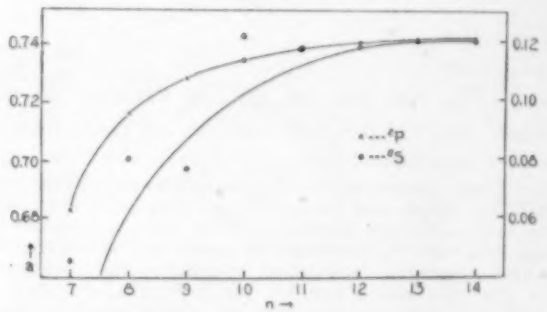


FIG. 2. Irregularities in $^2S$ series as shown by values of $a\ (=n^*-m)$ *vs.* $n$.

TABLE III. *Regular doublet law. Values of s from* $\Delta\nu=f(l)(Z-s)^4/n^3$.

| | 6*P* | 7*P* | 8*P* | 9*P* | |
|---|---|---|---|---|---|
| Tl I | 53.422 | 62.467 | 64.984 | 66.408 | |
| | −3.443 | −4.463 | −4.253 | −4.114 | |
| Pb II | 49.979 | 58.004 | 60.731 | 62.294 | |
| | −2.278 | −2.897 | −2.739 | | |
| Bi III | 47.701 | 55.107 | 57.992 | | |
| | 6*D* | 7*D* | 8*D* | 9*D* | 10*D* |
| Tl I | | 70.262 | 70.852 | 71.255 | 71.470 |
| Pb II | (inverted) | 56.587 | 56.511 | 66.341 | 66.367 |
| Bi III | | 60.615 | 62.025 | | |

general agreement is evident; particular deviations are discussed below as due to perturbations.

### Substantiations and Perturbations

The Zeeman pattern observations by Green and Loring[15] were used to check the present classification. A recalculation from the observed patterns was necessary, since the present classification changes Gieseler's assignment of several levels and includes several lines which were unclassified when their patterns were observed. Table IV is a revision of Table III of reference 15,

Table IV. *g-values for even levels of Pb II.*

| λ | $7S_{\frac{1}{2}}$ | $^4P_{1\frac{1}{2}}$ | $6D_{2\frac{1}{2}}$ | $6D_{1\frac{1}{2}}$ | $^4P_{2\frac{1}{2}}$ | $7D_{1\frac{1}{2}}$ | $7D_{2\frac{1}{2}}$ | $9S_{\frac{1}{2}}$ | $8D_{1\frac{1}{2}}$ | $8D_{2\frac{1}{2}}$ |
|---|---|---|---|---|---|---|---|---|---|---|
| 2203 | 2.02 | | | | | | | | | |
| 2719* | | 0.55 | | | | | | | | |
| 2948 | | | 1.29 | | | | | | | |
| 3016 | | | | 0.89 | | | | | | |
| 3452 | | | | | 1.41 | | | | | |
| 3455 | | | | | | | | | 1.07 | |
| 3714 | | | | | | | | | | 1.16 |
| 3718 | | | | | | | | 1.93 | | |
| 3786 | | 1.65 | | | | | | | | |
| 3827 | | | | | | | | | (.51 fr σ .92 fr π) | |
| 4153 | | | | | | | | 1.98 | | |
| 4242 | | | 1.29 | | | | | | | |
| 4245 | | | 1.35 | | | | | | | |
| 4386 | | | | .86 | | | | | | |
| 5042 | | | | | | 0.81 | | | | |
| 5372 | | | | | 1.67 | | | | | |
| 5545 | | | | | | | 1.18 | | | |
| 5609 | 2.00 | | | | | | | | | |
| 5876 | | | | | | .78 | | | | |
| 6660 | 2.02 | | | | | | | | | |
| Ave. | 2.01 | 1.65 | 1.31 | .87 | 1.54 | .80 | 1.18 | 1.96 | .99 | 1.16 |
| Theor. | 2.00 | 1.73 | 1.20 | .80 | 1.60 | .80 | 1.20 | 2.00 | .80 | 1.20 |

* There appears to be a confusion between λ2719.8 and λ2717.5. Green and Loring remark that λ2717.5 appears to have a pattern similar to λ3786, thus appropriate to the $6F_{2\frac{1}{2}}-sp^2\,{}^4P_{1\frac{1}{2}}$ transition to which λ2719.8 is assigned. (This assignment is required by the frequency difference in the two levels and by the hyperfine structure of λ2719.8.) However, the Zeeman pattern given by them for λ2719 leads to inconsistent results for the *g*-value of $7S_{\frac{1}{2}}$ if attributed to λ2717.5.

and gives the *g*-values for the various even levels, calculated from the unresolved patterns by the method of Shenstone and Blair,[16] assuming in each line that the odd level involved has the appropriate theoretical (i.e., unperturbed) *g*-value. Comparison with the theoretical *g*-values for the even levels shows good agreement. The effect of the mutual perturbation between the two levels $sp^2\,{}^4P_{1\frac{1}{2}}$ and $6d\,{}^2D_{1\frac{1}{2}}$, and between $6d\,{}^2D_{2\frac{1}{2}}$ and $sp^2\,{}^4P_{2\frac{1}{2}}$, is shown by the tendency to share *g*-values, thus decreasing the *g*-values of the $sp^2$ levels approximately as much as the *6d* level values are increased. Further evidences of these perturbations exist in the hyperfine structure of the levels, and in their positions, as discussed below.

Hyperfine structure data made available by Dr. J. L. Rose were used as a guide to assigning the $sp^2$ levels and as a further indication of perturbations existing between various even levels. Levels from $sp^2$ should show a larger separation in the components of the Pb 207 isotope (due principally to the increased interaction of the single *s* electron with the nucleus); and the isotope shift for Pb 206 and 208 should be different for the $sp^2$ levels as compared with the normal $s^2x$ levels. Inspection of the data in Dr. Rose's article immediately following shows that the $sp^2$ levels as assigned do have consistently larger hyperfine structure separations. These separations also substantiate the perturbations expected between such even terms as have equal *J*-values and are located in proximity to each other. Such perturbations would cause a sharing of the larger separations of the $sp^2$ levels with those from the normal $s^2s$ and $s^2d$ configurations. This sharing is shown by the fact that the sum of the isotope shifts for $sp^2\,{}^4P_{1\frac{1}{2}}$ and $6d\,{}^2D_{1\frac{1}{2}}$ is approximately equal to the sum of the shifts for $sp^2\,{}^4P_{2\frac{1}{2}}$ and $6d\,{}^2D_{2\frac{1}{2}}$. A similar effect on the hyperfine structure appears in the $8d\,{}^2D$ terms. Since $7d\,{}^2D_{1\frac{1}{2}}$ is single and $7d\,{}^2D_{2\frac{1}{2}}$ shows only a small structure (perhaps due to interaction with $sp^2\,{}^2D_{2\frac{1}{2}}$), the $8d\,{}^2D$ terms would be expected to show vanishingly small structure. The separation observed in the $8d\,{}^2D_{1\frac{1}{2}}$ level is thus due to the effect of the neighboring level $sp^2\,{}^2P_{1\frac{1}{2}}$, while the absence of such separation in the $8d\,{}^2D_{2\frac{1}{2}}$ level is in complete agreement with the absence of any neighboring term with $J=2\frac{1}{2}$.

Since the odd terms in the Pb II spectrum include only the $^2P$ and $^2F$ series from $6s^2mx$, no perturbations should occur, on account of the inequality of *J*-values for adjacent levels. This absence of perturbations is evident in the regularity of the effective quantum numbers of these series in Table II. On the other hand, the even terms show a mixing of the levels from $sp^2$ with the $6s^2ms$ and $6s^2md$ configurations. The

[15] Green and Loring, Phys. Rev. **43**, 459 (1933).
[16] Shenstone and Blair, Phil. Mag. **8**, 765 (1929).

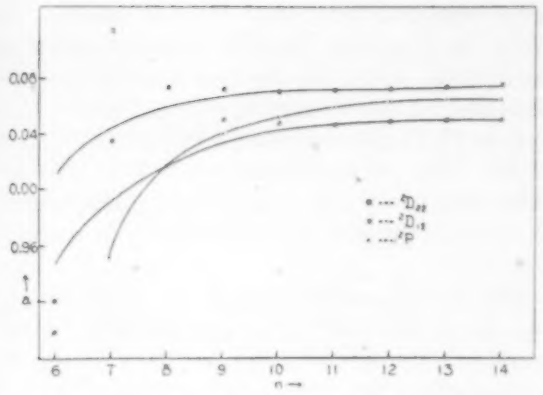


FIG. 3. Irregularities in $^2D$ series as shown by values of $a$ ($=n^*-m$) *vs.* $n$.

resulting mutual perturbations are particularly evident in the locations of the series members, and may be explained very satisfactorily, though qualitatively, by the concepts of Langer[17] and Shenstone and Russell.[18] They find that the perturbation between two interacting levels is a mutual repulsion whose magnitude depends on the overlapping of the wave functions of the two levels, and hence should increase with increasing proximity of the levels. If the quantum number discrepancy $a$ of the Rydberg series formula be plotted against the total quantum number $n$ (Fig. 2), the higher $6s^2ms$ series members are evidently regular; at $n=11$ and 10 an increasing deviation is apparent, due to repulsion by the $sp^2\,{}^2S_{\frac{1}{2}}$ level; at $n=9$ the effect of this perturbation is reversed in direction, causing the value of $a$ to be smaller than normal. The value of $a$ for the $8s$ term is too large, agreeing with the expected effect of the neighboring $sp^2\,{}^2P_{\frac{1}{2}}$ level. And finally, the $7s$ value of $a$ is also too large, due to the effect of $sp^2\,{}^4P_{\frac{1}{2}}$.

Similarly explainable effects are found in the case of the $^2D$ series, for which the effective quantum number discrepancy is plotted against $n$ in Fig. 3. Again the higher members are regular, but in the $^2D_{1\frac{1}{2}}$ terms at $n=10$ and 9 there appears a deviation due to the presence of the $sp^2\,{}^2P_{1\frac{1}{2}}$ level. This in turn causes a reversed effect upon $8d\,{}^2D_{1\frac{1}{2}}$, decreasing the effective quantum number below its normal value. The $7d\,{}^2D_{1\frac{1}{2}}$ level is

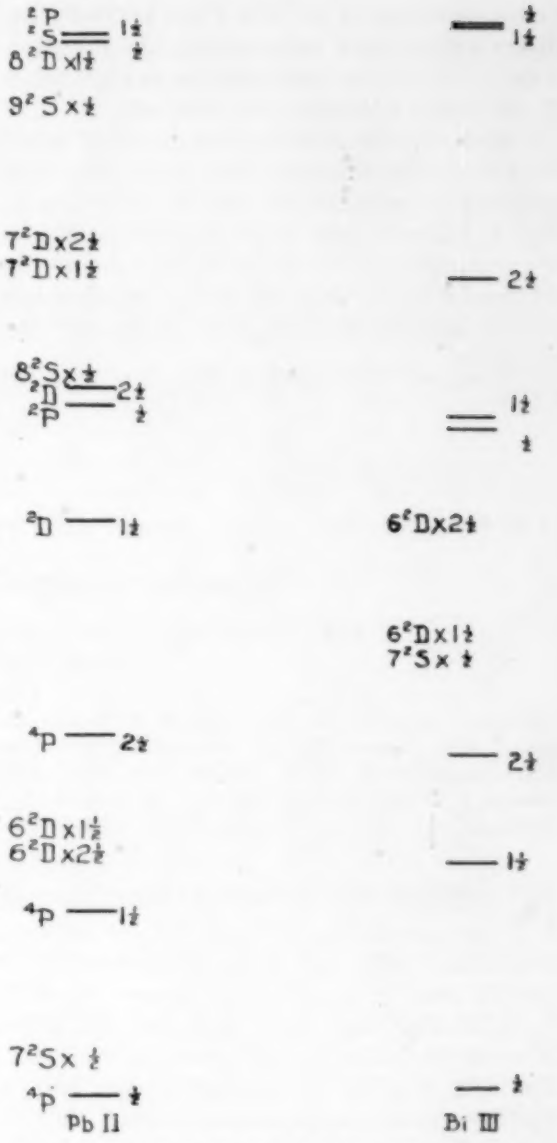


FIG. 4. $sp^2$ levels from Pb II and Bi III. (The $x$'s indicate the location of terms of the normal ($s^2nx$) series.)

affected by both $sp^2\,{}^2P_{1\frac{1}{2}}$ and $sp^2\,{}^2D_{1\frac{1}{2}}$, so a prediction of the net effect is not immediately possible; this is also true of the $6d\,{}^2D_{1\frac{1}{2}}$, affected by $sp^2\,{}^2D_{1\frac{1}{2}}$ and $sp^2\,{}^4P_{1\frac{1}{2}}$. In the case of the $^2D_{2\frac{1}{2}}$ series the deviations of the terms $n=10$, 9, 8 and 7 are due to repulsion by the $sp^2\,{}^2D_{2\frac{1}{2}}$ level; the relative magnitudes and directions of these displacements are in accord with expectation. Further, the $6d\,{}^2D_{2\frac{1}{2}}$ term is displaced in the direction of smaller effective quantum number

[17] Langer, Phys. Rev. **35**, 649 (1930).
[18] Shenstone and Russell, Phys. Rev. **39**, 415 (1932).

by the proximity of $sp^2\ {}^4P_{2\frac{1}{2}}$. These perturbation effects explain very satisfactorily the inversion of the $6d\ {}^2D$ and the abnormally large separations of the $7d$ and $8d$ doublets as observed.

The effect of the perturbations on the $sp^2$ levels is not so readily discussed, since the unperturbed arrangement is not so well known. Referring to Fig. 4, however, the larger separation of the ${}^4P_{1\frac{1}{2}}-{}^4P_{2\frac{1}{2}}$ levels in Pb II may well be due to the presence of the $6d\ {}^2D$ terms, both of which would tend to increase the separation. In Bi III[19] the effect does not occur, since the $6d$ doublet lies above the ${}^4P$ group. The difference in location of the $sp^3\ {}^2D_{2\frac{1}{2}}$ levels in the two spectra may be explained by the downward effect of the $7d\ {}^2D_{2\frac{1}{2}}$ term in Pb II and the upward effect of $6d\ {}^2D_{2\frac{1}{2}}$ in Bi III. The perturbations existing in the $sp^3$ levels with $J=\frac{1}{2}$ and $1\frac{1}{2}$ appear too complicated to admit of present interpretation on a qualitative basis.

The friendly cooperation of Dr. Rose by the loan of plates and the communication of unpublished hyperfine structure data is gladly acknowledged.

[19] McLay and Crawford, Proc. Roy. Soc. **A143**, 540 (1934).

JANUARY 15, 1935 PHYSICAL REVIEW VOLUME 47

# Hyperfine Structure of Singly Ionized Lead

JOHN L. ROSE, *Physics Department, New York University, University Heights, N. Y.*

(Received November 12, 1934)

Some one hundred and thirty lines of Pb II were observed with Lummer-Gehrcke plates and Fabry-Perot interferometers from 2300 to 10,000A. The isotope shifts between $Pb^{208}$ and $Pb^{206}$, and the h.f.s. splitting of $Pb^{207}$ were computed from the h.f.s. measurements of these lines for all of the levels of Pb II, classified by Earls and Sawyer, with the exception of $6s^26p^2P_{1/2,\ 3/2}$ and $6s6p^2\ {}^2P_{1/2}$. Parameters were obtained for equations derived by Breit and Wills for finding the h.f.s. constants, $a'$, $a''$, $a'''$, and $a(s)$, of the $6s6p^2$ configuration in intermediate coupling.

NUCLEAR spins for the three more abundant isotopes, $Pb^{208}$, $Pb^{206}$ and $Pb^{207}$, of ordinary lead were found from h.f.s. measurements of spectral lines by several investigators[1, 2, 3] to be $I=0$ for $Pb^{208}$ and $Pb^{206}$, and $I=\frac{1}{2}$ for $Pb^{207}$. Most of the lines observed were those of Pb I. The h.f.s. of a few of the more intense lines of Pb II was measured from which the isotope shift and $Pb^{207}$ splitting was found for several levels. In the present work an attempt was made to increase the intensity of the Pb II radiation from a hollow cathode tube in order to observe the h.f.s. of the weaker lines. The Paschen-Schüler type tube with a hollow iron cathode (2.5 cm diameter×7.5 cm), supported in the center of a brass tube (10 cm diameter×25 cm) serving as the anode, and the conditions of excitation, with the exception of the He pressure were similar to those used in the investigation of the h.f.s. of PbI[3]. It was found that a He pressure of about 1.0 cm of Hg and currents from 50 to 500 ma would produce a Pb II spectrum much more intense than that of Pb I. With these currents and no cooling of the cathode all of the h.f.s. components of Pb II were very sharp and it was possible to operate the tube with a current as high as 500 ma for several weeks continuously before a few grams of lead, previously placed in the cathode, were completely carried over as a fine powder to the anode. Any increase of current above 500 ma caused very little increase in the intensity of the Pb II spectrum, but a very small increase of current at this point showed a large gain in the radiation due to Pb I. At about 600 ma the more intense lines of both spectra seemed to be of about the same intensity and with larger currents the arc lines were decidedly the stronger. A large number of new lines always appeared with the above He pressure which had

[1] H. Kopfermann, Zeits. f. Physik **75**, 363 (1932).
[2] H. Schüler and E. G. Jones, Zeits. f. Physik **75**, 563 (1932).
[3] J. L. Rose and L. P. Granath, Phys. Rev. **40**, 760 (1932).

TABLE I. *Measured separation of h. f. s. components in Pb II lines.*‡
($\Delta\nu 10^{-3}$ cm$^{-1}$.)

| λ | Classification | $Pb^{203}$ | $Pb^{206}$ | $Pb^{207}$ | $Pb^{207}$ | $Pb^{207}$ |
|---|---|---|---|---|---|---|
| 8545.0 | $7P_{3/2}-p^3\,{}^2D_{5/2}$ | 0 | +338 | +673 | −438 | *X* |
| 6229.7 | $p^3\,{}^2D_{3/2}-9P_{1/2}$ | 0 | −345 | −681 | +443 | |
| 4788.1 | $p^3\,{}^2D_{3/2}-10P_{1/2}$ | 0 | −350 | −694 | +443 | |
| 4195.5 | $p^3\,{}^2D_{3/2}-11P_{1/2}$ | 0 | −341 | −692 | +438 | |
| 8395.6 | $7P_{3/2}-8S_{1/2}$ | 0 | ~0 | *X* | ~−60 | *X* |
| 4152.8 | $7P_{1/2}-9S_{1/2}$ | 0 | very small | *X* | ~−165 | *X* |
| 3261.0* | $7P_{3/2}-10S_{1/2}$ | | | (Single) | | |
| 2914.5* | $7P_{3/2}-11S_{1/2}$ | | | (Single) | | |
| 8335.0 | $p^3\,{}^2D_{3/2}-8P_{1/2}$ | | | (Same as λ5049) | | |
| 7558.7 | $7D_{5/2}-7F_{7/2}$ | 0 | −70 | −133 | +88 | |
| 6009.7 | $7D_{5/2}-8F_{7/2}$ | | | (Same as λ7558.7) | | |
| 5306.8 | $7D_{5/2}-9F_{7/2}$ | | | ( " " " ) | | |
| 4912.7 | $7D_{5/2}-10F_{7/2}$ | | | ( " " " ) | | |
| 7193.6 | $p^3\,{}^2D_{5/2}-6F_{7/2}$ | 0 | −348 | −692 | +436 | |
| 5111.9 | $p^3\,{}^2D_{5/2}-7F_{7/2}$ | 0 | −354 | −680 | +434 | |
| 4352.7 | $p^3\,{}^2D_{5/2}-8F_{7/2}$ | 0 | −353 | −698 | +440 | |
| 3971.3 | $p^3\,{}^2D_{5/2}-9F_{7/2}$ | | | (Same as λ7193.6) | | |
| 3746.9 | $p^3\,{}^2D_{5/2}-10F_{7/2}$ | | | ( " " " ) | | |
| 3601.8 | $p^3\,{}^2D_{5/2}-11F_{7/2}$ | | | ( " " " ) | | |
| 3501.9 | $p^3\,{}^2D_{5/2}-12F_{7/2}$ | | | ( " " " ) | | |
| 7013.2 | $7D_{3/2}-7F_{5/2}$ | | | (Single) | | |
| 6790.8 | $7P_{1/2}-8S_{1/2}$ | 0 | ~0 | *X* | (−100) | (+100) |
| 3718.2 | $7P_{1/2}-9S_{1/2}$ | 0 | very small | *X* | ~−168 | *X* |
| 2986.9* | $7P_{1/2}-10S_{1/2}$ | | | (Single) | | |
| 6660.0 | $7S_{1/2}-7P_{1/2}$ | 0 | +53 | *X* | +322 | −105 |
| 6518.2 | $8P_{3/2}-11S_{1/2}$ | | | (Single) | | |
| 6181.9 | $8P_{3/2}-10D_{5/2}$ | | | ( " ) | | |
| 6041.4 | $p^3\,{}^4P_{1/2}-7P_{1/2}$ | 0 | −413 | −657 | +956 | *X* |
| 5163.8 | $p^3\,{}^4P_{1/2}-7P_{3/2}$ | 0 | −412 | −659 | +916 | *X* |
| 5876.7* | $7P_{3/2}-7D_{5/2}$ | | | (Single) | | |
| 3827.2 | $7P_{3/2}-8D_{5/2}$ | 0 | +168 | *X* | ~+305 | *XX* |
| 3125.6* | $7P_{3/2}-9D_{5/2}$ | | | (Single) | | |
| 2845.2* | $7P_{3/2}-10D_{5/2}$ | | | ( " ) | | |
| 5608.8 | $7S_{1/2}-7P_{3/2}$ | 0 | +50 | −54 | +275 | ~−80 |
| 2717.5 | $7S_{1/2}-8P_{3/2}$ | 0 | (+50) | *X* | ~+274 | |
| 5544.6 | $7P_{3/2}-7D_{5/2}$ | 0 | +65 | +124 | −77 | *X* |
| 3714.0* | $7P_{3/2}-8D_{5/2}$ | | | (Single) | | |
| 3117.7* | $7P_{3/2}-9D_{5/2}$ | | | ( " ) | | |
| 2840.6* | $7P_{3/2}-10D_{5/2}$ | | | ( " ) | | |
| 2684.9* | $7P_{3/2}-11D_{5/2}$ | | | ( " ) | | |
| 2587.2* | $7P_{3/2}-12D_{5/2}$ | | | ( " ) | | |
| 2521.1* | $7P_{3/2}-13D_{5/2}$ | | | ( " ) | | |
| 5372.1 | $p^3\,{}^4P_{3/2}-5F_{7/2}$ | 0 | −283 | −570 | +387 | |
| 3451.7 | $p^3\,{}^4P_{5/2}-6F_{7/2}$ | 0 | −286 | −572 | +374 | |
| 2887.3 | $p^3\,{}^4P_{5/2}-7F_{7/2}$ | | | (Same as λ5372.1) | | |
| 5367.3 | $p^3\,{}^4P_{5/2}-5F_{5/2}$ | | | ( " " " ) | | |
| 3450.0 | $p^3\,{}^4P_{5/2}-6F_{5/2}$ | | | ( " " " ) | | |
| 2886 | $p^3\,{}^4P_{5/2}-7F_{5/2}$ | | | ( " " " ) | | |
| 5308.2 | $8P_{1/2}-12S_{1/2}$ | | | (Single) | | |
| 5109.6 | $p^3\,{}^2D_{5/2}-7F_{5/2}$ | | | (Same as λ7193.6) | | |
| 5049.3 | $p^3\,{}^2D_{3/2}-6F_{5/2}$ | 0 | −351 | −80 | −430 | |
| 3927.3 | $p^3\,{}^2D_{3/2}-7F_{5/2}$ | 0 | −360 | −84 | −432 | |
| 3463.6 | $p^3\,{}^2D_{3/2}-8F_{5/2}$ | 0 | −348 | −79 | −422 | |
| 3217.9 | $p^3\,{}^2D_{3/2}-9F_{5/2}$ | | | (Same as λ5049.3) | | |
| 3068.5? | $p^3\,{}^2D_{3/2}-10F_{5/2}$ | | | ( " " " ) | | |
| 5042.5* | $7P_{1/2}-7D_{3/2}$ | | | (Single) | | |
| 3455.0 | $7P_{1/2}-8D_{3/2}$ | 0 | +168 | *X* | +317 | *X* |
| 2873.0* | $7P_{1/2}-9D_{3/2}$ | | | (Single) | | |
| 2634.3* | $7P_{1/2}-10D_{3/2}$ | | | ( " ) | | |
| 2498.9* | $7P_{1/2}-11D_{3/2}$ | | | ( " ) | | |
| 4684.9 | $p^3\,{}^2D_{3/2}-9P_{1/2}$ | | | (Same as λ5049.3) | | |
| 3784.0 | $p^3\,{}^2D_{3/2}-10P_{1/2}$ | | | (Pattern masked by λ3785.9) | | |
| 3389.4 | $p^3\,{}^2D_{3/2}-11P_{1/2}$ | 0 | −353 | −76 | −421 | |
| 4476.3 | $p^3\,{}^4P_{3/2}-8P_{3/2}$ | | | (Same as λ5372.1) | | |
| 4386.4 | $6D_{3/2}-5F_{5/2}$ | 0 | −86 | ** | | |
| 3016.4 | $6D_{3/2}-6F_{5/2}$ | | | (Same as λ4386.4) | | |
| 2576.6 | $6D_{3/2}-7F_{5/2}$ | | | ( " " " ) | | |
| 4245.1 | $6D_{5/2}-5F_{7/2}$ | 0 | −202 | −425 | +288 | |
| 2948.5 | $6D_{5/2}-6F_{7/2}$ | | | (Same as λ4245.1) | | |
| 2526.7 | $6D_{5/2}-7F_{7/2}$ | | | ( " " " ) | | |
| 2326.2 | $6D_{5/2}-8F_{7/2}$ | | | ( " " " ) | | |
| 4242.5 | $6D_{5/2}-5F_{5/2}$ | | | ( " " " ) | | |
| 2947.5 | $6D_{5/2}-6F_{5/2}$ | | | ( " " " ) | | |
| 2526 | $6D_{5/2}-7F_{5/2}$ | | | ( " " " ) | | |
| 3785.9 | $p^3\,{}^4P_{5/2}-5F_{5/2}$ | 0 | −428 | −629 | +328 | |
| 2719.8 | $p^3\,{}^4P_{5/2}-6F_{5/2}$ | | | (Same as λ3785.9) | | |
| 2356.9 | $p^3\,{}^4P_{5/2}-7F_{5/2}$ | | | ( " " " ) | | |
| 3699.2 | $7P_{3/2}-p^3\,{}^2S_{1/2}$ | 0 | +383 | +689 | ¶ | *X* |
| 3665.6 | $6D_{3/2}-8P_{3/2}$ | 0 | −205 | −421 | +282 | |
| 2772.7 | $6D_{3/2}-9P_{3/2}$ | 0 | −206 | −412 | +295 | |
| 3649.0 | $7P_{3/2}-p^3\,{}^2P_{3/2}$ | 0 | +225 | *X* | +423 | *XX* |
| 3309.2 | $7P_{1/2}-p^3\,{}^2P_{1/2}$ | 0 | +227 | *X* | (+455) | *X* |
| 5857 | ? | 0 | ~0 | −131 | | |
| 4182.(5) | ? | 0 | −361 | −760 | (?) | |
| 3352 | ? | 0 | (−305)† | +187 | (?) | |
| 3284.(2) | ? | 0 | small | −350 | | |

‡ The following lines were observed and found to be single: λλ9063.7, 6081.5, 5074.6, 4582.3, 4296.6, 4113.4, 3987.6, $5F_{5/2}-mG$ ($m=5, \cdots 11$); λλ9050.7, 6075.8, 5070.7, 4579.1, 4293.8, 4110.8, 3985.2, $5F_{7/2}-mG$ ($m=5, \cdots 11$); λλ8719.7, 7739.8, 7165.1, 6791.7, 6533.1, 6345.0, 6203.7, 6094.0, $6F_{5/2}-mG$ ($m=8, \cdots 15$); λλ8710.1, 7732.3, 7158.7, 6785.9, 6527.8, 6339.8, 6198.8, 6089.4, $6F_{7/2}-mG$ ($m=8, \cdots 15$); λλ7050.7, 5767.9, 5155.8, 4804.5, 4581.3, 4428.7, 4319.2, 4237.6, $8P_{1/2}-mD_{3/2}$ ($m=9, \cdots 16$); λλ7632.2, 6160.2, 5472.4, 5081.2, 4833.7, 4665.5, 4544.8, 4454.9, $8P_{3/2}-mD_{3/2}$ ($m=9, \cdots 16$).

*X* This expected $Pb^{207}$ component was not observed. It is either too near to a stronger component to be resolved or of insufficient intensity to be photographed.

*XX* Two very weak $Pb^{207}$ components were not observed.

* The several components expected for this line are too close to each other to be resolved.

** The two $Pb^{207}$ components are masked by $Pb^{203}$ and $Pb^{206}$.

¶ The spectral range of the Lummer-Gehrcke plate used in observing λ3699.2 was a little more than 1.10 cm$^{-1}$. It is very probable that this component nearly coincided with the $Pb^{206}$ component in the next order of the interference pattern.

† λ3352 was not observed for uranium-lead and it is not certain that this apparent component is due to $Pb^{206}$. This may be a weak line very near to λ3352.

not been observed when working at much lower pressures.[3] The entire spectrum from 2200 to 11,000A was photographed in the first order of a 21-ft. concave grating[4] and it was found on measuring their wavelengths that very few of the new lines had been previously reported. A comparison of the h.f.s. patterns of ordinary lead with those of uranium-lead, which contained more than 90 percent of $Pb^{206}$, proved the unknown lines, which showed h.f.s., to be

[4] The Anderson grating used at present in this mounting is the property of Townsend Harris Hall, College of the City of New York.

definitely those of Pb. This is a very effective method of identifying Pb lines, especially those with observable isotope shifts. The strongest apparent component which is due to $Pb^{206}$ of uranium-lead always coincides with the next to the strongest apparent component of ordinary lead which is also due to $Pb^{206}$, the second abundant isotope of ordinary lead. Dr. L. T. Earls and Professor R. A. Sawyer, of the University of Michigan, who used a much smaller cathode and lower pressures of He, have observed these new lines. Practically all of them have been included in the new classification of Pb II lines which they have reported in the article immediately preceding this one.

## Hyperfine Structure Measurements

The h.f.s. patterns were investigated by the use of fused quartz and glass Fabry-Perot interferometers with silica-aluminum and silvered surfaces, and two Lummer-Gehrcke plates, one of crystal quartz (200×30×3.518 mm), the other of glass (130×15×4.991 mm). Interferometer spacers ranging from 1.78 mm to 25 mm in thickness were used. The h.f.s. data for the Pb II lines which could be observed and measured are tabulated in Table I. These measured separations of the apparent components of ordinary lead are considered accurate to $\mp 5.0\times10^{-3}$ $cm^{-1}$ except those indicated in the table as approximate values.

The isotopes, $Pb^{208}$ and $Pb^{206}$, with $I=0$ always give single lines but several components may be expected for $Pb^{207}$ with $I=\frac{1}{2}$. In lines of ordinary lead where there is an observable isotope displacement the strongest apparent component is always due to the most abundant isotope, $Pb^{208}$, and the next to the strongest apparent component to the next abundant isotope, $Pb^{206}$. The relative intensities and the number of weaker components, due to $Pb^{207}$ in the h.f.s. patterns, vary with the $J$-values of the terms for the lines. Table II shows for various $J$-values the theoretical relative intensities of the components expected for $Pb^{207}$. In Table I all of the components are given from left to right in the order of their expected relative intensities.

Table II. *Theoretically expected relative intensities for $Pb^{207}$ components.*

| For $I=1/2$ | | | | | | | | | | | | | | |
|---|---|---|---|---|---|---|---|---|---|---|---|---|---|---|
| $F\rightarrow$ | 0 ↓ 0 | 0 ↓ 1 | 1 ↓ 0 | 1 ↓ 1 | 1 ↓ 2 | 2 ↓ 1 | 2 ↓ 2 | 2 ↓ 3 | 3 ↓ 2 | 3 ↓ 3 | 3 ↓ 4 | 4 ↓ 3 | 4 ↓ 4 | 4 ↓ 5 |
| $J$ ↓ | | | | | | | | | | | | | | |
| 1/2→1/2 | 0 | 1 | 1 | 2 | . | . | . | . | . | . | . | . | . | . |
| 1/2→3/2 | | 2 | | 1 | 5 | . | . | . | . | . | . | . | . | . |
| 3/2→1/2 | | | 2 | 1 | | 5 | . | . | . | . | . | . | . | . |
| 3/2→3/2 | | | | 5 | 1 | 1 | 9 | . | . | . | . | . | . | . |
| 3/2→5/2 | | | | | 9 | | 1 | 14 | . | . | . | . | . | . |
| 5/2→3/2 | | | | | | 9 | 1 | | 14 | . | . | . | . | . |
| 5/2→5/2 | | | | | | | 14 | 1 | 1 | 20 | . | . | . | . |
| 5/2→7/2 | | | | | | | | 20 | | 1 | 27 | . | . | . |
| 7/2→5/2 | | | | | | | | | 20 | 1 | | 27 | . | . |
| 7/2→7/2 | | | | | | | | | | 27 | 1 | 1 | 35 | . |
| 7/2→9/2 | | | | | | | | | | | 35 | | 1 | 44 |

Table III. *Isotope shift and splitting of Pb II terms ($\Delta\nu10^{-3}$ $cm^{-1}$).*

| Term | | Term splitting for $Pb^{207}$, $I=1/2$ | Isotope shift of $Pb^{208}$ with respect to $Pb^{206}$ |
|---|---|---|---|
| $6s^27s^2S_{1/2}$ | | + 350 | − 53 |
| $8s^2S_{1/2}$ | | +1(00) | ∼ 0 |
| $9s^2S_{1/2}$ | | +2(00) | ∼ 0 |
| $ms^2S_{1/2}$, | $m\geqq10$ | 0 | 0 |
| $6p^2P_{1/2}$ | | No data | |
| $7p^2P_{1/2}$ | | ∼+ 80 | ∼ 0 |
| $mp^2P_{1/2}$, | $m\geqq8$ | 0 | 0 |
| $6p^2P_{3/2}$ | | No data | |
| $7p^2P_{3/2}$ | | ∼+ 20 | ∼ 0 |
| $mp^2P_{3/2}$, | $m\geqq8$ | 0 | 0 |
| $6d^2D_{3/2}$ | | ∼+ 90 | + 86 |
| $7d^2D_{3/2}$ | | 0 | 0 |
| $8d^2D_{3/2}$ | | − 250 | +168 |
| $md^2D_{3/2}$, | $m\geqq9$ | 0 | 0 |
| $6d^2D_{5/2}$ | | + 713 | +202 |
| $7d^2D_{5/2}$ | | + 221 | + 70 |
| $md^2D_{5/2}$, | $m\geqq8$ | 0 | 0 |
| $mf^2F_{5/2}$, | $m\geqq5$ | 0 | 0 |
| $mf^2F_{7/2}$, | $m\geqq5$ | 0 | 0 |
| $mg^2G_{7/2,\ 9/2}$, | $m\geqq5$ | 0 | 0 |
| $6s\,6p^2\ ^4P_{1/2}$ | | +159(4) | +413 |
| $^4P_{3/2}$ | | + 957 | +428 |
| $^4P_{5/2}$ | | + 957 | +283 |
| $^2D_{3/2}$ | | − 348 | +360 |
| $^2D_{5/2}$ | | +1120 | +348 |
| $^2P_{1/2}$ | | No data | |
| $^2P_{3/2}$ | | −36(2) | +227 |
| $^2S_{1/2}$ | | +18(08) | +383 |

## $Pb^{207}$ Term Splitting

The classification, kindly furnished by Dr. Earls and Professor Sawyer, for the lines whose h.f.s. had been observed made it possible to find the $Pb^{207}$ splitting and isotope shift for all the terms of Pb II with the exception of $6s^26p^2P_{1/2,\ 3/2}$ and $6s6p^2\ ^2P_{1/2}$. The lines to the former terms have wavelengths too short for the h.f.s. to be

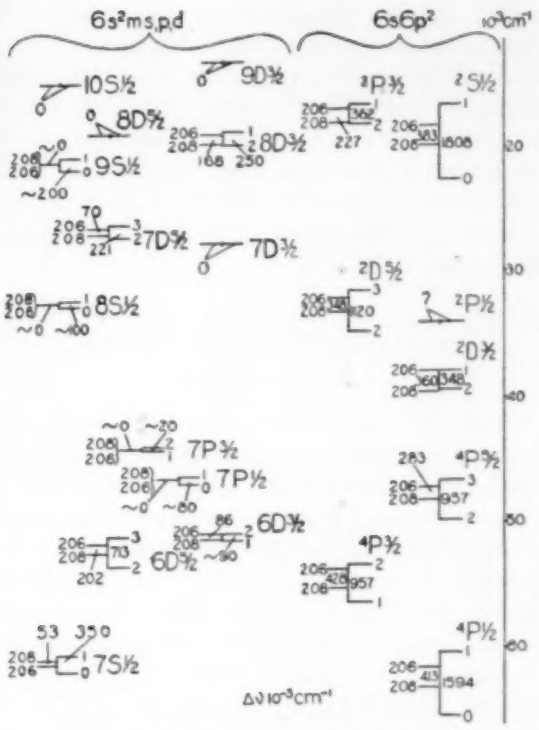


FIG. 1. Isotope shift between $Pb^{208}$ and $Pb^{206}$, and $Pb^{207}$ splitting of Pb II terms. Higher terms for $6s^2ms$, $p$, $d$ and all $6s^2mf$, $g$ terms, which are not included in the diagram, are single. No data for $6s^26p^2\,{}^2P_{1/2,\,3/2}$ and $6s6p^2\,{}^2P_{1/2}$.

easily resolved and no line to the latter term was found with sufficient intensity to photograph its interference pattern. The calculated $Pb^{207}$ term separations are shown in the second column of Table III. A negative sign indicates that the h.f.s. levels for the term are inverted. All of the terms in which splitting was found are included in the energy level diagram in Fig. 1. The $Pb^{207}$ levels with the $F$-values and calculated separation are indicated on the right side of the h.f.s. diagram for each term. Many of the $Pb^{207}$ term separations listed represent an average of several values. These values could be found independently by using the h.f.s. data for different lines or groups of lines which have a common term. The largest errors are expected in the values of the splitting for $8s^2S_{1/2}$, $9s^2S_{1/2}$, and $p^2\,{}^2S_{1/2}$. The separation for $8s^2S_{1/2}$ was determined from the patterns of two lines λλ8395.6 and 6790.8. Only one $Pb^{207}$ component could be observed for the former line and the measurements for the latter are not very accurate. In each of the lines to $9s^2S_{1/2}$ the position of the $Pb^{207}$ component had to be determined with respect to a very broad apparent component which actually consisted of three unresolved components. The value of the splitting for $p^2\,{}^2S_{1/2}$ was calculated indirectly from the observed structure of λ3699.2. This is a very weak line which required more than ten hours to photograph its pattern and its proximity to other lines made it very difficult to measure. The best photographs showed only one component which could be due to $Pb^{207}$. In making a calculation for the position of other possible components it was assumed that the observed component was the most intense one expected for $Pb^{207}$, and that the center of gravity of the $Pb^{207}$ term was between the $Pb^{208}$ and $Pb^{206}$ terms and displaced with respect to $Pb^{208}$ by a little more than 60 percent of the displacement for $Pb^{206}$ with respect to $Pb^{208}$. The latter assumption was used on the basis that this type of isotope displacement has been observed for all terms of both Pb I and Pb II where the shift could be measured. The calculations showed that the next to the strongest $Pb^{207}$ component, in the interference pattern for the Lummer-Gehrcke plate used, would nearly coincide with the $Pb^{208}$ component in an adjacent order and would not be resolved. If this is the case the separation for the $^2S_{1/2}$ level is approximately 1.808 $cm^{-1}$. A very large separation for this term is in agreement with the equations discussed below. The error expected in the above result will be several times that in the individual measured separations of the components of λ3699.2.

## ISOTOPE SHIFT

According to the data for several series of lines from $m^2F$ levels ending on a common level, the isotope shift between $Pb^{208}$ and $Pb^{206}$ is practically the same for all lines ending on the same level. It appears that the displacements must be attributed to the lower levels rather than the $^2F$ terms. In the last column of Table III the shifts are based on the assumption that the isotope separation for $^2F$ terms is zero. Isotope shifts for lead have been discussed by Rosenthal and Breit[5, 6] and the shifts listed are in general

[5] J. E. Rosenthal and G. Breit, Phys. Rev. **41**, 459 (1932).
[6] G. Breit, Phys. Rev. **42**, 348 (1932).

agreement with theory. The shifts observed in λλ6660.0 and 5608.8 and contributed to 7P terms by Kallman and Schüler[7] were not in accordance with the theory which predicted the shift to be the result of a displacement in the $7S$ term and opposite in direction to the shifts for terms of the $6s6p^2$ configuration. Additional data for other lines, recently classified by Earls and Sawyer, definitely prove that the above shifts are the result of a displacement between the $Pb^{208}$ and $Pb^{206}$ levels for the $7S$ term and in the direction suggested by theory. For the $6D$ terms where a negligible shift is expected, it was pointed out[5] that the shifts observed in these terms were the results of perturbations and could be contributed to certain terms with the same $J$-values of the $6s6p^2$ configuration. (In the above paper $p^2\,{}^2D_{3/2,\,5/2}$ are now classified as $p^2\,{}^4P_{3/2,\,5/2}$.) In the same way shifts for $7D_{5/2}$ and $8D_{3/2}$ can be explained as the result of $6s6p^2$ terms in the proximity of these $D$ terms. No doubt some of the $ms^2S_{1/2}$ terms are perturbed to some extent by $6s6p^2$ terms with $J=\frac{1}{2}$ but the isotope displacement was too small to be observed for the higher terms and for $7S_{1/2}$ it was opposite in direction to the displacements for $6s6p^2$ terms. When the isotope shifts for the $mD$ terms are added to the observed shifts for the proper $6s6p^2$ terms the displacements due to this configuration are nearly the same for all terms. This is what one would expect for terms with the same electron configuration, as a result of nuclear field perturbations.

A very weak component, attributed to a lesser abundant isotope, $Pb^{204}$, was observed by Schüler and Jones[2] for λλ7228, 5201 and 5005 of Pb I and λ5609 of Pb II. These lines were photographed with long exposures during the course of the present work but a faint ghost appeared in each order of the interference pattern and the position of the ghost in orders nearest the center, where the dispersion is large, was too near the position of the reported $Pb^{204}$ component to be certain of the existence of the latter. The relative position of the ghost in any one order varied with the order of interference and in the fourth order from the center, the ghost was in a position which would not interfere with the observance of a $Pb^{204}$ isotope. The failure to observe any $Pb^{204}$ component in this order and other orders farther from the center may have been due to the small dispersion in these orders. Another set of interferometer plates, which do not produce the same type of ghost, are now available and will be used in re-photographing the above lines, and also λλ6660 and 4386, whose patterns should show a $Pb^{204}$ component.

[7] H. Kallman and H. Schüler, Ergebnisse der Exakten Naturwissenschaften **11**, 134–175 (1932).

## Intermediate Coupling for $6s6p^2$ Configuration

With the above $Pb^{207}$ term separations it is possible to make a comparison with theory for the h.f.s. constants of the $6s6p^2$ configuration. In order to do this it is first necessary to consider the gross structure of the $6s6p^2$ terms. The position of levels in intermediate coupling can be obtained as the solution of certain algebraic equations (secular equations) which involve the interaction integrals $G^1$, $X$ and $a$.[8, 9, 10] By using the ${}^3P_{0,\,1,\,2}$ and ${}^1P_1$ levels of the $6s6p$ configuration in Pb III, $G^1$ was found to be $3.6\times10^4$ cm$^{-1}$ and $a=1.24\times10^4$ cm$^{-1}$. Then, by using the levels ${}^3P_{0,\,2}$, ${}^1D_2$, ${}^1S_0$ of the $6s^26p^2$ configuration of Bi II, the values $X=3.36\times10^3$ cm$^{-1}$ and $a=1.22\times10^4$ cm$^{-1}$ were obtained. Since the $a$'s as calculated from these two configurations agree very well it is reasonable to suppose that the values of the parameters so obtained are valid for the $6s6p^2$ of Pb II.

The energy matrix was calculated in $ls$ coupling with the values $G^1$, $X$ and $a$.[9] From this one readily obtains the energies and expressions for wave functions in intermediate coupling in terms of wave functions corresponding to $ls$ or $jj$ coupling. The calculated energies, referred to the midpoint between ${}^4P_{5/2}$ and ${}^2D_{5/2}$, are shown in comparison with the experimental values of Earls and Sawyer in Fig. 2. (In this figure slightly different scales are used in plotting the two sets of data.) The levels $W=27.4\times10^3$ cm$^{-1}$ and $W=9.7\times10^3$ cm$^{-1}$ are undoubtedly ${}^2S_{1/2}$ and ${}^2P_{1/2}$, respectively. The assignments for all the other levels could be made without difficulty.

[8] $G^1$ is Slater's radial exchange integral between the $s$ and $p$ electrons, $X=3/25F^2$ is the interaction integral between the two $p$ electrons, and $a$ is the magnetic interaction of the $p$ electrons.

[9] M. H. Johnson, Jr., Phys. Rev. **39**, 197 (1932).

[10] G. Breit and L. A. Wills, Phys. Rev. **44**, 470 (1933).

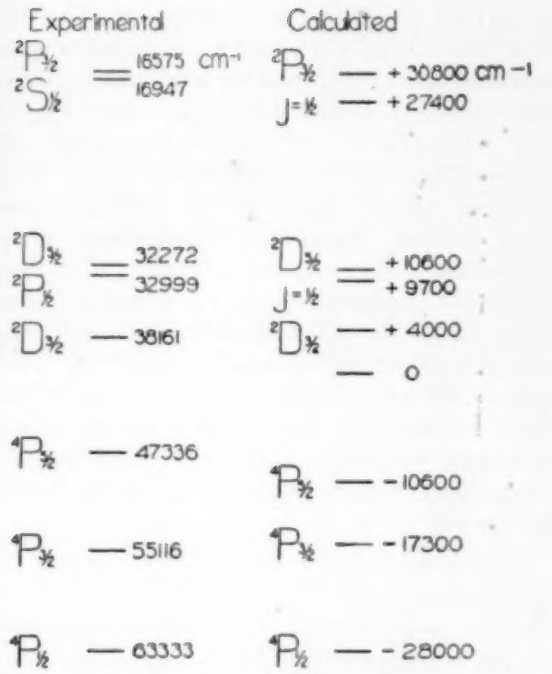


FIG. 2. Pb II $6s6p^2$ term values. The calculated energies are referred to the midpoint between $^4P_{5/2}$ and $^2D_{5/2}$.

The calculated results, neglecting perturbations due to even terms of other configurations, are in as good agreement as could be expected with the experimental values. This indicates that the assignment of these levels to the $6s6p^2$ configuration is essentially correct. At the same time deviations of levels from calculated positions are connected with decreased isotope shifts, showing that the isotope shift is due to the $6s$ electron. The wave functions determined are given by the following transformation matrices:

| | | $^2D_{5/2}$ | $^2P_{5/2}$ |
|---|---|---|---|
| $J=5/2$ | $^2D'_{5/2}$ | 0.89 | −0.463 |
| | $^2P'_{5/2}$ | .463 | .89 |

| | | $^2D_{3/2}$ | $^4P_{3/2}$ | $^2P_{3/2}$ |
|---|---|---|---|---|
| $J=3/2$ | $^2D'_{3/2}$ | 0.943 | 0.0873 | −0.327 |
| | $^4P'_{3/2}$ | − .119 | .99 | − .0805 |
| | $^2P'_{3/2}$ | .319 | .114 | .943 |

| | | $^4P_{1/2}$ | $^2P_{1/2}$ | $^2S_{1/2}$ |
|---|---|---|---|---|
| $J=1/2$ | $^4P'_{1/2}$ | 0.935 | −0.138 | 0.327 |
| | $^2P'_{1/2}$ | .305 | .775 | − .531 |
| | $^2S'_{1/2}$ | − .184 | .605 | .775 |

where the unprimed states are for *ls* coupling and the primed for intermediate coupling. The transformation from *jj* into intermediate coupling can now be obtained by multiplying the above matrices by the transformation from *ls* to *jj* coupling given in Table VIII of Breit and Wills.[10] The coefficients of the *jj* to intermediate coupling transformation are just the $c$'s of the above reference, so that the separation factors, $A$, in intermediate coupling can be immediately obtained from their formulae:

$$A(^2D_{5/2}) = 0.763a' + 0.042a'' - 0.461a''' + 0.200a(s) \quad (1)$$

$$A(^4P_{5/2}) = .646a' + .160a'' + .461a''' + .200a(s) \quad (2)$$

$$A(^2D_{3/2}) = .871a' + .302a'' - .463a''' - .176a(s) \quad (3)$$

$$A(^4P_{3/2}) = .926a' - .192a'' + .236a''' + .268a(s) \quad (4)$$

$$A(^2P_{3/2}) = 1.137a' + .019a'' + .226a''' - .159a(s) \quad (5)$$

$$A(^4P_{1/2}) = .306a' - .061a'' + 2.033a''' + .759a(s) \quad (6)$$

$$A(^2P_{1/2}) = 1.110a' - .221a'' - .956a''' + .088a(s) \quad (7)$$

$$A(^2S_{1/2}) = .252a' - .050a'' - 1.100a''' + .805a(s). \quad (8)$$

In these equations the h.f.s. coupling constants, $a'$, $a''$, $a(s)$, denote the values of $A$ for the $p_{3/2}$, $p_{1/2}$, and $6s$ electrons respectively; $a'''$ is an analogous constant which owes its existence to the fact that there are non diagonal matrix elements of the nuclear magnetic field between $p_{1/2}$ and $p_{3/2}$ states. The sum rule equations[11, 12] require a knowledge of $A$ for all of the levels of the $6s6p^2$ configuration in order to be solved for $a'$, $a''$, and $a(s)$, but with the above equations these constants together with $a'''$ can be obtained when $A$ is accurately known for any four of the eight possible levels. When various values of $A$, calculated directly from the observed $Pb^{207}$ splittings for $6s6p^2$ terms in Table II, were substituted in the equations it was impossible to find reasonable values for the constants. This result was not surprising since one would expect the perturbations between these terms and even terms of other configurations with the same $J$-values to have an effect on the $Pb^{207}$ splitting for

[11] S. Goudsmit, Phys. Rev. **37**, 663 (1931).
[12] R. A. Fisher and S. Goudsmit, Phys. Rev. **37**, 1057 (1931).

terms in which an effect for the isotope displacements was observed. For the $^2D$ terms of the $6s^2md$ configuration the $Pb^{207}$ splitting would be expected to be very little different from the splitting for $6s^2mf$ terms which was found to be zero. The fact that large splittings were found in $^2D$ terms only where isotope shifts were observed and that a large inverted splitting was observed for $8D_{3/2}$, in the proximity of $p^2\,{}^2P_{3/2}$ with inverted levels, and between two single terms $7D_{3/2}$ and $9D_{3/2}$, indicate that the splitting in $^2D$ terms must be attributed to perturbations by $6s6p^2$ terms.

More reasonable values for the constants were found when the splitting for the perturbed $6s^2md$ terms was taken into account. The sum of the $A$'s for the perturbed and perturbing term was used in the calculations with Eqs. (1)–(8) because the sum rule applies to $A$ values in such perturbations. Consistent results could not be found when Eq. (8) was used. This is no doubt due to the error in the calculated value for the separation of the levels of $^2S_{1/2}$ and because of some perturbation effect between this term and $9S_{1/2}$ which could not be readily observed. The best results were obtained by using the sum of Eqs. (1) and (2) with a value of $A$ from $6D_{5/2}$, $7D_{5/2}$, $^2D_{5/2}$, $^4P_{5/2}$; Eq. (3) with $A$ from $^2D_{3/2}$; Eq. (4) with $A$ from $^4P_{3/2}$ and $6D_{3/2}$; and Eq. (6) with $A$ from $^4P_{1/2}$. From the above four equations $a(s)=1.89$, $a''=0.402$, $a'=0.078$, and $a'''=0.07$ were determined. The result for $a'$ is higher than expected and a plus value for $a'''$ is meaningless. The expected values for these constants, $a'=a''/17$ and $a'''=-5a'/16$, are very small and are quite sensitive to experimental error. Even in cases where there are no perturbations, it is almost impossible, experimentally to determine with sufficient accuracy $A$ values which will give good results for $a'$ and $a'''$. The value of $a''$ is in good agreement with the following experimental values found from other spectra, Pb I,[3] 0.370; Bi I,[11, 12] 0.375 and 0.390; Bi II,[12] 0.340. The value of $a(s)$ for Pb II also compares favorably with other experimental values, Bi II,[12] 1.60; Bi III,[12] 1.80; Bi IV,[13] 2.34; Bi V,[12] 2.6.

In conclusion the writer wishes to express his appreciation to Dr. Earls and Professor Sawyer for their cooperation in sending unpublished data on the classification of Pb II which they have corrected and extended, to Professor G. Breit for his interest and many suggestions throughout the progress of this investigation, and to the National Research Council for a grant-in-aid, a part of which was used to obtain apparatus for this research.

[12] A. B. McLay and M. F. Crawford, Phys. Rev. **44**, 986 (1933).

# The Far Infrared Absorption of Benzene

R. BOWLING BARNES, W. S. BENEDICT* AND C. M. LEWIS,* *Palmer Physical Laboratory, Princeton University*

(Received December 1, 1934)

The absorption of benzene has been studied from 40–135$\mu$ under high resolution. Five weak bands, interpreted as difference bands, have been found in the liquid. The observations lend strong support to the plane symmetrical hexagonal model for benzene.

ALTHOUGH the infrared, ultraviolet and Raman spectra of benzene have been extensively studied[1] no general agreement yet exists concerning the equilibrium structure and vibrational states of this important molecule. Accordingly we have examined its absorption in the hitherto unexplored far infrared region (40–135$\mu$). The work of Shapiro, Gibbs and Johnson has demonstrated the existence of a low frequency vibrational interval (160 $cm^{-1}$) in the ground state of the molecule. If benzene has a structure of low symmetry this frequency, or one related to it, might appear in the far infrared spectrum as an active fundamental.

The spectrometer used has been described recently.[2]

In this investigation we first used a cell 3 cm in length, with windows of crystal quartz 0.3 mm in thickness. When filled with benzene vapor at the saturation vapor-pressure at room temperature, no absorption was found from 40–110$\mu$. It was then filled with liquid benzene (Kahlbaum's thiophene free, carefully dried over sodium, but otherwise not further purified). Absorption was now practically complete in this region. Reduction of the layer of benzene to 3.5 mm thickness gave good relative transmissions throughout the region. The transmission curve is given in Fig. 1. The slit-width was 2$\mu$, and two points were taken per slit width. The absorption is seen to be fairly constant throughout the region, with no outstanding structure, but with maxima at 87, 117, 140, 168 and 216 $cm^{-1}$. These maxima we interpret as $Q$ branches of individual vibrational transitions and the remaining absorption as due to overlapping of the undefined $P$ and $R$ branches. Comparison with the results of Leberknight and Silverman, who worked with comparable resolving power in the near infrared, shows that this is the expected band structure in liquid benzene. In the vapor the $P$ and $R$ branches stand out more distinctly. It is, of course, not excluded that other weaker bands, in addition to the five named, may be present.

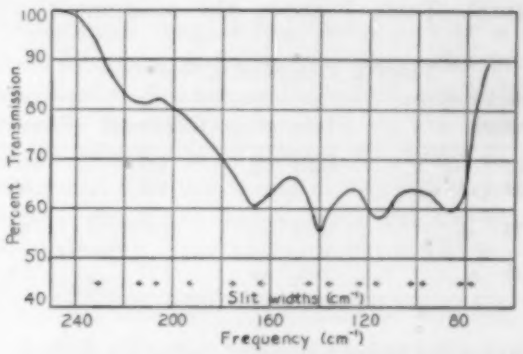


FIG. 1. Far infrared transmission of benzene.

## DISCUSSION

The absence of any absorption in the vapor, or with thin layers of liquid, would seem to prove the absence of a fundamental vibrational frequency in the region studied. A thickness of 0.01 mm of liquid is sufficient to give the fundamental band at 6$\mu$. Even after making allowance for the $\nu$-factor in the expression for absorption intensities, our bands are seen to be associated with transitions 15–40 times less probable than the 6$\mu$ fundamental. The number and irregularity of the bands observed precludes the possibility of

* National Research Fellow.

[1] Infrared: Silverman, Phys. Rev. **41**, 486 (1932); Leberknight, Phys. Rev. **43**, 969 (1933); Kettering and Sleator, Physics **4**, 39 (1933).
Ultraviolet: Shapiro, Gibbs and Johnson, Phys. Rev. **38**, 1170 (1931); Kistiakowsky and Nelles, Phys. Rev. **41**, 595 (1932).
Raman: Grassmann and Weiler, Zeits. f. Physik **86**, 321 (1934).
Correlation: Dietz and Andrews, J. Chem. Phys. **1**, 62 (1933); Wilson, Phys. Rev. **45**, 706; **46**, 146 (1934).
Also references to earlier work therein cited.

[2] R. Bowling Barnes, Rev. Sci. Inst. **5**, 237 (1934).

their all being overtones or combinations of very low frequencies, as there can, on any reasonable choice of force constants, be only two such frequencies, associated with puckering of the benzene ring, and one of these is doubtless 160 $cm^{-1}$. Our bands must therefore be interpreted as difference bands; and the four strongest maxima are immediately seen to correspond each with the difference of a Raman and an infrared fundamental. Table I shows the assignment, the frequencies being numbered following Wilson.

TABLE I. *Assignment of frequencies.*

| Raman | | Infrared | | Calculated | Observed |
|---|---|---|---|---|---|
| 1605 | $\nu_8$ | 1483 | $\nu_{19}$ | 122 | 117 |
| 1584 | $\nu_1+\nu_6$ | | | 101 | 87 |
| 1178 | $\nu_{10}$ | 1038 | $\nu_{11}$ | 140 | 140 |
| 849 | $\nu_9$ | 672 | $\nu_{18}$ | 177 | 168 |

The agreement is satisfactory, particularly as the Raman frequencies have been observed in the liquid and the infrared in the vapor.

These results lend convincing support to Wilson's assignment of the frequencies on the basis of the plane symmetrical hexagonal model (symmetry group $D_{6h}$). The observed differences are in all cases allowed by the selection rules and no other allowed differences between observed frequencies would fall in this region. The following other differences, involving inactive Raman and infrared bands, whose approximate positions can however be calculated from Wilson's formulae, might appear in our region: $\nu_{12}-\nu_6$; $\nu_7-\nu_{12}$; $\nu_5-\nu_{17}$; $\nu_3-\nu_{17}$; $\nu_3-\nu_{14}$; $\nu_5-\nu_{14}$. Of these, the first two are most probable, involving the lowest frequencies. An assignment such as $\nu_{12}=693$ would place both these bands in reasonable observed positions, 87 and 156 $cm^{-1}$ but, lacking data of comparable accuracy on the weak combination bands in the nearer infrared, such assignments are risky.

On any model of less symmetry, the possible number of difference bands observable would be much greater: if there were no center of symmetry, differences of two Raman bands, such as $849-606=243$ would be expected to appear rather strongly; our data agree with the whole body of Raman and infrared data in excluding this possibility. If the ring is puckered (symmetry $D_{3d}$, as postulated by Dietz and Andrews) the number of possible differences is not prohibitively increased and this model might possibly be made to fit previously existing data. However, on this model the *ungerade* ring-puckering vibration (Wilson's $\nu_{16}$) would be active. If the 160 $cm^{-1}$ observed by Shapiro, Gibbs and Johnson is $\nu_4$, as seems highly probable,[3] $\nu_{16}$ must lie in our region. There is a faint possibility that $\nu_{16}<80$ $cm^{-1}$, but in that case $\nu_4+\nu_{16}$ would fall in our region and should appear strongly. Hence the non-appearance of any band of sufficient intensity to qualify as a fundamental or first combination provides a decisive spectroscopic proof of the plane model for benzene.

[3] If the *upper* state of the ultraviolet absorption system is puckered, all vibrational differences involving *gerade* puckering frequencies of the *lower* state may appear, according to the Teller-Herzberg selection rules, Zeits. f. physik. Chemie **B21**, 410 (1933); if both states are plane, only even overtones of the lower state fundamentals are allowed. Thus 160 may be $\nu_4$ or, less probably in our opinion, $2\nu_4$.

# The Zeeman Effect of the Spectra of Arsenic

J. B. GREEN AND W. M. BARROWS, JR., *Mendenhall Laboratory of Physics, Ohio State University*

(Received October 26, 1934)

*Zeeman Effect in Arsenic:* Zeeman patterns of the spectra of As I, As II and As III have been measured. The results give $g$-values that are in general agreement with perturbation theory, although it appears that Goudsmit's method of adding an $s$-electron to parts of a configuration is not sufficiently accurate.

THE Zeeman patterns of the spectrum of arsenic from 2200 to 6500 Angstroms were photographed with the apparatus previously described.[1] One important alteration in the arrangement of the source has been made.

Above and forward of the holes, which admit the pole-pieces into the vacuum-box, are two five-eighths inch tapped holes, directly opposite one another. Into these are screwed hard rubber plugs with close-fitting threads, well covered with stopcock grease. The left-hand plug (as seen looking forward) is drilled and tapped to receive a one-quarter inch, twenty-thread screw, while the right-hand one has a blind, three-sixteenths inch smooth side hole, extending about three-quarters of its length from the inside. A brass rod about five inches long, consisting of three inches of three-sixteenths inch round rod and two inches of one-quarter inch, twenty male thread, is inserted in the right plug and screwed into the left plug, after being greased to insure air-tightness. This rod forms the axle for a horizontal lever arm of three-sixteenths inch brass rod, which is provided with a long brass bushing. A short helical spring pushes this bushing away from the right plug and a washer stops it at the beginning of the threaded part of the axle. The axle is screwed in or out of the left plug until the lever arm is in the plane of the disk. The lever arm is free to turn about the axle in this vertical plane. On the inner end of the lever arm, vertically above the center of the disk, is a brass fixture, through which is drilled a vertical hole, tapped to accommodate a No. 5–40 machine screw. On the side of the fixture opposite the lever arm (toward the back of the box) is a set-screw, which also has a No. 5–40 thread.

A one-eighth inch round brass rod, about seven inches long, is now threaded with a No. 5–40 die and screwed into the hole in this fixture until, when the arm is horizontal, the rod just touches the uppermost point of the disk, in which position it is secured by means of the set-screw. The upper end of the rod then protrudes about two inches above the top of the box, through a one-inch hole cut in the box for this purpose.

On the forward end of the lever arm (on the opposite side of the axle) is fastened a lead counterweight of sufficient mass so that only a slight pressure is exerted on the disk by the vertical rod. This pressure may be increased at will by screwing brass weights onto the top of the rod. Now if the disk is set rotating, the magnetic field is on, the vacuum-box (and therefore the disk) is connected to the negative terminal and the vertical rod (through the lever arm and axle) to the positive terminal of a source of direct current, the arc will operate. The disk becomes its negative electrode and the vertical rod its positive electrode. The magnetic field is in such a direction that as soon as a current flows through the rod it suffers a backward force. This force produces a torque about the axle which tends to lift the upper electrode, thus striking the arc. When the arc blows out, as it will in a magnetic field, the current ceases, the torque vanishes and the electrode falls back against the disk, whereupon the process is repeated indefinitely. By this means an average current of one ampere through the arc will produce a spectrum considerably brighter than was obtained by the former method with a current of three amperes.

The insertion of rubber gaskets between the pole-pieces and the vacuum box, to insulate the box from the frame of the magnet, which

is grounded, necessarily widens the pole-gap slightly, so that the field intensity is reduced to some 36,000 gauss at ninety amperes actuating current.

Since arsenic cannot be successfully cast or alloyed in large proportion in air, the following method was used to introduce it into the arc:

The rod which was to become the upper electrode was provided with an axial hole one-sixteenth inch in diameter, extending inward about one and one-quarter inches from one end. This hole was filled with finely powdered arsenic, which was firmly tamped down. The rod was then placed in the arc in the usual manner with the filled end down. With this arrangement the arc would operate for about an hour before the arsenic was exhausted.

A fairly large hole was cut in the back-plate of the vacuum-box at a point slightly higher than the pole-gap. Over this hole was soldered a flanged, tapered bushing, into which fits a tapered, hollow plug with a stopcock grease seal. The longitudinal hole in this plug is covered with a plate-glass window cemented to the plug. Through this window the source may be observed in operation, either with the naked eye or through a small direct-vision spectroscope, without interfering with the beam which enters the spectrograph. If the plug be removed, a long-shanked screw-driver may be inserted into the box for adjustment of the set-screw, without removing the back-plate.

The hole in the box, through which projects the upper end of the electrode, is closed by means of the same hollow brass cap previously used.[1] By removing this cap and the tapered plug in the back-plate, the electrode may be adjusted, or removed and replaced without disturbing the back-plate.

The complete Zeeman patterns and then the *p*-components were exposed for forty-eight hours, with a slit-width of 0.045 mm, the source being in an atmosphere of hydrogen at a pressure of ten millimeters of mercury. In the meantime a small tank of helium became available. It was found that the arsenic spectrum was increased in intensity and the bands were less objectionable when the vacuum-box contained helium at 10 mm pressure. Accordingly, the *s*-components were photographed with helium replacing the hydrogen as residual gas and the exposure was reduced to sixteen hours. This exposure brought out considerably more lines in the arsenic spectrum than the others.

## As I

The spectrum of As I has been partially classified by Meggers and DeBruin[2] and by Rao.[3] These classifications are in substantial agreement, that of Rao's being the more recent and more complete.

Table I summarizes the results of the present investigation of the Zeeman effect as As I.

The third column gives the classification of each line (Rao).

In the fifth column are recorded the displacements, in terms of the unit $L$, of the various components from the center of the pattern. In the cases of unresolved patterns these displacements are measured to the centers of intensity of the groups of *s*-components. The figures in parentheses refer to *p*-components and the others to *s*-components.

The last two columns give the *g*-values calculated for the levels; $g_a$ is that of the level first mentioned in the classification and $g_b$ of the other.

The $4s^24p^3$ configuration has been studied by Inglis[4] and by Inglis and Johnson[5] and the *g*-formulae calculated on the basis of the perturbation theory. The results calculated according to this method are compared with observations in Table II.

No very definite conclusion can be drawn from this comparison. The levels of As I are so close to *LS* coupling that the *g*-values are almost normal. A striking discrepancy is seen in the *g*-value of $^2P_{1/2}$, which should not change with coupling. This comes about as a result of the pattern of λ2991, which shows a marked departure from the *g*-value computed from λ2745. A similar disturbance in the same level of Sb I[6] has been noticed and attributed to hyperfine structure of this level. The *g*-value of $^2P_{3/2}$ is in quite good agreement with the present theory.

Johnson[7] and Goudsmit[8] have studied the $4s^24p^25s$ configuration from the standpoint of the addition of an *s*-electron to a $^3P$ set of levels.

TABLE I. *Zeeman patterns of As I.*

| λ | ν | Classification | Pattern | $g_a$ | $g_b$ |
|---|---|---|---|---|---|
| 2288.2 | 43689 | $4p^2D_{5/2}-5s^2P_{3/2}$ | (0) 1.090 | 1.208 | 1.327 |
| 2349.9 | 42542 | $4p^2D_{3/2}-5s^2P_{1/2}$ | (0) .830 | .811 | .736 |
| 2369.8 | 42185 | $4p^2P_{3/2}-5s^2D_{3/2}$ | (.73) 1.08 | 1.32 | .84 |
| 2437.3 | 41017 | $4p^2D_{3/2}-5s^4P_{3/2}$ | (1.35) — | .81 | 1.71 |
| 2493.0 | 40101 | $4p^2D_{3/2}-5s^4P_{1/2}$ | 0 (.901) 1.716 | .815 | 2.617 |
| 2745.1 | 36418 | $4p^2P_{1/2}-5s^2P_{3/2}$ | (.331) .993 1.659† | .663 | 1.326 |
| 2780.3 | 35956 | $4p^2P_{3/2}-5s^2P_{3/2}$ | (0) 1.324 | 1.319 | 1.329 |
| 2860.6 | 34948 | $4p^2P_{1/2}-5s^2P_{1/2}$ | (0) .704 | .687 | .721 |
| 2898.8 | 34487 | $4p^2P_{3/2}-5s^2P_{1/2}$ | (.292) 1.040 1.597† | 1.319 | .743 |
| 2991.1 | 33424 | $4p^2P_{1/2}-5s^4P_{3/2}$ | (.505) 1.217 2.217† | .711 | 1.717 |
| 3033.0 | 32961 | $4p^2P_{3/2}-5s^4P_{3/2}$ | (.618) 1.489 | 1.283 | 1.695 |

† Stronger lines.

TABLE II.* *$4s^24p^3$ configuration of As I.*

| | $^2P_{3/2}$ | $^2P_{1/2}$ | $^2D_{5/2}$ | $^2D_{3/2}$ | $^4S_{3/2}$ |
|---|---|---|---|---|---|
| $g$ *LS* | 4/3 | 2/3 | 6/5 | 4/5 | 2 |
| $g$ obs. | 1.313 | .687 | 1.208 | .813 | — |
| $g$ calc. | 1.317 | 2/3 | 6/5 | .822 | 1.994 |

* In this table, as well as Tables III, IV, VI, VII the well-resolved lines have been weighted more heavily in calculating the $g_{obs.}$ values taken from the lists of lines.

TABLE III. *The $4s^24p^25s$ configuration of As I.*

| | | Referred to $^4P_{5/2}$ | | | | |
|---|---|---|---|---|---|---|
| Level | ν | Obs. | Calc. | $g_{calc.}$ | $g_{obs.}$ | $g_{LS}$ |
| $^4P_{1/2}$ | 30,000 | −2204 | −2098 | 2.620 | 2.617 | 2.667 |
| $^4P_{3/2}$ | 29,084 | −1288 | −1368 | 1.722 | 1.706 | 1.733 |
| $^4P_{5/2}$ | 27,796 | (0) | (0) | 1.600 | —— | 1.600 |
| $^2P_{1/2}$ | 27,558 | 238 | 223 | .713 | .736 | .667 |
| $^2P_{3/2}$ | 26,088 | 1708 | 1788 | 1.345 | 1.327 | 1.333 |

TABLE IV.* *The 4s4p5s configuration of As I*

| Level | ν | Referred to 23838 | Calc. | $g_{calc.}$ | $g_{obs.}$ | $g_{LS}$ |
|---|---|---|---|---|---|---|
| $^4P_{1/2}$ | 30,000 | −6162 | −6242 | 2.572 | 2.617 | 2.667 |
| $^4P_{3/2}$ | 29,084 | −5246 | −5234 | 1.718 | 1.706 | 1.733 |
| $^4P_{5/2}$ | 27,796 | −3958 | −3958 | 1.591 | —— | 1.600 |
| $^2P_{1/2}$ | 27,558 | −3720 | −3824 | .761 | .736 | .667 |
| $^2P_{3/2}$ | 26,088 | −2250 | −2284 | 1.329 | 1.327 | 1.333 |
| $^2D_{5/2}$ | 19,879 | +3958 | +3958 | 1.209 | —— | 1.200 |
| $^2D_{3/2}$ | 19,859 | +3978 | +4000 | .819 | .84 | .800 |
| $^2S_{1/2}$ | 15,882 | +7956 | +8140 | 2.000 | —— | 2.000 |

* This same configuration has been studied by Schlapp (Proc. Roy. Soc. Edin. **54**, 109 (1934)), a reprint of which has just been received (Nov. 16, 1934).

Using the matrices calculated by Johnson we find the following results, which are compared with the observations in Table III.

From this table it is seen that $^2P_{3/2}$ shows a great discrepancy, in that the observed $g$-value is lower than the *LS*-value, while that calculated on the basis of Johnson's matrix is higher. This can only mean that even so close to *L–S* coupling as this configuration is, the perturbing effect of the $(^1D_2+s)$ must be taken into account.

More recently, Johnson[9] has studied the $p^2s$ configuration, taking this into account, and the above-mentioned discrepancy then disappears. Table IV gives the comparison.

## As II

The spectrum of As II has been partially classified by Rao.[10] A number of levels have not been completely identified and are designated by letters.

Following is Table V, showing the data relative to the observed patterns of As II. Data followed by # were supplied by the authors upon the basis of the present observations.

Two levels tentatively identified as $5d^3D_2$ and $5d^3F_2$ have been included and several transitions involving them have been classified. It is certain that each of the levels has a $j$-value of two and their apparent $g$-values are consistent with these classifications. Two additional transitions between known levels, apparently not observed by Rao, have been classified and included in Table II.

While, in general, Rao's classifications appear to be correct, the configuration $4s^24p4d$ still seems to be in doubt, especially $4d^1D_2$ and $4d^1P_1$, the Zeeman patterns of whose combinations are inconsistent. In addition to these levels, the

TABLE V. *Zeeman patterns of As II.*

| λ | ν | Classification | Pattern | $g_a$ | $g_b$ |
|---|---|---|---|---|---|
| 2830.5 | 35319 | $4d^2F_3 - F$ | (0) 0.914 | | |
| 2831.3 | 35310 | $4d^2F_2 - D$ | (0) 1.279 | 0.58 | 0.93 |
| 2884.5 | 34657 | $4d^2F_3 - E$ | (0) 1.276 | | |
| 2890.2 | 34589 | $4d^2F_2 - D$ | (.30) 1.01 | 1.07 | 0.95 |
| 3053.5 | 32740 | $4d^2F_2 - 4f^2F_3$ | (0) 1.607 | 0.58 | 1.09 |
| 3058.1 | 32691 | $4d^2F_2 - A$ | (0) 1.289 | | |
| 3116.7 | 32076 | $4d^2F_3 - B$ | (0) 1.165 | | |
| 3843.1 | 26013 | $sp^3{}^3D_3 - 5p^3P_2$ | (0) 1.256 | 1.345 | 1.433 |
| 3931.3 | 25430 | $sp^3{}^3D_1 - 5p^3P_1$ | 0.529 (.877) 1.376 | 0.519 | 1.386 |
| 3945.9 | 25336 | $sp^3{}^3D_2 - 5p^3D_2$ | (0) 1.485 | 1.183 | 1.334 |
| 3948.7 | 25318 | $sp^3{}^3D_2 - 5p^3P_1$ | (0) 1.031 | 1.159 | 1.406 |
| 4006.3 | 24954 | $sp^3{}^3D_3 - 5p^3D_3$ | (0) 1.327 | 1.320 | 1.334 |
| 4065.5 | 24590 | $4d^2D_2 - D$ | .302† .607 .888* | 1.217 | 0.912 |
| 4157.6 | 24045 | $5p^3P_1 - 6s^2P_2$ | (0) .988 | 1.389 | 1.121 |
| 4197.6 | 23816 | $4d^2D_2 - E$ | (0) .83 | | |
| 4208.0 | 23758 | $4d^2P_1 - G$ | (0) 1.226 | | |
| 4225.9 | 23657 | $5p^3D_2 - d$ | (0) .97 | | |
| 4243.3 | 23560 | $5p^1P_1 - 5d^2F_2$ # | (0) .640 | 0.812 | 0.698 |
| 4297.5 | 23263 | $5s^2P_1 - 5p^1D_2$ | .643† 1.05 —* | 1.43 | 1.05 |
| 4299.5 | 23252 | $sp^3{}^3D_2 - 5p^3D_2$ | (0) 1.174 | 1.179 | 1.170 |
| 4315.9 | 23164 | $sp^3{}^3D_1 - 5p^3D_1$ ¶ | (0) 1.002 | | |
| 4324.1 | 23120 | $5p^3P_0 - e$ | (0) .730 | ÷ | 0.730 |
| 4336.9 | 23052 | $sp^3{}^3D_2 - 5p^3D_1$ | (0)† (.280) .894† 1.183 1.463 | 1.183 | 0.897 |
| 4352.3 | 22970 | $5s^1P_1 - 5p^1S_0$ | (0) 1.078 | 1.078 | ÷ |
| 4353.1 | 22966 | $5p^3P_1 - 6s^2P_1$ ¶ | (0) 1.206 | | ÷ |
| 4359.9 | 22930 | $5p^3P_2 - 5d^2D_2$ # | .777 1.110† 1.433† 1.744* | 1.433 | 1.110 |
| 4371.4 | 22870 | $sp^3{}^3D_3 - 5p^3D_2$ | (0) 1.509 | 1.341 | 1.174 |
| 4404.6 | 22692 | $5p^3S_1 - f$ | .410† 1.131 —* | 1.874 | 1.143 |
| 4413.7 | 22651 | $4d^2P_1 - D$ ¶ | .743† 1.071 1.439 | | |
| 4427.4 | 22581 | $4d^2P_1 - C$ | (0) .983 | | |
| 4431.8 | 22558 | $4d^2D_1 - 4f^2F_2$ | (0) .946 | 0.895 | 0.93 |
| 4466.6 | 22382 | $4d^2D_2 - F$ | (0) .985 | | |
| 4507.9 | 22177 | $5p^3P_1 - e$ | 0.723 1.389* | 1.389 | 0.723 |
| 4516.1 | 22137 | $5p^3S_1 - 6s^2P_2$ | .440† 1.152 1.893* | 1.893 | 1.165 |
| 4528.6 | 22076 | $4d^2D_2 - 4f^2F_2$ | .423 .842† 1.285† 1.685* | 1.285 | 0.842 |
| 4539.9 | 22021 | $4d^2D_2 - 4f^2F_2$ | (0) .77 | 1.29 | 1.03 |
| 4549.2 | 21976 | $5p^3D_1 - 5d^2F_2$ # | (0) .55 | 0.90 | 0.67 |
| 4552.4 | 21960 | $5s^2P_1 - 5p^3S_1$ | 1.419 1.895* | 1.419 | 1.895 |
| 4591.0 | 21776 | $5p^3D_3 - 5d^2F_3$ # | .220 .698† 1.174† 1.654* | 1.174 | 0.698 |
| 4602.7 | 21720 | $4d^1D_2 - E$ | (0) 1.440 | | |
| 4617.3 | 21652 | $4d^1D_2 - D$ | (0) .917 | 0.94 | 0.93 |
| 4630.1 | 21592 | $5p^3P_1 - d$ | (0) 1.494 | | |
| 4632.6 | 21580 | $sp^3{}^3D_1 - 5p^1P_1$ # [Rao $4d^1D_2 - C$] | (.325) .497 .808 | 0.497 | 0.808 |
| 4672.7 | 21395 | $5p^1D_2 - f$ | (0) 1.087 | 1.046 | 1.128 |
| 4707.8 | 21235 | $4d^2D_3 - B$ | (0) .593 | | |
| 4730.9 | 21132 | $5s^2P_1 - 5p^2P_2$ | (0) 1.440 | 1.423 | 1.434 |
| 4787.3 | 20883 | $5s^2P_2 - 5p^1D_2$ | (–) .585 (.959) 1.040† 1.491† 1.943 | 1.491 | 1.045 |
| 4799.7 | 20829 | $5p^3D_1 - b$ | (.232) .921 1.086 | 0.906 | 1.104 |
| 4888.8 | 20450 | $5s^2P_0 - 5p^3P_1$ | (0) 1.390 | ÷ | 1.390 |
| 4985.6 | 20052 | $5s^2P_1 - 5p^2P_1$ | (0) 1.413 | 1.430 | 1.395 |
| 5105.7 | 19580 | $5s^2P_1 - 5p^3S_1$ | (0) (.439) 1.085† 1.492 1.902 | 1.492 | 1.902 |
| 5107.8 | 19572 | $5s^1P_1 - 5p^1D_2$ | (0) 1.025 | 1.075 | 1.050 |
| 5231.5 | 19110 | $5s^2P_1 - 5p^3P_0$ | (0) 1.428 | 1.428 | ÷ |
| 5331.5 | 18751 | $5s^2P_2 - 5p^3P_2$ | (0) 1.464 | 1.492 | 1.436 |
| 5385.5 | 18563 | $5p^2P_1 - b$ | (.263) 1.10 1.37 | 1.38 | 1.12 |
| 5472.0 | 18270 | $5s^1P_1 - 5p^3S_1$ | (.853) — 1.91 | 1.06 | 1.91 |
| 5498.0 | 18183 | $5s^2P_0 - 5p^3D_1$ | (0) .887 | ÷ | 0.887 |
| 5558.3 | 17986 | $5s^2P_1 - 5p^3D_2$ | (0) (.289) .903† 1.150 — | 1.439 | 1.171 |
| 5651.6 | 17689 | $5s^2P_2 - 5p^3D_3$ | (0) 1.13 | 1.49 | 1.31 |
| 5657.2 | 17672 | $5s^2P_2 - 5p^3P_1$ | (0) 1.558 | 1.502 | 1.389 |
| 6022.6 | 16599 | $5s^2P_0 - 5p^1P_1$ | (0) .810 | ÷ | 0.810 |
| 6110.7 | 16360 | $5s^1P_1 - 5p^3P_1$ | 1.073 1.386* | 1.073 | 1.386 |
| 6170.3 | 16202 | $5s^2P_1 - 5p^1P_1$ | (.606) .819 1.423 | 1.423 | 0.819 |

* Measured only in perpendicular polarization.
† Stronger lines.
¶ Apparently incorrect classifications.

levels $C$, $E$ and $d$ give inconsistent patterns, while those called $D$, $b$, $e$, $f$ have definitely $j$-values of 3, 1, 1, 2, respectively.

The $g$-values of the $4s^24p5s$ configuration have been calculated according to Houston's method[11] and are compared with the experimental values in Table VI. The agreement is excellent.

TABLE VI. *$4s^24p5s$ configuration of As II.*

| Level | Referred to C. of G. | $\epsilon$ | $g_{calc.}$ | $g_{obs.}$ | $g_{LS}$ |
|---|---|---|---|---|---|
| $^1P_1$ | 79972 | +2225 | 2.402 | 1.073 | 1.075 | 1 |
| $^3P_2$ | 81281 | + 926 | 1 | 1.500 | 1.492 | 1.500 |
| $^3P_1$ | 83662 | −1455 | −1.571 | 1.427 | 1.424 | 1.500 |
| $^3P_0$ | 84059 | −1852 | −2 | ÷ | ÷ | ÷ |

The calculation of the $g$-values of the $4s^24p5p$ configuration is much more complicated, since six parameters must be adjusted to fit three linear equations and give the roots of a quadratic ($j=0$), a cubic ($j=2$), and a quartic ($j=1$) within a reasonable degree of accuracy. By using Johnson's[7] matrices and the following values of the parameters

$\alpha=3900$, $\gamma=-1560$, $a_1=1840$,
$\beta=1600$, $\delta=7360$, $a_2=380$,

the $g$-values were calculated, with Marvin's[12] suggestion of replacing the diagonal term of the energy $W$ by $W_0-g_1\omega+g\omega$ and neglecting terms in $\omega^2$. The comparison of theory and experiment is given in Table VII.

TABLE VII. *The $4s^24p5p$ configuration of As II.*

| Level | ν | Referred to $^3D_3$ Obs. | Calc. | $g_{calc.}$ | $g_{obs.}$ | $g_{LS}$ |
|---|---|---|---|---|---|---|
| $^1P_1$ | 67460 | −3869 | −3845 | 0.800 | 0.812 | 1.000 |
| $^3D_1$ | 65872 | −2281 | −2200 | 0.905 | 0.895 | 0.500 |
| $^3D_2$ | 65675 | −2084 | −2035 | 1.180 | 1.174 | 1.167 |
| $^3P_0$ | 64552 | − 961 | − 960 | ÷ | ÷ | ÷ |
| $^3P_1$ | 63610 | − 19 | 12 | 1.405 | 1.389 | 1.500 |
| $^3D_3$ | 63591 | (0) | (0) | 1.333 | 1.325 | 1.333 |
| $^3P_2$ | 62530 | 1061 | 1030 | 1.435 | 1.433 | 1.500 |
| $^3S_1$ | 61702 | 1889 | 1753 | 1.890 | 1.896 | 2.000 |
| $^1D_2$ | 60399 | 3192 | 3175 | 1.052 | 1.046 | 1.000 |
| $^1S_0$ | 57002 | 6589 | 6590 | ÷ | ÷ | ÷ |

The $g$-sums are 4.992 instead of 5.00 for $j=1$, and 3.655 instead of 3.667 for $j=2$, quite within experimental error, and the general agreement of each level is quite satisfactory.

Several other lines attributed to As II by Rao[10] were also measured and are listed in Table VIII, together with other pertinent infor-

TABLE VIII. *Unclassified lines of As II.*

| | Pattern | | $j_a$ | $j_b$ | $g_a$ | $g_b$ | Suggested combinations |
|---|---|---|---|---|---|---|---|
| 2603.0 | 38406 | (0) 0.704 | | | | | |
| 2959.7 | 33777 | (0) 1.090 | | | | | |
| 3004.0 | 33280 | (.300) 1.198 | 1? | 1? | 1.05 | 1.35 | |
| 4119.8 | 24266 | (0) 1.258 | | | | | |
| 4228.4 | 23643 | (0) 1.302 | | | | | |
| 4302.3 | 23237 | (0) 1.529 | | | | | |
| 4412.3 | 22658 | (0) .497 | 0 | 1 | 0.497 | | $^3D_1$, $j=0$ |
| 4421.1 | 22612 | .498 1.415* | 1 | 1 | 0.498 | 1.415 | $^3D_1$, $^3P_1$ |
| 4447.7 | 22478 | .821 1.179* | 1 | 1 | 0.821 | 1.179 | |
| 4456.9 | 22431 | (0) 1.903 | | | | | |
| 4458.8 | 22421 | (0) 1.025 | | | | | |
| 4474.6 | 22342 | (0) .943 | | | | | |
| 4532.4 | 22057 | .54† 1.00 1.47 | 2 | 1 | 1.47 | 1.00 | $^3P_2$, $^1P_1$ |
| 4543.7 | 22003 | (0) 1.042 | | | | | |
| 4580.9 | 21824 | 0 .44† .97† 1.48* | 2 | 2 | 0.45 | 0.98 | $^3F_2$, $^1D_2$ |
| 4619.6 | 21641 | (0) 1.188 | | | | | |
| 4627.8 | 21602 | 1.05† 1.50 —* | 2 | 1 | 1.50 | 1.95 | $^3S_1$, $^3P_2$ |
| 5043.4 | 19822 | (0) .853 | | | | | |
| 5161.3 | 19370 | (.565) .867 1.462 | 1 | 1 | 1.454 | 0.875 | $^3P_1$, $^1P_1$ |
| 5497.1 | 18186 | (0) 1.044 | | | | | |
| 5685.7 | 17583 | (0) .917 | | | | | |
| 5838.2 | 17124 | (.07) 1.468 | 1 | 1 | 1.43 | 1.50 | $^3P_1$, $^3P_1$ |

* Measured only in perpendicular polarization.
† Stronger lines.

mation gleaned from their Zeeman patterns.

## As III

Of the spectrum of As III only two lines were found to be resolved, the principal doublet of this spectrum[13]

| | | | | | |
|---|---|---|---|---|---|
| 3922.6 | 25486 | $5s^2S_{1/2}-5p^2P_{3/2}$ | (0.347) | 1.005† | 1.666 |
| 4037.2 | 24763 | $5s^2S_{1/2}-5p^2P_{1/2}$ | (0.669) | 1.327 | |

† Stronger lines.

yielding $g$-values

| | |
|---|---|
| $^2S_{1/2}$ | 1.996 |
| $^2P_{1/2}$ | 1.333 |
| $^2P_{3/2}$ | 0.658 |

which are, within experimental error, the $LS$-values, 2, 4/3, 2/3.

In conclusion, the authors wish to express their gratitude to Dr. R. A. Loring for his many suggestions and valuable assistance during the progress of this work.

### BIBLIOGRAPHY

1. Green and Loring, Phys. Rev. **30**, 574 (1927); **43**, 457 (1933).
2. Meggers and De Bruin, Bur. Standards J. Research **3**, 765 (1929).
3. Rao, Proc. Roy. Soc. **A125**, 244 (1929); Proc. Phys. Soc. London **44**, 594 (1932).
4. Inglis, Phys. Rev. **38**, 377 (1931).
5. Inglis and Johnson, Phys. Rev. **38**, 1642 (1931).
6. Löwenthal, Zeits. f. Physik **57**, 828 (1929); Green and Loring, Phys. Rev. **31**, 707 (1928).
7. Johnson, Phys. Rev. **38**, 1628 (1931).
8. Goudsmit, Phys. Rev. **35**, 1325 (1930).
9. Johnson, Phys. Rev. **39**, 197 (1932).
10. Rao, Proc. Phys. Soc. (London) **44**, 343 (1932); Ind. J. Phys. **7**, 561 (1933).
11. Houston, Phys. Rev. **33**, 297 (1929).
12. Marvin, Phys. Rev. **44**, 818 (1933).
13. Rao and Narayan, Zeits. f. Physik **57**, 867 (1929).

# The Spectrum of AsO

F. A. JENKINS AND L. A. STRAIT, *University of California*

(Received December 3, 1934)

The band-heads of two systems due to AsO have been measured, and the following equations deduced as the best representation of the vibrational structure

$$A: \quad \nu = \begin{cases} 31{,}655.8 \\ 30{,}631.1 \end{cases} + 683.8(v'+\tfrac{1}{2}) - 9.42(v'+\tfrac{1}{2})^2 - 966.6(v''+\tfrac{1}{2}) + 4.92(v''+\tfrac{1}{2})^2$$

$$B: \quad \nu = \begin{cases} 39{,}862.0 \\ 38{,}838.3 \end{cases} + 1098(v'+\tfrac{1}{2}) - 6(v'+\tfrac{1}{2})^2 - 966.6(v''+\tfrac{1}{2}) + 4.92(v''+\tfrac{1}{2})^2.$$

The intensity distribution in system $A$ is normal, but in system $B$ the $v'=0$ progression is predominant. This is explained by predissociation, and a value of 4.93 volts is found for the heat of dissociation of AsO.

THE only previous measurements of the bands here ascribed to diatomic arsenic oxide are those of de Watteville,[1] who photographed the ultraviolet spectrum of a flame fed with different arsenic solutions. Because of the small dispersion used, his measurements were accurate to only 0.5A. In the present work, the spectrum was excited by a discharge through the vapors of arsenic and arsenic oxide in a sealed tube, and, considered in connection with de Watteville's work, the experimental conditions indicate that the bands belong to the oxide. This origin is verified, as shown below, by a comparison of the bands with those of the homologous molecules PO and NO. Arsenic consists of a single isotope of mass-number 75, and the chief interest of this spectrum lies in the fact that it extends our knowledge of the spectra of the oxides of the nitrogen group a step further.

## EXPERIMENTAL DATA

The discharge tube was made entirely of quartz, with a constricted portion 5 cm long and 3 mm in diameter. A plane window was fused on one end, and the other end was sealed off after the introduction of the arsenic oxide and 2 cm of helium. Arsenic was prepared by the thermal decomposition of arsine, and subsequently oxidized by contact with the air. The discharge was obtained by using external electrodes connected to a power oscillator[2] of 5 kw capacity oscillating at a wavelength of 80 m. At room temperature the spectrum of pure helium was obtained, but upon heating to about 400°C the discharge turned a greenish blue. In this stage the spectrum of AsO was strong enough to be photographed in the second order of the 21-foot grating with an exposure of ½ to 4 hours. Iron comparison spectra taken before and after the bands showed no relative shift. In the region λ2327 to λ3091 standards were taken from Jackson's measurements[3] of the iron arc wavelengths.

Two band systems were found, of which that of shorter wavelength corresponded to de Watteville's description. Fig. 1 shows the two regions of the spectrum containing the most intense portions of these systems. The rotational structure is only partially resolved. Each head is a close doublet, and, as will be seen from the measurements of Table I, the double heads are associated in pairs of a constant frequency separation which is the same (1024 $cm^{-1}$) in both systems. Hence we evidently have a wide electronic doublet, which represents a splitting of the lower state because this state is common to the two systems (cf. Eqs. (1) and (2), below). The two components of the close doublets are probably $R$ and $Q$ heads in system $A$, which is shaded to the red, and $P$ and $Q$ heads in system $B$, which is shaded to the violet. In deriving equations to represent the vibrational structure, the $Q$ heads

[1] M. C. de Watteville, Zeits. f. wiss. Phot. **7**, 279 (1909).

[2] The electrical circuit used here, and a description of the demountable oscillator tube, will be found in a paper by D. H. Sloan, R. L. Thornton and F. A. Jenkins to appear soon in the Rev. Sci. Inst.

[3] C. V. Jackson, Proc. Roy. Soc. **A130**, 395 (1931).

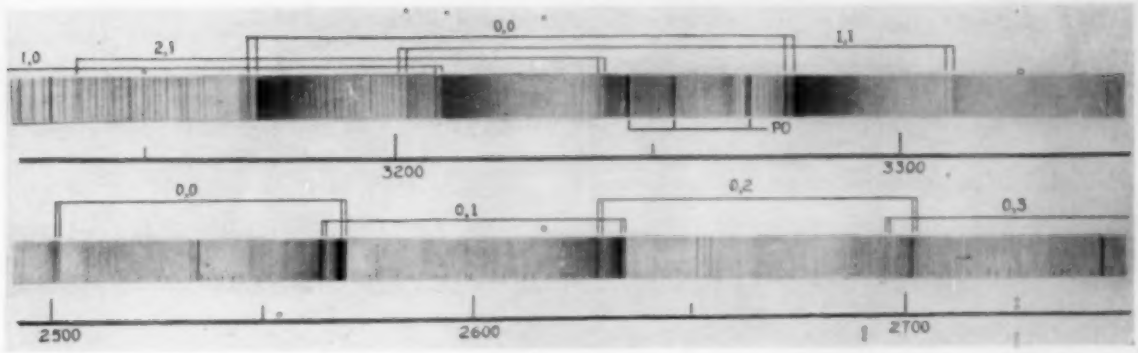


FIG. 1. Enlargements of the AsO bands from first order plates. In the upper system (system *A*), the 0,0 band of the corresponding system in PO appears as an impurity.

TABLE I. *Band-head frequencies in the spectrum of AsO.*

*System A*

| $v'$ \ $v''$ | 0 | 1 | 2 |
|---|---|---|---|
| 0 | 31,531.8 (3) | 30,564.2 (0) | |
| | 31,513.9 (8) | 30,556.6 (3) | |
| | 30,505.5 (8) | 29,552.3 (3) | |
| | 30,487.9 (10) | 29,531.9 (3) | |
| 1 | 32,192.8 (4) | 31,236.9 (1) | |
| | 32,179.1 (5) | 31,221.8 (4) | |
| | 31,167.0 (4) | 30,212.2 (2) | |
| | 31,153.3 (6) | 30,197.2 (4) | |
| 2 | 32,835.6 (1) | 31,878.7 (0) | — |
| | 32,824.7 (2) | 31,866.9 (3) | 30,919.6 (2) |
| | — | 30,855.0 (3) | 29,910.0 (1) |
| | — | 30,842.4 (6) | 29,896.6 (3) |
| 3 | | — | |
| | | 32,494.5 (1) | |
| | | — | |
| | | — | |

*System B*

| $v'$ \ $v''$ | 0 | 1 | 2 | 3 |
|---|---|---|---|---|
| 0 | 39,929.7 (4) | 38,971.9 (7) | 38,024.6 (4) | 37,086.6 (1) |
| | 39,913.9 (2) | 38,957.5 (3) | 38,010.6 (2) | 37,073.3 (1) |
| | 38,903.7 (9) | 37,947.4 (10) | 37,001.7 (8) | 36,065.3 (2) |
| | 38,887.1 (5) | 37,930.7 (6) | 36,988.1 (4) | 36,053.1 (1) |

were used exclusively. Thus in system *A* the second and fourth heads listed in Table I under each vibrational transition were used, while in system *B*, the first and third were used. The results were as follows:

System *A*

$$\nu = \begin{cases} 31{,}655.8 \\ 30{,}631.1 \end{cases} + 683.8(v'+\tfrac{1}{2}) - 9.42(v'+\tfrac{1}{2})^2 - 966.6(v''+\tfrac{1}{2}) + 4.92(v''+\tfrac{1}{2})^2, \quad (1)$$

System *B*

$$\nu = \begin{cases} 40{,}410.5 \\ 39{,}386.8 \end{cases} - 966.6(v''+\tfrac{1}{2}) + 4.92(v''+\tfrac{1}{2})^2. \quad (2)$$

The mean deviation from the values given by Eqs. (1) and (2) is 0.5 $cm^{-1}$. However, this does not represent the error of measurement, as is shown by the fact that the combination differences show systematic discrepancies due to the finite distance of the $Q$ heads from the origins. Further data on the rotational structure would be necessary if the vibrational constants in these equations were to be much improved.

Another band of system *B* was observed by de Watteville at 40,996.4 and 41,016.6. No trace of this occurs on our plates. If it actually belongs to this system, it probably represents the high-frequency component of the 1,0 band. With this assignment, the value of $\Delta G_1'$ becomes 1086.9, and the system origins are approximately 39,867 and 38,843 $cm^{-1}$. The levels of Fig. 2a are drawn using these values.

## DISCUSSION

Fig. 2 represents the known electronic states of NO, PO and AsO, with the vibration frequencies, $\omega_e$, associated with each and the observed

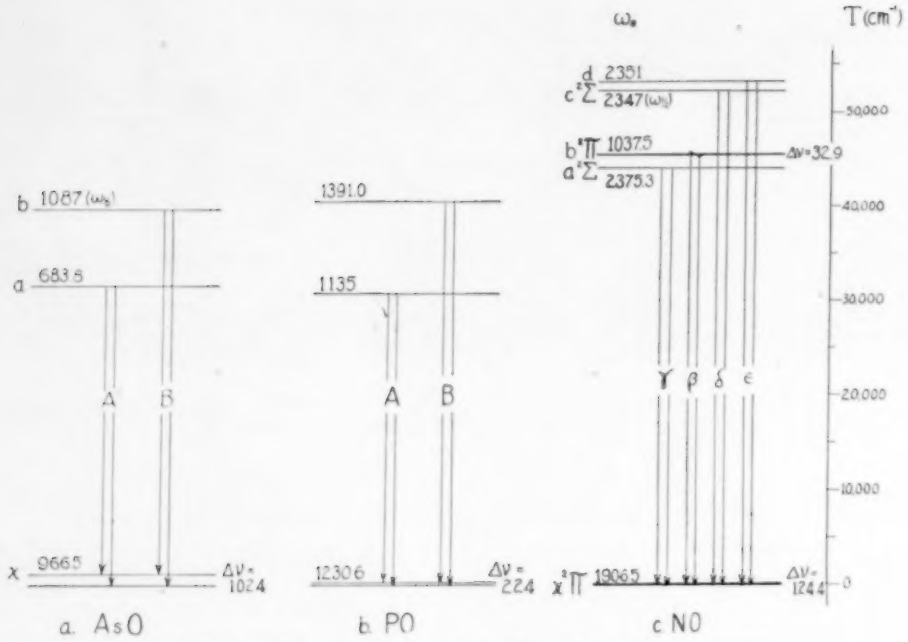


FIG. 2. Known electronic states of the oxides of the nitrogen group.

transitions. In PO, the higher-frequency system (Geuter's *B* system) has been measured very completely by Ghosh and Ball,[4] while the data on the *A* system are taken from unpublished work by R. Grinfeld and one of us. The analogy between the spectra of AsO and PO is very close. In each case we have one loosely-bound and one tightly-bound excited state. The latter was assumed by Ghosh and Ball to correspond to the $a^2\Sigma$ state in NO, and the same analogy can be carried over to the *b* state of AsO. That the *a* state of AsO is of the same character is shown by the similarity of the *A* and *B* systems with regard to number of heads and variations in the separation of the close double heads, the chief difference being that the binding is much weaker in the *a* state. The *A* system shows none of the characteristics of a $^2\Pi$, $^2\Pi$ system, and hence is not the analogue of the $\beta$ system of NO. More probably it is to be correlated with the $\delta$ system, whose upper state is $c\ ^2\Sigma$.

It will be seen from Table I that only the $v'=0$ progression is observed in system *B*. This is the more remarkable because the vibration frequencies in the upper and lower states are not very different, so that we should expect by the Franck-Condon principle the occurrence of fairly long sequences. It indicates strongly the existence of predissociation for the states above $v'=0$. A similar effect is found in the $\beta$ system of NO, where the breaking-off occurs at $v'=4$, and has been ascribed to predissociation by Kaplan.[5] The possible observation of a 1,0 band in the flame spectrum by de Watteville does not rule out the possibility of predissociation, since it is well known that bands from predissociated states may appear in emission at higher pressures.[6]

The marked difference in intensity between the electronic doublet components of system *B*, which can be seen from the visual estimates given in parentheses in Table I and also from inspection of Fig. 1, is another peculiarity of this system, undoubtedly related to the predissociation. The low-frequency component is about twice as strong. Some preferential effect of the predissociation for one of the components of the upper state ($F_1$ or $F_2$ if it is $^2\Sigma$) is here indicated.

A fairly exact value of the heat of dissociation of AsO can be obtained from the predissociation limit. The height of the $v=0$ level of the *b* state is 39,929 $cm^{-1}$, or 4.93 volts. The products of dissociation are almost certainly two normal

[4] P. N. Ghosh and G. N. Ball, Zeits. f. Physik **71**, 362 (1931).

[5] J. Kaplan, Phys. Rev. **37**, 1406 (1931).

[6] G. Herzberg, Erg. Exakt. Naturw. **10**, 207 (1931).

atoms, $^4S$ and $^3P$ of As and O, respectively, since there are a number of repulsive states derived from this combination. Furthermore, a linear extrapolation to convergence of the vibrational levels of the normal state gives 46,943 $cm^{-1}$, and such a procedure usually leads to values which are 20 to 30 percent too high. Therefore we conclude that 4.93 volts is a reliable value for the heat of dissociation.

During the present investigation, there appeared a report of work on the AsO bands by Shawhan and Morgan.[7] Their analysis of system $A$ is different from ours, in that the electronic doubling is given as 644 $cm^{-1}$, and the vibration frequency in the upper state 372 $cm^{-1}$. In view of the good agreement we find for the doubling in the two systems, and of the fact that 372 $cm^{-1}$ is almost impossibly low in comparison to 966 for the normal state, there seems no doubt as to the correctness of our values for this system. These authors have apparently mistaken the vibration frequency in the upper state for the electronic difference. Their analysis of system $B$ is in essential agreement with ours, and extends it to higher vibrational states in the upper state by the equation $G'=1098(v'+\frac{1}{2})-6(v'+\frac{1}{2})^2$. Assuming the correctness of these constants, we calculate the origins of system $B$ to be 39,862.0 and 38,838.3 $cm^{-1}$. In their preliminary report, Shawhan and Morgan give no statement about the specific bands with $v'>0$ which are observed, nor about their intensities. It is stated, however, that the bands were excited in the arc and the flame in emission, and also observed in absorption in the flame. If our conclusions are correct as to the predissociation, it seems probable that these additional bands were observed in absorption.

[7] E. N. Shawhan and F. Morgan, Phys. Rev. **47**, 199A (1935) (St. Louis Meeting, 1934).

JANUARY 15, 1935 PHYSICAL REVIEW VOLUME 47

# A New Type of Expansion in Radiation Problems

W. W. HANSEN,* *Stanford University*

(Received August 9, 1934)

A new type of expansion of $\mathbf{i}(1)e^{ikr_{12}}/r_{12}$ is developed. Here $\mathbf{i}$ is a vector function of the spherical coordinates denoted by 1 and $r_{12}$ is the distance between two points denoted by 1 and 2. This expansion is used in the solution of Maxwell's equations and a simple general expression is found for the energy radiated from a known current distribution. A brief application to Dirac's theory of radiation is given. An expansion for $\mathbf{i}(1)/r_{12}$ is developed which can be used to find the vector potential due to a steady current distribution.

THE well-known expansion of $e^{ikr_{12}}/r_{12}$ in terms of spherical harmonics and half-order Bessel functions provides a method of evaluating $\int(e^{ikr_{12}}/r_{12})\rho(1)d\tau_1$, which is a solution of the inhomogenous wave equation. But the same method is not very satisfactory for the solution of the corresponding vector wave equation because in any coordinates except Cartesian it is rather difficult to keep the various components separate. In the present paper a new type of expansion is found which avoids this difficulty.

Guided somewhat by the expansion for the scalar case we anticipate an expansion of the form

$$\mathbf{i}(1)e^{ikr_{12}}/r_{12}=\sum a_{kl}\mathbf{A}_k'(2)\mathbf{A}_l(1)\cdot\mathbf{i}(1). \quad r_2>r_1 \quad (1)$$

Here vectors are in bold faced type, and the $\mathbf{A}$'s are solutions of the vector wave equation; $\mathbf{A}'$ is to bear the same relation to $\mathbf{A}$ as the Hankel function does to the Bessel function in the scalar case.

Now from each solution of the scalar wave equation we can construct three and only three independent solutions of the vector wave equation; for example in Cartesian coordinates we have only to multiply the scalar function by each of the three unit vectors. There are, of course, an infinite number of possible sets of functions but the ones most suited for present purposes are constructed as follows. Let $\xi$ be a solution of the scalar wave equation, say

* National Research Fellow at Massachusetts Institute of Technology.

$$\xi=\left(\frac{(2l+1)(l-m)!}{8l(l+1)(l+m)!}\right)^{\frac{1}{2}}\frac{1}{(kr)^{\frac{1}{2}}}J_{l+\frac{1}{2}}(kr)P_l^m(\cos\theta)e^{im\varphi}. \tag{2}$$

Then we use the three vector functions[1] defined by

$$\mathbf{A}_{1lm}=(l(l+1))^{\frac{1}{2}}\nabla\xi_{lm}\,;\qquad \mathbf{A}_{2lm}=k\nabla\times(\mathbf{r}\xi_{lm})=-(1/k)\nabla\times\mathbf{A}_{3lm}\,;\qquad \mathbf{A}_{3lm}=-(1/k)\nabla\times\mathbf{A}_{2lm}. \tag{3}$$

$\mathbf{A}'$ is obtained by replacing the $J(kr)$ in $\xi$ by $H^{(1)}(kr)$. If $k$, $l$ and $m$ were to range through all allowed values the resulting set of functions would be complete but here $k$ is always considered as constant.

To determine the coefficients $a_{kl}$ we first investigate the normalizing integrals and the orthogonality of our functions. Integrating between spheres of radius $R_1$ and $R_2$ we find

$$\begin{aligned}
&(2l+1)\int\mathbf{A}_1'\cdot\bar{\mathbf{A}}_1'd\tau=(lI_{l-1}+(l+1)I_{l+1}), && \int\mathbf{A}_2'\cdot\bar{\mathbf{A}}_2'd\tau=I_l,\\
&(2l+1)\int\mathbf{A}_3'\cdot\bar{\mathbf{A}}_3'd\tau=((l+1)I_{l-1}+lI_{l+1}), && \int A_1'\cdot\bar{\mathbf{A}}_2'd\tau=0,\\
&(2l+1)\int\mathbf{A}_1'\cdot\bar{\mathbf{A}}_3'd\tau=(l(l+1))^{\frac{1}{2}}(I_{l-1}-I_{l+1}), && \int\mathbf{A}_2'\cdot\bar{\mathbf{A}}_3'd\tau=0,\\
&I_l=\frac{\pi k^2}{2}\int_{R_1}^{R_2}\left|\frac{1}{(kr)^{\frac{1}{2}}}H^{(1)}_{l+\frac{1}{2}}(kr)\right|^2r^2dr\sim\frac{R_2-R_1}{2}, && k(R_2-R_1)\gg l.
\end{aligned} \tag{4}$$

We note that the functions are not quite orthogonal. As things work out it seems much simpler not to orthogonalize. Some of these results are obtained most easily by using the polar coordinate components of the $\mathbf{A}$'s, others by using Cartesian components. The polar components are quite simple expressions but the Cartesian components are a little hard to write down and since their use is quite essential, both here and in the integrals to follow, it is worth while to indicate that they may be obtained rather directly in the following way. It is readily seen that the $z$ components of $\mathbf{A}_1$, $\mathbf{A}_2$, $\mathbf{A}_3$ may be obtained by operating on $\xi$ with the following

$$\begin{gathered}
(l(l+1))^{\frac{1}{2}}\partial/\partial z,\\
k\left(y\frac{\partial}{\partial x}-x\frac{\partial}{\partial y}\right),\quad \left(2+x\frac{\partial}{\partial x}+y\frac{\partial}{\partial y}+z\frac{\partial}{\partial z}\right)\frac{\partial}{\partial z}+k^2z;
\end{gathered} \tag{5}$$

the other components are obtained similarly after cyclic permutations of $x$, $y$, $z$ in the operators above. If now we write our solutions of the scalar wave equation $\xi$ in Whittaker's general form,[2] the operations are readily carried out and on putting $P_l^m(\cos u)\sin u e^{im\nu}$ for Whittaker's $f(u,v)$ we find the various Cartesian components expressed as functions of polar coordinates. The components of $\mathbf{A}'$ may be found similarly or by substituting $H^{(1)}$ for $J$ in the components of $\mathbf{A}$.

We next evaluate the following integrals

$$\begin{aligned}
&\int_{R_1}^{R_2}\mathbf{A}_1'(2)\frac{e^{ikr_{12}}}{r_{12}}d\tau_2=\frac{4\pi i}{k}\left[\frac{1}{2l+1}(lI_{l-1}+(l+1)I_{l+1})\mathbf{A}_1(1)+\frac{(l(l+1))^{\frac{1}{2}}}{2l+1}(I_{l-1}-I_{l+1})\mathbf{A}_3(1)\right], \qquad r_1<R_1\\
&\int_{R_1}^{R_2}\mathbf{A}_2'(2)\frac{e^{ikr_{12}}}{r_{12}}d\tau_2=(4\pi i/k)I_l\mathbf{A}_2(1),\\
&\int_{R_1}^{R_2}\mathbf{A}_3'(2)\frac{e^{ikr_{12}}}{r_{12}}d\tau_2=\frac{4\pi i}{k}\left[\frac{(l(l+1))^{\frac{1}{2}}}{2l+1}(I_{l-1}-I_{l+1})\mathbf{A}_1(1)+\frac{1}{2l+1}((l+1)I_{l-1}+lI_{l+1})\mathbf{A}_3(1)\right].
\end{aligned} \tag{6}$$

[1] The first two of these are essentially functions used for different purposes by Mie and others. See G. Mie, Ann. d. Physik **25**, 377 (1908); H. Bateman, *Electrical and Optical Wave Motion*.

[2] Whittaker and Watson, *Modern Analysis*, 4th ed., Par. 18. 61.

The above are obtained by using Cartesian components and the expansion of $e^{ikr_{12}}/r_{12}$ in spherical coordinates. We may remark that equations almost identical with (4) and (6) are obtained if $\mathbf{A}'$ and $\mathbf{A}$ are interchanged.

Considering the left-hand side of Eq. (1) as a function of the variables 2 (with $r_2 > r_1$) it must be possible to expand it in a series of $A'$s; doing this we find the expansion coefficients to be $(4\pi i/k)\bar{\mathbf{A}}(1)\cdot\mathbf{i}(1)$. Thus we have

$$\mathbf{i}(1)e^{ikr_{12}}/r_{12} = (4\pi i/k)\sum \mathbf{A}_s'(2)\bar{\mathbf{A}}_s(1)\cdot\mathbf{i}(1). \qquad r_2 > r_1 \quad (7)$$

Here $s$ includes all the numbers needed to characterize an $\mathbf{A}$.

## Solutions of Maxwell's Equations and an Expression for the Radiation from a Given Current Distribution

The principal use of this expansion seems to be in connection with Maxwell's equations. Suppose that the charge and current are confined to a finite region, say a sphere of radius $R$, and that they vary sinusoidally in time so that they can be written $\mathbf{i}(xyz)e^{-i\omega t}$, $\rho(xyz)e^{-i\omega t}$. Then all the other quantities will also have a common factor $e^{-i\omega t}$; this we will remove. Then we easily find

$$\begin{aligned} \mathbf{A} &= (i/\omega)\sum a_s \mathbf{A}_s', \\ \mathbf{E} &= (-1/c)\sum (a_{2lm}\mathbf{A}_{2lm}' + a_{3lm}\mathbf{A}_{3lm}'), \\ \mathbf{B} &= (-i/c)\sum (a_{2lm}\mathbf{A}_{3lm}' + a_{3lm}\mathbf{A}_{2lm}'), \\ a_s &= \int \bar{\mathbf{A}}_s\cdot\mathbf{i}\,d\tau, \quad r > R. \end{aligned} \qquad (8)$$

(We use Heaviside-Lorentz units.) The scalar potential is not written since if $\mathbf{i}$ and hence $\mathbf{A}$ are known, everything else may be found without knowledge of $\rho$ or the scalar potential—the converse is not true, of course.

It should be noted that in any practical case, such for example as the computation of the field due to a radio antenna, the series all converge very rapidly because near the origin the $\mathbf{A}$'s vanish like higher and higher powers of $r$ as $l$ increases. Thus $\mathbf{A}_{31m}$ is finite at the origin, $\mathbf{A}_{32m}$ is proportional to $r$ near $r=0$, etc.

From these results it is possible to find a particularly simple expression for the total energy radiated per unit time by a given current distribution. The result is

$$\int \mathbf{S}\cdot d\sigma = (1/2c)\sum (|a_{2lm}|^2 + |a_{3lm}|^2). \quad (9)$$

The form of this last expression suggests that its scope can be extended to include coordinate systems other than spherical. Thus if we consider a complete orthogonal set of vector functions which includes among others $\mathbf{A}_1$, $\mathbf{A}_2$ and $\mathbf{A}_3$ a measure of the radiation from a current distribution is the square of the "norm on the subspace" spanned by $\mathbf{A}_2$ and $\mathbf{A}_3$. To go further we must decide what it is that distinguishes $\mathbf{A}_2$ and $\mathbf{A}_3$ from other functions, for instance $\mathbf{A}_1$. One essential distinction is that $\mathbf{A}_2$ and $\mathbf{A}_3$ have zero divergence, while $\mathbf{A}_1$ has zero curl; the reason this is important is that a current distribution with zero curl cannot radiate and a function with zero curl will have no component in the subspace spanned by the functions with zero divergence.[3] The other important characteristic is of course that $\mathbf{A}_2$ and $\mathbf{A}_3$ are solutions of a wave equation with the proper value of $k$. Suppose now we know a complete set of solutions of the scalar wave equation in some coordinates other than spherical; from each of these we can construct three solutions of the vector wave equation, one lamellar and two solenoidal. All the latter functions could of course be obtained (assuming them to be orthogonal inside a sphere) by a rotation of the subspace spanned by $\mathbf{A}_2$, $\mathbf{A}_3$; but the norm on the subspace is invariant under this rotation so that the total radiation can be computed exactly as before by summing the squares of the coefficients of the expansion of $\mathbf{i}$.

The only restriction on the functions used that has not been mentioned is that it must be possible to normalize the functions in the same way the $\mathbf{A}$'s are normalized, i.e., so that the average value of $|\mathbf{A}|^2$ over the surface of a sphere becomes asymptotic to $(\sin(kr+\delta)/r)^2$ as

[3] Provided the function vanishes properly at infinity. The lamellar function obtained by dividing a current which is zero outside a finite region into lamellar and solenoidal parts satisfies this requirement.

$r \to \infty$. Unless some rational way can be found to normalize the functions resulting from other choices of coordinates this seems to limit the method outlined above to spherical polar, prolate spheroidal, oblate spheroidal, confocal ellipsoidal coordinates, and those designated by Eisenhart[4] as Type VI.

## Treatment of the Quantum-Mechanical Radiation Problem

The functions $\mathbf{A}_2$, $\mathbf{A}_3$ may be made the basis of a rather neat treatment of Dirac's[5] theory of the radiation from an atom. Thus consider a large spherical hohlraum of radius $R$ and let this be filled with radiation describable by a vector potential $\mathbf{A}(\nabla \cdot \mathbf{A} = 0)$. This $\mathbf{A}$ can be expanded in a series in which only functions of the type $\mathbf{A}_2$ and $\mathbf{A}_3$ will appear.

$$\mathbf{A} = \sum u_s \mathbf{A}_s. \tag{10}$$

The $u_s$ are functions of the time only and we may treat them as coordinates, since if we know them we know the radiation field. Introducing momenta conjugate to these coordinates, and changing units for convenience, we can write the energy of the field in Hamiltonian form

$$\begin{gathered} W = \sum (\tfrac{1}{2} p_s^2 + 2\pi^2 \nu_s^2 q_s^2); \quad q_s = \alpha_s^{\frac{1}{2}} u_s; \\ p_s = (1/\alpha_s^{\frac{1}{2}})(\partial W/\partial u_s); \quad \alpha_s = (1/c^2)(R/2). \end{gathered} \tag{11}$$

If now there is an atom in the hohlraum and we know the energy of interaction between it and the field, we can treat this interaction as a perturbation and so find the probability that the atom will change (say) from state two to state one and a radiation field oscillator of type $s$ will simultaneously change from the $n$th to the $(n+1)$st state. Taking the interaction energy to be $(1/c)\mathbf{A} \cdot i e^{2\pi i \nu t}$ the result is

$$\frac{(n+1)R}{2h\nu c\alpha_s} \left| \frac{1}{c} \int \mathbf{A}_s \cdot i d\tau \right|^2. \tag{12}$$

For the reverse transition $(n+1)$ is replaced by $n$. The radius of the hohlraum $R$ enters because there are $2Rd\nu/c$ radiation components in $d\nu$ of type $s$ and one must sum over these. Remembering that $n = \rho_\nu c^3/8\pi h\nu^3$ we see that we obtain both the $A$ and $B$ coefficients of Einstein. Thus

$$\mathbf{A}_{s,\,21} = (c/h\nu) \left| (1/c) \int \mathbf{A}_s \cdot i d\tau \right|^2. \tag{13}$$

If for convenience we put the atom at the origin of coordinates the point of the present method of calculation is plain; the dipole, quadrupole, etc., types of radiation are completely and naturally separated. Thus transitions involving radiation of type $\mathbf{A}_{31m}$ are generally much stronger than those associated with $\mathbf{A}_{32m}$ or $\mathbf{A}_{21m}$ because the former is finite at the origin whereas the latter two vanish like $r$. We notice that the designations dipole, quadrupole, etc., are not sufficient to describe the various types of radiation, for example, radiation of type $\mathbf{A}_{21m}$ is in general weak compared with the dipole type $\mathbf{A}_{31m}$ but has almost the same symmetry properties. To get a complete description then radiation of the third type with $l = 1, 2 \cdots$ will be called electric dipole, quadrupole, etc., and radiation of the second general type will be designated as magnetic dipole, etc.

Without more definite knowledge of the current distribution it cannot be said whether the electric quadrupole or the magnetic dipole will be stronger; one easily can think of cases where either one but not the other is zero.[6]

The relative intensities of the various Zeeman components can be computed by the present method but the results will not be given as they have already been obtained as far as the quadrupole terms.[7, 8] These formulas can be derived from quite general principles by group theory or by the methods first used for the dipole case by Honl[9] and Kronig and Goudsmit.[10] In connection with the latter we may mention that for given $l$ a sum of $\mathbf{A}_s$ can be built up which gives radiation that is unpolarized and with intensity independent of angle.

---

[4] L. P. Eisenhart, Annals of Math. **35**, 284 (1934); Phys. Rev. **45**, 427 (1934).

[5] P. A. M. Dirac, Proc. Roy. Soc. **A114**, 243 (1927).

[6] For examples of actual cases where the magnetic dipole term is important see E. U. Condon, Astrophys. J. **79**, 217 (1934).

[7] A. Rubinowicz, Zeits. f. Physik **53**, 267 (1929).

[8] H. C. Brinkman, Dissertation, Amsterdam.

[9] H. Honl, Zeits. f. Physik **31**, 340 (1925).

[10] R. de L. Kronig and S. Goudsmit, Naturwiss. **13**, 90 (1925).

It is of interest to note that exactly the same results for the Einstein $A$ coefficients can be obtained by computing in a classical way the radiation from an atom with a given current distribution. By Eq. (9) it is seen that the Einstein $A$ is that given by Eq. (13) except for a factor of two that appears in such cases as this.[11]

## The Vector Potential in the Steady Current Case

It is of some interest to investigate the expansion of $\mathbf{i}(1)/r_{12}$ even though use of the expansion does not seem to lead to any results not previously known, with the possible exception of a formula similar to Eq. (9) for the inductance of a coil. We might start by letting $k$ approach zero in the expressions above but this is likely to be rather awkward as the $\mathbf{A}$'s all approach zero while the $\mathbf{A}''$s become infinite. All told it seems best to start anew in the same way as before by inventing three vector functions satisfying a vector Laplace equations and developing an expansion of $\mathbf{i}(1)/r_{12}$ in terms of these. Such functions are

$$\begin{aligned}
&\boldsymbol{A}_1=\mathbf{r}\xi-[1/(2l+3)]\nabla(r^2\xi),\\
&\boldsymbol{A}_2=\nabla\times\boldsymbol{A}_1=\nabla\times(\mathbf{r}\xi),\\
&\boldsymbol{A}_3=\nabla\times\boldsymbol{A}_2=\cdot\nabla\nabla\boldsymbol{A}_1, \qquad (14)\\
&\xi=\left[\frac{(l-m)!}{l(l+1)\,(l+m)!}\right]^{\frac{1}{2}} r^l P_l{}^m e^{im\phi}.
\end{aligned}$$

The functions $\boldsymbol{A}'$ are the same except that the $r^l$ in $\xi$ is replaced by $r^{-l-1}$ and the $-1/(2l+3)$ in the definition of $\boldsymbol{A}_1$ is changed to $+1/(2l-1)$. In the limit $k\to 0$ and taking no account of constant factors

$$\mathbf{A}_2\to\boldsymbol{A}_2,\quad \mathbf{A}_1\to\boldsymbol{A}_3,\quad \mathbf{A}_3\to\boldsymbol{A}_3 \text{ and } \mathbf{A}_3-(l+1)\mathbf{A}_1\to\boldsymbol{A}_1.$$

[11] J. Frenkel, *Elementary Theory of Wave Mechanics*, Oxford, p. 134.

There is an interesting crossing over of the functions in the integrals that follow

$$\int_{R_1}^{R_2}\frac{\boldsymbol{A}_1'(2)}{r_{12}}d\tau_2=U_1\boldsymbol{A}_3(1),$$

$$\int_{R_1}^{R_2}\frac{\boldsymbol{A}_2'(2)}{r_{12}}d\tau_2=U_2\boldsymbol{A}_2(1),$$

$$\int_{R_1}^{R_2}\frac{\boldsymbol{A}_3'(2)}{r_{12}}d\tau_2=U_3\boldsymbol{A}_1(1), \qquad r_1<R_1$$

with

$$U_1=[4\pi/(2l-1)^2(2l-3)(l+1)](1/R_1{}^{2l-3}-1/R_2{}^{2l-3}),$$

$$U_2=[4\pi/(2l-1)(2l+1)](1/R_1{}^{2l-1}-1/R_2{}^{2l-1}),$$

$$U_3=(4\pi l/2l+1)(1/R_1{}^{2l+1}-1/R_2{}^{2l+1}).$$

Also

$$\int_{R_1}^{R_2}\boldsymbol{A}_i'\cdot\bar{\boldsymbol{A}}_j'd\tau=0 \quad (i\neq j)$$

$$\int_{R_1}^{R_2}\boldsymbol{A}_i'\cdot\bar{\boldsymbol{A}}_i'd\tau=U_i,$$

and

$$\mathbf{i}(1)/r_{12}=\sum\boldsymbol{A}_s'(2)\bar{\boldsymbol{A}}_s(1)\cdot\mathbf{i}(1). \qquad r_1<r_2$$

If the vector potential and the magnetic field due to a given steady current are determined by means of this expansion, it will be found that $B$ is apparently a linear combination of $\boldsymbol{A}_2$ and $\boldsymbol{A}_3$. Actually, however, the terms in $\boldsymbol{A}_2$ vanish because their coefficients depend on integrals of the form $\int\boldsymbol{A}_3\cdot\mathbf{i}d\tau$ and these are zero because $\nabla\cdot\mathbf{i}=-(1/c)\dot{\rho}=0$. We note that the electric field due to a stationary charge distribution can also be expressed by using $\boldsymbol{A}_3$ only.

This work was done while the author was a National Research Fellow at Massachusetts Institute of Technology and he wishes to thank the National Research Council for their aid, and Professor J. C. Slater for extending the hospitality of the laboratory.

# Note on Charge and Field Fluctuations

J. R. OPPENHEIMER, *Department of Physics, University of California*

(Received December 3, 1934)

The field fluctuations which arise from the possibility of creating positron-electron pairs are computed. These fluctuations, which are inescapable in all field measurements, give a simple interpretation of Heisenberg's results on charge fluctuations, and of the divergences which appear in his calculations. The pair-induced fluctuations in the radiation field are in general small of order $\alpha$ compared to those which arise from the corpuscular character of the radiation.

THE fluctuations in charge density to be expected on the basis of the positron theory of Dirac have recently been studied by Heisenberg.[1] Consider a large enclosure of volume $V$, in which there are known to be $N_k$ electrons of momentum $\mathbf{k}$, and $M_k$ positrons of momentum $\mathbf{k}$. Consider further a small volume of dimensions $L_1$, $L_2$, $L_3$, and ask for the average value of the charge in this volume over a time $T$. This is, of course, with $e$ the electronic charge,

$$\bar{e}=e(\bar{m}-\bar{n}); \quad \bar{n}=(L_1L_2L_3/V)\sum_k N_k; \qquad \bar{m}=(L_1L_2L_3/V)\sum_k M_k.$$

The charge in this volume will, however, fluctuate about its mean value, and these fluctuations $(\Delta e)^2$ can now be divided, as Heisenberg has shown, into three sets of terms:

($\alpha$) vacuum terms, which are present when $N=M=0$, and which have no analogue in non-relativistic theory.

($\beta$) terms linear in $N_k$, $M_k$. These reduce to their classically expected value

$$(\Delta e)^2=e^2(\bar{n}+\bar{m}) \tag{1}$$

for space time regions large compared to those within which the electrons and positrons can be localized. When, however, for all electrons and positrons present

$$T\ll\hbar(m^2c^4+c^2k^2)^{-\frac{1}{2}}; \quad L_i\ll\hbar(m^2c^2+k_i^2)^{-\frac{1}{2}}$$

($k_i$ the component of momentum parallel to $L_i$), then these fluctuations tend to vanish. The deviations from (1) under these circumstances are an immediate consequence of the limitations on the localizability of the particles.

($\gamma$) negative terms quadratic in the $N$'s and $M$'s, which give the familiar reduction, to be expected on the basis of the exclusion principle, in the fluctuations of a dense Fermi gas.

It is with the vacuum terms that Heisenberg is chiefly concerned. These not only do not vanish, but for a sharply limited spatio temporal region are infinite. This result can only be interpreted as a consequence of the infinite disturbance produced when we try to measure the charge in a sharply defined region; and Heisenberg has, in fact, shown that if we take the boundaries of our spatial volume "spread out" over a distance $b$, then we get in general finite fluctuations. Thus

$$\begin{aligned}(\Delta e)^2 &\sim e^2L^2/bcT \text{ for } cT\ll b\ll L;\ cT\ll\lambda=\hbar/mc.\\ &\sim e^2L^2\lambda/bc^2T^2 \text{ for } cT\ll b\ll L;\ cT\gg\lambda.\end{aligned} \tag{2}$$

These conclusions lose at once their paradoxical character, if we consider the experimental arrangement by which we might measure the charge. To do this it is only necessary to measure the normal component of the electric field over the surface of the volume in which we are interested. These field measurements will give fluctuating results, and these fluctuations will correspond to those of the charge within the volume. We have thus to consider the fluctuations in the longitudinal component of the electric intensity, averaged over a time $T$, and a slab of dimensions $L_1$, $L_2$, $L_3$.

These field fluctuations are given by an integral of the form

$$(\Delta\mathcal{E}_{||})^2 = \frac{2^6\pi^{-4}e^2}{L_1^2L_2^2L_3^2c^2T^2}\int d\mathbf{k}\int d\mathbf{k}'\frac{\epsilon\epsilon'-\mathbf{k}\cdot\mathbf{k}'-\mu^2}{\epsilon\epsilon'|\mathbf{k}-\mathbf{k}'|^2}\Pi \tag{3}$$

[1] W. Heisenberg, Verh. d. Sächs. Akad. **86**, 317 (1934).

with

$$\epsilon=(\mu^2+k^2)^{\frac{1}{2}};\quad \epsilon'=(\mu^2+k'^2)^{\frac{1}{2}} \text{ and } \mu=mc/\hbar=1/\lambda.$$

$$\Pi=\frac{\sin^2(c/2)(\epsilon+\epsilon')T}{(\epsilon+\epsilon')^2}\cdot\frac{\sin^2\frac{1}{2}(k_1-k_1')L_1}{(k_1-k_1')^2}\cdot\frac{\sin^2\frac{1}{2}(k_2-k_2')L_2}{(k_2-k_2')^2}\cdot\frac{\sin^2\frac{1}{2}(k_3-k_3')L_3}{(k_3-k_3')^2}.$$

The integrand differs from that given by Heisenberg for the charge fluctuations essentially by the factor $|\mathbf{k}-\mathbf{k}'|^{-2}$. This integral converges, and may be evaluated when we make limiting assumptions about the relative magnitude of the lengths $cT$, $L_i$, $\lambda$. We thus find

| for | | $(\Delta\mathcal{E}_{\parallel})^2\sim$ |
|---|---|---|
| all $L_i\gg\lambda$<br>$cT\gg\lambda$<br>$L\leqq cT$ | | $\dfrac{e^2\lambda}{L_1L_2L_3c^2T^2}$ |
| all $L_i\gg cT$<br>$cT\ll\lambda$<br>$L_i\leqq\lambda$ | | $\dfrac{e^2}{L_1L_2L_3cT}$ |
| all $L_i\ll\lambda$<br>$L_i\ll cT$<br>$cT\leqq\lambda$ | $L_1\backsimeq L_2\backsimeq L_3\backsimeq L$ | $\dfrac{e^2}{L^3c^2T^2}$ |
| all $L_i\ll\lambda$<br>$L_i\ll cT$<br>$cT\leqq\lambda$ | $L_1\ll L_2$;<br>$L_2\backsimeq L_3=L$ | $\dfrac{e^2}{L^2c^2T^2}\ln(L/L_1)$ |

(4)

If we apply these results to field measurements in a rectangular slab of area $L^2$, and thickness $b$, and use $\sqrt{(\Delta e)^2}\sim L^2\sqrt{(\Delta\mathcal{E}_{\parallel})^2}$, we get at once for the charge fluctuations the values (2) given by Heisenberg, and the further value, for the case $L\ll cT$

$$(\Delta e)^2\sim e^2(L^2/c^2T^2)\ln(L/b),$$

which is also in agreement with Heisenberg's formulae. We thus see that the infinite fluctuations which we find for a sharply limited volume arise from the measurement of fields in infinitely thin slabs; for these an infinite charge density is required, and the charge fluctuations correspond to the pairs created in the neighborhood of these surface charges.

The calculations of field fluctuations can be extended to include those of the radiation field, which are of the same order of magnitude as those of the longitudinal field. Thus the fluctuations in the average value of the total electric intensity are given by an integral of the form (3), but with an extra factor

$$\frac{(\mathbf{k}-\mathbf{k}')^2\{(\mathbf{k}-\mathbf{k}')^2(\epsilon\epsilon'-\mathbf{k}\cdot\mathbf{k}'-\mu^2)+(\epsilon+\epsilon')^2(\epsilon\epsilon'+3\mathbf{k}\cdot\mathbf{k}'+5\mu^2)\}}{(\epsilon\epsilon'-\mathbf{k}\cdot\mathbf{k}'-\mu^2)[(\epsilon+\epsilon')^2-(\mathbf{k}-\mathbf{k}')^2]^2}.$$

The corresponding integrals can again be evaluated under limiting assumptions about the magnitude of $L$, $cT$, $\lambda$ and lead to results whose order of magnitude agrees in every case with (4).

These fluctuations in the radiation field are not in principle separable from the fluctuations arising from the corpuscular character of electromagnetic radiation. These latter fluctuations have been studied by Bohr and Rosenfeld,[2] who give for them

$$(\Delta\epsilon_r)^2\sim\hbar cL^{-4} \qquad \text{for } L\gg cT,$$

$$(\Delta\epsilon_r)^2\sim\hbar cL^{-2}(cT)^{-2} \qquad \text{for } cT\gg L.$$

To these must be added the fluctuations arising from the creation of matter by the field measurements, so that the total fluctuations are, for instance,

$$(\Delta\epsilon)^2\sim\hbar cL^{-2}(cT)^{-2}(1+e^2/\hbar c);\qquad L\ll cT;\ L\ll\lambda.$$

$$(\Delta\epsilon)^2\sim\hbar cL^{-2}(cT)^{-2}(1+e^2/mc^2L);\quad L\ll cT;\ L\gg\lambda.$$

From the form of these expressions it seems quite doubtful whether the physical significance of the modifications introduced by the pairs can be legitimately evaluated without taking into account the atomicity of the electric charge with which the field measurements are necessarily made.

[2] N. Bohr and L. Rosenfeld, Det. Kgl. Dansk. Vid. Selskap. **12**, 8 (1933).

# Note on the Production of Pairs by Charged Particles

J. R. OPPENHEIMER, *Department of Physics, University of California*

(Received December 3, 1934)

We compute the internal conversion by pair-production of the radiation emitted in the impact of charged particles. When the energy available for pair-production is large compared to $mc^2$, this simple method gives a valid estimate of pair-production by the impact. For electrons of very high energy the probability of pair-production increases as $[\ln (E/mc^2)]^3$.

THE production of pairs by charged particles of high energy has been considered by Furry and Carlson,[1] and by Heitler and Nordheim.[2] In both of these researches the probability of pair production is calculated by an application of the systematic Born-Møller perturbation theory for relativistic impacts. We want here to consider a rather simpler method of treating the problem for the case that the energy available for pair production is very large compared to $mc^2$.

Consider first pair production by the impacts of a heavy charged particle on a nucleus, where we may take the velocity of the particle $v \ll c$, and where, in order that large energies may be available for pair production, we shall suppose that $\mu v^2 \gg mc^2$, where $\mu = M_1M_2/(M_1+M_2)$ is the reduced mass of particle and nucleus. For this case the impact of the two heavy particles and the electromagnetic field produced by the impact can be computed purely classically, and we have to study the production of pairs by this field. For the components of this field of frequency $\nu \gg \nu_0 = mc^2/h$, the wavelength is small compared to the region, of order $\hbar/mc$, in which pair production is important, so that the radiation field of the impact may, despite $v \ll c$, be supposed in this limit to contribute essentially to pair production.

It is easy to calculate the effect of this radiation field, if we neglect altogether the diffraction zone field of the charges. To do this we may use the classical expression for the intensity of the continuous x-ray spectrum. If mass and charge of the two particles are $M_1$, $Z_1e$; $M_2$, $Z_2e$, respectively, then for unit incident flux of impacting particles the intensity per unit frequency of emitted radiation is given by the well-known formula of Kramers

$$I_\nu = 32\pi^2 3^{-\frac{1}{2}} \frac{e^6 Z_1^2 Z_2^2 \zeta^2}{\mu^2 v^2 c^3}, \qquad (1)$$

for $$\nu \leqslant \bar{\nu} = \mu v^2/2h,$$

where $\zeta = (M_1Z_2 - M_2Z_1)/(M_1+M_2)$ is the effective charge. This radiation is dipole radiation, for which the internal conversion coefficient by production of pairs is known.[3] For $\nu \gg \nu_0$, it is given with good approximation by

$$(2\alpha/3\pi)[\ln (2\nu/\nu_0) - 3/5]; \quad \alpha = e^2/\hbar c. \qquad (2)$$

If we take from (1) the number of quanta emitted per unit frequency per unit time, we get, using (2), for the cross section for pair production

$$\sigma = 2Q \int^{\bar{\nu}} (d\nu/\nu)[\ln (2\nu/\nu_0) - 3/5];$$

with $$Q = 16 \cdot 3^{-5/2} \alpha^2 \frac{e^4 Z_1^2 Z_2^2 \zeta^2}{\mu^2 v^2 c^2}, \qquad (3)$$

where the lower limit of the integral over $\nu$ is of order $\nu_0$. For $\bar{\nu} \gg \nu_0$, we thus get

$$\sigma = Q[\ln (\bar{\nu}/\nu_0)]^2. \qquad (4)$$

The estimate which Heitler and Nordheim give for this case is just

$$\sigma \sim Q. \qquad (5)$$

This result they have obtained by applying Born's approximation to the impact of the two heavy particles and the calculation of their field. Although the validity of this method of

[1] W. H. Furry and J. F. Carlson, Phys. Rev. **44**, 237 (1933).

[2] W. Heitler and L. Nordheim, J. de Physique **5**, 449 (1934).

[3] L. Nedelsky and J. R. Oppenheimer, Phys. Rev. **44**, 948 (1933).

treating an impact with $Z_1Z_2 \gg 1$, $v \ll c$, can hardly be established, it probably gives correct results for the special case of the Coulomb field. On the other hand, the fields calculated by Heitler and Nordheim are just the diffraction zone fields which we have neglected; they, in turn, have neglected the radiation field entirely. The fact that for large $\bar{\nu}/\nu_0$, (4) is larger in order of magnitude than (5), may be regarded as a justification for our neglect of the diffraction zone fields, and of the validity, for $\bar{\nu} \gg \nu_0$, of (4). For $\bar{\nu} \sim \nu_0$, on the other hand, (4) and (5) give contributions of the same order of magnitude, so that both fields must be considered.

This same method can be applied to pair production by electrons of energy $E \gg mc^2$. Here we have again to limit ourselves to impacts in which the reaction of the pairs on the impacting electron can be neglected. This restriction, which is also involved in the calculations of Carlson and Furry, means that the energy of the pair shall be only a small part of $E$. As was observed by these authors, and as follows also from our calculations, this restriction does not, for large $E$, affect the order of magnitude of the results. The neglect of the diffraction zone parts of the field of the particles is here even less open to question than in the case of heavy charges.

We have now, however, to use in place of (1) the expression for the continuous radiation from high energy electrons in a Coulomb field, for which Bethe and Heitler[4] give, for $h\nu \ll E$, $h\nu \gg mc^2$,

$$I_\nu = \frac{32\pi Z^2 e^6}{3m^2c^3} \ln (\bar{\nu}^2/\nu\nu_0) \tag{6}$$

with $\bar{\nu} = E/h$.

This radiation is no longer dipole radiation; but for $\nu \gg \nu_0$, the dominant term in the internal conversion coefficient for multipole radiation[5] is again given by

$$(2\alpha/3\pi) \ln (\nu/\nu_0) \tag{7}$$

We thus find, for the cross section for pair production

$$\sigma = (32/9\pi)\alpha^2 Z^2 (e^4/m^2c^4) \int^{\bar{\nu}} (d\nu/\nu) \ln (\nu/\nu_0)[2 \ln (\bar{\nu}/\nu_0) + \ln (\nu_0/\nu)]$$

$$\simeq (64/27\pi)\alpha^2 Z^2 (e^4/m^2c^4)[\ln (\bar{\nu}/\nu_0)]^3. \tag{8}$$

The calculation of internal conversion, and of the radiation by heavy ions, will be unaffected by the screening of the nuclear field by atomic electrons. But as Bethe and Heitler[4] have shown, for $E > mc^2/\alpha Z^{\frac{1}{3}}$, (6) must be modified. Instead we have, again for $h\nu \ll E$,

$$I_\nu = (32\pi Z^2 e^6/3m^2c^3) \ln (199/Z^{\frac{1}{3}}), \tag{9}$$

which leads to

$$\sigma \simeq (16/9\pi)\alpha^2 Z^2 (e^4/m^2c^4) \ln (199/Z^{\frac{1}{3}})[\ln (\bar{\nu}/\nu_0)]^3. \tag{10}$$

Formulae (8) and (10) show that the probability of pair production by a very high energy electron differs from that for a gamma-ray of the same energy by a factor of the order $\alpha[\ln (\bar{\nu}/\nu_0)]^2$. This is in complete agreement with the conclusions of Furry and Carlson. For energies of $5 \times 10^9$ volts, (10) gives for the ratio of these probabilities about 10 percent.

[4] H. Bethe and W. Heitler, Proc. Roy. Soc. **A146**, 83 (1934).

[5] For $\nu \gg \nu_0$, radiation corresponding to multipoles of very high order will be present; for these the use of the asymptotic value (7) for the internal conversion coefficient may be questioned. The true value of the internal conversion coefficient will be smaller than (7). This correction will not affect the dominant term of the result.

# On the Born-Infeld Field Theory of the Electron

EUGENE FEENBERG, *Research Laboratory of Physics, Harvard University*

(Received November 12, 1934)

Since the field equations of the Born-Infeld field theory impose no essential restrictions on the world lines of the singularities, a dynamical condition, equivalent to equations of motion, must be added to complete the theory. The variation problem from which Born and Infeld obtain equations of motion by varying the world lines of the singularities does not appear to be susceptible of generalization to include radiation reaction and, moreover, the equations of motion are not invariant in form under a Lorentz transformation. The definition of a magnetic charge and current vector (which vanishes for an isolated singularity in uniform rectilinear motion) makes possible the derivation from the energy-momentum conservation laws of a relation (Eq. (32)) which is the formal analogue of the dynamical assumption, in the classical theory of electromagnetic mass, that the total force on the electron, including the self-reaction, vanishes. This result is not, however, equivalent to equations of motion because the non-classical part of the field arising from the non-linear character of the field equations always adjusts itself, for arbitrary motion of the singularity, to maintain the relation. In the coordinate system in which the singularity is momentarily at rest the relation simplifies notably and points to a new dynamical condition which appears to be singled out from all other possible conditions by its compelling simplicity. The resulting equations of motion contain the usual radiation resistance term and also higher order terms in the self-interaction.

## I. INTRODUCTION

IN the Born-Infeld[1] theory the electron appears as a coulomb singularity with which is associated in a natural and unforced manner a definite spatial distribution of charge upon which external fields act. The way in which the field changes in going from one world point to a near by point is determined by a system of field equations which also imply the existence of an energy-momentum tensor satisfying a set of divergence equations interpreted as energy-momentum conservation laws.

The principal result of this paper is the derivation from the energy-momentum conservation laws of an equation which is the formal analogue of the dynamical assumption, in the classical theory of electromagnetic mass, that the total force on the electron, including the self-reaction, vanishes. A simple assumption then leads to dynamical equations of motion containing radiation resistance and higher order terms, whereas the method used by Born and Infeld to set up equations of motion does not appear to be susceptible of generalization to include radiation resistance.

## II. THE FIELD EQUATIONS

The building material out of which the Born-Infeld theory is constructed is a single anti-symmetric field tensor of the second rank $p_{kl}$, satisfying the set of divergence equations[2]

$$\partial p^{kl}/\partial x^l = 0. \tag{1}$$

In space vector form (1) becomes[3]

$$\nabla \cdot D = 0, \quad \nabla x H = \partial D/c\partial t. \tag{2}$$

The electron at rest under the action of no forces is characterized by the assumptions that $H$ vanishes identically and $D$ is spherically symmetric. Then necessarily

$$D = -e\nabla(1/r) \tag{3}$$

with $e$ an arbitrary constant of integration which is set equal to the experimental value of the electronic charge. Since $D$ is the gradient of a scalar function its curl vanishes; also the divergence of $H$ vanishes (trivial since $H$ vanishes identically). Hence the stationary electron is described by a field tensor (3) which satisfies the set of equations

$$\begin{aligned} &\nabla \cdot D = 0, \quad \nabla \cdot H = 0, \\ &\nabla x H = 0, \quad \nabla x D = 0. \end{aligned} \tag{4}$$

Turning now to the case of an electron in uniform rectilinear motion we see that (2) and

[1] M. Born and L. Infeld, Proc. Roy. Soc. **A144**, 425 (1934).

[2] To avoid unessential complications only invariance under Lorentz transformations is required of the tensor equations.

[3] Except where otherwise stated the notation throughout is taken from reference 1.

(3) and the fact that $D$ and $H$ together form the six vector $p_{kl}$ imply that the field tensor of the moving electron satifies the complete set of Maxwell's equations[4]

$$\partial p^{kl}/\partial x^l=0, \quad \partial p^{*kl}/\partial x^l=0. \qquad (M)$$

This result is summarized in the statement that the Eqs. (1) and the assumption that the field of the stationary electron is given by (3) imply that the field tensor $p_{kl}$ for a system of electrons, each in uniform rectilinear motion, satisfies the complete set of Maxwell's equations $(M)$. It is of course well known that $M$ possesses solutions (in terms of the retarded potentials for a point charge) for a singularity or group of singularities with arbitrary world lives. Such solutions will be written $\bar{p}_{kl}$.

Interaction between the singularities is brought into the theory through the "Hamiltonian"[5] function $\mathbf{H}=(1+P)^{\frac{1}{2}}-1$ and the variation problem[6]

$$\delta\int\int\int\int \mathbf{H}dxdydzdt=0, \qquad (5)$$

which is to be solved by varying the field tensor $p_{kl}$ subject to the restriction that the comparison tensors remain solutions of (1) and are all equal on the boundaries of the region of integration. It is understood that the world lines of the electrons (the lines in $xyzt$ space on which $p_{kl}$ possesses a singularity of the second order) are not varied nor is any comparison tensor admitted which possesses singularities except on these lines. A necessary and sufficient condition that the variation of the integral vanish is then

$$\partial f^{*kl}/\partial x^l=0 \qquad (6)$$

with $f_{kl}=p_{kl}(1+P)^{-\frac{1}{2}}$. (1) and (6) together will be referred to as the Born-Infeld field equations and denoted by the symbol BI.

The field tensor $p_{kl}$ defined by (3) and the corresponding tensor $f_{kl}$ are, in fact, solutions of the Born-Infeld field equations. Thus for a single unperturbed singularity in uniform rectilinear motion both the Born-Infeld field equations and Maxwell's equations are simultaneously satisfied. This circumstance is of decisive importance in determining the form of the equations of motion.

## III. The Energy-Momentum Tensor

From the field equations Born and Infeld derive energy-momentum conservation equations

$$\partial T_k{}^l/\partial x^l=0, \qquad (7)$$

in which[7]

$$T_k{}^l=(\mathbf{H}+\tfrac{1}{2}f_{rs}p^{rs})\delta_k{}^l-f_{mk}p^{ml} \qquad (8a)$$

$$=\tfrac{1}{2}\{((1+P)^{\frac{1}{2}}+(1+P)^{-\frac{1}{2}}-2)\delta_k{}^l - (f_{mk}p^{ml}+f^{ml}p_{mk}-\tfrac{1}{2}f_{rs}p^{rs}\delta_k{}^l)\}. \qquad (8b)$$

The second form in the definition of $T_k{}^l$ is needed for later developments. It is instructive for the study of the relation between the field and particle forms of the conservation laws to consider the explicit form of the field tensors and the tensor $T_k{}^l$ in the neighborhood of a singularity. A number of definitions are needed for use at this point and later, namely: ${}^v p_{kl}(t)$ the field associated with a singularity, in uniform rectilinear motion, which at the time $t$ is coincident with and moving with the accelerated singularity, ${}^a p_{kl}$ the acceleration field of the classical point charge, ${}^e p_{kl}$ the external field which causes the non-uniform motion, $\bar{q}_{kl}$ the difference between the actual field and the field of a classical point charge moving with the singularity, $\tilde{q}_{kl}$ the difference between the complete field and the sum of external field and classical field, and finally $q_{kl}$ the sum $\tilde{q}_{kl}+{}^e p_{kl}+{}^a p_{kl}$. Then

$$\begin{aligned} \bar{p}_{kl}&={}^v p_{kl}+{}^a p_{kl}, \\ p_{kl}&=\bar{p}_{kl}+\bar{q}_{kl}, \\ &=\bar{p}_{kl}+\tilde{q}_{kl}+{}^e p_{kl}, \\ &={}^v p_{kl}+q_{kl}. \end{aligned} \qquad (9)$$

The assumption that ${}^e p_{kl}$ is small in comparison with unity permits us to write it as a solution of Maxwell's equations. We wish to express the field quantities in terms of ${}^v p_{kl}$, ${}^v f_{kl}$ and $q_{kl}$ retaining only first order terms in $q_{kl}$. The results are

[4] $p_{kl}{}^*$ is the dual tensor; see reference 1, p. 432.
[5] Reference 1, p. 436; $P$ designates the invariant $\frac{1}{2}p_{rs}{}^*p^{*rs}=-\frac{1}{2}p_{rs}p^{rs}$.
[6] Reference 1, p. 436.
[7] Reference 1, p. 436; from the definition of $f_{rs}$, $f_{mk}p^{ml}=f^{ml}p_{mk}$.

$$
\begin{aligned}
&\tfrac{1}{2}p_{rs}p^{rs}=\tfrac{1}{2}\,{}^{v}p_{rs}\,{}^{v}p^{rs}+{}^{v}p_{rs}q^{rs},\\
&\mathbf{H}=\mathbf{H}^{v}-\tfrac{1}{2}\,{}^{v}f_{rs}q^{rs},\\
&(1+P)^{-\frac{1}{2}}=(1+P^{v})^{-\frac{1}{2}}+{}^{v}f_{rs}q^{rs}/(1+P^{v}),\\
&f_{kl}={}^{v}f_{kl}\{1+{}^{v}f_{rs}q^{rs}/2(1+P^{v})^{\frac{1}{2}}\}+q_{kl}/(1+P^{v})^{\frac{1}{2}},\\
&f_{mk}p^{ml}={}^{v}f_{mk}\,{}^{v}p^{ml}+{}^{v}f_{mk}q^{ml}+{}^{v}f^{ml}q_{mk}+\tfrac{1}{2}\,{}^{v}f_{mk}\,{}^{v}f^{ml}\,{}^{v}f_{rs}q^{rs},\\
&T_{k}{}^{l}={}^{v}T_{k}{}^{l}+{}^{q}T_{k}{}^{l},\\
&{}^{v}T_{k}{}^{l}=(\mathbf{H}^{v}+\tfrac{1}{2}\,{}^{v}f_{rs}\,{}^{v}prs)\delta_{k}{}^{l}-{}^{v}f_{mk}\,{}^{v}p^{ml},\\
&{}^{q}T_{k}{}^{l}=-{}^{v}f_{mk}q^{ml}-{}^{v}f^{ml}q_{mk}+\tfrac{1}{2}\,{}^{v}f_{rs}q^{rs}\delta_{k}{}^{l}+\tfrac{1}{2}(F^{v}\delta_{k}{}^{l}-{}^{v}f_{mk}\,{}^{v}f^{ml})\,{}^{v}f_{rs}q^{r},
\end{aligned}
\tag{10}
$$

(with $F=-P/(1+P)=\frac{1}{2}f_{rs}f^{rs}$). In these equations ${}^{v}p_{rs}$, ${}^{v}f_{rs}$, $q_{rs}$ may be replaced by $\bar{p}_{rs}$, $\bar{f}_{rs}$, $\bar{q}_{rs}$.

As a direct consequence of (7) and (10)

$$
\begin{aligned}
\frac{\partial}{\partial x^{l}}\,{}^{q}T_{k}{}^{l}&=-\frac{\partial}{\partial x^{l}}\,{}^{v}T_{k}{}^{l}\\
&=-\frac{\dot{v}_{i}}{c}\frac{\partial}{\partial v_{i}}\,{}^{v}T_{k}{}^{4},
\end{aligned}
\tag{11}
$$

and

$$
\begin{aligned}
-\int\int\int\frac{\partial}{\partial x^{l}}\,{}^{q}T_{k}{}^{l}d\tau&=\frac{\dot{v}_{i}}{c}\frac{\partial}{\partial v_{i}}\int\int\int\,{}^{v}T_{k}{}^{4}d\tau\\
&=\frac{d}{cdt}\int\int\int\,{}^{v}T_{k}{}^{4}d\tau,
\end{aligned}
\tag{12}
$$

integrating about the singularity over a region on the surface of which $P$ is small in comparison with unity. A simple calculation yields[8] (letting $\beta=(1-v^{2}/c^{2})^{-\frac{1}{2}}$)

$$
\begin{aligned}
\int\int\int\,{}^{v}T_{k}{}^{4}d\tau&=(4\pi c/b^{2})m_{0}v_{k}\beta, \quad k=1,2,3,\\
&=(4\pi c/b^{2})m_{0}c\beta, \quad k=4.
\end{aligned}
\tag{13}
$$

The left-hand member of (12) must therefore be interpreted as external force plus radiation resistance. In this way the field conservation laws are transformed into a form appropriate to the particle standpoint. However, the Eqs. (12) are not equations of motion for, as will be shown, the field equations do not in any way restrict the motion.

[8] $m_0$ is the electronic mass; reference 1, p. 446. $b$ is the "absolute" field; reference 1, p. 437.

## IV. The Charge and Current Densities

The equation[9]

$$\partial f^{kl}/\partial x^{l}=4\pi\rho^{k} \tag{14}$$

defines the electric charge and current densities $\rho^{k}$. Let us add the equation

$$\frac{\partial}{\partial x^{l}}p^{*kl}=\frac{\partial}{\partial x^{l}}\bar{q}^{*kl}=4\pi\sigma^{k}, \tag{15}$$

defining the four vector $\sigma^{k}$, and interpret $\sigma^{k}$ as the magnetic charge and current density vector. The preceding discussion enables us to state at once that $\bar{q}_{kl}$ and $\sigma^{k}$ vanish identically in the case of an isolated singularity in uniform rectilinear motion.

## V. The Field Equations for Arbitrary Motions of the Singularities

In this section we show, by sketching a method for the calculation of $\bar{q}_{kl}$, that the field equations do not impose any essential restrictions on the motion of the singularities. It is supposed that the world lines of the singularities are arbitrarily prescribed, subject to the broad restriction that the curvature of any given world line should never exceed in order of magnitude the curvature in the world line of a classical particle moving in the field of all the other singularities. This restriction insures that in the neighborhood of a singularity

$$\partial\bar{f}^{*kl}/\partial x^{l}=O({}^{v}p_{rs}). \tag{16}$$

($O(x)$ is a function which vanishes with the first

[9] Reference 1, p. 441.

power of $x$.) With prescribed world lines $\bar{p}_{kl}$ is a known function of the space-time coordinates, a solution of (1) and hence $\bar{q}_{kl}$ must satisfy the Eq. (1):

$$\partial \bar{q}^{kl}/\partial x^l = 0. \tag{17}$$

Because of (17) there exists a potential vector $\chi_k$ in terms of which

$$\bar{q}_{rs}{}^* = \frac{\partial}{\partial x^r}\chi_s - \frac{\partial}{\partial x^s}\chi_r. \tag{18}$$

Then in the neighborhood of a singularity the field Eq. (6) becomes, with the help of the remark following (10),

$$\frac{\partial}{\partial x^l}\left[(1+\bar{P})^{-1}\left(g^{kr}\frac{\partial}{\partial x^r}\chi^l - g^{ls}\frac{\partial}{\partial x^s}\chi^k\right)\right] - \bar{f}^{*kl}\frac{\partial}{\partial x^l}\left[(1+\bar{P})^{-1}\bar{f}^{*rs}\frac{\partial}{\partial x^r}\chi_s\right] = -\frac{\partial}{\partial x^l}\bar{f}^{*kl} + O(\bar{q}_{rs}{}^2), \tag{19}$$

a set of four non-homogeneous linear partial differential equations of the second order in the unknown functions $\chi_k$ if the remainder term $O(\bar{q}_{rs}{}^2)$ is neglected. The appropriate solution of (19) determines a field tensor $\bar{q}_{kl}$ which is a solution of (17) and also determines the field tensor $\tilde{q}_{kl}$ by means of the equations $\tilde{q}_{kl} = \bar{q}_{kl} - {}^*p_{kl}$. The Eq. (19) is also obtained if $\bar{p}_{kl}$ is interpreted as the *sum* of the fields of the classical point charges on prescribed world lines. $\bar{q}_{rs}$, the difference between $p_{rs}$ and $\bar{p}_{rs}$, is then the non-classical part of the field arising from the nonlinear character of the field equations and, with neglect of the remainder term, is given throughout space by the appropriate solution of (19).

## VI. The Born-Infeld Equations of Motion

The preceding discussion brings up the question how is it possible for Born and Infeld to derive equations of motion from the field equations? The answer is simply that their equations of motion are not consequences of the field equations, but are obtained from the variation problem (5) by putting in place of $p_{rs}$ the tensor ${}^*p_{rs} + {}^e p_{rs}$ and varying the world line in the resulting definite function of the position and velocity of the singularity. It is clear that two distinct variation principles are thus associated with Eq. (5); one yielding the field equations, the other the equations of motion. In this manner they obtain a Lagrangian function[10]

$$\Lambda(r(t), v(t), t) = m_0 c^2/\beta - \int\int\int \varphi_l{}^{(e)}\, {}^*\rho^l d\tau, \tag{20}$$

in which $\varphi_l{}^{(e)}$ is the potential four vector of the external field and ${}^*\rho^l$ is the charge four vector for a singularity in uniform rectilinear motion with the velocity $v$. More generally we might return to the variation problem and, using an approximation to the field of the classical point charge more accurate than ${}^*p_{rs}$, obtain a correction term to be added to (20) of the form (for small values of the velocity)

$$\sum_{i=0}^{N}\sum_{j=1}^{N} a_{ij} v^{(i)} \cdot v^{(j)}, \tag{21}$$

which would contribute a sum of odd derivatives of the velocity to the equations of motion.[11] It does not seem possible to obtain a radiation resistance term (an even derivative of the velocity) from any modification of this form of the variation problem.

In addition to the difficulty in connection with the radiation resistance there is another which seems more fundamental. The equations of motion will be invariant in form only if $\Lambda\beta$ is a scalar invariant. But since the time cross section for the space integration depends on the coordinate system in which the integral is defined, the quantity $\beta\int\int\int\int \varphi_l{}^{(e)}\, {}^*\rho^l d\tau$ is not in general a scalar invariant. This non-invariant result from an apparently invariant procedure appears to arise from the fact that the equation $\delta\int_{t_1}^{t_2}\Lambda dt = 0$ follows from $\delta\int\int\int\int H dx dy dz dt = 0$ only if the space and time integrations separate (i.e., the limits for the time integration are independent of the space coordinates). However the

[10] Reference 1, p. 449.

[11] See Courant-Hilbert *Methoden der Mathematischen Physik*, p. 171 for statement of the variation problem and derivation of the Euler equations for the general case in which $\Lambda$ is a function of derivatives of arbitrary order.

statement that the space and time integrations separate is not invariant and different equations of motion are obtained for different choices of the coordinate system in which the separation occurs.

The interaction of an electron with a plane monochromatic wave supplies a simple illustration of the preceding remarks.[12] In a coordinate system in which the electron is moving momentarily in the direction of propagation of the wave with velocity $v$ the quantity $\beta\int\int\int\varphi_l^{(e)}\rho^l d\tau$ has the value

$$\frac{2e}{cy}\left(\int_0^\infty \frac{\sin yz}{(1+z^4)^{\frac{1}{4}}}dz\right)\beta\frac{dx^l}{dt}\varphi_l^{(e)}(x, y, z, t)$$

with $y=2\pi r_0/\lambda\beta=(2\pi r_0/\lambda_0)(1+v/c)$ ($\lambda_0$ the wavelength measured by an observer moving with the electron). Now $y$ is obviously not invariant, consequently neither is $\Lambda\beta$.

## VII. An Alternative Form of the Conservation Equations

The analysis is facilitated by writing the Eqs. (6) and (15) in the equivalent forms

$$\frac{\partial}{\partial x^k}f_{lm}+\frac{\partial}{\partial x^l}f_{mk}+\frac{\partial}{\partial x^m}f_{kl}=0, \tag{22}$$

$$\frac{\partial}{\partial x^k}p_{lm}+\frac{\partial}{\partial x^l}p_{mk}+\frac{\partial}{\partial x^m}p_{kl}=8\pi\sigma_{klm}, \tag{23}$$

in which $\sigma_{klm}$ is a complete antisymmetric tensor of the third order related to $\sigma^k$ through the equation[13]

$$\sigma_{klm}=j_{klmn}\sigma^n. \tag{24}$$

To begin, Eq. (14) is multiplied by $p_{km}$:

$$p_{km}\frac{\partial}{\partial x^l}f^{kl}=4\pi p_{km}\rho^k.$$

Then

$$\frac{\partial}{\partial x^l}(p_{km}f^{kl})-f^{kl}\frac{\partial}{\partial x^l}p_{km}=4\pi p_{km}\rho^k,$$

$$-f^{kl}\frac{\partial}{\partial x^l}p_{km}=-\tfrac{1}{2}\frac{\partial}{\partial x^m}(f^{kl}p_{kl})$$

$$+\tfrac{1}{2}p^{kl}\frac{\partial}{\partial x^m}f_{kl}+4\pi f^{kl}\sigma_{klm},$$

$$\tfrac{1}{2}p^{kl}\frac{\partial}{\partial x^m}f_{kl}=\frac{\partial}{\partial x^l}(p^{kl}f_{km}). \tag{25}$$

From these results and the identity $f^{kl}\sigma_{klm}=-f_{km}{}^*\sigma^k$ follows[14]

$$\frac{\partial}{\partial x^l}\{p_{km}f^{kl}+p^{kl}f_{km}-\tfrac{1}{2}f_{rs}p^{rs}\delta_m{}^l\}=4\pi(p_{km}\rho^k+f_{km}{}^*\sigma^k). \tag{26}$$

Now if the conservation Eq. (7) is multiplied by two and added to (26) there is obtained the symmetrical and strikingly simple equation

$$\frac{\partial}{\partial x^m}((1+P)^{\frac{1}{2}}+(1+P)^{-\frac{1}{2}})=4\pi(p_{km}\rho^k+f_{km}{}^*\sigma^k). \tag{27}$$

Let us fix attention on a particular singularity $e_i$ and integrate (27) over the space between two surfaces $S$ and $S'$ enclosing $e_i$. $S$ is taken such that in a coordinate system in which the singularity is instantaneously at rest it is spherical and centered at $e_i$; moreover it is assumed possible to take the radius of $S$ so great that on $S$ the scalar invariant $P$ is small in comparison with unity. (This assumption excludes the interesting case of two singularities separated momentarily by a distance of less than $10^{-12}$ cm.) That value of the radius is taken for which $P$ is roughly as small as possible. $S'$ is any surface having arbitrarily small linear dimensions and symmetric with respect to reflection through the singularity. Then, letting $\mathbf{M}=(1+P)^{\frac{1}{2}}+(1+P)^{-\frac{1}{2}}-2$,

$$\int\int\int_{S-S'}\frac{\partial}{\partial x^m}\mathbf{M}d\tau=\int\int_S\mathbf{M}\cos(x^m, s)ds$$

$$+\int\int_{S'}\mathbf{M}\cos(x^m, s)ds, \quad m=1, 2, 3. \tag{28}$$

On $S$

$$\mathbf{M}\leqq\tfrac{1}{4}P^2=(D^2-H^2)^2/4b^4. \tag{29}$$

[12] Compare reference 1, p. 450.

[13] $j_{klmn}$ is the complete antisymmetric tensor of the fourth order; see reference 1, p. 431

[14] With the identity $p^{*kl}f_{km}{}^*=p_{km}f^{kl}-\frac{1}{2}p_{rs}f^{rs}\delta_m{}^l$ the left-hand member of (26) can be written in symmetrical form.

$D$ has the same order of magnitude on $S$ as the perturbing field ${}^{e}p_{rs}$ there or at $e_i$ arising from the other singularities in the field (merely another way of saying that $S$ is so chosen that on it $P$ is roughly as small as possible). Now, even for a radiation field, $r^2(D^2-H^2)^2<O({}^{e}p_{rs}{}^2)$ and consequently

$$\left|\int\int_S \mathbf{M}\cos(x^m, s)ds\right| < O({}^{e}p_{rs}{}^2),\ m=1,2,3. \quad (30)$$

The other surface integral is uniformly bounded, independent of the linear dimensions of $S'$, because the singularity of the argument at $e_i$ is only of the second degree. Moreover a reflection through the singularity merely changes the sign of the argument without changing its value (in the limit as the linear dimensions of $S'$ approach zero). Hence

$$\lim_{S'\to 0}\int\int_{S'} \mathbf{M}\cos(x^m, s)ds=0, \quad m=1,2,3,$$

and[15]

$$\int\int\int \nabla\mathbf{M}d\tau=0 \quad (31)$$

with neglect of terms having the order of magnitude $O(ep_{rs}{}^2)$. Thus (27) implies

$$\int\int\int (p_{km}\rho^k+f_{km}{}^{*}\sigma^k)d\tau=0, \quad m=1,2,3, \quad (32)$$

neglecting again quadratic terms in the perturbing field at $e_i$. Classical analogy suggests interpreting $(p_{km}\rho^k+f_{km}{}^{*}\sigma^k)d\tau$ as the force on the charge occupying the element of volume $d\tau$. With this interpretation (32) is equivalent to the statement that the total force on the electron vanishes. But since the BI field equations do not determine the motion neither can (32) which is a consequence of the field equations. The electrons may move as they please, but always the non-classical part of the field, $\tilde{q}_{rs}$, which is determined from the motion by the field equations has just the value required to insure the truth of (32). This remark applies with equal force to Eq. (12) which is indeed equivalent to (32). It is better then not to attach too much significance to the above interpretation although it cannot be said to be false and does point unmistakably to a reasonable dynamical assumption.

Hitherto only three of the Eqs. (27) have been considered. But, from (10),

$$\mathbf{M}=\mathbf{M}^{v}+\tfrac{1}{2}F^{v}\,{}^{v}f_{rs}q^{rs}+O(q_{rs}{}^2) \quad (33)$$

and hence both the Eqs. (32) and the equation obtained by applying to (27) for $m=4$ an integration over the interior of $S$ are contained in the set of equations

$$4\pi\int\int\int (p_{km}\rho^k+f_{km}{}^{*}\sigma^k)d\tau=\delta_m{}^4\left\{\frac{\partial}{2c\partial t}\int\int\int F^{v}\,{}^{v}f_{rs}q^{rs}d\tau-\int\int\int F^{v}\,\frac{\dot{v}_i}{c}\,\frac{\partial}{\partial v_i}(1+P^{v})^{\frac{1}{2}}d\tau\right\}. \quad (34)$$

[15] Wherever a volume integration appears it is understood that the integration is over the region inclosed by $S$.

## VIII. The Conservation Equations in the Coordinate System in Which the Singularity is Instantaneously at Rest

The equation

$$\frac{\partial}{\partial x^l}{}^{v}f^{kl}=4\pi\,{}^{v}\rho^k+\frac{\dot{v}_i}{c}\,\frac{\partial}{\partial v_i}{}^{v}f^{k4} \quad (35)$$

defines the unperturbed charge four vector ${}^{v}\rho^k$ which is associated with a singularity moving with the instantaneous velocity $v$. Let

$${}^{q}\rho^k=\rho^k-{}^{v}\rho^k \quad (36)$$

represent the distortion in the charge and current densities produced by the acceleration and the external field. Then

$$p_{km}\rho^k={}^{v}p_{km}\,{}^{v}\rho^k+q_{km}\,{}^{v}\rho^k+p_{km}\,{}^{q}\rho^k. \quad (37)$$

Symmetry considerations lead at once to the conclusion

$$\int\int\int {}^{v}p_{km}\,{}^{v}\rho^{k}d\tau=0. \tag{38}$$

Furthermore the integral over $p_{km}\,{}^{q}\rho^{k}$ can be expressed in a simple form. For

$$\frac{\partial}{\partial x^{l}}f^{kl}=4\pi({}^{v}\rho^{k}+{}^{q}\rho^{k}) \tag{39}$$

and hence, using (10),

$$4\pi\,{}^{q}\rho^{k}=\frac{\dot{v}_i}{c}\frac{\partial}{\partial v_i}{}^{v}f^{k4}+\frac{\partial}{\partial x_l}(f^{kl}f_{rs}q^{rs}/2(1+P)^{\frac{1}{2}})+\frac{\partial}{\partial x^{l}}(q_{kl}/(1+P)^{\frac{1}{2}})+O(q_{rs}^{2}). \tag{40}$$

Accordingly, after some calculation (for which see appendix),

$$4\pi p_{km}\,{}^{q}\rho^{k}=-\frac{1}{2}\frac{\partial}{\partial x^{l}}({}^{v}f_{km}\,{}^{v}f^{kl}\,{}^{v}f_{rs}q^{rs})-\frac{\dot{v}_i}{c}{}^{v}f_{km}\,{}^{v}f^{k4}\frac{\partial}{\partial v_i}(1+P^{v})^{\frac{1}{2}}+O(q_{rs}^{2}), \tag{41}$$

and, combining (37), (38) and (41) with (34)

$$4\pi\int\int\int(q_{km}\,{}^{v}\rho^{k}+{}^{v}f_{km}{}^{*}\sigma^{k})d\tau=\frac{1}{2c}\frac{\partial}{\partial t}\int\int\int(F\,{}^{v}\delta_{m}{}^{4}-{}^{v}f_{km}\,{}^{v}f^{k4})\,{}^{v}f_{rs}q^{rs}d\tau$$

$$-\int\int\int(F\,{}^{v}\delta_{m}{}^{4}-{}^{v}f_{km}\,{}^{v}f^{k4})\frac{\dot{v}_i}{c}\frac{\partial}{\partial v_i}(1+P^{v})^{\frac{1}{2}}d\tau. \tag{42}$$

The surface integral discarded to obtain (42) is bounded by the quantity[16] $2\pi|q_{rs}|(e^{3}/b^{3}r^{4})=2\pi(e/b)|q_{rs}|(r_0/r)^{4}$ which falls off with decreasing interaction at least as rapidly as the cube of the external field ($r$ is roughly the smallest linear dimension of $S$). Now $F^{v}=({}^{v}B^{2}-{}^{v}E^{2})/b^{2}$, ${}^{v}f_{k4}\,{}^{v}f^{k4}=-{}^{v}E^{2}/b^{2}$ and $b^{2}\,{}^{v}f_{km}\,{}^{v}f^{k4}(m\neq 4)$ is just the vector product of ${}^{v}E$ and ${}^{v}B$. Consequently $(F^{v}\delta_{m}{}^{4}-{}^{v}f_{km}\,{}^{v}f^{k4})$ vanishes in the coordinate system in which the electron is momentarily at rest and also

$$\frac{\partial}{\partial t}\{(F^{v}\delta_{m}{}^{4}-{}^{v}f_{km}\,{}^{v}f^{k4})\,{}^{v}f_{rs}\}=0(\dot{v}).$$

Letting the superscript $O$ designate this coordinate system, (42) reduces to[17]

$$\int\int\int({}^{o}q_{4m}\,{}^{o}\rho^{4}+{}^{o}f_{km}{}^{*}\,{}^{o}\sigma^{k})d\tau^{o}=0. \tag{43}$$

It must be considered as significant that the unpleasant distortion charge vector ${}^{q}\rho^{k}$ drops out of (32) to leave just (43) when the problem is set up in the one coordinate system (the instantaneous rest system) which is physically singled out from all others. Finally to bring out explicitly the manner in which classical and non-classical terms enter into (43) it is written in the suggestive form

$$\int\int\int({}^{a}p_{4m}{}^{o}+{}^{c}p_{4m}{}^{o})\,{}^{o}\rho^{4}d\tau^{o}=-\int\int\int({}^{o}\tilde{q}_{4m}\,{}^{o}\rho^{4}+{}^{o}f_{km}{}^{*}\,{}^{o}\sigma^{k})d\tau^{o}. \tag{44}$$

---

[16] $r_0=(e/b)^{\frac{1}{2}}=2.28\times10^{-13}$ cm; see reference 1, p. 446.

[17] Note that ${}^{o}\rho^{4}$ is $({}^{v}\rho^{4})_{v=0}$ and not the quite distinct quantity $(\rho^{4})_{v=0}$.

It is clear that neither side of (42) constitutes a four vector or possesses transformation properties simply related to those of a four vector. This circumstance is not surprising for only under exceptional conditions is it true that the space integral of a four vector possesses any simple transformation properties.

## IX. The Equations of Motion

The noteworthy feature of (44) which makes it important and justifies the laborious analysis by means of which it is derived is the occurrence in it of the integral $\int\int\int({}^{a}p_{4m}{}^{o}+{}^{e}p_{4m}{}^{o}){}^{o}\rho^{4}d\tau^{o}$, which differs only slightly from the quantity which in the classical electromagnetic theory is interpreted as the total force on the electron and required to vanish in order to supply the theory with dynamical equations of motion. The difference is only that in the classical expression the acceleration field of a volume distribution of charge appears in the place of ${}^{a}p_{4m}{}^{o}$. Here, just as in the classical theory, a dynamical condition is needed to determine the motion. But (44) leaves no doubt as to the simplest physically satisfactory condition. We must require that the motion shall be such that the right-hand member of (44) which represents a completely unclassical "force" on the electron shall vanish. Then the equation

$$\int\int\int({}^{a}p_{4m}{}^{o}+{}^{e}p_{4m}{}^{o}){}^{o}\rho^{4}d\tau^{o}=0 \qquad (45)$$

determines the required motion. The vanishing of $\bar{q}_{kl}$ and $\sigma_k$ when the motion of the singularity is uniform and rectilinear suggests that (45) is a condition which makes the departure from the classical field small, or even, in a rough sense, as small as possible. In this respect the condition (45) is related to the Born-Infeld equations of motion. In terms of the field tensors measured in an arbitrary coordinate system (45) can be written

$$\frac{1}{\beta}\frac{dx^{om}}{dx^{k}}\int\int\int({}^{a}p_{4m}{}^{o}+{}^{e}p_{4m}{}^{o}){}^{o}\rho^{4}d\tau^{o}$$

$$=-\frac{dx^{j}}{cdt}\int\int\int({}^{a}p_{kj}+{}^{e}p_{kj}){}^{o}\rho^{4}d\tau^{o}=0. \qquad (46)$$

The integration over $d\tau^{o}$ in (46) implies a cut perpendicular to the $t^{o}$ axis, the time cross section for an observer moving with the electron. For this reason the substitution of ${}^{o}\rho^{4}d\tau$ for ${}^{o}\rho^{4}d\tau^{o}$ in (46) is not permitted although ${}^{o}\rho^{4}d\tau$ is a scalar invariant.

There remains the problem of exhibiting explicitly the equations of motion implicit in (45). For small values of the velocity the electric field in the neighborhood of a classical point charge, computed from the retarded potentials, is given by

$$D(x,y,z,t)=e1\{1/r^{2}-1\cdot\dot{v}/2c^{2}r+(1\cdot\ddot{v}/8c^{4})r-(1\cdot v^{iv}/15c^{5})r^{2}+(1\cdot v^{v}/48c^{6})r^{3}\cdots\}$$

$$+e\{-\dot{v}/2c^{2}r+2\ddot{v}/3c^{3}-(3\ddot{v}/8c^{4})r+(2v^{iv}/15c^{5})r^{2}-(5v^{v}/144c^{6})r^{3}+\cdots\}. \qquad (47)$$

$r$ is the scalar distance from the point $x, y, z$ at which the field is wanted to the instantaneous position of the electron. 1 is the unit vector from the electron to the point $x, y, z$. Also[18]

$$b\,{}^{o}\rho^{4}=\frac{e}{2\pi r_{0}^{3}(r/r_{0})(1+(r/r_{0})^{4})^{\frac{1}{2}}}. \qquad (48)$$

Letting ${}^{o}D^{e}$ represent the external electric field (45) becomes

$$b\int\int\int{}^{o}D^{e}\,{}^{o}\rho^{4}d\tau^{o}=\int\int\int\left\{\frac{2\dot{v}}{3c^{2}r}-\frac{2\ddot{v}}{3c^{3}}+\frac{\ddot{v}}{3c^{4}}r-\frac{v^{iv}}{9c^{5}}r^{2}+\frac{v^{v}}{36c^{6}}r^{3}\right\}\frac{e^{2}d\tau^{o}}{2\pi r_{0}^{3}(r/r_{0})(1+(r/r_{0})^{2})^{\frac{1}{2}}} \qquad (49)$$

or, introducing the symbol $G(m, n)$ for the integral

[18] Reference 1, p. 444.

$$\int_0^\infty \frac{x^m dx}{(1+x^4)^{n/2}},$$

$$b\int\int\int {}^\circ D^\epsilon\, {}^\circ\rho^4 d\tau^\circ = (4e^2/3c^2r_0)G(0,3)\dot v - (4e^2/3c^3)G(1,3)\ddot v + (2e^2r_0/3c^4)G(2,3)\dddot v$$
$$-(2e^2r_0^2/9c^6)G(3,3)v^{iv} + (e^2r_0^3/18c^8)G(4,3)v^v. \quad (50)$$

Now[19]

$$G(4,3)=G(0,3)=\tfrac{1}{2}G(0,1)=0.9270=(3c^2r_0/4e^2)m_0, \qquad G(1,3)=G(3,3)=0.5. \quad (51)$$

Using the substitution[20] $x=\tan\frac{1}{2}w$

$$G(2,3)=\tfrac{1}{2}\left(\frac{\partial}{\partial\theta}\int_0^{\pi/2}\frac{d\omega}{(1-\sin^2\theta\sin^2\omega)^{\frac{1}{2}}}\right)_{\theta=\pi/4}=0.422. \quad (52)$$

(By "Peirce's Tables" p. 121.)
Eq. (50) now takes the form

$$b\int\int\int {}^\circ D^\epsilon\, {}^\circ\rho^4 d\tau^\circ = m_0\dot v - (2e^2/3c^3)\ddot v + (2e^2/3c^3)(r_0/c)\{0.422\dddot v - 0.167(r_0/c)v^{iv} + 0.077(r_0/c)^2 v^v\}. \quad (53)$$

We see that the equations of motion contain the usual radiation resistance term $(2e^2/3c^3)\ddot v$ and additional terms which are important when the electron interacts with very high frequency radiation. But clearly the derivation of the right-hand member of (53) from (54) involves approximations which limit its validity, for the problem of interaction with radiation, to wavelengths somewhat greater than the characteristic length $2\pi r_0$ (perhaps, $h\nu \leqq (137/3)m_0c^2$).[21]

The generalization of (53) to an arbitrary coordinate system is accomplished by going back to (46) or more simply by introducing two four vectors $\beta F_k$, $\beta G_k$ taking the values

$$(F_1, F_2, F_3)=b\int\int\int {}^\circ D^\epsilon\, {}^\circ\rho^4 d\tau^\circ, \qquad F_4=0,$$
$$(G_1, G_2, G_3)=0, \qquad G_4=\frac{2e^2}{3c^4}\left\{\dot v^2 - 0.422\frac{r_0}{c}3\dot v\cdot\ddot v + \cdots\right\} \quad (54)$$

when the velocity of the singularity vanishes. Then

$$F_k=\frac{b^2}{\beta}\frac{dx^{\circ l}}{dx^k}\int\int\int {}^\circ p_{l4}\, {}^\circ\rho^4 d\tau^\circ$$
$$=b^2\frac{dx^j}{dx^4}\int\int\int {}^\circ p_{kj}\, {}^\circ\rho^4 d\tau^\circ, \quad (55)$$

or

$$(F_1, F_2, F_3)=b\int\int\int\left\{{}^\circ D+\frac{1}{c}(v\times {}^\circ H)\right\}{}^\circ\rho^4 d\tau^\circ, \qquad F_4=-\frac{b}{c}\int\int\int v\cdot {}^\circ D\, {}^\circ\rho^4 d\tau^\circ. \quad (56)$$

The equations of motion have the form

[19] Reference 1, p. 440, p. 446.
[20] Reference 1, p. 439.
[21] A more fundamental restriction implied by the consistent neglect of quadratic terms in the external field is $|\dot b| \ll c^2/r_0$.

$$-(F^k+G^k)=\frac{d}{dt}m_0\beta\frac{dx^k}{dt}-\frac{2e^2}{3c^3}\frac{d}{dt}\beta\frac{d}{dt}\beta\frac{dx^k}{dt}+\cdots. \tag{57}$$

The plane wave fields,

$$({}^sD,\ {}^sH)=(A,\ B)e^{2\pi i(\nu t-(lx+my+nz)/\lambda)}$$

lead to the force vector

$$(F_1,\ F_2,\ F_3)=eg\left(\frac{2\pi r_0}{\lambda_0}\right)\left\{{}^sD+\frac{1}{c}(v\times{}^sH)\right\}, \tag{58}$$

in which ${}^sD$ and ${}^sH$ are evaluated at the singularity and $g(2\pi r_0/\lambda_0)$[22] is a factor less than unity representing the fact that the grip which the field obtains on the electron decreases in strength as the frequency goes up. It is important to note that the $\lambda_0$ occurring in the argument of $g$ is the wavelength for an observer moving with the singularity. Thus $g(2\pi r_0/\lambda_0)$ is a scalar invariant, but not a constant.

Appendix: derivation of Eq. (41).

From (40)

$$4\pi p_{km}\,{}^q\rho^k=p_{km}\frac{\dot v_i}{c}\frac{\partial}{\partial v_i}{}^vf^{k4}+\frac{\partial}{\partial x^l}\{\tfrac12(f_{rs}q^{rs})f_{km}f^{kl}+f_{km}q^{kl}\}-\left(\frac{\partial}{\partial x^l}p_{km}\right)(f^{kl}-{}^vf^{kl}), \tag{59}$$

$$\begin{aligned}-\left(\frac{\partial}{\partial x^l}p_{km}\right)(f^{kl}-{}^vf^{kl})&=(f^{kl}-{}^vf^{kl})\left(\frac{\partial}{\partial x^k}p_{ml}+\frac{\partial}{\partial x^m}p_{lk}\right)\\&=-\tfrac12(f^{kl}-{}^vf^{kl})\frac{\partial}{\partial x^m}p_{kl}\\&=-\frac{\partial}{\partial x^m}\{\tfrac12(f_{rs}q^{rs})f_{kl}f^{kl}+f_{kl}q^{kl}\}+\tfrac12p^{kl}\frac{\partial}{\partial x^m}(f_{kl}-{}^vf_{kl}),\end{aligned} \tag{60}$$

$$\begin{aligned}\tfrac12p^{kl}\frac{\partial}{\partial x^m}(f_{kl}-{}^vf_{kl})&=-\tfrac12p^{kl}\left\{\frac{\partial}{\partial x^k}(f_{lm}-{}^vf_{lm})+\frac{\partial}{\partial x^l}(f_{mk}-{}^vf_{mk})\right\}\\&\quad-\tfrac12\frac{\dot v_i}{c}\frac{\partial}{\partial v_i}\{\delta_m{}^4\,{}^vf_{kl}+\delta_k{}^4\,{}^vf_{lm}+\delta_l{}^4\,{}^vf_{mk}\}p^{kl}\\&=\frac{\partial}{\partial x^l}\{\tfrac12(f_{rs}q^{rs})f^{kl}f_{km}+f^{kl}q_{km}\}-\tfrac12\left(\frac{\dot v_i}{c}\frac{\partial}{\partial v_i}{}^vf_{kl}\right)p^{kl}\delta_m{}^4+\left(\frac{\dot v_i}{c}\frac{\partial}{\partial v_i}{}^vf_{km}\right)p^{k4}.\end{aligned} \tag{61}$$

Combined, these equations yield

$$4\pi p_{km}\,{}^q\rho^k=-\frac{\partial}{\partial x^l}{}^qT_m{}^l-\frac{\dot v_i}{c}\frac{\partial}{\partial v_i}{}^vT_m{}^4+\tfrac12\frac{\partial}{\partial x^l}({}^vf_{km}\,{}^vf^{kl}\,{}^vf_{rs}q^{rs})-\frac{\dot v_i}{c}{}^vf_{km}\,{}^vf^{k4}\frac{\partial}{\partial v_i}(1+P^v)^{\frac12}+O(q_{rs}^2) \tag{62}$$

$$=\tfrac12\frac{\partial}{\partial x^l}({}^vf_{km}\,{}^vf^{kl}\,{}^vf_{rs}q^{rs})-\frac{\dot v_i}{c}{}^vf_{km}\,{}^vf^{k4}\frac{\partial}{\partial v_i}(1+P^v)^{\frac12}+O(q_{rs}^2). \tag{41}$$

The writer is indebted to colleagues in the Research Laboratory for many helpful criticisms and to Mr. Julian Knipp for checking certain calculations.

[22] Reference 1, p. 450 for explicit form and tabulated values.

# Directions of Discontinuous Changes in Magnetization in Monocrystal Bars and Disks of Silicon-Iron

R. F. CLASH, JR. AND F. J. BECK, JR., *Sloane Physics Laboratory, Yale University*

(Received December 3, 1934)

## INTRODUCTION

BECK and McKeehan,[1] expecting to find a crystallographic dependence of the Barkhausen effect, looked for it in a stationary disk subjected to a rotating field of constant magnitude. They measured, with a two-element galvanometer (G. E. oscillograph) the amplified impulses in two search coils about the disk with their axes at right angles. The measurement of the rectangular components of a single discontinuity in magnetization, thus picked out, permits its relocation in the plane of the disk. They were unsuccessful in proving any important influence of crystal structure but McKeehan and Clash[2] in a preliminary report of further work done by the improved method described below, were able to show that the expected dependence existed. The principal improvement in technique consisted in the use of a cathode-ray oscillograph which provides a means whereby the two amplified component impulses could be impressed upon a single moving element, the electron beam, and thus reintegrate the parts into a vector representing the nearly discontinuous increment in magnetization, $\Delta\mathbf{I}$. The excursions of the luminous spot on the fluorescent screen would then be nothing more than two dimensional reconstructions of the initial $\Delta I$'s. The modifications that were necessary in the apparatus warrant complete description at this time.

We now have data taken on a number of specimens which appear to justify the working hypothesis earlier presented.[2]

## APPARATUS

### 1. Effect-producing mechanism

In Fig. 1 a side view of the revised mechanism is shown. The self-supporting field coils used by Beck and McKeehan have been replaced by a machined brass casting, $G$, to which a removable two-section magnetizing coil, $F$, $F$, may be clamped. Each of these sections is wound with 317 turns of No. 16 B. and S. gauge (0.1291 cm) enameled copper wire with single covered cotton insulation. The coil pair in series aiding produces a field intensity of 34.7 oersteds ampere$^{-1}$ as found by calibration with a Hibbert standard. In addition to increasing the field range the new arrangement gave improved mechanical performance.

The mirror system shown at $E$, $E'$ provides a convenient reference frame for making observations. Thirty-six small aluminum-on-glass mirrors, mounted at 10° intervals on the periphery of a hard rubber disk, form successive reflecting surfaces for a convergent beam of light, refocused (after reflection) on the ceiling of the room. Successive coincidences of the moving images with a stationary image (from a fixed mirror $E'$) provide a convenient method of counting the 10° intervals. One moving image is double, furnishing a conspicuous starting point for counting the intervals. A reflection is designated by an integer, $N$, ranging from 0 to 35 ($N=0$ for the double moving image).

A new rectangular search coil system (see Fig. 2) has been constructed in which the two coils $J$, $J$, have equal areas and numbers of turns. Also the specimen, $K$, may be placed at a position similarly related to both coils, so that the coils become equivalent. Each coil is wound with a total of 5000 turns of No. 40 B. and S. gauge (0.0080 cm) enameled copper wire (2500 turns per channel). The windings of the two channels, $L$, $L$, of a coil are connected in series aiding, and have a total resistance of about 2100 ohms. The angular position of the coil system is adjustable and easily determined from a calibrated circular scale on the mounting.

Special precautions were taken to insure uniform rotation of the effect-producing mechanism with a minimum of mechanical vibration. The driving torque was furnished by a single phase,

[1] F. J. Beck, Jr., and L. W. McKeehan, Phys. Rev. **41**, 385 (1932); **42**, 714–720 (1932).
[2] L. W. McKeehan and R. F. Clash, Jr., Phys. Rev. **45**, 839–840 (1934).

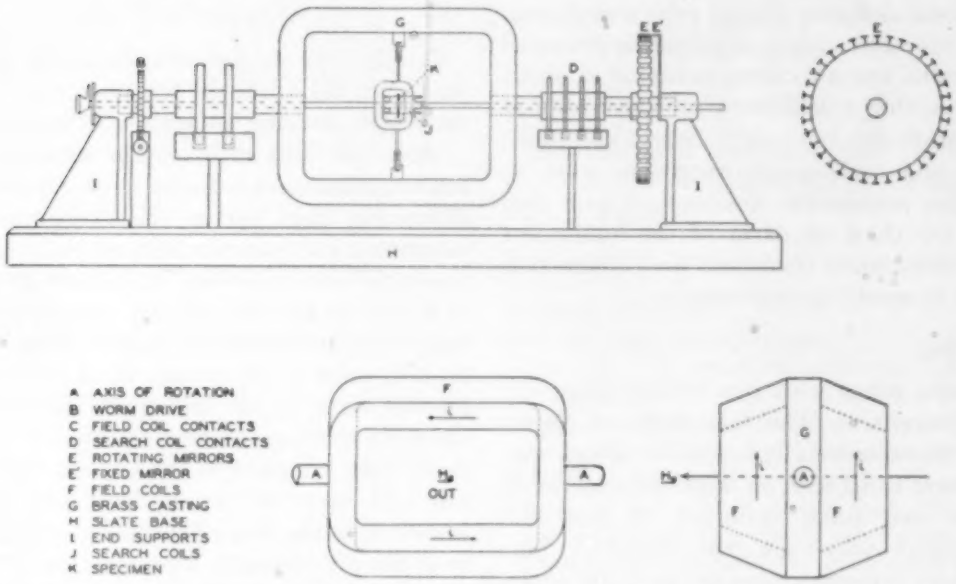


FIG. 1. Side view of the revised rotating mechanism, axial view of mirror system, and side and axial views of the new field coils clamped to the supporting brass casting.

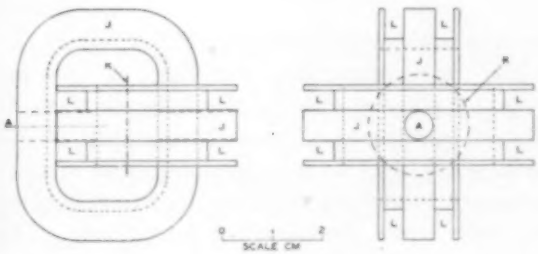


FIG. 2. Side and axial views of the new search coils. Note the equivalence of the two rectangular sections and their positions relative to the stationary specimen. Forms are of hard rubber. *A*, axis of rotation; *J*, search coil form; *K*, specimen; *L*, channel for windings.

60 cycle, 1/50 h.p., 1200 r.p.m., Westinghouse synchronous motor working through 5000 : 1 reduction gears. Motor and one reduction gear were mounted rigidly and "floated" on a hair-felt pad, this assembly being located about 180 cm from the mechanism proper. One section of the connecting drive shaft was a (0.95 cm) lead pipe. The magnetic field and search coil system were thus rotated about the stationary specimen once in 250 seconds.

## 2. The amplifiers

Two 4-stage resistance-capacity coupled audio-frequency amplifiers were constructed. The circuit constants are shown in Table I. One side of each search coil was connected directly to the grid of its respective amplifier while the other was grounded, thus impressing the induced emf's directly on the input grids. The PJ-11 gave satisfactorily low noise output.[3] The grid bias of the output tube made it necessary to adjust the signal "sense" so as to produce positive grid swings from this bias value. This eliminated distortion, but confined observations to excursions occurring in one quadrant of the oscillograph screen. The total voltage amplification realized from this circuit was about 147,000.

TABLE I. *Circuit constants of amplifier.*

| Stage | Tube | $E_b$ | $E_g$ | $R_p$ | $R_g$ | $C$ |
|---|---|---|---|---|---|---|
| 1 | PJ-11 | 180v | −1.2v | 0.1 Meg. | ——— | 0.1μf |
| 2 | UX-240 | 270v | 0 | 0.75 " | 5 Meg. | 0.1μf |
| 3 | UX-240 | 270v | 0 | 0.75 " | 5 " | 0.1μf |
| 4 | UX-240 | 225v | −4.5v | 0.25 " | 5 " | 0.1μf |

## 3. The oscillograph

Some difficulty was experienced in finding a cathode-ray oscillograph with sufficient photographic intensity and deflector plate sensitivity. Finally a DuMont[4] Type 54 (5 inch screen, 2 sets

[3] G. F. Metcalf and T. M. Dickinson, Physics **3**, 11 (1932).

[4] We very gratefully acknowledge the help and sugges-

of orthogonal deflector plates) tube was chosen. This was operated with an accelerating potential of 2000 volts, and a focusing potential of about 325 volts, giving a deflector plate sensitivity of approximately 0.4 mm volt$^{-1}$. Search coil leads, windings and oscillograph excursions were so related that permissible observations were confined to the third quadrant of the fluorescent screen. Experimental conditions were adjusted as necessary to meet this requirement.

## 4. Operation

Data were taken with this revised apparatus by two procedures. The first involved photographing the excursions by means of a laboratory-made camera fitted with an adjustable aperature F1.9 lens and using standard 35 mm film (supersensitive gray-back panchromatic). Successive short exposures were taken at 10° intervals giving a complete set of data in 250 seconds. It was found that optimum photographic contrast was obtained for an exposure time equal to the ($F$ setting)$^2$/120 seconds. For longer exposures general illumination of the fluorescent screen produced excessive halation on the film. The most conspicuous excursions were then traced by a sharp pencil on thin translucent paper, and their angles relative to the oscillographic axes measured with a protractor.

The other procedure necessary in some cases, was to count individual excursions occurring within 10° intervals having lengths greater than an arbitrary minimum $r$. This was accomplished by successively placing opaque circular screens of proper radii over the center of the fluorescent screen. This required two workers, one for counting, the other for recording while the photographic experiments were easily conducted by a single operator.

It is of importance to remark that adequate shielding of the apparatus from mechanical, acoustical and electromagnetic disturbances was necessary. Each amplifier had two independent sets of batteries and separately shielded compartments for each stage. Further, the mechanism proper was enclosed in a copper box, and all exposed leads carefully shielded.

tions of Mr. Allen B. DuMont in finding a cathode-ray oscillograph meeting our requirements.

### Reference System

In Fig. 3 we have drawn the search coil axes, $S_x$, $S_y$, in an arbitrary position with the field vector, $\mathbf{H}_a$, making an angle $\gamma$ with the positive $S_x$ direction. This angle may be adjusted at will, but remains constant during a run. Obviously the differential field vector $d\mathbf{H}_a/dt$ is constant in magnitude and leads the field vector by 90° when the latter has a constant magnitude and rotates at a uniform rate. It will also be noted from the figure that our previously defined integer, $N$, has its zero value at the instant $\mathbf{H}_a$ is parallel to the fiducial mark on the stationary specimen. Now since the oscillograph axes correspond to $S_x$ and $S_y$ we may at once find the angle $\psi$ between the reference mark on the specimen and $\Delta I$ if $\theta$ is known ($\theta$ is the angle between $S_x$ and $\Delta I$ found from the photograph). By inspection we see that

$$\psi = \theta - \gamma + 10N, \tag{1}$$

$$\phi = \psi - 10(N+9), \tag{2}$$

where $\phi$ is the angle between $d\mathbf{H}_a/dt$ and $\Delta\mathbf{I}$.

The high impedance coupling of the ungrounded plate of a pair of the deflector plates to ground introduced a non-orthogonality of the oscillograph axes as photographed, and made it necessary to add a correction term to $\theta$, depending only upon its observed magnitude. This correction ranged from 0° to 5°.

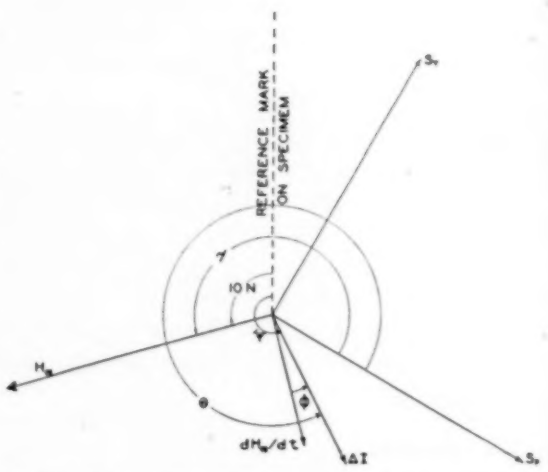


FIG. 3. Reference system. The reader must conceive of all vectors as rotating with respect to the dotted line which is fixed on the plane of the specimen. All of these vectors except $\Delta\mathbf{I}$ are fixed relative to one another.

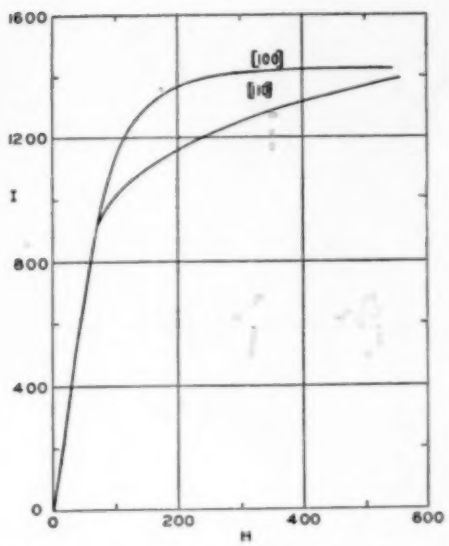


FIG. 4. Magnetization of silicon-iron single crystals along [100] and [110] directions as a function of the magnetizing force in oersteds.

## Specimens

All the disk and bar specimens, except the polycrystal disk of specially processed[5] electrical sheet steel were cut from material very kindly furnished us by Dr. W. E. Ruder of the General Electric Company's Research Laboratories. This stock was in strip form and had the following average composition.

| C | Mn | P | S | Si |
|---|---|---|---|---|
| 0.05 | 0.15 | 0.038 | 0.026 | 3.24 |

A small ellipsoid was ground from this material and analyzed magnetically by the modified Curie balance since described by McKeehan.[6] Fig. 4 shows the magnetization curve obtained for the two crystallographic directions, [100] and [110]. The characteristic magnetic anisotropy of single crystals of silicon-iron is revealed.

No. 1 (100) disk
Diameter—1.33 cm
Thickness—0.022 cm
Demagnetizing factor—0.16

No. 2 (100) disk
Diameter—1.51 cm
Thickness—0.018 cm
Demagnetizing factor—0.12

No. 3 [100] disk
Diameter—2.54 cm
Thickness—0.0457 cm
Demagnetizing factor—0.17.

The projected crystallographic directions for the disks (of the form <100>) are indicated in Figs. 5, 6 and 7.

Polycrystal disk (processed electrical sheet steel)
Diameter—1.51 cm
Thickness—0.0328 cm

(100) Bar—1.90×0.28×0.05 cm³
Axis of bar 14.9° from [100], normal to plane of bar at 75.1° from [100].

(110) Bar—1.92×0.28×0.05 cm³
Axis of bar 21.3° from [110], normal to plane of bar at 68.7° from [110].

Polycrystal bar—1.92×0.29×0.05 cm³. This specimen was cut from the same strip as were the two above, but consisted of a large number of small random grains.

## RESULTS

All three of the bar specimens gave a single sharply defined linear trace on the oscillograph screen. The trace lengths were also approximately equal for corresponding directions of $\mathbf{H}_a$. Table II gives the angles between the bar length and the observed $\Delta I$'s for all three specimens at two values of $\mathbf{H}_a$. It will be noted that all observed

TABLE II. *Azimuth angles. Bar specimens.*

| Spec. | (100) | | (110) | | Polycrystal | |
|---|---|---|---|---|---|---|
| $N$ \ $\mathbf{H}_a$ | 86.9 | 156.3 | 86.9 | 156.3 | 86.9 | 156.3 |
| 4 | | | | | | |
| 5 | 181 | 181 | 175 | 175 | 179 | 180 |
| 6 | 178 | 178 | 177 | 176 | 177 | 178 |
| 7 | 177 | 177 | 179 | 178 | 177 | 180 |
| 8 | 178 | 178 | 176 | 176 | 178 | 180 |
| 9 | 177 | 177 | 179 | 177 | 177 | 176 |
| 10 | 179 | 177 | 176 | 176 | 179 | 178 |
| 11 | 178 | 179 | 176 | 174 | 179 | 178 |
| 12 | 179 | 179 | 176 | 176 | 179 | 178 |
| 13 | 181 | 180 | | | 176 | 177 |
| 14 | | | | | | |
| 22 | | | | | | |
| 23 | 0 | 0 | 358 | 354 | 0 | 0 |
| 24 | 358 | 359 | 355 | 355 | 359 | 0 |
| 25 | 359 | 358 | 356 | 356 | 0 | 0 |
| 26 | 356 | 358 | 355 | 355 | 359 | 359 |
| 27 | 358 | 357 | 358 | 359 | 0 | 359 |
| 28 | 1 | 358 | 359 | 358 | 359 | 0 |
| 29 | 0 | 0 | 357 | 357 | 358 | 359 |
| 30 | 358 | 359 | 357 | 356 | 0 | 358 |
| 31 | 1 | 359 | | | 357 | 1 |
| 32 | | | | | | |

[5] N. P. Goss, United States Patent No. 1,965,559, also see reference Trans. A. S. M. 1934 (in press).
[6] L. W. McKeehan, Rev. Sci. Inst. **5**, 265 (1934).

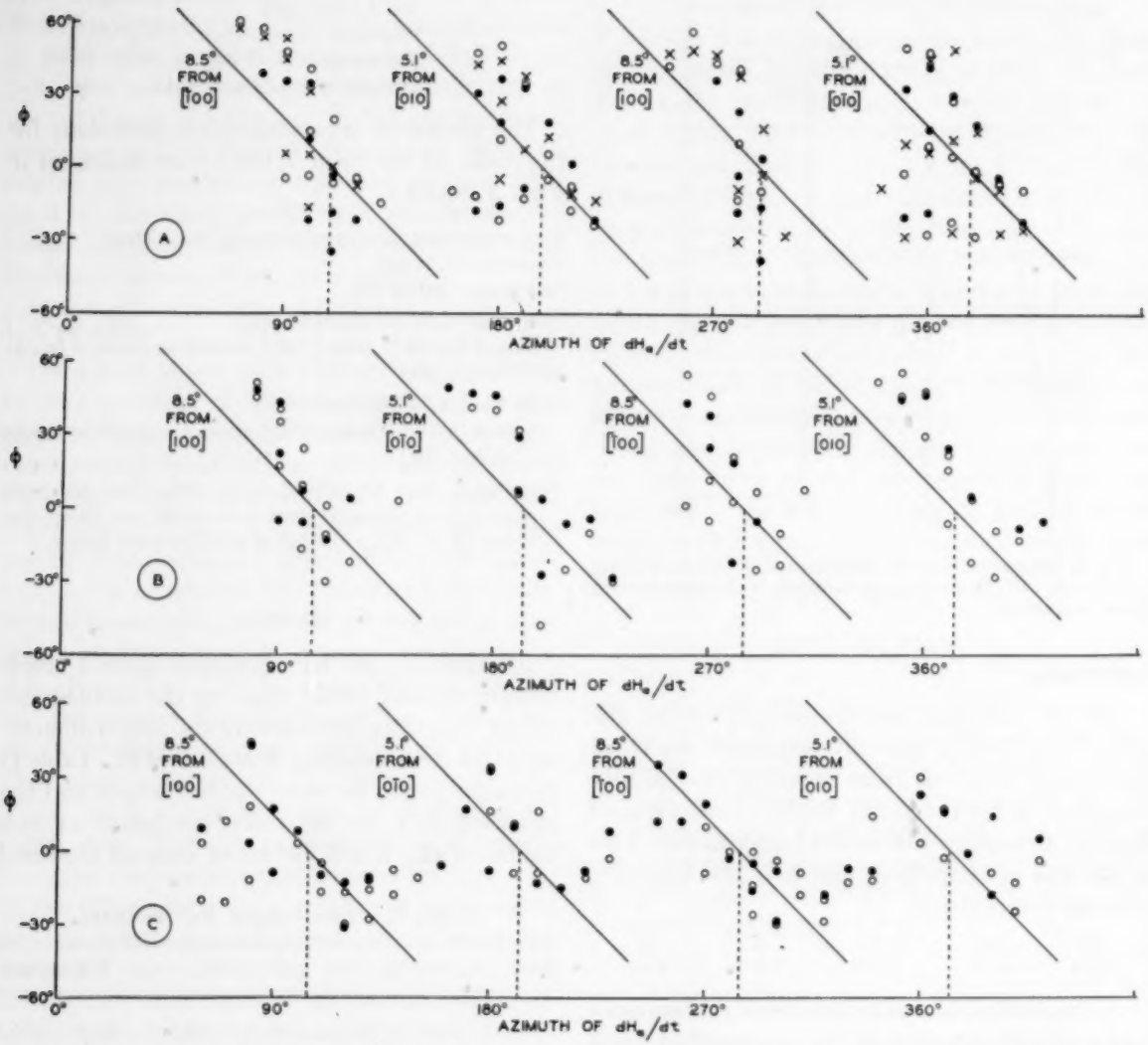


FIG. 5. Photographic results for No. 1 (100) silicon-iron disk. *A*, unannealed, three runs; x $I=1363$, o $I=1360$, ● $I=1369$; *B*, annealed, two runs o $I=1358$, ● $I=1353$. The sum of the ordinate and abscissa of an observed point represents the angle between $\Delta\mathbf{I}$ and the arbitrary zero line on the specimen. Points lying on the full diagonal lines represent $\Delta\mathbf{I}$'s parallel to the projected crystal direction as indicated. The dotted lines represent the angles at which $d\mathbf{H}_a/dt$ is parallel to the respective crystal directions as marked. The crystallographic dependence consists in the occurrence of frequent $\Delta\mathbf{I}$'s when $d\mathbf{H}_a/dt$ is in the near vicinity of a direction of easiest magnetization, and a crowding of points near the diagonal lines.

changes in magnetization are parallel to the long axes of the bars.

In passing it should be noted that one revolution of the mechanism carries the bar through an ordinary hysteresis cycle since only that component of $\mathbf{H}_a$ which is parallel to the length of such a bar is effective in magnetizing it appreciably. As is to be expected the rotating linear pattern has two zeros and two maxima per cycle, these latter occurring when the steep parts of the hysteresis curve are being traversed.

The bar data indicate at once that our first concept of these changes as due to reversals of single domains along axes of a single form, here <100>, is incorrect and that more complicated processes occur. These data have a further significance in that they show the equivalence of the two search-coil-plus-amplifier systems. The same results were obtained by having the two systems "trade" components. This is an im-

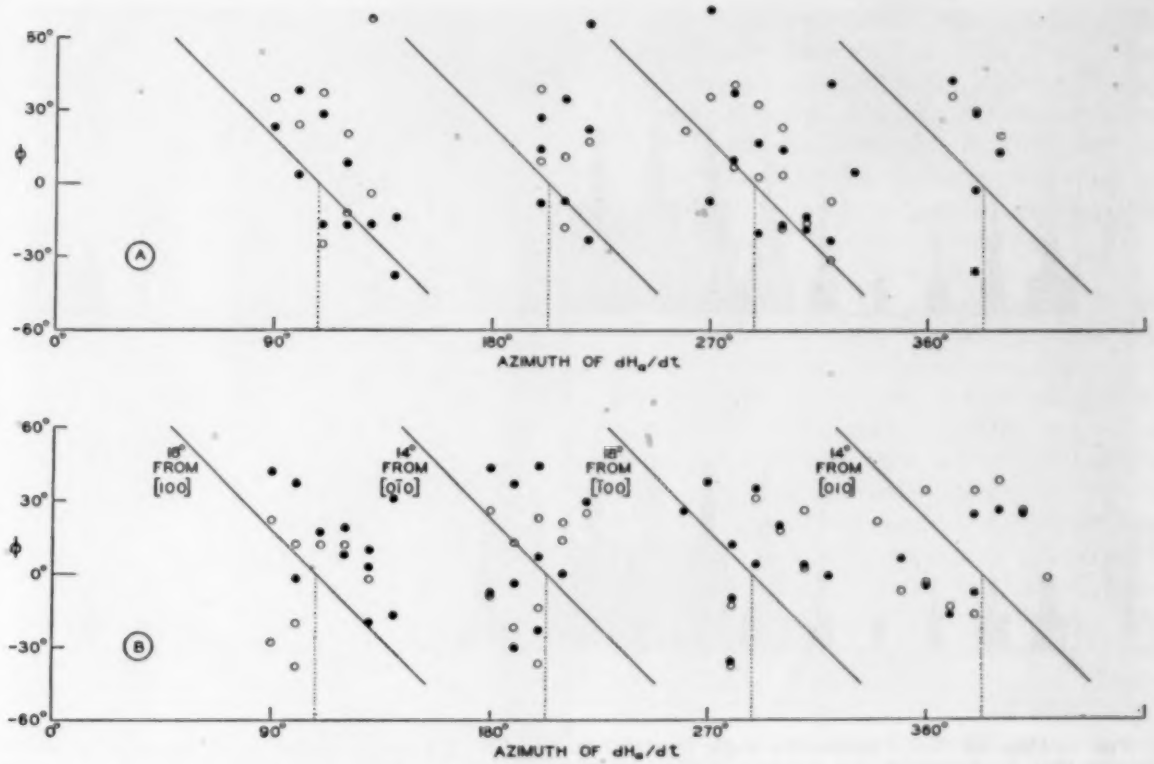


FIG. 6. Photographic results for No. 2 silicon-iron disk. *A*, annealed, two runs ○ $I=1273$, ● $I=1273$; *B*, annealed, two runs ○ $I=1360$, ● $I=1358$. See caption of Fig. 5 for explanation.

portant verification since it directly tests the operation of the apparatus under simple conditions.

Fig. 5 and Fig. 6 show the data obtained from photographs for two (100) single crystal disks of silicon-iron. It is important to note that the crystallographic dependence here shows up so clearly because only excursions too short for resolution are present when $d\mathbf{H}_a/dt$ is parallel to directions of the form <110>. The "counting" method is necessary in cases where excursions long enough for photographic recording occur at all angles. Fig. 7 is an example. This specimen is the one used previously by Beck and McKeehan in which no apparent crystallographic dependence was found. The unweighted angles, $\psi$, then studied are now seen to be of secondary importance and our attention is directed to those azimuths of $d\mathbf{H}_a/dt$ for which excursions of greater length are found. We naturally assume that these correspond to larger increments in magnetization.

The results of the counting method as applied to the "Goss" processed electrical sheet steel disk are shown in Fig. 8. The diagram, while not as striking, indicates the same type of fourfold symmetry exhibited by the single crystal of Fig. 7. The colloid concentration pattern,[7] Fig. 9[8] for a section of this material shows that there is a preference for surface magnetization along the rolling direction.

The disk specimens under the present experimental conditions exhibit several noteworthy characteristics. In the first place many excursions occur for which the corresponding $\Delta\mathbf{I}$'s have components antiparallel to the applied field, $\mathbf{H}_a$. This, of course, means that changes in magnetization take place for which the magnetic potential energy relative to the applied field shows an increase. This need not disturb us since

[7] L. W. McKeehan and W. C. Elmore, Phys. Rev. **46**, 226 (1934).

[8] Mr. W. C. Elmore of this laboratory kindly furnished us with this photograph.

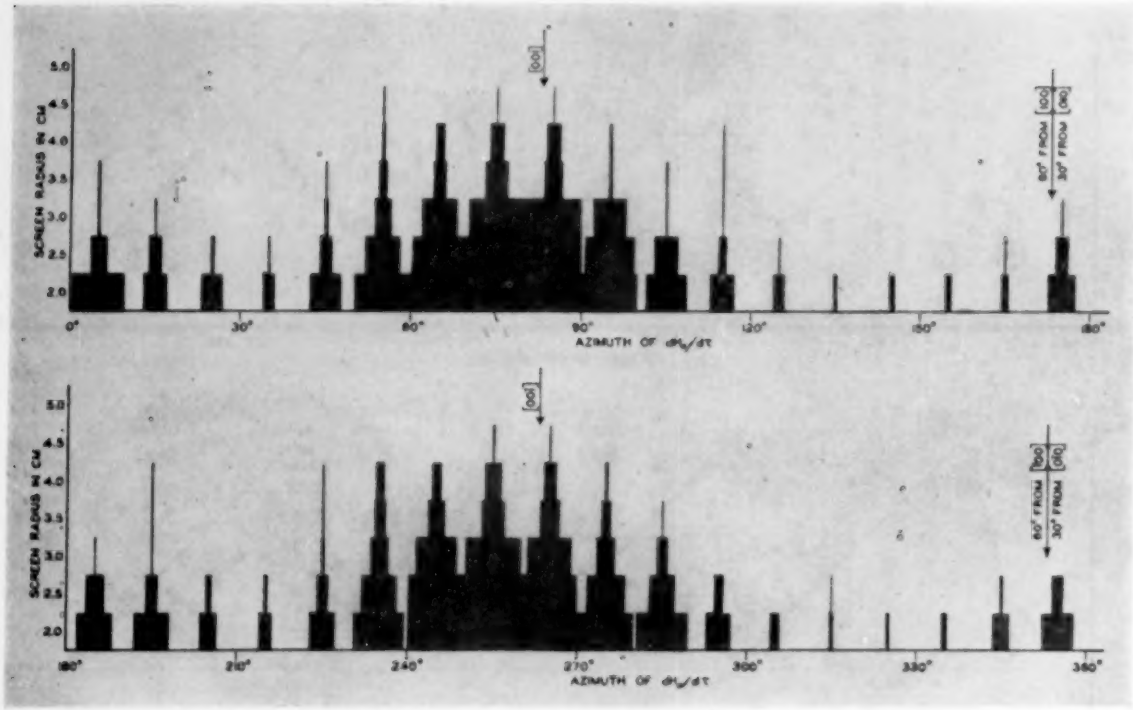


FIG. 7. Data for No. 3 silicon-iron single crystal disk. $I=1190$. The number of discontinuities having lengths greater than $r$ are plotted as a function of the position of $d\mathbf{H}_a/dt$. The width of a band represents the number counted in the interval required for $d\mathbf{H}_a/dt$ to rotate through 10°. A band "10"" in width represents 30 discontinuities which is the value assigned to intervals having too many excursions for accurate count.

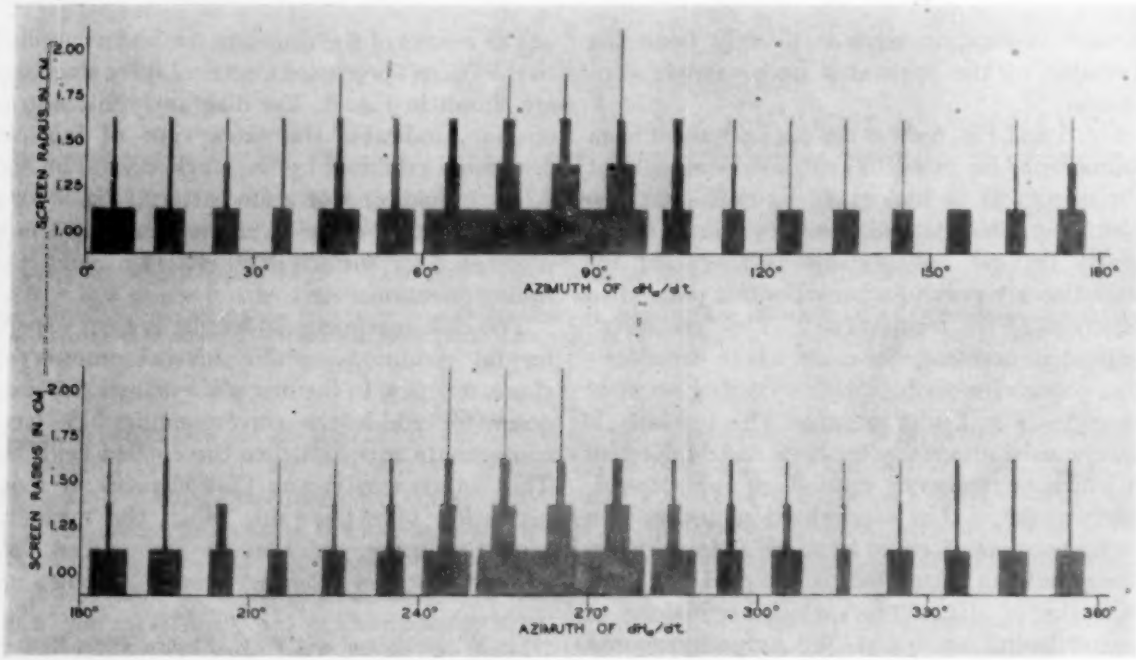


FIG. 8. Results for disk of silicon sheet steel furnished by N. P. Goss. $\mathbf{H}_a=139$. See Fig. 7 for explanation. Here the width of a band represents 25 discontinuities. The zero azimuth is parallel to the direction of rolling, 90° and 270° representing the transverse direction.

FIG. 9. Colloid concentration pattern for a section of the disk of silicon sheet steel furnished by N. P. Goss. The rolling direction is along the scratch on the left side of the pattern.

we expect large variations in the macroscopic field intensity from point to point inside the crystal at magnetizations below saturation. These local fields may be conceived of as causing the resulting $\Delta I$'s observed. Hence the anomaly is apparent rather than real.

A second peculiarity noted only in the case of the disk specimens is the occurrence of many curved and zigzag traces. These indicate a change in direction of $\Delta I$ during the time of tracing. We appear to have passed from the simple one-dimensional bar specimen to the case where two degrees of magnetic freedom exist. Certainly such behavior as observed is unlikely if a single domain accounts for each observed effect by simple reversal of moment. On this simple picture the (110) bar should have yielded a dual set of linear traces. As it did not, we now have two strong experimental points in favor of a "complicated" process.

The final important characteristic of disk specimens is obtained from Figs. 7 and 8 and from visual observation of the oscillograph excursions; namely, the longer excursions appear more frequently when $d\mathbf{H}_a/dt$ is in the near vicinity of a direction of easiest magnetization. The evidence strongly supports a crystallographic dependence of the Barkhausen effect.

As pointed out earlier[2] we look to the work of Sixtus and Tonks[9] for an explanation of the effects observed here. Under this view an observable and nearly discontinuous change in magnetization is conceived of as originating at a favorable nucleus, rapidly traveling to an end point and exhibiting on a much finer scale the same properties as those ascribed to the abnormally large discontinuities that have been produced in strained ferromagnetics. Such a change in magnetization would involve numerous ferromagnetic domains which together give complicated $\Delta I$'s under the conditions of macroscopic fields. This fits the marked angular spreading found which is in accord with Brion's work.[10] It furthermore anticipates a crystallographic dependence since larger regions would be involved if the process progressed mostly by reversals. This is obvious since a reversed domain subjects its end-on neighbors to the maximum favorable field variation. A train of reversals would then proceed farthest and produce the largest $\Delta I$ if occurring when $d\mathbf{H}_a/dt$ coincided nearly with a direction for easy reversal. In the partly magnetized specimen below the knee of the curve a traveling reversal still finds the individual domains oriented along the few crystallographically stable directions, but of course, with a different distribution among these permitted directions than is appropriate to the demagnetized state.

We wish to express our sincere thanks to Professor N. I. Adams, Jr. for his help in connection with the design of the amplifiers and to Professor L. W. McKeehan for his continued interest and encouragement throughout the course of the investigation.

[9] K. J. Sixtus and L. Tonks, Phys. Rev. **35**, 1441 (1930); **37**, 930 (1931); **39**, 357 (1932); **42**, 419 (1932); L. Tonks and K. J. Sixtus, ibid. **41**, 539 (1932); **43**, 70–80; **43**, 931 (1933).

[10] H. Brion, Ann. d. Physik **15**, 167 (1932).

# The Time of Relaxation in Crystals of Rochelle Salt

R. D. SCHULWAS-SOROKIN AND M. V. POSNOV, *Physical Technical Institute, Leningrad, U.S.S.R.*

(Received July 3, 1934)

A semiquantitative theory of the action of mechanical and electrical forces is given, using the concept of two relaxtion times. The theory is shown to offer qualitative explanations of numerous features of the experimental results such as the phenomenon of "creep" and the asymmetrical rates of polarization and depolarization observed by Kurchatov and Staub. Experiments on the dielectric constant and power loss have been made over a range from 1 to 1000 hertz, and dispersion curves have been obtained. The theory is applied to explain various features of the results.

## INTRODUCTION

DURING the last few years a number of papers have been published devoted to the study of the anomalous properties of crystals of Rochelle salt, the majority dealing with their electric or mechanical properties. If we try to systematize the results obtained, we may present them in the following form (Table I), in which the principal results of various authors for the polarization ($P$) and deformation ($x$) are given.

## THEORY

From the table it is clear that the deformation and polarization vary similarly. Since Rochelle salt is piezoelectric, it seemed to us that the whole of the polarization in the crystal, irrespective of whether it was obtained by applying electric or mechanical stresses, might be of piezoelectric origin. Both mechanical and electric fields produce deformation in the crystal. The dipole, or ionic group forming part of the molecule is displaced relative to its equilibrium position during the deformation of the lattice. Because of the absence of a center of symmetry in the Rochelle salt crystal, this displacement gives rise to an electric moment. Since the processes in Rochelle salt are reversible, provided the stresses are not too high, we may make use of the method of thermodynamic potential to test the above hypothesis. If we consider isothermal processes, the expression for the thermodynamic potential will be[1]

$$\zeta = \tfrac{1}{2}c_{kl}x_kx_l - e_{ik}\mathcal{E}_ix_k - \tfrac{1}{2}\eta_{il}\mathcal{E}_i\mathcal{E}_l.$$

The polarization is $P_i = e_{ik}x_k + \eta_{il}\mathcal{E}_l$, (1)

while the mechanical stress is $M_k = -c_{kl}x_k + e_{ik}\mathcal{E}_i$. In the particular case when the crystal is cut along the axes, the polarization in an electrical field applied along the axis $a$ is

$$P_1 = e_{14}x_4 + \eta_{11}\mathcal{E}_1, \qquad (1')$$

since $e_{11}=e_{12}=e_{13}=e_{15}=e_{16}=0$ and $\mathcal{E}_2=\mathcal{E}_3=0$. The mechanical stress $M_k=0$. In order to determine the value of $x_4$ we require only the value of $M_4$: $M_4 = -c_{44}x_4 + e_{14}\mathcal{E}_1 = 0$ since all $c_{4k}=0$ except $c_{44}$ whence $x_4=(e_{14}/c_{44})\mathcal{E}_1$. Putting this value of $x_4$ in (1′) we get

$$P_1 = (e_{14}^2/c_{44}+\eta_{11})\mathcal{E}_1 = (d_{14}^2c_{44}+\eta_{11})\mathcal{E}_1 = \eta'_{11}\mathcal{E}_1,$$

where $e_{14}=d_{14}c_{44}$. This expression is true for all crystals of the rhombic system, and it shows that the polarization in an applied electrical field is not only dependent on $\eta_{11}$ but also on the product $d_{14}^2c_{44}$, whereas one measures experimentally $\eta'_{11}=d_{14}^2c_{44}+\eta_{11}$. In crystals where $d_{14}$ is of the order $10^{-8}$ e.s.u./dyne, and $c_{44}=10^{11}$ dyne/cm² the first term will be of the order $10^{-5}$, i.e., negligibly small compared with $\eta_{11}$, which is of the order of unity in most crystals.

In Rochelle salt, $d_{14}$ varies between $4\cdot10^{-5}$ e.s.u./dyne and $2.6\cdot10^{-4}$ e.s.u./dyne[4] and $c_{44}=1.64\cdot10^{11}$ dyne/cm²,[7] so that the first term is of the order $10^3$, and is very large compared with $\eta_{11}$. Consequently the whole of the polarization in crystals of Rochelle salt is dependent on the first term. This is seen particularly clearly from Staub's[2] work, although his experiments did not show the mechanism of this displacement. For reflections from the surface, (1,0,0), i.e., the plane perpendicular to the axis $a$, Staub did not observe any change in intensity, and it is necessary to conclude that this is a result of the fact

[1] W. Voigt, Lehrb. d. Kristallphys. pp. 414, 563, 816 (1928).

TABLE I. *Summary of previous results.*

| No. | Polarization as function of various factors | Form of function and numerical value | Deformation as function of various factors | Form of function and numerical value |
|---|---|---|---|---|
| 1 | $P=f(\mathcal{E})$ | Saturated<br>870[3] e.s.u. 850[9] e.s.u. | $x=f(\mathcal{E})$ | Saturated<br>$7.5\cdot10^{-4}$[11] $5\cdot10^{-5}$ calculated from refs. (3) and (4) |
| 2 | $P=f(M)$ | Saturated<br>940[4] e.s.u. | $x=f(M)$ | Saturated[6]<br>$4.5\cdot10^{-5}$ calculated from refs. (7) and (4) |
| 3 | $P=f(T°)$ | Two Curie points<br>+22.5°[4] and −15°[10] | $x=f(T°)$ | Two Curie points<br>+23° and −15°;[8] +25°[2] |
| 4 | $P=f(t)$ | "Creep" of charge<br>$t=3$ min.[4] | $x=f(t)$ | Slow recovery of deformation after removal of field<br>$t=2$ min.[2] |
| 5 | $t_\rho=f(T°)$ | Increase of $t_\rho$ with decrease of temperature[4] | $t_x=f(T°)$ | Increase of $t_x$ with decrease of temperature[2] |

Remarks: $\mathcal{E}$—electric field, $M$—mechanical stress, $T°$—temperature, $t$—time, $t_\rho$ and $t_x$ relaxation time.

that $d_{11}=0$ and $x_1=0$. Further, Staub did not observe any changes in the position of the interference spots under the action of the electric field, but this can be accounted for by the insufficient accuracy of measurement which, according to the determinations of this author, was equal to 0.3 percent, or $3\times10^{-3}$ of the measured magnitude, while the deformation which should give the displacement in the interference spots was of the order $10^{-5}$.

From this point of view we can give a semi-quantitative theory of the behavior of Rochelle salt: under the action of a constant mechanical stress, and also under the action of a constant electric field.

(1) For a *constant applied mechanical stress* in the absence of an electric field we can suppose the motion of a dipole with the lattice to be represented by the equation[12]

$$r\dot{x}_4+c_{44}x_4=M_4, \tag{2}$$

where $M_4$ is the applied stress to which the displacement of the dipole is proportional and $r$ is a "viscosity" constant. Solving this equation, we get

$$x_4=(1-e^{-t/\theta})M_4/c_{44}, \tag{3}$$

where $M_4/c_{44}$ is the final value of the deformation, and $\theta=r/c_{44}$. Since the rotation takes place in a medium with large frictional forces, $\theta$ is large and the approach to this final value of $x_4$ and consequently of the polarization also, occurs very slowly. If we neglect the second term in Eq. (1′) because $\mathcal{E}$, = the polarization will be given by

$$P_1=e_{14}x_4=(1-e^{-t/\theta})e_{14}M_4/c_{44}$$
$$=d_{14}M_4(1-e^{-t/\theta}). \tag{4}$$

(2) For an applied *electrical field* we can represent the motion of a dipole by the equation

$$\rho\dot{x}_4+\beta x_4=\mathcal{E}_1, \tag{2′}$$

from which

$$x_4=(1-e^{-t/\tau})\mathcal{E}_1/\beta=d_{14}\mathcal{E}_1(1-e^{-t/\tau}), \tag{3′}$$

where $\beta=1/d_{14}$ and $\tau=\rho/\beta=\rho d_{14}$.

From Eq. (1) we get for the polarization if we neglect $\eta_{11}$ in agreement with the preceding argument

$$P_1=e_{14}x_4=d_{14}{}^2c_{44}\mathcal{E}_1(1-e^{-t/\tau}), \tag{4′}$$

from which we see that for an applied electrical field also the final value of the polarization is not attained instantaneously.

[2] Staub, Helv. Phys. Acta. p. 2 (1933).
[3] Kobeko and Kurchatov, Zeits. f. Physik **66**, 192 (1930).
[4] Schulwas-Sorokin, Zeits. f. Physik **73**, 700 (1932); **77**, 541 (1932).
[5] Isely, Phys. Rev. **24**, 569 (1924).
[6] S. Bloomenthal, Physics **4**, 172 (1933).
[7] Mandell, Proc. Roy. Soc. **A116**, 623 (1927).
[8] R. M. Davies, Nature **120**, 332 (1927).
[9] Oplatka, Helv. Phys. Acta. (1933).
[10] B. Kurchatov and I. Kurchatov, Phys. Zeits. d. Sow. **3**, 321 (1933).
[11] Sawyer and Tower, Phys. Rev. **35**, 269 (1930).
[12] We can neglect the inertial forces because $r$ and $\rho$ are large and the accelerations are consequently small.

The final magnitude of polarization obtained with a given deformation should be the same irrespective of whether the deformation was produced by an electric field or a mechanical stress. From Eqs. (4) and (4′), it follows that

$$M_4 = d_{14} c_{44} \mathcal{E}_1, \qquad (5)$$

i.e., we get the electrical equivalent of the mechanical stress. From Eq. (5) it is possible to determine the field necessary to produce a given polarization, if the mechanical stress required to produce the same polarization is known. If we take, for example, the polarization $P = 500$ e.s.u., this is obtained with a mechanical stress $M_2' = 12$ kg/cm² applied at an angle of 45° to the axes $b$ and $c$; $M_4 = \frac{1}{2} M_2' = 6$ kg/cm². Corresponding to a load $M_2'$, $d_{14} = 10.8 \cdot 10^{-5}$ e.s.u./dyne.[13] Putting this value in Eq. (5), we get

$$\mathcal{E}_1 = \frac{6 \cdot 10^6 \cdot 300}{1.08 \cdot 10^{-4} \cdot 1.64 \cdot 10''} = 102 \frac{\text{volt}}{\text{cm}}.$$

In Fig. 20 of the monograph of I. V. Kurchatov *Rochelle Electricity*, the curve $P = f(\mathcal{E})$ for a crystal of 1 cm thickness at +14°C is given. From this curve we get a polarization of 500 e.s.u. at $\mathcal{E}_1 = 130$ volt/cm. Similar calculations for a polarization of 300 e.s.u. give $\mathcal{E}_1 = 27$ volt/cm while the value required to produce this polarization experimentally is 50 volt/cm. As we pass to smaller stresses, i.e., into the region of "small polarizibility," the calculated value is considerably less than that actually required to produce the given polarization.

From our point of view, the phenomenon of saturation must be regarded as follows: an increase in the mechanical stress and electric field increases the deformation of the lattice, and consequently the angle formed between the position of the dipole for a given load, and its position before loading. However, there is a certain stress (field) at which the lattice is deformed so much that its smallest dimension is less than or equal to, the greatest dimension of the dipole, so that the latter can no longer rotate. When this limiting deformation of the lattice is reached, the bonds between certain ions in the lattice and the dipoles increase rapidly and the coefficients $c_{44}$ and $\beta = 1/d_{14}$ in Eqs. (2) and (2′) increase very considerably, producing a decrease in $\theta$ and $\tau$ for large stresses and electric fields. The decrease of $d_{14}$ with increasing mechanical stress was in fact observed by us. The influence of the electric field on $d_{14}$ is described later.

We are thus led to introduce *two* "times of relaxation" $\theta$ and $\tau$. Unfortunately we are not able to predict their theoretical values, as we can say little definitely about the two quantities $r$ and $\rho$. In this respect, therefore, the theory remains qualitative, and must be further investigated to be made completely satisfying. In terms of these concepts we can obtain, however, a fairly complete interpretation of the experimental results.

## Experiments with Static Mechanical Loads

Experiments have previously been made[4] on a crystal 12 mm long along the $a$ axis. The external stress was applied in a direction of 45° to the $b$ and $c$ axis. Fig. 1 gives the experimental results for the polarization as a function of the time elapsed since the application of the load. From these curves one can readily determine the time of relaxation $\theta$ for mechanical deformation of the crystal.* The curve of $\theta$ is given in Fig. 2 (continuous curve).

If we write $\theta = r/c_{44}$ and substitute $r = 10^{13}$ e.s.u. according to Tammann and Hesse[14] and $c_{44} = 3.28 \cdot 10^{11}$ dynes/cm² as measured by Mandell[7] for our experimental arrangement, we obtain a value $\theta = 30$ sec. agreeing well in order of magnitude with our experimental values.

A similar order of magnitude was found by Staub for the time of restoration of intensity of interference spots, after removal of the electric field, when the crystal is left under the influence of the internal mechanical stresses. As both the coefficient of "internal" viscosity and the elastic coefficients are functions of temperature, $\theta$ must be also. In the range from +25°C to −15°C the curve is hyperbolic and $\theta$ varies inversely with the temperature. At −15°C, $r$ becomes very large, so that at lower temperatures the linear dimensions of the lattice are less than the greatest dimension of the dipoles. The latter are then

[13] Schulwas-Sorokin, Zeits. f. Physik **73**, 700, 704 (1932).

* The idea of explaining the phenomenon of "creep" as the time of relaxation belongs to Professor J. Frenkel.

[14] Tammann and Hesse, Zeits. f. an. u. allg. Chemie **156**, 256 (1926).

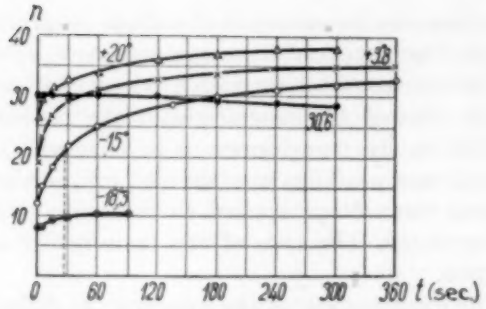


FIG. 1. The "creep" of polarization for an applied mechanical stress.

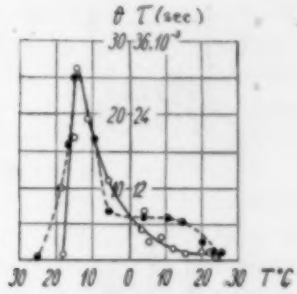


FIG. 2. The relaxation times as functions of temperature.

no longer involved in the deformation and as a consequence there is a considerable decrease in the polarization, as this is now produced only by the ions and electrons.

In general the appearance of "creep" is sharply defined only for small stresses. As the stress is increased the time of relaxation decreases, and at stresses corresponding to saturation[4] the polarization occurs instantaneously. $\theta$ is thus a function of the stress.

## Polarization in Static Electrical Fields

On the basis of the theory given above we can interpret some of the puzzling features of previous experiments on Rochelle salt. The behavior of the crystal is characterized by an "electrical time of relaxation" $\tau$ which is a function of the piezoelectric modulus and of the coefficient $\rho$ which may be called the "coefficient of electrical viscosity," but whose theoretical value is unknown. Since $d_{14}$ is a function of the field, $\tau$ will also be a function of the field.

According to the measurements of I. Kurchatov[15] and of Staub[2] $\tau$ is very small. Both authors also observed an asymmetry in the velocities of the processes of polarization and of depolarization. This asymmetry can be explained from the present point of view if we assume that in the polarization process in an electrical field the appropriate time of relaxation is $\tau$, while the depolarization occurring after removal of the field depends only on the internal mechanical stresses, the rate being determined by the mechanical time of relaxation $\theta$. We can, therefore, also understand the relation between the rate of depolarization and the quantity of electricity stored in the crystal, which from our point of view is proportional to the mechanical tension in the crystal (cf. Eq. (4)) and $\theta$ is a function of this tension.

[15] I. Kurchatov, Phys. Zeits. d. Sow. **5**, 200 (1934).

## Experiments with Alternating Fields

In 1931 Errera[16] studied the dispersion of the dielectric constant in Rochelle salt. The measurements were made in strong fields and extended over a frequency range of $3.4\times10^2$ to $10^6$ $H_z$. Frayne[17] investigated the phenomenon at higher frequencies. It was the aim of the present work to study the behavior of Rochelle salt in weak fields and at lower frequencies than those used by Errera, since the large values of the relaxation time which we obtained with static experiments suggested that the dispersion curve would be anomalous.

### Method of study. Experimental arrangement

The capacity bridge method (Fig. 3) was used for measuring the dielectric constant and the power factor. The arms $C_1$ and $C_2$ consisted of two almost equal, symmetrically mounted condensers of about 1200 cm capacity. Both condensers were placed in a shielded box, and in addition were shielded from one another. The moving plates were connected together, and to the screen at the point $A$. Both condensers were graduated so that it was possible to select a given ratio between the arms of the bridge. The arm $C_3$ contained a precision fixed condenser of 3600 cm capacity. This condenser, when necessary, was connected in parallel with a liquid variable resistance from $0.3\cdot10^6\Omega$ to $300\cdot10^6\Omega$. The arm $C_4$ consisted of a variable air condenser with

[16] J. Errera, Phys. Zeits. **32**, 369 (1931).
[17] J. S. Frayne, Phys. Rev. **20**, 97 (1922); **21**, 348 (1923).

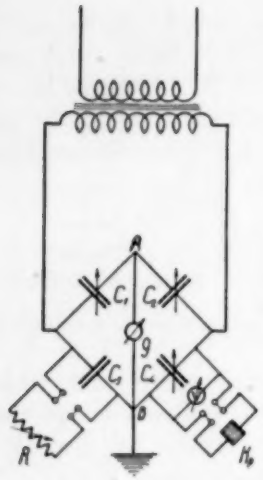


FIG. 3. The capacity bridge which was used for measuring the D.K.

capacity equal to 900 cm, and a condenser of 2550 cm capacity. This condenser was connected in parallel with that containing the crystal. All parts of the bridge were shielded, and the shields earthed. A dynatron generator supplied the alternating potential. The dynatron generator possesses the great advantage over other generators of low frequency in that no inductance coupling is necessary, and the frequency generated is determined by the natural period of the circuit itself. In order to obtain a given frequency it is only necessary to satisfy the condition: $L/CR=R_{in}$, where $R_{in}$ is the internal resistance of the valve, $L$ the self-inductance, $C$ the capacity and $R$ the ohmic resistance of the oscillating circuit.[18] The necessity of obtaining very low frequencies demanded the use of high self-induction, and thus $R$ had also to be large in order to avoid using a generator of very large dimensions. At very low frequencies the quantity $L/CR$ became much less than $R_{in}$ and it was therefore necessary (1) to select valves with low internal resistance, (2) to reduce $R_{in}$ by increasing the positive potential on the control grid. In this way it was possible to adjust the dynatron scheme to obtain frequencies over continual range from 1000 to 0.5. Since the oscillating circuit, in addition to the constant self-induction, contained an adjustable condenser and a variable self-inductance in the form of a multi-layer solenoid with movable core, it was easily possible to obtain any frequency in the above-mentioned range. The potential from the generator valves reached an amplifier through a potential divider which allowed the magnitude of the potential applied to the transformer to be changed. The transformer windings were divided into sections, so that the voltage applied to the bridge could be regulated. The core of the transformer was earthed.

The measurement of the frequency in different parts of the spectra was made in different ways: from 1000 to 60 hertz the measurements were made with a string frequency meter according to the system of A. I. Belov,[19] by using the fundamental tone for the high frequencies, and the overtones for the low frequencies. Frequencies from 65 to 6 hertz were measured with the frequency meter of Hartmann and Braun with which the region from 14 to 6 hertz was measured by overtones. Finally, the lowest frequencies were measured with a stop watch while listening to the clicks in a telephone, or by watching the vibrations of the pointer of a d.c. voltmeter. On account of the fact that the generator produced a series of overtones in addition to the fundamental tone, it was necessary to filter the current in the bridge in order to make measurements on the fundamental tone, or to use an indicator of the resonance type. The former method presents considerable difficulty because of the large range of frequencies (11 octaves), and consequently we selected the latter. A potential divider connected to an Edelmann string galvanometer was placed in the diagonal of the bridge. With the potential divider it was possible to regulate the potential difference on the galvanometer, and to increase the sensitivity of the indicator according to the balancing of the bridge. The galvanometer could be tuned to any frequency by tightening or slackening the string. Since a platinum wire 2.5$\mu$ thick was rapidly destroyed by frequent tightening or loosening, a platinum strip 2$\mu$ thick, placed on edge, was used. As the width of the strip was 40$\mu$ its strength was many times greater[20] than that of the wire. The use of this strip did not decrease the sensitivity of the apparatus appreciably, since the loss of sensi-

[18] Colebrook, Exp. Wireless 1931, p. 581.

[19] A. I. Belov, Wireless Telegraphy and Telephony, No. 56, 535 (1929) (in Russian).

[20] N. V. Nickolsky suggested the use of this strip, which he prepared, and we wish to express our gratitude to him.

tivity, as a result of the increased mechanical stress, was compensated by a considerable decrease in the ohmic resistance of the string, which was 108Ω. The sensitivity of the galvanometer for constant potential difference varied from 0.1 volt to $2\cdot10^{-5}$ volt, depending on the tension of the string. At resonance the sensitivity was considerably greater.

## Experimental Results

### A. The influence of frequency on the polarization

Following the lines of the theory given in a previous section for the case of harmonically varying mechanical or electrical fields, we replace the right-hand sides in Eqs. (2) and (2′) by $M_4$ sin $\omega t$ or $\mathcal{E}_1$ sin $\omega t$, respectively. The particular solutions for the forced vibrations then become for the two cases

$$x_4=[M_4/c_{44}(1+\omega^2\theta^2)^{\frac{1}{2}}]\sin(\omega t-\delta_1) \quad (6)$$

and

$$x_4=[\mathcal{E}_1/\beta(1+\omega^2\tau^2)^{\frac{1}{2}}]\sin(\omega t-\delta), \quad (6')$$

where, as previously, $\beta=1/d_{14}$ and $\mathcal{E}=\rho d_{14}$.

The quantities

$$S=1/c_{44}(1+\omega^2\theta^2)^{\frac{1}{2}} \text{ and } D=d_{14}/(1+\omega^2\tau^2)^{\frac{1}{2}} \quad (7)$$

will be referred to as the "dynamic modulus of elasticity" and the "dynamic piezo-modulus," respectively. If we assume, in accordance with the above, that the origin of the polarization in Rochelle salt is mainly piezoelectric, we get the mechanical equivalent of the electrical field. The amplitude of the deformation is

$$x_4=D\mathcal{E}_1=SM_4, \quad (8)$$

whence $M_4=D\mathcal{E}_1/S$, i.e., the electric field of amplitude $\mathcal{E}_1$ multiplied by $D/S$ can produce the same effect as an alternating mechanical stress of amplitude $M_4$. The amplitude of the polarization in a crystal acted upon by an alternating electric field of amplitude $\mathcal{E}_1$ will be[21]:

$$P_1=\mathrm{E}x_4=(D/S)x_4=(D^2/S)\mathcal{E}_1.$$

Substituting in this, the values of $D$ and $S$, we get

$$P_1=d_{14}^2c_{44}\frac{(1+\theta^2\omega^2)^{\frac{1}{2}}}{1+\tau^2\omega^2}\mathcal{E}_1=K\frac{(1+\theta^2\omega^2)^{\frac{1}{2}}}{1+\tau^2\omega^2}\mathcal{E}_1. \quad (9)$$

[21] $\mathrm{E}=D/S$ is the dynamic piezo-constant.

The factor multiplying $\mathcal{E}_1$ in the expression for the polarization is the apparent coefficient of polarization, which we shall denote by $\eta_4$. The expression $\eta_4$ at $\omega=\infty$ becomes zero, and when $\omega=0$ it becomes equal to that obtained for a constant field (see Eq. (4′)).

Since $K$ is constant, the expression $(1+\theta^2\omega^2)^{\frac{1}{2}}/(1+\tau^2\omega^2)$ determines the way in which the polarization depends on the frequency, if the measurements at all frequencies are made with a constant amplitude of the field $\mathcal{E}_1$. By taking the first derivative of this equation, and setting it equal to zero, we find the value of $\omega_m$, at which the polarization is a maximum or minimum,

$$\omega_m=(\theta^2-2\tau^2)^{\frac{1}{2}}/\tau\theta. \quad (10)$$

The negative sign of the second derivative, if we substitute the value of $\omega_m$ from (10) shows that the function has a maximum. Dropping $2\tau^2$ with respect to $\theta^2$ in the numerator of Eq. (10) (as $\theta\gg\tau$), we find

$$\tau=1/\omega_{\max}. \quad (11)$$

The experimental curves are given in Fig. 4. Since the amplitude of the field $\mathcal{E}_1$ is the same at all frequencies, the course of $P_1=f(\omega)$ will also be the same. The two curves in the upper part of the plot refer to two crystals: the curve $\alpha$ refers to a slab, whose thickness in the direction of the axis $a$ was 3.4 mm, while curve $\beta$ is for a crystal of thickness 34 mm. The scale on the right refers to the thin slab, and that on the left to the thick. Further, the curve $\alpha$ was taken at $\mathcal{E}_{eff}=26$ volt/cm, and the curve $\beta$ at $\mathcal{E}_{eff}=3.5$ volt/cm.

We see that both curves have a sharp maximum. For the thicker crystal $\tau=4.2\cdot10^{-3}$ sec. at 16°C, and for the thinner crystal $\tau=4.7\cdot10^{-3}$ sec. at 15°C.

In order to test the agreement between the experimental curve and the function of Eq. (9), the factor $(1+\theta^2\omega^2)^{\frac{1}{2}}/(1+\tau^2\omega^2)$ was calculated for various frequencies for a crystal whose time of relaxation was also $\tau=4.2\cdot10^{-3}$ sec.

The form of this relation is given in Fig. 4 (dashed curve). The form of both curves is similar. It seems to us that this similarity supports our hypothesis.

Unfortunately, we must be content for the present with a qualitative agreement between

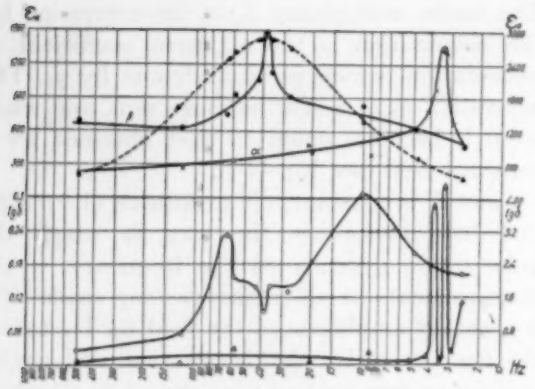

FIG. 4. The apparent dielectric coefficient (upper curves) and the power factor (lower curves) as functions of the frequency.

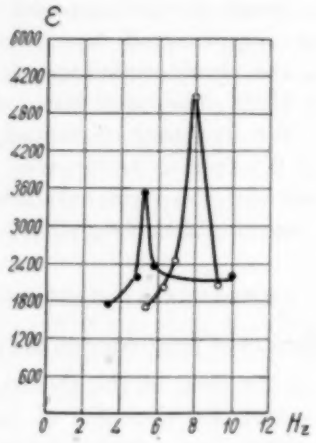


FIG. 5. The displacement of the position of dispersion maxima with the field.

the experimental and theoretical curves, since the value of the coefficient $d_{14}$ for such small electric fields, and correspondingly small mechanical stresses, is not known. If we use this divergence between the theoretical and experimental magnitudes, we may make an estimate of the value of $d_{14}$ (and possibly also of $s_{44}$) for these small fields, and we find that it must be of the order of $10^{-5}$ to$10^{-6}$ e.s.u./dyne which means that $d_{14}=f(\varepsilon_1)$ must pass through a maximum.

### B. The relation between the time of relaxation and the field

In Eq. (6′) we saw that $\tau$, the electric time of relaxation, is equal to $\rho d_{14}$, where $d_{14}$ is the piezo-modulus, and $\rho$ is the coefficient of "electric viscosity." The piezo-modulus in its turn is a function of the mechanical stress. The function $d_{14}=f(M_4)$ is approximately hyperbolic[13] and may be written with sufficient accuracy in the form: $d_{14}M_4=\text{const}$. If we substitute in this expression the equivalent of $M_4$ from Eq. (5), we get $d_{14}^2 c_{44}\varepsilon_1=C$. Assuming that $c_{44}$ is independent of the field, we get

$$d_{14}=C_1/\varepsilon_1^{\frac{1}{2}}. \tag{12}$$

For the weak fields with which we are determining the time of relaxation, we may suppose that $\rho$ is independent of the field. It then appears that $\tau=Q_1/\varepsilon^{\frac{1}{2}}$. It has been actually shown by experiment that the shift of the position of the maximum in the dispersion curve is dependent on the magnitude of the applied field. With an increase of field, the maximum is displaced towards higher frequencies. Two maxima in the dispersion curves for one and the same crystal at the same temperature, but with different field strengths, are shown in Fig. 5.

We see from Table II that the value of $Q'$ remains constant for each crystal (column six). The maximum deviation from the mean is 7 percent for the thick crystal, and 2 percent for the thin, when the field is varied from 2 to 7 times.

TABLE II. *Values of* $\omega_{max}$ *and* $\tau$ *for Rochelle salt crystals.*

| $N$ | $\varepsilon_1 \frac{\text{volt}}{\text{cm}}$ | $\varepsilon_1^{\frac{1}{2}}$ | $\omega_{max}$ | $\tau\cdot10^3$ (sec.) | $\tau\times\varepsilon_1^{\frac{1}{2}}\cdot10^3$ |
|---|---|---|---|---|---|
| | | (a) crystal thickness 18 mm | | | |
| 1 | 3.6 | 1.9 | 157 | 6.4 | 12.1 |
| 2 | 8.35 | 2.9 | 232 | 4.3 | 12.5 |
| 3 | 11.6 | 3.4 | 301 | 3.3 | 11.2 |
| 4 | 23.9 | 4.9 | 450 | 2.2 | 10.8 |
| | | (b) crystal thickness 2.08 mm | | | |
| 1 | 24 | 4.9 | 14.5 | 70 | 34 |
| 2 | 33.6 | 5.8 | 17.8 | 56 | 33 |
| 3 | 57.8 | 7.6 | 20.3 | 49 | 37 |

### C. The influence of the field on the dielectric constant.

The influence of the field on the dielectric constant was measured by Errera.[16] He found that the dielectric constant increased proportionally to the field. Our first experiments showed that this is not right for our range of frequencies, but here there must be a more complicated relation. Indeed, we have shown that the coefficient of polarization as a function of the field has a sharp maximum for weak fields, the position of

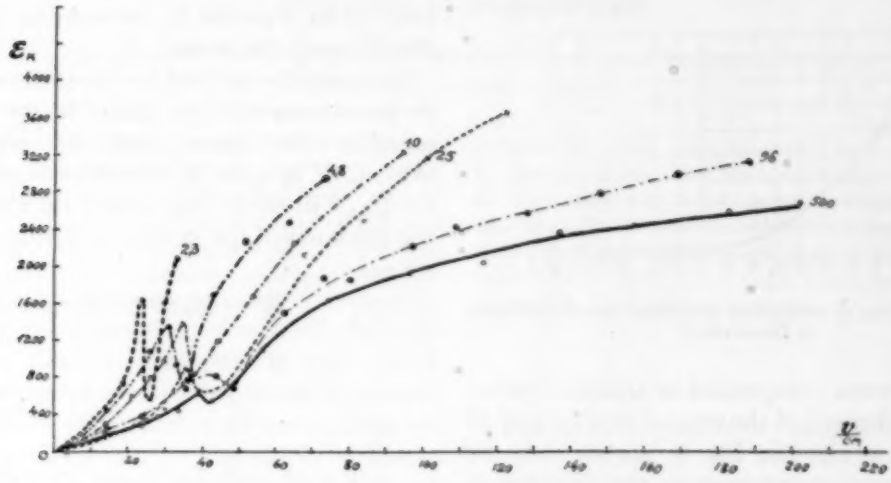

FIG. 6. The apparent dielectric coefficient as a function of the field for various frequencies.

which varies with the frequency (Fig. 6). This maximum decreases with increasing frequency and becomes scarcely perceptible at 500 $H_z$. For the field larger than about 40 volt/cm (depending on the thickness of the crystal) (Fig. 6) the coefficient of polarization increases, but not linearly with the field.

**D. The relation between the time of relaxation $\tau$ and temperature.**

Curves similar to those given in Fig. 4 for 16°C were taken at different temperatures. At all temperatures between −15° and +25°C, a maximum was obtained. These maxima for certain temperatures are given in Fig. 7 where we see that as the temperature is reduced the maximum shifts towards smaller frequencies, i.e., $\omega_m$ decreases. With temperatures below −15°C and above +25°C, no maxima were found in the frequency interval used. (In the figure the curves for the temperatures −25° and +25.5°C are drawn on a greatly enlarged scale.)

The values of $\tau$ calculated from the experimental data according to Eq. (11) are plotted in Fig. 2 (dashed curve), for the crystal the thickness of which was 35 mm and the field $\mathcal{E}=3.5$ volt/cm. We see that the variation with temperature is quite similar to the variation of $\theta$ with temperature (Fig. 2).

This similarity for the temperature relation of the mechanical and electrical times of relaxation, obtained by such different methods, appears to support still further our view of the mechanism of the production of polarization in Rochelle salt. The electric time of relaxation is $\rho d_{14}$. The piezomodulus $d_{14}$ is known to be a function of the temperature and at −16° and +25°C it becomes very small. The quantity $\rho$ probably depends on the temperature also, but as yet it is difficult to say what will be the character of this relation. It is thus easy to understand why the relation between $\tau$ and temperature is so complex.

**E. The relation between the time of relaxation $\tau$ and the thickness of the crystal**

I. V. Kurchatov studied the effect of crystal thickness on the magnitude of the apparent dielectric constant, and thus of the field necessary to produce saturation. This has been described in his monograph *Rochelle Electricity*. We have studied the effect of crystal thickness on the speed of attaining complete polarization. The

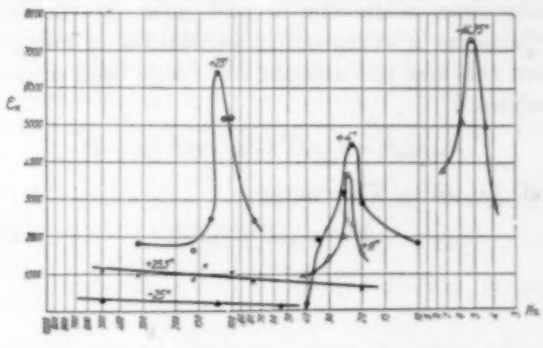

FIG. 7. The displacement of the position of dispersion maxima at different temperatures.

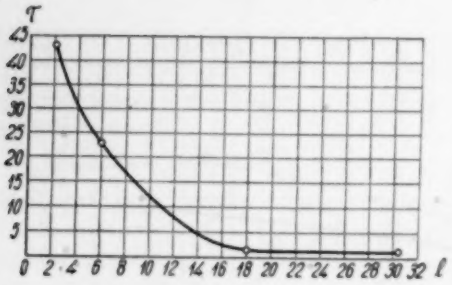


FIG. 8. The time of relaxation as a function of thickness of the crystal.

relation between $\tau$ (expressed in arbitrary units) and the thickness $l$ of the crystal in a field of 25 volt per cm is given in Fig. 8. We see that the time of relaxation decreases as the thickness is increased, but after a certain thickness, which probably depends on the field strength, the time of relaxation does not change. At present it is difficult to explain this effect of crystal thickness. Probably it is necessary to study the question in connection with the effect of field strength on the magnitude of the polarization, and on the time of relaxation in crystals of Rochelle salt.

### Losses in Crystals of Rochelle Salt

According to the hypotheses developed above for the process of polarization in crystals of Rochelle salt, the energy of the electric field must be spent in deforming the crystal. Eq. (2′) can be written in the form:

$$e_{14}\rho\dot{x}_4+(e_{14}/d_{14})x_4=e_{14}\mathcal{E}_1 \sin \omega t,$$

where we have on the right the magnitude of the force. Multiplying both sides of this equation by $\dot{x}_4$, i.e., by the velocity of deformation, we get on the right side the work done by the field in unit time, while the second term on the left represents a symmetrical oscillation of energy, and the first the amount of energy used up per second.

$$e_{14}\rho\dot{x}_4\dot{x}_4=e_{14}\rho D^2\mathcal{E}_1{}^2\omega^2 \cos^2(\omega t-\delta)$$

(cf. Eq. (6′)). The energy

$$W=e_{14}\rho D^2\mathcal{E}_1{}^2\omega^2/2 \qquad (13)$$

used up in a period in overcoming the friction should equal the losses.

In the bridge method the losses are determined by measurement of the power factor. From this quantity the losses may be expressed as $W=\omega C\mathcal{E}^2l^2$ tg $\varphi$, or by substitution of the value $C=Q\eta_k/l$ where $Q$—the area of the electrodes $l$—the thickness of the crystal, and $\eta_k$ from Eq. (13) we get

$$W=(Ql\omega D^2\mathcal{E}_1{}^2/S) \text{ tg } \varphi.$$

If we refer this equation to unit volume and equate it to the value of the energy in Eq. (13), we get

$$\text{tg } \varphi=e_{14}\rho\omega S/2=[d_{14}\rho\omega/2(1+\theta^2\omega^2)^{\frac{1}{2}}] \qquad (14)$$

since $e_{14}=d_{14}/s_{44}$, and $d_{14}\rho=\tau$. This relation between tg $\varphi$ and the frequency should show a minimum at $\omega_m=1/\tau$, i.e., at just that frequency at which the dielectric coefficient is a maximum. Our curves for tg $\varphi=f(\omega)$ do in fact pass through a minimum at the relaxation frequency, but on either side of this minimum there are two symmetrically placed maxima, whose appearance we have as yet been unable to explain. The value of tg $\varphi$ at the relaxation frequency, calculated from Eq. (14), after substituting the experimental values of $\omega$ and $\theta$, was 0.002 for the thick crystal, and 0.14 for the thin. The values obtained by measurement were 0.09 and 0.12, respectively. Within the frequency range used, tg $\varphi$ should be practically independent of the frequency, since $(\theta\omega)^2$ is large compared with unity and tg $\varphi$ should depend only on the times of relaxation $\tau$ and $\theta$.

However, we see that there is a very distinct frequency relationship. It seems to us that the cause of this may lie in the fact that in the equation of motion we considered the displacement as proportional to the deformation, instead of equal to the deformation itself.

In conclusion we wish to express our gratitude to Professor J. Frenkel for suggesting this problem, and to Professor W. Fredericks for his interest and critical consideration of our results.

# Properties of Rochelle Salt

HANS MUELLER, *The George Eastman Laboratory, Massachusetts Institute of Technology*

(Received November 12, 1934)

Measurements of the dielectric, pyroelectric, optical and electro-optical properties of Rochelle salt, and a theory correlating all observations are given. The theory is based on the assumptions that all properties depend on the inner field $F=E+fP$, and that the Curie point changes with temperature. The theory explains the observed variation of the susceptibility with temperature and field strength, the anomalies of the quadratic electro-optical effect, the pyroelectric effect, the hysteresis loop, the abnormal temperature variation of the birefringence and the change of these properties if the piezoelectric deformations are prevented. It is shown that the electro-optical effect is a Kerr effect. A longitudinal Kerr effect is discovered. A small crystal represents a single Weiss region, but large crystals show a Barkhausen effect.

ROCHELLE salt is noted for its large piezoelectric effect and its anomalous dielectric behavior. The dielectric anomalies occur only for fields in the direction of the *a*-axis. They are very similar to the magnetic properties of ferromagnetic substances. However unlike ferromagnetism, the anomalies disappear not only above a critical temperature, but vanish also for low temperatures. There exist two Curie points, 23.7° and −18°. The piezoelectric effect varies in the same manner as the dielectric polarization. Both have sharp maxima at the Curie points and shows hysteresis and saturation at temperatures between the Curie points. Connected with the dielectric anomalies is the existence of a series of other effects, namely: the linear and quadratic electro-optic effect,[1] the electro-caloric effect,[2] the change of specific heat at the Curie points,[3] the pyroelectric effect,[4] unipolar conduction, and an abnormal temperature coefficient of the birefringence. It has been shown[5] that the rhombic hemiedric crystal structure does not change at the Curie points, but the intensity of some x-ray reflections shows an abnormal change with temperature and electric field.[6]

Two theories have been advanced to explain these properties. Cady's[7] theory takes into account the secondary effect of piezoelectricity. Kobeko and Kurtschatov[8] assume the existence of free dipoles in the crystal and develop a theory analogous to Weiss's theory of ferromagnetism. Neither theory is entirely satisfactory. Cady's theory does not explain the optical properties and Weiss's theory, as used by Kurtschatov,[8, 9] cannot account for the change of the dielectric properties when the piezoelectric deformations are prevented. A satisfactory explanation of all observations can only be given by a combination of both theories.

## EXPERIMENTAL DIFFICULTIES

Our investigations show, that it is possible to obtain reproducible data on Rochelle salt, provided the following conditions are fulfilled.

The crystal must be able to deform freely. Mechanical constraints alter radically all its properties.[10] Since good contact[11] between crystal and electrodes is required, the electrodes must be of small mechanical rigidity. Electrodes of conducting paint, graphite or metal foil[12] were found equally suitable and give the same results. The tinfoil electrode, provided it is properly attached, was found most convenient. The electrodes must cover the entire face of the crystal. Uncovered edges are a source of constraining forces for the interior part of the crystal. The

[1] F. Pockels, Göttinger Nachrichten, 1895.
[2] P. Kobeko and I. Kurtschatov, Zeits. f. Physik **66**, 192 (1930).
[3] P. Kobeko and J. Nelidov, Phys. Zeits. d. Sow. **1**, 382 (1932).
[4] J. Valasek, Phys. Rev. **17**, 475 (1921); **20**, 639 (1922); **19**, 478, 529 (1922); **24**, 560 (1924).
[5] H. M. Krutter and B. E. Warren, Phys. Rev. **43**, 500 (1933).
[6] H. Staub, Helv. Phys. Acta. **7**, 1, 480 (1934).
[7] W. G. Cady, Phys. Rev. **33**, 278 (1929).
[8] I. B. Kurtschatov, Seignette—*Electricity*, Monograph, 1933.
[9] B. and I. Kurtschatov, Phys. Zeits. d. Sow. **3**, 321 (1933).
[10] C. B. Sawyer and C. H. Tower, Phys. Rev. **35**, 269 (1930).
[11] Busch, Helv. Phys. Acta **6**, 315 (1933).
[12] Electrodes of evaporated silver (A. Zeleny and J. Valasek, Phys. Rev. **46**, 450 (1934)) were found to be unsatisfactory since the crystal effloresces in the vacuum.

crystal is either suspended on strips of tinfoil attached to the electrodes, or supported on knife edges along the lines for which the piezoelectric displacements vanish.

The temperature must be accurately controlled. The dielectric and optical measurements provide very accurate means to ascertain that the entire crystal has the same temperature as the bath. It was found necessary to wait more than two hours before temperature equilibrium was reached. The temperature is measured with two or more separate thermocouples, one of which is attached to one electrode, and a type $K$ potentiometer.

Surface conductivity is practically eliminated by annealing the crystal for several hours at 45°, and drying it for about 20 minutes over phosphorous pentoxide. Dehydration of the surface layer must be avoided. For a properly annealed and dried crystal the electric strength is more than 20 kv/cm.

The influence of the electrolytic conduction is minimized by the use of a.c. methods. We have verified[11] that the dielectric properties are the same for frequencies up to 5000 cycles.

In measurements with d.c. voltages the complications due to conductivity are avoided by making all observations immediately after the voltage is applied, and by grounding both electrodes immediately afterwards. The next observation is made with the field reversed. After a few preliminary trials it is possible to set the measuring device very close to the correct setting and readings can be made before the field has appreciably changed.

## The Crystals

All crystals were grown, cut, and some also foiled by the Brush Development Company. The uniformity of the results gathered on more than twenty different crystals testifies for the purity of the material. In Table I we give the dimensions of the crystals which were used in the final measurements.

Table I. *Length in direction* (mm).

| No. | 1 | 2 | 3 | 4 | 5 | 6 | 7 | 8 |
|---|---|---|---|---|---|---|---|---|
| *a* | 3.1 | 2 | 2.2 | 25 | 25 | 8.1 | 20 | 34 |
| *b* | 60 | 37 | 55 | 1.5 | 25 | 13.8 | 50 | 10 |
| *c* | 100 | 56 | 31 | 25 | 1.5 | 29.6 | 90 | 10 |

## Experimental Methods

Dielectric measurements were performed with the following methods:

(a) Bridge measurements with a General Radio capacitance bridge, using 1000 cycle a.c. of a tuning fork oscillator. The bridge output is amplified with a two stage resistance coupled amplifier. The substitution method was used. The crystals are suspended in sealed glass tubes, which are immersed in the bath whose temperature is controlled by a mercury regulator.

(b) Determination of the a.c. capacity while the crystal is under the influence of a d.c. voltage. For this purpose the bridge arm is modified, as shown in Fig. 1.

(c) The same arrangement in Fig. 1 is connected in parallel with the condenser of an audio-frequency oscillator. The change of capacitance with field strength produces a frequency change of the oscillator.[12]

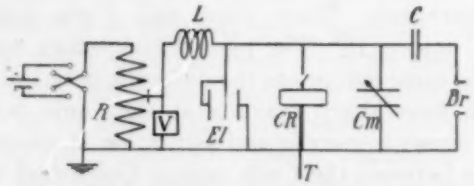


Fig. 1. Modified bridge arm. $V$ voltmeter, *El* electrometer, *CR* crystal condenser, *Cm* measuring condenser, $L=60$ henry, $C=2$ mf.

(d) Investigation with the cathode-ray oscillograph. Sawyer and Tower's[10] method is improved by the use of the arrangement shown in Fig. 2. The resistance $R$ serves to correct for the power loss in the crystal. The cathode-ray oscillograph uses the R.C.A. tube 905. Measurements with 500 cycles are found to be more reliable than with 60 cycles.

## Optical and Electro-Optical Investigations

All optical investigations were made with monochromatic light of $\lambda=5461$A furnished by a Hg arc and a filter. The optical system consists of a polarizing nicol, a Babinet compensator, a low power microscope with the analyzing nicol between ocular and objective and a system of

[12] Demonstrated at the meeting of the A. A. P. T., December, 1933.

lenses and stops to produce a parallel pencil of light. The compensator permits measurements of a change of optical path of 1/150λ. The light passes through the crystal in the direction of one of the axes and is polarized at 45° to the other two axes. The crystal is mounted in a brass tube which passes horizontally through the temperature bath. The tube is closed by two sets of plane parallel windows. The orientation of the crystal is adjusted by moving the whole bath, which is mounted on a movable platform. In making the adjustment we made use of the fact that the linear electro-optical effect must vanish if the light passes in the direction of the *b* or *c* axes. The surfaces of the crystals, where the light enters and leaves, are polished and parallel. For measurements above 40° it is necessary to protect the polished faces with a cover glass, attached with balsam in xylene, otherwise the surface soon becomes opaque due to efflorescence. The voltage is furnished by a kenotron outfit, and measured with a galvanometer and high resistances.

### Pyroelectric Measurements

This experiment required a particularly careful mounting of the crystal. Two rings of fused quartz hold it in a small brass tube in the center of a large well stirred temperature bath. All leads are shielded and insulated with quartz capillaries. The temperature is changed in steps of about 2° and, after every change, temperature equilibrium is attained. The method of Gaugain[14] was used for qualitative observations, but for quantitative measurements the compensation method of Ackermann[15] was employed. We constructed a quartz insulated Harms-condenser with a capacity of 1158 mmf and used an Edelmann-Lutz string electrometer at a sensitivity of 0.01 volt per scale division.

### Evaluations and Correction

The dielectric constant in the *a* direction was calculated by using for the geometrical capacitance $C_g = A/4\pi t$. Busch[11] has used Kirchhoff's correction for the edge effect, but if one takes into account the large ratio between the dielectric constant in the *a* direction and the constants in the *b* and *c* directions, one realizes that this edge effect is negligible. For the same reason the Chaumont correction for the Kerr effect can be omitted. We have varied the ratio of electrode area to thickness by a factor 10 without discovering any influence of the edge effects.

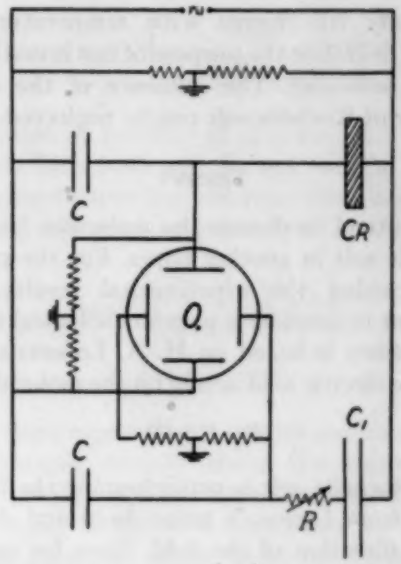


FIG. 2. Oscillograph connections. *O* oscillograph, $C = 0.03$ mf, $C' = 0.6$ mf, *Cr* crystal.

In the range where the polarization $P$ is not proportional to the field $E$, we assume that the a.c. measurements give $\kappa_E = \partial P/\partial E$ for the value of $E$ corresponding to the superposed d.c. voltage.

The cathode-ray oscillograms are evaluated with the help of calibration curves. From Fig. 2 it is evident that the oscillograms are not true $P(E)$ curves. To construct these curves the photographs were projected on cross-section paper and the necessary corrections applied.

The optical and electro-optical measurements give $(n_a - n_b)/\lambda$, etc. The thickness of the crystals made it necessary to carry out all observations on an interference line of high order. The order number $S$ was not determined. Its value can be estimated by using Valasek's[4] values of the indices of refraction $n_a$ (of light, whose electric vector oscillates in the *a* direction), $n_b$ and $n_c$. Though we are not able to give the absolute values of the birefringence, we can measure

[14] W. Voigt, *Lehrbuch der Kristallphysik*, p. 239.
[15] Ackermann, Ann. d. Physik **46**, 197 (1915).

accurately its change with temperature and electric field. For the purpose of our investigation this is sufficient. The influence of the optical activity of Rochelle salt can be neglected.

## Theory

We intend to discuss the molecular theory of Rochelle salt in another paper. For the purpose of discussing the experimental results, it is sufficient to consider a phenomenological theory. This theory is based on H. A. Lorentz's result that the electric field acting on the molecules is

$$F=E+fP. \tag{1}$$

Since Rochelle salt is orthorhombic the factor $f$ differs from Lorentz's value $4\pi/3$ and depends on the direction of the field. Since for ordinary dielectrics $F$ and $E$ are proportional, we assume that the dielectric polarization, the piezoelectric deformation $y_s$, the electro-optical effects and the change of scattering of x-rays depend on $F$ in the same manner as they depend on $E$ in normal dielectrics. We postulate therefore

$$y_s=\delta_{14}F. \tag{2}$$

The available data[16] are not sufficient to decide whether a term in $F^3$ should be introduced in (2). Since in the important temperature range $fP$ is much larger than $E$, this postulate agrees with the observed proportionality of $y_s$ with $P$. The dielectric polarization is given by

$$P=\alpha F-\beta F^3. \tag{3}$$

The linear term is the result of four effects

$$\alpha=\alpha_1+\alpha_2+\alpha_3+\alpha_4,$$

where $\alpha_1$ is the optical polarizability, $\alpha_2$ is due to the displacement of ions in the lattice, $\alpha_3=e_{14}\delta_{14}$ is due to the piezoelectric back polarization[16] $e_{14}y_s$ and $\alpha_4$ gives the contribution of dipoles. In a finite plate $\alpha_3$ depends on the geometrical dimensions of the crystal, and vanishes if the deformations are prevented. $\alpha_3$ and $\alpha_4$ are responsible for a marked temperature dependence of $\alpha$.

The term $\beta F^3$ may be due to the existence of a cubic term in (2) or it is due to the orientation of dipoles. The present data do not require the introduction of higher powers of $F$ in (3).

The quadratic electro-optical effect is proportional to $F^2$. If $\Delta_a$ designates the change of $(n_b-n_c)/\lambda$ produced by an electric field, we assume

$$\Delta_a=\rho_aF^2;\quad \Delta_b=\rho_bF^2;\quad \Delta_c=\rho_cF^2. \tag{4}$$

This definition requires

$$\rho_a+\rho_b+\rho_c=0. \tag{5}$$

Since $\Delta_a$ represents a change of the polarization of light passing through the crystal in the direction of the applied field, we shall call it a "longitudinal Kerr effect." The "longitudinal Kerr constant" $\rho_a$ can be calculated with the help of (5) from the "transversal Kerr constants" $\rho_b$ and $\rho_c$.

From (1) and (3) we get

$$E=(1-\alpha f)F+\beta fF^3.$$

The Curie points are the temperatures where $\alpha f=1$. We introduce therefore as "Curie temperature" $\Theta$

$$\Theta=\alpha fT \tag{6}$$

and get the fundamental equation

$$P=(1-\Theta/T)F+\beta fF^3. \tag{7}$$

The Curie temperature $\Theta$ is a function of the temperature. The dielectric properties at the temperature $T$ are analogous to the magnetic properties of a ferromagnetic substance whose Curie point is at the temperature $\Theta(T)$. While the concept of a variable Curie point, or Curie temperature, is new, the ideas on which this concept is based are identical with those of Kurtschatov, Bernal and Fowler,[17] and of Debye. (Theory of the dielectric properties of liquids with polar molecules.)

The experimental Curie points $T_c$, defined as the temperatures where the transition from the normal to the "ferro"-dielectric state occurs, are the solutions of the equation $\Theta(T)=T$.

It is convenient to assume that within small temperature ranges $\Theta$ is a linear function of the

[16] S. Bloomenthal, Physics **4**, 172 (1933).

[17] Bernal and Fowler, J. Chem. Phys. **1**, 515 (1933).

absolute temperature $T$. For temperatures $t$ (centigrades) near the Curie points we can therefore write

$$T-\Theta=\gamma(t-t_c), \tag{8}$$

where $(1-\gamma)$ is the slope of $\Theta(T)$ at the Curie point. If $T>\Theta$ the dielectric behavior is normal; if $T<\Theta$ the anomalies occur. We consider the two cases separately.

**$T < \Theta$**

For very small fields $E$ the dielectric susceptibility $\kappa_0$ follows a law similar to the Curie-Weiss law for ferromagnetism

$$\frac{1}{\kappa_0}=\frac{f}{\Theta}(T-\Theta).$$

Near the Curie point this leads to the approximation

$$\frac{1}{\kappa_0}=\frac{f\gamma}{T_c}(t-t_c)=\frac{t-t_c}{C}. \tag{9}$$

The Kerr effect for small fields is

$$\Delta=\frac{\rho T^2}{(T-\Theta)^2}E^2=KE^2\leqq\frac{\rho T_c^2}{\gamma^2(t-t_c)^2}E^2, \tag{10}$$

where the last expression holds only near the Curie point. $K$ is Kerr's constant as usually defined. Eqs. (9) and (10) are limiting laws for $E\to 0$. The larger $(T-\Theta)$ the wider their range of validity.

In the range where the term $\beta f F^3$ is small, but not negligible, we can make the development

$$F=\frac{1}{1-\Theta/T}E-\frac{\beta f}{(1-\Theta/T)^4}E^3.$$

This leads to

$$\kappa_E=\kappa_0(1-GE^2) \tag{11}$$

with

$$G=\frac{3\beta f}{(\Theta/T)(1-\Theta/T)^3}$$

or near the Curie point

$$\left(\frac{1}{G}\right)^{\frac{1}{2}}=\frac{\gamma}{T_c}\left(\frac{1}{3\beta f}\right)^{\frac{1}{2}}(t-t_c)=g(t-t_c). \tag{12}$$

For the Kerr effect the second approximation gives

$$\Delta=KE^2\left[1-\frac{2\beta f}{(1-T/\Theta)^3}E^2\right]. \tag{13}$$

The range of validity of (11) and (13) is very limited. They hold only for not very large fields and temperatures not too near the Curie point. At the Curie point we get $\kappa_0=\infty$

$$\kappa_E=\frac{1}{f}\left[\frac{1}{3}\left(\frac{1}{\beta f E^2}\right)^{\frac{1}{2}}-1\right]$$

and

$$\Delta=\rho(E/\beta f)^{\frac{1}{2}}. \tag{14}$$

The best experimental results are obtained at temperatures slightly above the Curie point, where the second approximation holds for small fields only. Hence it is important to develop general formulas which hold for large fields. Using (7) and (4) we get for the Kerr effect

$$E/(\Delta)^{\frac{1}{2}}=R(t-t_c)+Q\Delta, \tag{15}$$

where

$$R=\frac{\gamma}{T_c\rho^{\frac{1}{2}}}=\frac{1}{(K)^{\frac{1}{2}}}\frac{1}{(t-t_c)}, \tag{16}$$

$$Q=\beta f/\rho^{\frac{1}{2}}. \tag{17}$$

A similar formula can be derived for the susceptibilities. We introduce

$$X=\frac{(\kappa_0-\kappa_E)f^2}{(1+f\kappa_0)(1+f\kappa_E)}.$$

Near the Curie point $\kappa_0$ and $\kappa_E$ are very large, and hence $X$ is given with sufficient accuracy by

$$X=(\kappa_0-\kappa_E)/\kappa_0\kappa_E. \tag{18}$$

Eq. (7) leads then to

$$E/(X)^{\frac{1}{2}}=M(t-t_c)+NX, \tag{19}$$

where

$$M=\gamma/fT_c(3\beta)^{\frac{1}{2}};\quad N=1/3f^2(3\beta)^{\frac{1}{2}}. \tag{20}$$

**$T < \Theta$**

In this temperature range we get a spontaneous polarization $P_0$. With $E=0$ Eq. (7) gives

$$P_0^2=(F_0/f)^2=(1/\beta f^2T)(\Theta-T), \tag{21}$$

where $F_0$ is the spontaneous inner field. Near the Curie point we get

$$P_0^2=(\gamma/\beta f^2 T_c)(t_c-t)=h(t_c-t). \quad (21')$$

This spontaneous polarization, since it depends on temperature, manifests itself in the same way as an ordinary pyroelectric effect. The crystallographic symmetry of Rochelle salt does not permit an ordinary pyroelectric effect. Its apparent pyroelectricity is due to this spontaneous polarization. The existence of this effect is therefore no violation of Neumann's principle. The direction of $P_0$ is parallel to the $a$-axis, "the direction of easy polarization" but the sign of $P_0$ is not determined by the theory.

The spontaneous field produces a spontaneous Kerr effect

$$\Delta_0=(\rho/\beta f T)(\Theta-T) \quad (22)$$

or, near the Curie point

$$\Delta_0=(\rho\gamma/\beta f T_c)(t_c-t)=\nu(t_c-t). \quad (22')$$

This effect is superposed upon the normal change of birefringence with temperature and produces an anomalous temperature variation of the birefringence.

The spontaneous field $F_0$ is also responsible for the temperature dependence of the scattering of x-rays. The energy necessary to produce $P_0$ leads to a change of the specific heat.

The range of spontaneous polarization extends from $-18°$ to $+23.7°$. The difference $\Theta-T$ has a maximum at about 0°, where it is about 10°. Consequently the dielectric properties of Rochelle salt are not comparable with the magnetic properties of iron at room temperature, but they are analogous to the ferromagnetic properties near the Curie point. This fact justifies the use of Eq. (7) for the "ferro-electric" temperature range.

The susceptibility for small fields ($E=0$, $F=F_0$) is given by

$$\kappa_0=T/2f(\Theta-T)-1/f.$$

Near the Curie points this leads again, by neglecting small terms, to a law similar to the Curie-Weiss law

$$\frac{1}{\kappa_0}=\frac{2f\gamma}{T_c}(t_c-t)=2\frac{t_c-t}{C}. \quad (23)$$

The Kerr effect for small fields $dE$ is

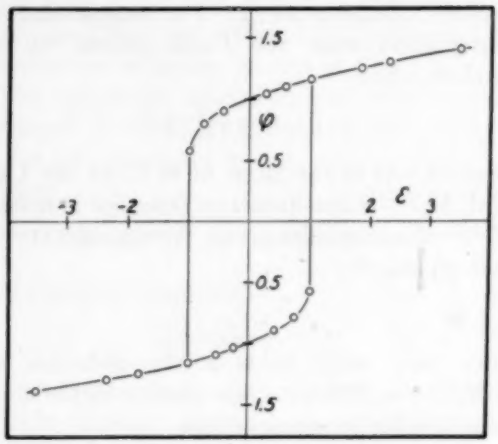


FIG. 3. Theoretical hysteresis curve.

$$d\Delta=\frac{p}{\pm[(\beta f/T)(\Theta-T)]^{\frac{1}{2}}}dE;$$

hence the quadratic electro-optical effect is in first approximation proportional to the absolute value of the applied field. Near the Curie points we get

$$\Delta=[L/(t_c-t)]^{\frac{1}{2}}|E|, \quad (24)$$

where $L=\rho^2 T_c/\gamma\beta f$.

For larger fields the theory gives a hysteresis loop of the form shown in Fig. 3. In this diagram we have plotted $\varphi=F/F_0$ versus $\epsilon=E/E_c$ where $E_c$ is the coercive field

$$E_c=\frac{2}{3T}\frac{1}{(3\beta f T)^{\frac{1}{2}}}(\Theta-T)^{\frac{1}{2}}. \quad (25)$$

Near the Curie point we have

$$E_c=\tfrac{2}{3}g^{\frac{1}{2}}(t_c-t)^{\frac{1}{2}}. \quad (26)$$

The "reduced" hysteresis loop in Fig. 3 is the same for all temperatures $T<\Theta$. Since we have always $P\gg E$ the loop for $P(E)$ is similar to the $F(E)$ loop. The remanent polarization is identical with the spontaneous polarization $P_0$.

In the experiments hysteresis loops are observed, but they do not show the large Barkhausen jumps predicted by the theory. We believe that this is due to the interaction between polarization and piezoelectric deformation. The deformation cannot change with infinite velocity. Hence the loop is smoothed out in a way which

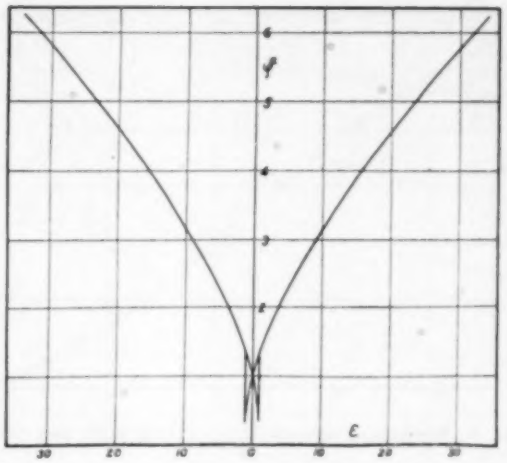


FIG. 4. Kerr effect between the Curie points. Theoretical curve.

depends on the elastic properties of the crystal. The formulas for $P_0$ and $E_c$ can therefore not be exactly verified, but they give the correct order of magnitude and the temperature dependence of the height and width of the loops.

For fields large compared with $E_c$ we have by no means saturation as is usually stated. Since we are always near the Curie point, we must expect a further increase of $P$ with $E$. Also, the Kerr effect does not show saturation. Fig. 4, which has been constructed by using Eq. 7, shows how this effect should vary with the applied field for any temperature between the Curie points. For small fields we get a quadratic hysteresis loop. For large fields the Kerr effect is nearly proportional to the absolute value of the applied field.[18]

We wish to develop here the theory only as far as it has a relation to our experimental work. There are no difficulties in applying it to the electro-caloric effect, the change of specific heat, the change of x-ray scattering, the linear electro-optical and the piezoelectric effect.

[18] Previously the author (Phys. Rev. **40**, 1051 (1932)) has proposed another explanation for this curious behavior of a quadratic effect. While the fundamental idea is the same as in this paper, the mathematical formulation cannot be accepted. The older theory requires an increase of the slope of the $\Delta(E)$ curves with increasing values of $(\theta - T)$ and of $E$. The present theory gives according to (24) a smaller Kerr effect for larger values of $(\theta - T)$ and a slightly decreasing slope for increasing field strengths. The experiments definitely support the conclusions of the present theory.

Eighteen of the above equations are subject to experimental verification. They are used to determine the values of $C$, $g$, $R$, $Q$, $M$, $N$, $h$, $v$ and $L$. Near the Curie point these 9 constants depend only on the values of $\gamma$, $f$, $\beta$ and $\rho$. We have therefore a series of possibilities to cross check our theory by the following relations between the experimental constants:

$$g=(M^2/C)^{\frac{1}{4}}, \quad (27) \qquad v=R/Q, \quad (30)$$

$$Q=\tfrac{1}{3}(R/g)^3, \quad (28) \qquad L=1/RQ, \quad (31)$$

$$N=\tfrac{1}{3}CM, \quad (29) \qquad h=9NM. \quad (32)$$

These six relations reduce the number of independent quantities to three and we are therefore not able to determine all four quantities $\gamma$, $f$, $\beta$ and $\rho$ but only the combinations

$$f\gamma=T_c/C. \ (33) \ ; \ \beta f^4=1/27N^2. \ (34) \ ; \ \rho f^2=v/h. \ (35)$$

These equations hold for both Curie points. The value of $\gamma$ is positive for the upper, and negative for the lower Curie point. $\rho$ and $\beta$ will vary with temperature, but $f$ is a constant.

## EXPERIMENTAL RESULTS

All data[19] are given in c.g.s.e. units. The error limits are estimated from the variation of the data on different crystals. Data on the same crystal are reproducible and give much smaller error limits.

### $T > \Theta$

*The susceptibility* $\kappa_0$. Method: a.c. bridge. Crystals 1, 2 and 3 were used for the temperature range from $-180°$ to $-15°$ and $+20°$ to $+50°$. Fig. 5 gives the reciprocal susceptibility *versus* temperature of two crystals above the upper Curie point. We call attention to the analogy between this curve and the curves for the paramagnetic susceptibility of iron and nickel[20] above the Curie point. Between 34° and 50° the

[19] In making the measurements I have been assisted by a number of students. Credit must be given to Miss Lucy M. Groat, who performed a large part of the optical and electro-optical determinations, to Mr. J. E. Forbes, for the dielectric measurements with the a.c. bridge, to Mr. E. B. Bradford for the investigations with the cathode-ray oscillograph and to Mr. L. Tarnopol for the investigation of the pyroelectric effect.

[20] Weiss and Foëx, Arch. de Geneve **31**, 89 (1911).

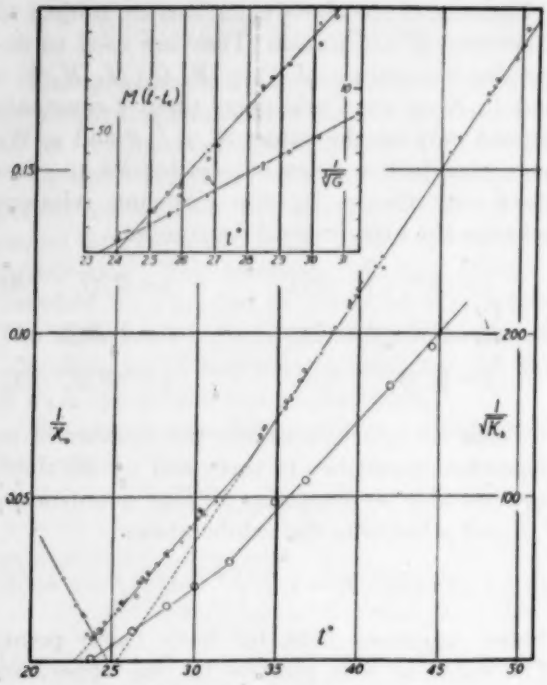


FIG. 5. Curie-Weiss law for $1/\kappa_0$. (o crystal 1, x crystal 2) and for $K_b^{-1}$ (crystal 6). Inset: $G^{-1}$ and $M(t-t_c)$. (o crystal 2, x crystal 3).

measurements on all three crystals follow very accurately the law

$$1/\kappa_0=(1/c_i)(T-T_i) \qquad (36)$$

with $c_1=136\pm0.5$ and $T_1=273+25.3\pm0.05$. Between 25° and 32° the results can be represented by the same law, but with

$$c_2=178\pm5 \qquad T_2=273+23\pm0.5.$$

The Curie point is at $23.67\pm0.03°$. In view of the great difficulties in getting reproducible results for temperatures very near the Curie point, we feel justified in assuming $T_2=T_c$ and $C=c_2$.

Since the low temperatures could not always be kept constant for a sufficiently long period the data in Fig. 6 are less accurate. As was first noticed by Valasek, the susceptibility can again, within small temperature ranges, be represented by the law (36) but this is more a matter of convenience than of necessity. We get

| | | | | |
|---|---|---|---|---|
| from | −18° to −28° | $c_3=-93.8=C'$ | $T_3=273-17.9=T_c'$ |
| " | −28 to −42 | $c_4=-68.5$ | $T_4=273-20.6$ |
| " | −42 to −80 | $c_5=-47.9$ | $T_5=273-27.1$ |
| " | −100 to −140 | $c_6=-80.6$ | $T_6=273+16.6$ . |

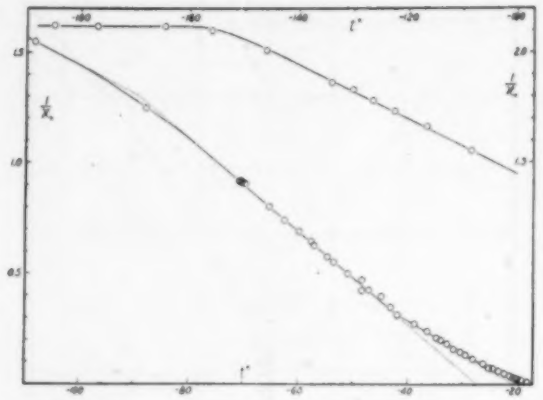


FIG. 6. Reciprocal susceptibility of Rochelle salt below −18°.

Below −160° the dielectric constant is independent of temperature.

The experimental law (37) is compatible with Eq. (9) provided

$$\Theta=T/[1+(1/c_if)(T-T_i)]. \qquad (37)$$

The large values of $c_i$ justify our assumption (8). Eq. (37) will serve to determine $\Theta(T)$.

Crystals 4 and 5 were used to measure the dielectric constants $\epsilon$ in the $b$ and $c$ direction. Since the corrections for the edge effect are here very large no accurate values can be given. For 25° we find approximately $\epsilon_b=10$, $\epsilon_c=9.6$. Both constants show a definite increase with temperature. We find $(1/\epsilon_b)(d\epsilon_b/dt)=0.007$ and $(1/\epsilon_c)\times(d\epsilon_c/dt)=0.003$. At the Curie points no abnormal change is observed.

*The susceptibility* $\kappa_E$. Method: a.c. bridge with bridge arm in Fig. 1. Crystals 2 and 3 were measured between 22° and 35°. Above 32° no change of $\kappa$ with field was observed. Fig. 7 shows that Eq. (11) is verified. From the initial slopes of these curves we find $G^{-1/3}$ (see Fig. 5) and verify the theoretical law (12). Fig. 5 gives

$$g=1.05\pm0.02.$$

Verification of (11) has also been given by Kurtschatov[8] but we cannot agree with his conclusion that the deviations from this law require the introduction of higher powers of $F$ in Eq. (7). The deviations are due to the fact that (11) is an approximation. Eq. (7) can be verified by testing the validity of the general law (19). This is done

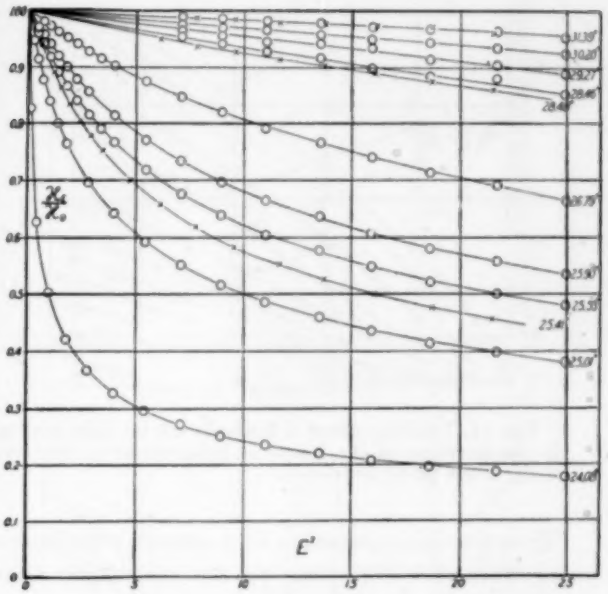

FIG. 7. Change of the susceptibility with field intensity; o crystal 2; x crystal 3.

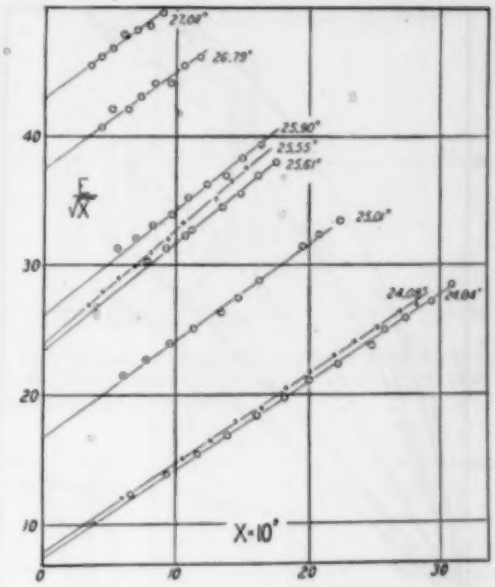

FIG. 8. $E/X^{\frac{1}{2}}$ *versus* $X=(\kappa_0-\kappa_E)/(\kappa_0/\kappa_E)$.

in Fig. 8. The slope of the straight line varies slightly, but does not show any regular change with temperature. Its average value is

$$N=800\pm80.$$

The ordinate for $X=0$ must be proportional to $(t-t_c)$. This is verified in Fig. 5, which gives $t_c=23.75$ and

$$M=13.5\pm0.4.$$

### OBSERVATIONS WITH THE CATHODE-RAY OSCILLOGRAPH

The oscillograms do not give accurate determinations, but they are a convenient method to demonstrate and verify the previous observations. The photographs in Fig. 9 illustrate the change of the $P(E)$ curves as one approaches the upper Curie point. From these photographs the $Q(E)$ curves are constructed in Fig. 10, $Q$ is the charge per cm². Since $P\gg E$ we can approximate $Q=F/f$ and get from (7)

$$E=[(t-t_c)/C]Q+\beta f^4Q^3. \qquad (38)$$

The curves in Fig. 10 are drawn according to this law, with the values $t_c=23°$, $C=170$, $\beta f^4=1.10^{-7}$. Curves similar to Fig. 9 are obtained

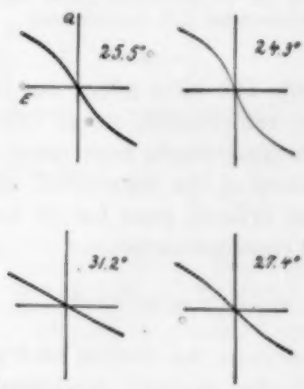

FIG. 9. Photographs of cathode-ray oscillograms showing the dependence of polarization on the field above the Curie point.

below the lower Curie point. (See Fig. 16.) The oscillogram as well as the measurements of $\kappa_E$ give the same results if the direction of $E$ is reversed.

### THE QUADRATIC ELECTRO-OPTICAL EFFECT

Crystal 7 was investigated for light passing in the $c$ direction, and crystal 6 was used in all three orientations. Preliminary investigations, using six other crystals, showed that the effect is reproducible, provided the effect of conduction

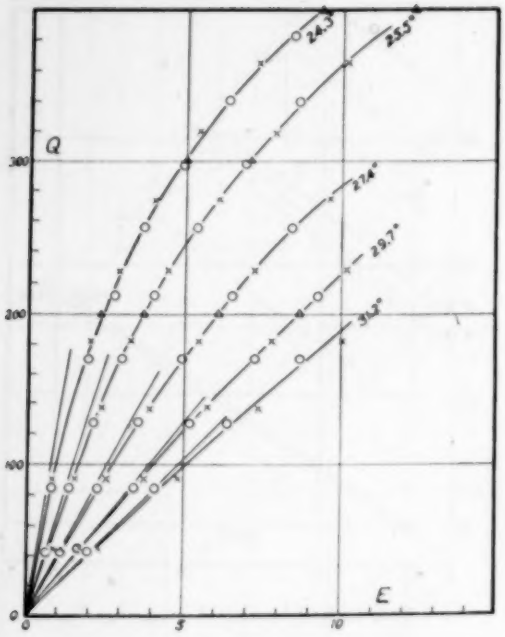


FIG. 10. Dependence of the induced charge $Q$ on the applied field $E$ for temperatures above the Curie point. $o$, $x$ observed values for $\pm E$, $\Delta$ calculated.

is eliminated. The Kerr effect was observed to exist in the temperature range from $-30°$ to $+45°$ but measurements were made only above $0°$. Comparison of the transversal effects, made on the same crystal, gave for all temperatures and fields a constant ratio

$$\Delta_b/\Delta_c = \rho_b/\rho_c = -95/70.$$

In both directions the electric field produces an increase of the natural birefringence. Since $n_a > n_b > n_c$ we must consider $\rho_b$ as a negative, $\rho_c$ as a positive quantity. According to (5) there exists therefore for Rochelle salt a longitudinal Kerr effect

$$\rho_a = -(\rho_b + \rho_c) = (25/70)\rho_c.$$

The longitudinal effect is again an increase of birefringence. The existence, direction and magnitude of this longitudinal effect was directly verified in a separate experiment, in which the light passed through pin holes in the electrodes. Only observations at room temperature were made. At this temperature the effect is nearly proportional to the absolute value of the field. The result of this experiment casts serious doubt

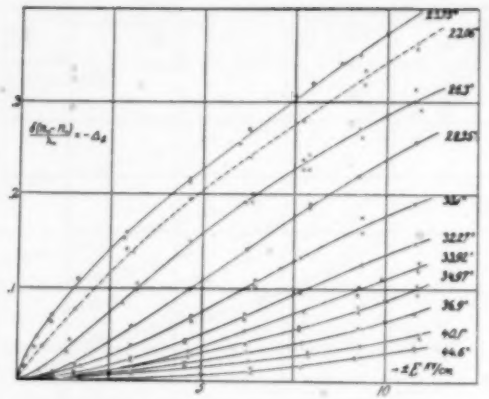

FIG. 11. The Kerr effect in Rochelle salt for light passing in the direction of the $b$ axis at temperatures above the upper Curie point (crystal 6).

upon the interpretation of a similar experiment of Valasek.[4] We come to the conclusion that Valasek observed not the linear, but the longitudinal quadratic electro-optical effect. Our observations contradict his statement that the change of birefringence is reversed with reversal of the field. It is linear, but it cannot be reversed.

Fig. 11 gives the observations in the $b$ direction of crystal 6. Above 40° the Kerr effect is normal and follows the law (10). Between 34° and 40° the data can be represented by Eq. (13) and give

$$1/(K_b)^1 = 10.3(t - 25.7°).$$

The data are not accurate enough to verify the temperature variation of the coefficient of $E^2$ in Eq. (13). Below 32° we get (from Fig. 12)

$$1/(K_b)^1 = 6.9(t - 23.6).$$

The variation of $K_b^{-1}$ is plotted in Fig. 5 and we notice the similarity with the curve for $1/\kappa_0(T)$. The results below 32° are used in Fig. 12 to verify Eq. (15) and they give

$$R_b = 6.9 \pm 0.2 \quad \text{and} \quad Q_b = 150 \pm 20.$$

More accurate results could be obtained with the large crystal 6. The results in Fig. 13 satisfy again Eq. (15) and give

$$R_c = 10.1 \pm 0.2; \quad Q_c = 307 \pm 10.$$

From (16) and (17) follows

$$\rho_b/\rho_c = R_b/Q_b \cdot Q_c/R_c = 1.4.$$

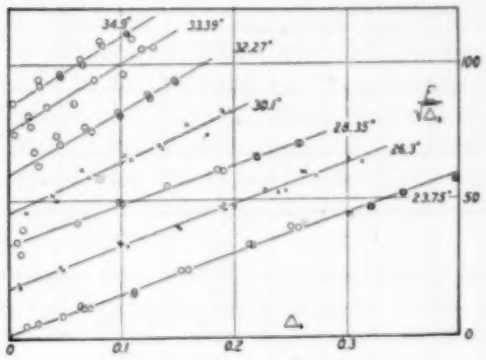


FIG. 12. Verification of Eq. (15).

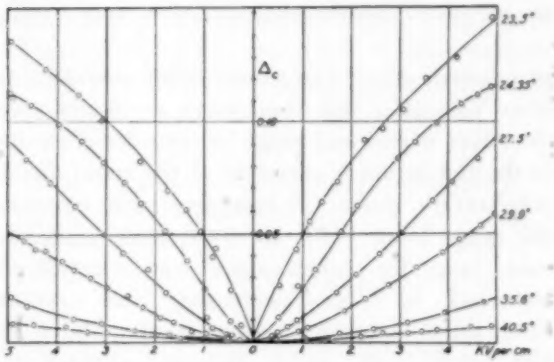


FIG. 13. The Kerr effect above the Curie point for light passing in the $c$ direction (crystal 7).

The observations on different crystals agree therefore with the result $\rho_b/\rho_c = 95/70$ found from measurements on the same crystal.

## $T < \Theta$

*Influence of the piezoelectric back polarization.* Four crystals, all of the same cross section $1'' \times 1''$ and varying in thickness from $\frac{1}{4}''$ to $1''$ were cut with their faces at 45° to the $b$ and $c$ axes, and inserted in the device of Fig. 14. This device permits a pressure to be exerted on the crystal and thus the piezoelectric deformation is partly prevented during either half cycle or the entire cycle of the applied a.c. voltage. The change of the dielectric properties with pressure was investigated with the bridge and the oscillograph. Even the slightest pressure reduces the capacitance of the crystal, when measured with the bridge, to less than 5 percent of its original value. The influence of constraints is particularly interesting in the measurements of the hysteresis

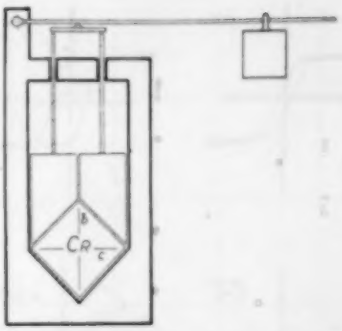

FIG. 14. Device for preventing the piezoelectric deformations. The pressure can be applied to either vertical rod by removing the cross piece.

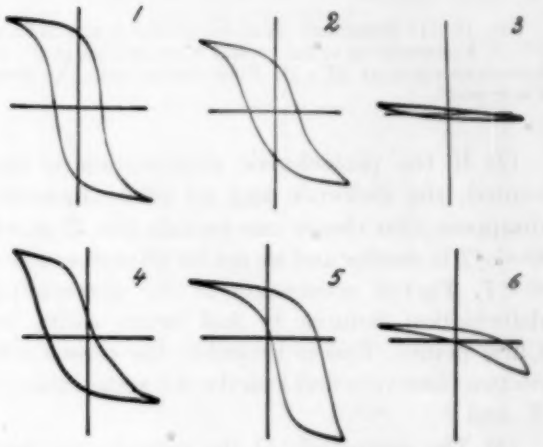


FIG. 15. The change of the hysteresis curve of Rochelle salt with pressure. $t = 0°$. (1) Free crystal, (2) pressure 1 kg/cm² on both sides, (3) pressure 7 kg/cm² on both sides, (4) pressure 2 kg/cm² on right side only, (5) pressure 3 kg/cm² on left side, (6) pressure 7 kg/cm² on left side. Maximum field 2 kv/cm.

loops. Fig. 15 shows that the loop for a "free" crystal is symmetrical, but with the help of pressure we can produce any direction and degree of asymmetry.[21] For very large pressures the loop disappears,[10] but usually the crystal breaks before a photograph can be taken.

These observations lead to the conclusions:

(1) Most investigators[22] have not realized the importance of mechanical constraints. Their asymmetric results are probably produced by the crystal holder.

---

[21] R. David, Helv. Phys. Acta **7**, 647 (1934), reports the same result. This paper appeared after completion of our investigation.

[22] Oplatka, Phys. Zeits. **34**, 296 (1933); references 4 and 6.

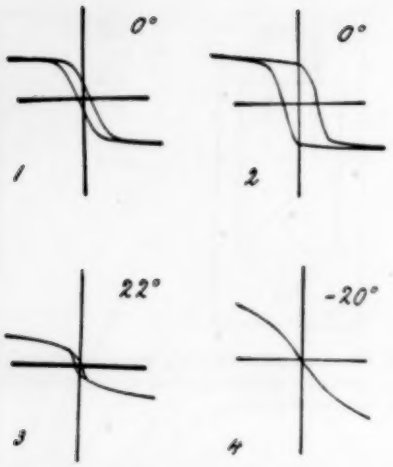


FIG. 16. (1) Hysteresis curve for crystal 3 mm thick at 0°; (2) hysteresis curve for crystal 12 mm thick at 0°; (3) hysteresis curve at 22°; (4) $P(E)$ curve below the lower Curie point.

(2) If the piezoelectric deformation is prevented, the dielectric and all other anomalies disappear. Our theory can explain this. If $\alpha_3=0$, $\Theta=\alpha f T$ is smaller and we get for all temperatures $\Theta<T$. Partial prevention of the piezoelectric deformation reduces $\Theta$ and hence shifts the Curie points. This is probably the reason why no two observers find exactly the same values of $T_c$ and $T_c'$.

(3) The magnitude of the piezoelectric back polarization is determined by $y_s$ and hence depends on the size and shape of the crystal. The elastic problem involved is too complicated to predict a law for this dependence. The hysteresis loop, as was pointed out, depends to a considerable degree on this interaction between polarization and piezoelectric deformation, and hence on size and shape of the crystal.

This dependence is shown in Fig. 16. For thin crystals the hysteresis loop is flat and the remanent polarization is small. Thick crystals give a steep loop[23] and a large remanent polarization.

## THE PYROELECTRIC EFFECT

This effect was discovered by Valasek,[4] but it has been questionable[11] whether it is not a false

[23] I. Kurtschatov, Phys. Zeits. d. Sow. **5**, 200 (1934). The forces exerted by the electrodes are perhaps responsible for this effect.

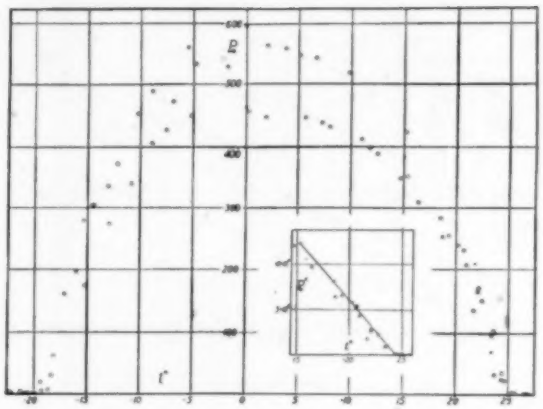

FIG. 17. Pyroelectric effect of Rochelle salt. $o$ total charge per cm² and $x$ remanent polarization of the same crystal.

pyroelectric effect. Our results differ considerably from Valasek's, but they leave no doubt that the effect is real and must be considered as due to the temperature variation of the spontaneous polarization. About 30 complete runs, covering the range from $-70°$ to $+40°$ were made. In some runs the temperature was successively increased, in others decreased. Five crystals were tested. All give the same result: Above 25° and below $-18°$ no pyroelectric charges are produced. The effect appears and disappears very suddenly at the Curie points. It is very large and of opposite signs at these temperatures. The reversal of sign occurs near 0°C. Fig. 17 shows the change of the total charge per cm² with temperature. With the same crystal the data are reproducible, but the larger the thickness of the crystal the larger the polarization. The magnitude of the piezoelectric moment is identical with the remanent polarization as measured in the hysteresis loop. The results on all crystals verify at both Curie points the Eq. (21′). The data on crystal 8 give the largest values of $P_0$. We find from Fig. 17 $h\geqq 1.5\ 10^4$ and at the lower Curie point $h'=2.65\ 10^4$. The maximum moment at 0° is $P_0(O)=600$ e.s.u. Since our observations, Fig. 15 and Fig. 16, show that pressure and the finite thickness of the crystal tend to reduce $P_0$, and since a crystal is never entirely free, we must expect that these values of $h$ are smaller than their theoretical values.

Further observations of the pyroelectric effect are discussed in a later section.

### The Kerr Effect of the Spontaneous Field

The temperature dependence of the indices of refraction of Rochelle salt has been measured by Müttrich[24] and Valasek.[4] Both report a linear variation, but Valasek's data are not accurate enough to show the expected effect, and Müttrich's result is based on observation at a few temperatures only.

We have measured the temperature variation of $n_c-n_a/\lambda$ and $n_a-n_b/\lambda$ between $-30°$ and $+50°$. The temperature change was performed in the same manner as for the piezoelectric measurements. To satisfy the condition $E=0$ the crystal No. 6 was wrapped in tinfoil with small holes for the passage of light. Each curve in Figs. 18 and 19 is the result of observations at over 100 different temperatures. Above 24° the data can be represented by

$$\frac{n_c-n_a}{\lambda}=-4.159-\frac{S_b}{2.960}+0.0644_6t-0.00040_5t^2,$$
$$\frac{n_a-n_b}{\lambda}=6.689+\frac{S_c}{1.384}-0.134t-0.00054_3t^2, \tag{39}$$

where $S_b$ and $S_c$ are whole numbers. To get agreement with the values of $n_a$, $n_b$, $n_c$ given by Valasek we must have

$$S_b=292\pm4\,;\quad S_c=90\pm2.$$

The curve $(n_b-n_c)/\lambda$ is found by subtraction. Below $-20°$ the change is linear.

$$\frac{n_c-n_a}{\lambda}=-4.392-\frac{S_b}{2.96}+0.0322t,$$
$$\frac{n_a-n_b}{\lambda}=6.968+\frac{S_c}{1.384}-0.155t. \tag{40}$$

At both Curie points the curves show a sharp break. We interpret this as due to the Kerr effect of the spontaneous inner field. Since in all cases the break is in the direction of increasing birefringence, this interpretation is consistent with the observations of the Kerr effect. Extrapolating (39) to temperatures below 24° and extrapolating (40) to temperatures above $-18°$ and calculating the difference between the

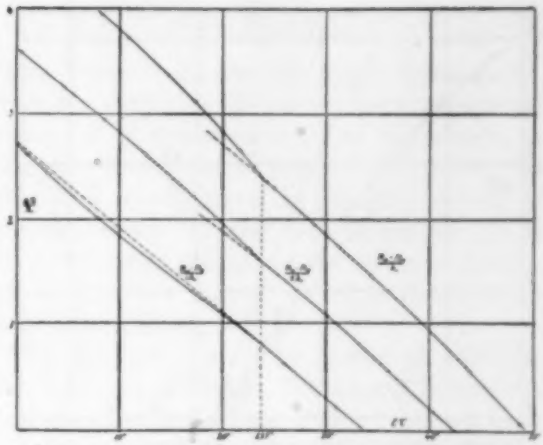

FIG. 18. Temperature dependence of the birefringence of Rochelle salt above 0°.

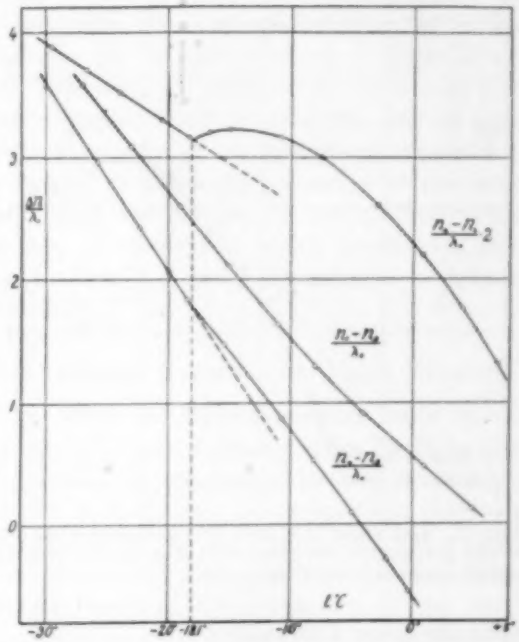

FIG. 19. Temperature dependence of the birefringence of Rochelle salt below 0°.

extrapolated and actual values of $(n_c-n_a)/\lambda$, etc., we get in Fig. 20 the Kerr effect of $F_0$. In agreement with the fact that $\rho_b>\rho_c$ we find at the upper Curie point $\Delta_0 b>\Delta_0 c$. At the lower Curie point $\Delta_0 b=\Delta_0 c$. This indicates that the longitudinal Kerr effect disappears at lower temperature. Figs. 20 and 21 verify (22′) and give

$$\nu_b=0.040\pm0.001$$

[24] Müttrich, Pogg. Ann. **121**, 193 (1864).

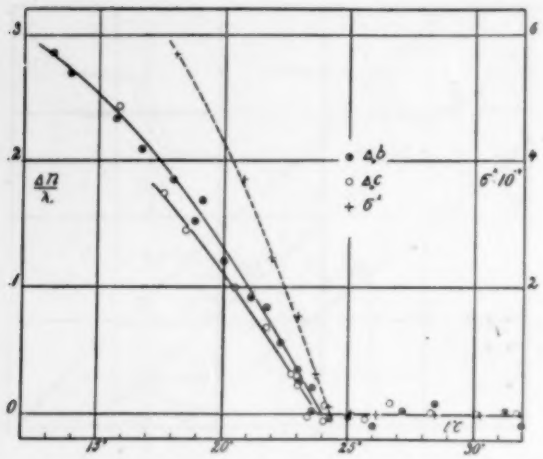

FIG. 20. Kerr effect produced by the spontaneous inner field and pyroelectric moment $\sigma = P_0$ of crystal 6 (measurement with Gaugain's method) near the upper Curie point.

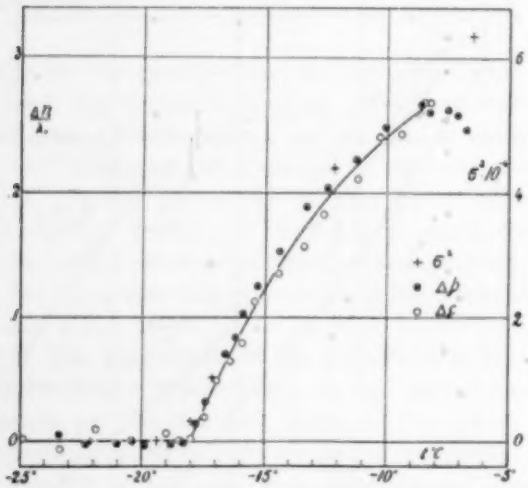

FIG. 21. Kerr effect produced by the spontaneous inner field and pyroelectric moment $\sigma = P_0$ of crystal 6 (Gaugain's method) near the lower Curie point.

and at the lower Curie point

$$v_b' = -0.046.$$

## DIELECTRIC MEASUREMENTS

Fig. 5 includes some data of $1/\kappa_0$ for $t < t_c$. The points seem to verify the law (23). They are on a straight line with a slope twice as large as the line for $t > t_c$.

We find that the bridge measurements give for $\kappa_0$ the same values as the ones calculated from the slope of the hysteresis loops at the points $E = 0$.

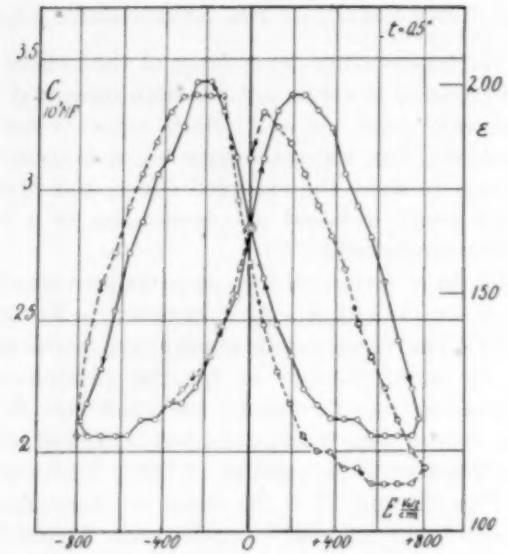

FIG. 22. Variation of the capacitance of Rochelle salt at 0.5° with the electric field. The curve is the derivative of a hysteresis curve.

The existence of the hysteresis loops can also be demonstrated with the help of bridge-measurements with a superposed d.c. field. Fig. 22 evidently represents the derivative $dP/dE$ of a hysteresis curve.

The theoretical value of the coercive field $E_c$ can, for obvious reasons, never be reached. With $g = 1.05$ Eq. (26) gives

$$E_c = (t_c - t)^{\frac{1}{2}} \times 210 \text{ volt/cm}.$$

The experiments (Figs. 16, 22 and 23) give a coercive field of this order of magnitude. $E_c$ increases faster than $(t_c - t)$ but not as fast as $P_0 = h(t_c - t)^2$. Since the conduction of the crystal influences the width of the observed loops no accurate measurements of $E_c$ have been possible. By comparison of loops obtained with 60 and 500 cycle a.c. we are able to approximate the proper compensation for the power loss due to conduction.

## THE KERR EFFECT

For small fields a quadratic hysteresis loop is observed (Fig. 23). For large fields, Fig. 24, the effect shows the peculiar behavior predicted by the theory. (Fig. 4.) The initial slope of the curves follows the law 24 and gives ($t_c = 25°$).

$$L_c = (3.0 \pm 0.1)10^{-4}.$$

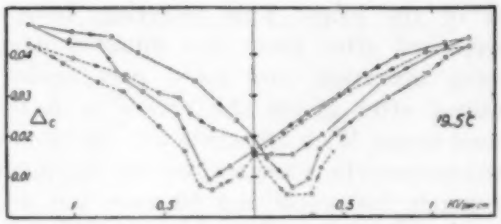

FIG. 23. Hysteresis loop of the Kerr effect (crystal 7).

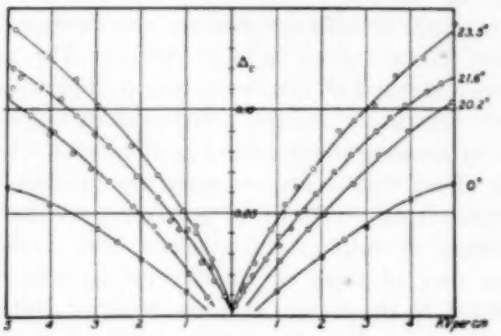

FIG. 24. The Kerr effect of Rochelle salt between the Curie points. $c$ direction, crystal 7.

## COMPARISON WITH THE THEORY

The experimental results verify all our theoretical conclusions. It remains only to be shown that the values of the experimental constants are consistent with each other. This is done by testing the six relations (27) to (32).

| | *Calculated* | *Observed* |
|---|---|---|
| $g=\left(\frac{M^2}{C}\right)^{\frac{1}{3}}$ | $1.01\pm0.03$ | $1.05\pm0.02$ |
| $Q_c=\frac{1}{3}\left(\frac{R_c}{g}\right)^3$ | $300\pm30$ | $307\pm10$ |
| $N=\frac{1}{9}CM$ | $800\pm50$ | $800\pm80$ |
| $h=9NM$ | $(9.7\pm0.9)10^4$ | $>1.5\ 10^4$ |
| $r_b=\frac{R_b}{Q_b}=1.4\frac{R_c}{Q_c}$ | $(4.6\pm0.5)10^{-2}$ | $(4.0\pm0.1)10^{-2}$ |
| $L_c=\frac{1}{R_cQ_c}$ | $(3.2\pm0.2)10^{-4}$ | $(3.0\pm0.1)10^{-4}$. |

For the quantities related to the behavior above the Curie point the agreement is excellent. For the quantities related to the "ferro" dielectric properties the theory gives values of the correct order of magnitude. From (33), (34) and (35) we get

$$f\gamma=1.67\pm0.006,$$

$$\beta f^4=(5.8\pm0.7)10^{-8},$$

$$\rho_c f^2=(4.7\pm1.0)10^{-8}.$$

These values hold for the upper Curie point. From the definition (8) follows $\gamma<1$. Hence the factor $f$ is of the same order of magnitude, as Lorentz's factor $4\pi/3$. We are not facing the difficulties encountered in Weiss's theory of ferromagnetism. If the cubic term in (7) is interpreted with the help of the theory of dipoles, it is easy to show that $\beta f^4$ should be of the above order of magnitude.

The constant $\rho$ shall be compared with the Kerr constant of liquids. For normal liquids the Kerr constant $K$ is about $5\times10^{-8}$ and we have

$$\rho=K[3/(\epsilon+2)]^2.$$

Hence for liquids $\rho$ has the same order of magnitude as $K$, while for Rochelle salt the largest value of $\rho$ is smaller than $10^{-8}$. The quadratic electro-optical effect of Rochelle salt can therefore be considered to be a real Kerr effect. The large magnitude of this and all other effects is not due to an anomalous structure of the crystal or abnormal properties of the molecules. They are due to the electric interaction between the molecules, which produces a very large inner field $F$ under the influence of a small outer field.

## BARKHAUSEN EFFECT AND WEISS REGIONS

The theory of ferromagnetism leads to the existence of a pyromagnetic effect for iron. This effect, which is analogous to the pyroelectric effect of Rochelle salt, has never been observed, and this has led to the conclusion that a block of iron consists of a large number of elementary magnetic regions. The existence of the pyroelectric effect in Rochelle salt indicates therefore that here a small crystal represents a single "Weiss region."[25] The directions of "easy polarization" are the $+a$ and $-a$ directions. Theoretically the pyroelectric moment could reverse its direction. Such a reversal has never been observed, even when the crystal was cooled while it was under the influence of an electric field of 1000 volt/cm. The direction of $P_0$ seems

[25] Or there may be a large number of elementary regions but most of them are polarized in the same direction. This would explain why we get much better agreement for $L_c$ and $r_c$ than we get for $h$.

to be determined by some small internal asymmetries, as for instance, small internal stresses which have not been removed by annealing. In accordance with the hypothesis of a single Weiss region no Barkhausen discontinuities could be observed for small crystals.

This hypothesis raises two questions, namely: (a) Why are the Weiss regions in Rochelle salt much larger than in ferromagnetism? and (b) how large may a crystal be to represent only a single region?

To question (a) we propose the following answer: Because there exists electric but no magnetic conduction. In magnetism a spontaneous polarized region produces an outer magnetic field which causes the neighboring regions to become polarized in the opposite direction. In Rochelle salt this effect does not exist because the free charges on the surface of a region are quickly neutralized by conduction.

In order to answer question (b) three large crystals with cross sections between 10 and 50 $cm^2$ were investigated. The observations indicate that such large crystals contain a large number of oppositely polarized Weiss regions.[26] The evidence is not conclusive, but interesting enough to be reported.

The previously discussed method shows a very small, and sometimes no pyroelectric effect for large crystals.

The existence of a Barkhausen effect was demonstrated in two ways: The electric field in the crystal was slowly and continuously increased with the help of an induction regulator in the primary of the kenotron outfit. In series with the crystal was an induction coil. A second coil, loosely coupled to the first, was connected to an audiofrequency amplifier feeding a loudspeaker. In the voltage range which corresponds to the steep part of the hysteresis loop a large number of sharp clicks could be heard. A thyratron operated counter recorded between 70 and 120 discontinuities for crystal 7. No such discontinuities occur in the saturation range, and they disappear for temperatures above the Curie point.

The oscillograph gave for these crystals a rapidly and irregularly flickering line in the steep part of the loops. This flickering, however, disappeared after about five minutes of continuous operation, and could only again be obtained after giving the crystal a rest for several hours. With 500 cycle a.c. the phenomenon continues for a longer time, and by applying alternately 500 cycle and 60 cycle a.c. for 3 minutes, the flicker phenomenon continued to appear for two hours. We have no explanation for this curious behavior. Successful attempts were made to observe directly the existence of many Weiss regions in large crystals. The well-known method of demonstrating pyroelectricity with electrically charged powders is also successful for showing the pyroelectric effect of Rochelle salt. Best results are obtained by heating the crystal from $-30°$ to $0°$ and using Bürker's[27] mixture of sulphur, lycopodium and carmine. The pair of faces of small crystals, which is normal to the $a$ axis, appears brightly colored, one face red, the other yellow. For large crystals, however, each face shows a system of red and yellow patches, occasionally arranged in a regular checkered pattern, red and yellow spots alternating about 2 to 3 cm apart and arranged in lines at 45° to the $b$ and $c$ axes. Usually however the pattern is quite irregular and further work is required before any conclusion can be drawn.

## Conclusion

The experiments verify the proposed theory within the limits of experimental errors. Measurements near the lower Curie point, where the conductivity is negligible, would furnish more accurate data. The measurements give values of $f$, $\gamma$, $\beta$ and $\rho$ which are of the correct order of magnitude. They give only the product $f\gamma$ and it is not possible to calculate $f$ and $\Theta(T)$ without introducing a further assumption.

This new assumption is based on the fact that the Curie-Weiss law (37) is satisfied with excellent precision for all temperatures above 34°. The analogy with the corresponding law in ferro- and paramagnetism suggests that above 34° $\Theta$ is constant. We emphasize that this assumption is arbitrary and may have to be changed. From it follows $\Theta = T_1$ for $t > 34°$ and

[26] Results which support this conclusion have been reported by Kurtschatov, Phys. Zeits. d. Sow. **4**, 125 (1933).

[27] K. Bürker, Ann. d. Physik **1**, 474 (1900).

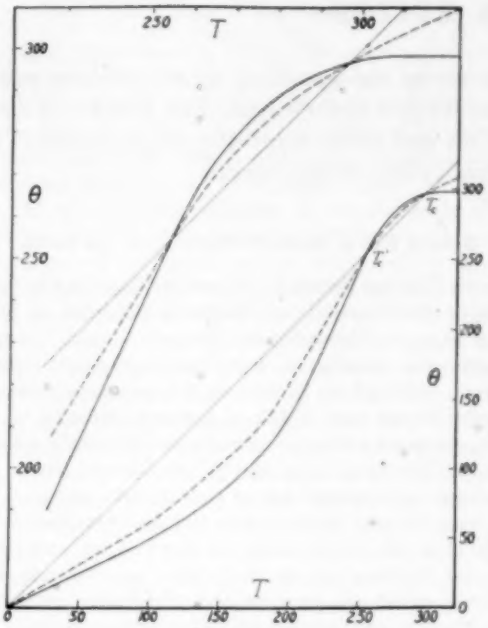


FIG. 25. Change of the Curie temperature Θ with temperature, assuming $f=2.19$, and for $f=4\pi/3$.

hence

$$f=T_1/c_1=2.19\pm0.01.$$

With the help of (37) and the values of $c_i$ and $T_i$ we are now able to construct the curve $\Theta(T)$ given in Fig. 25. Between the Curie points $\Theta(T)$ is calculated from the data on $P_0$ and $\Delta_0$. The dotted curve corresponds to the assumption $f=4\pi/3$ but the assumption $f<4\pi/3$ is not inconsistent with any observation.

With the help of this curve and the values of $\beta$ and $\rho$ we can calculate all our experimental results. From it follows the value of the inner field. The magnitude of the spontaneous inner field at 0° for instance is found to be 0.77 $10^6$ volt/cm.

This paper is an attempt to explain the anomalous properties of Rochelle salt without making any assumptions concerning the molecular mechanism involved. It gives the fundamental relations on which an atomistic theory can be based.

# LETTERS TO THE EDITOR

*Prompt publication of brief reports of important discoveries in physics may be secured by addressing them to this department. Closing dates for this department are, for the first issue of the month, the twentieth of the preceding month; for the second issue, the fifth of the month. The Board of Editors does not hold itself responsible for the opinions expressed by the correspondents.*

## Band Spectrum of Arsenic Oxide (AsO)

At the St. Louis meeting of the American Physical Society (November 30, 1934) we reported on the results of an investigation of the band spectrum of arsenic oxide (AsO) in emission and absorption.[1] Two systems of double double-headed bands were observed. In a paper to be presented by Jenkins and Strait at the Los Angeles meeting of the American Physical Society (December 21–22, 1934), a confirmation of these observations is recorded (Bulletin of the American Physical Society 9, No. 6, p. 7). There is, however, a discrepancy in the vibrational analysis of the *A*-system. On the basis of measurements of wavelengths on a Hilger $E_1$ quartz spectrograph, we found these bands to be represented within the error of observation by means of a formula requiring a doubling of the initial state. Jenkins and Strait have, however, represented these bands by a formula which does not require the doubling of the initial state. Either formula represents equally well our observations on the $E_1$ quartz spectrograph so that without more accurate observations a choice is not possible.

We have repeated our observations in the second order of a 21-foot concave grating having 30,000 lines to the inch and also on a Hilger E185 quartz spectrograph. In the latter case, the band system was excited by passing 5 amperes at 1000 volts d.c. through a discharge tube containing the vapor of $As_2O_3$. We have thus been able to extend the band systems previously observed and to increase the accuracy of our measurements. We now find that the *A*-system can be best represented without a doubling of the initial state. There is no change in the analysis of the *B*-system.

The results of a similar investigation by Connelly[2] have been received after our results had been prepared for publication. Except for minor differences in the numerical values of the vibrational constants, his results agree with those which we obtain. We have, however, been able to extend the *B*-system to $v'=6$ whereas Connelly's recorded observations stop with $v'=4$ and Jenkins and Strait observed only the $v'=0$ progression and attributed the absence of further progressions to predissociation. It also may be of interest to note that in the form of excitation used in our experiments both sub-bands were of approximately equal intensity.

FRANK MORGAN
E. N. SHAWHAN

Mendenhall Laboratory of Physics,
Ohio State University,
December 18, 1934.

[1] E. N. Shawhan and Frank Morgan, Phys. Rev. **47**, 199 (1935).
[2] Connelly, Proc. Phys. Soc. **46**, 790 (1934).

## Rate of Fall of Meteoric Material on the Earth

In the *Physical Review* for November 15, 1934 Dr. G. N. Lewis of the University of California publishes an interesting paper on *Genesis of the Elements*. In this paper he suggests the genesis of stony meteors from metallic meteors. Although he himself, in this paper, publishes no estimate of the rate of fall of meteoric material on the earth, the press notices of the article did contain such an estimate. The figure appearing in the *Literary Digest*, and elsewhere, was nineteen feet in sixty million years.

It may be that your readers will be interested in the result of a calculation based on the relative amount of material reaching the earth in the form of telescopic meteors, naked-eye meteors and meteorites of various sizes. We have previously published papers on the daily and annual numbers of telescopic meteors, naked-eye meteors and meteorites. We have also published calculations on the masses of meteors of various magnitudes. Recently it occurred to us that a plot showing for each magnitude the total amount of material reaching the earth could be made. This indicated that the meteoric material in the space through which the earth is passing is distributed, as far as useful data are available, approximately according to the probability curve.

It should be said that, because of recent work, we are using for the telescopic meteors somewhat higher numbers than the usual estimates in the past. We are also using distinctly higher numbers for the meteorites. For the masses of individual meteors our figure is of the same order of magnitude, but slightly higher, than most which have been published. Yet when we integrate the probability curve and obtain the total amount of meteoric material reaching the earth each year, we obtain a smaller figure than the previous estimates. These previous estimates have, of course, been based to a much smaller extent on observation and calculation. Our result is that the annual amount of meteoric material per square mile is ten grams. At this rate the radius of the earth would be increased one inch in about $2\times10^{10}$ years. The estimate for the age of the earth given in Russell-Dugan-Stewart's *Astronomy* is $5\times10^{9}$ years. So in the lifetime of the earth, according to this estimate, the radius of the earth would be increased only a fraction of an inch by meteoric material falling at the present rate.

The more complete paper is to appear in Contributions of the University of Iowa Observatory.

C. C. WYLIE

University of Iowa,
Iowa City, Iowa,
December 28, 1934.

### Light of the Night Sky

In a recent letter in *Nature*, Hamada[1] has proposed the identification of the $X_1$ and $X_2$ lines in the light of the night sky as members of the Goldstein bands of nitrogen. It is the purpose of this note to call attention to some of my recent work with these bands and to propose an explanation for these hitherto unexplained bands.

At the Berkeley meeting of the American Physical Society in June 1934, I reported the discovery of some new members of the second-positive system of nitrogen. Three of the five bands discussed by me were the Goldstein bands. At that time I also called attention to the fact that these three bands were probably present in the light of the night sky.[2] Further study of these bands showed that they were not second-positive bands, and a new discussion was given in which it was proposed that the three visible bands belonged to a system which arose in a transition from a new electronic level of nitrogen to the $B^3\pi$ level, the initial state of the well-known first-positive bands. They were identified as the $(v',12)$, $(v',11)$ and $(v',10)$ bands of a new system. The two ultraviolet bands were identified as the (0,1) and (0,0) bands of another system for which the $B^3\pi$ state was also the lower state.

The bands observed by me were reported as three-headed and degraded to the red. The Goldstein bands as given by Hamada are four-headed and also degrade to the red. In my most recent note[3] I gave the wavelengths of the three shortest wavelength heads as 4732, 4435 and 4174, while those given by Hamada are 4730, 4434 and 4167. If we use Hamada's wavelengths, an even more convincing argument can be obtained in favor of my identification of the lower state as the $B^3\pi$ level. The three bands are identified as the $(v',11)$, $(v',10)$ and $(v',9)$ bands rather than as given above. If further, we calculate the wave-number differences between the four components of any one of the Goldstein bands and compare them with the differences between the components of one of the first-positive bands, it is seen that there is a remarkably good agreement between these differences and hence we obtain additional evidence that the lower state is the $B^3\pi$ level.

It is possible to calculate the $(v',0)$ band of this system and one obtains for it a frequency of 38,300 $cm^{-1}$. This gives the energy of the initial state of these bands as 97,595 $cm^{-1}$ or about 12.05 volts. From this we can calculate the $(v',3)$ and $(v',2)$ bands and their shortest wavelength heads fall at 3004 and 2863A, respectively. This suggests that the ultraviolet bands 3010 and 2864 are not the (0,1) and (0,0) bands of a new system but that they are the above predicted bands. A reexamination of the plates indicates that there is another head at 3004A and hence the identification of these bands is strengthened. It is necessary, however, to account for the presence of the ultraviolet bands in the absence of the visible ones. It was on the basis of this experimental fact that the two ultraviolet bands were assigned to another system. If the initial state should turn out to be a very unstable one as has been suggested by Hamada, such an anomaly in intensity distribution would be possible, since similar anomalies have been frequently reported by me in the case of the first-positive system. The suggestion that a level at 12.05 volts be unstable is a very reasonable one since the energy required for the dissociation of a nitrogen molecule into two $^2D$ atoms is 12.08 volts.

Finally we wish to point out that the Goldstein bands have not been included in any of the tables of band-systems with which I am familiar, and that it is for that reason that they were announced as a new band system.

JOSEPH KAPLAN

University of California at Los Angeles,
December 20, 1934.

[1] Hamada, Nature **134**, 851 (1934).
[2] Kaplan, Nature **134**, 289 (1934).
[3] Kaplan, Phys. Rev. **46**, 534 (1934).

---

### Absorption and Scattering of Neutrons

In a study of the artificial radioactivity induced by neutron bombardment[1] we have observed both large increases and decreases in the activity when various substances are interposed between the target and the neutron source. With the source 7 cm from a silver target we find the activation to be doubled by filling the solid angle with water[2] and increased many more times when the target is completely surrounded with water or even when a large quantity of water is placed behind either the source or the target. When the neutrons first pass through water and then through 2 cm of $H_3BO_3$, the activation of silver and copper targets decreases to approximately 10 percent of the values obtained without the $H_3BO_3$, in agreement with the observation of Fermi. In addition we find similar effects with chlorine and bismuth. Thus with a 2 cm absorbing layer we find for the activity induced in copper the following values, taking the effect with no absorber as 100: KCl 55, NaCl 40, $CCl_4$ 30, and $BiONO_3$ 50. The absorption is negligibly small with NaF, NaI, BeO, and CuO; and $NH_4NO_3$ and S appear to cause small increases in the activation.

The neutron source consisting of 75 millicuries of radon in powdered beryllium was obtained through the courtesy and cooperation of Dr. L. R. Taussig and the University of California Medical School. A screen-walled tube counter[3] was used to count the electrons emitted by the activated targets and the target and counter were enclosed in an evacuated chamber. Initial counts with Ag, Cu and Al gave as high as 200 decompositions per minute and the half-life values for these elements checked the results of Fermi.

W. F. LIBBY
W. M. LATIMER

Department of Chemistry,
University of California,
Berkeley, California,
December 27, 1934.

[1] Fermi, Proc. Roy. Soc. **A146**, 483 (1934).
[2] Fermi and others, La Ricerca Scientifica [5] **2**, Nos. 7–8 (1934).
[3] Libby, Phys. Rev. **46**, 196 (1934).

### Production of Induced Radioactivity by the Cosmic Radiation

Examination of the "bursts" or "Stösse" obtained on a Compton-Bennett world-survey type of cosmic-ray meter converted to continuous recording at the Huancayo Magnetic Observatory, Peru (altitude 3300 meters, geomagnetic latitude, 0°) gives the surprising information that a number of the bursts are double—and in one case, doubtfully triple. The records were obtained on a relatively open time scale, 138 mm per hour or 2.3 mm per minute, and at the low sensitivity of $1.5\times10^7$ ions per mm. In all, with one brass and one lead shield, each 2.5 cm thick, 14 double bursts occurred with time-separation between the two bursts of less than one minute, the total number of bursts recorded with this screening arrangement being 927 obtained during 1344 hours of recording. This is 94 times the number to be expected on statistical grounds. Out of the 634 obtained during 1524 hours recording with an additional lead shield of 2.5-cm thickness, 5 were double with time-separation of less than one minute, or 164 times the number expected statistically. The time-intervals between the two bursts constituting a double varied between 23 and 55 sec. ±3 sec. We are therefore led to believe that the lead is responsible for the production of these particular doubles, for the ratio, actual to expected, was raised by the additional lead, although the actual number was reduced.

It seems that we are here dealing with an example of induced radioactivity. The time-differences between the original and second bursts of the doubles is not constant but the differences tend to group around one or two values, 26 seconds and 44 seconds. The number of bursts is too small to be able to draw any very definite conclusion about the distribution in time after the original burst and so state that the disintegrations follow the laws of radioactive decay, especially when the differences tend to group around two values. The pertinent data regarding the doubles and the one doubtful triple are given in Table I.

TABLE I. *Data concerning double bursts and one doubtful triple burst.*

| Ions produced ($\times10^6$) 1st | 2nd | 3rd | Time-interval (sec.) 1st to 2nd | to 3rd | Ions produced ($\times10^6$) 1st | 2nd | 3rd | Time-interval (sec.) 1st to 2nd | to 3rd |
|---|---|---|---|---|---|---|---|---|---|
| Shields: brass and lead, 2.5 cm each | | | | | | | | | |
| 3.0 | 3.0 | | 55±3 | | 1.6 | 8.2 | | 23±3 | |
| 12.3 | 12.3 | | 47 " | | 1.6 | 14.2 | 6.3 | 52 " | 36±3 |
| 2.3 | 3.5 | | 32 " | | 5.0 | 6.7 | | 29 " | |
| 6.3 | 4.7 | | 29 " | | 10.2 | 1.7 | | 44 " | |
| 3.2 | 4.8 | | 26 " | | 3.4 | 1.7 | | 44 " | |
| 1.6 | 13.0 | | 34 " | | 13.8 | 3.4 | | 47 " | |
| 3.3 | 4.9 | | 44 " | | | | | | |
| Shields: brass, lead and lead, 2.5 cm each | | | | | | | | | |
| 1.4 | 2.7 | | 50±3 | | 1.8 | 3.5 | | 39±3 | |
| 9.1 | 19.6 | | 50 " | | 3.5 | 5.3 | | 23 " | |
| 3.5 | 3.5 | | 26 " | | | | | | |

In these experiments the sensitivity was low so that no single alpha-particle effect could have been detected, and the circuit was so arranged that no rate of change of potential effects could affect the measurements. The average number of ions produced during the double bursts was $5.3\times10^6$ in the first burst and $5.6\times10^6$ in the second, ranging from 1.5 to $19.6\times10^6$ as may be seen from the table. Further results will be published shortly.

This work was made possible by a grant of instruments from the Cosmic-Ray Committee of the Carnegie Institution of Washington. Material assistance in securing the data was given by Messrs. R. H. Mansfield and O. W. Torreson, members of the staff of the Huancayo Magnetic Observatory, to whom acknowledgment is here made.

J. E. I. CAIRNS

Department of Terrestrial Magnetism,
Washington, D. C.,
December 28, 1934.

---

### Theory of the Piezo-Resistive Effect

It is herein meant by the piezo-resistive effect that change in electrical resistance which a homogeneous body undergoes when subjected to mechanical stress. From the experiments of Mildred Allen on bismuth[1] one is led to assume that in the most general case the changes of resistance are a linear function of the components of the applied stress. In tensor notation the law of the piezo-resistive effect is, therefore:

$$\Delta r_i = R_i - r_i = \sum_{j=1}^{6} \rho_{ij} X_j; \quad i = 1, 2 \cdots 6, \tag{1}$$

wherein $\Delta r_i$ is the resistance change, $r_i$ is the resistance in the direction $i$ in the unstressed state, $R_i$ is the resistance in the stressed state, $\rho_{ij}$ are to be the piezo-resistive constants, $X_j$ are the stress components of Love in the notation of Goranson,[2] and the axes of reference are the crystallographic.

The reduction of the constants must be by the so-called geometric method utilizing Neuman's hypothesis, so that for certain rotations or reflections depending upon the symmetry of the crystal, (1) takes the following form in the new (primed) system:[3]

$$r_i' = R_i' - r_i' = \sum_{j=1}^{6} \rho_{ij} X_j', \tag{2}$$

where it may be shown that the $R_i'$'s transform exactly as do the stress components given by Love,[4] and because of their higher symmetry

$$r_i' = r_i; \quad r_i = 0 \text{ if } i = 4, 5 \text{ or } 6. \tag{3}$$

Let the theory be illustrated for the bismuth crystal in which according to Bridgman[5] the $X$ axis is the digonal and the trigonal axis is $Z$. Thus the transformations for the $X_j$'s as well as for the $R_i$'s for the rotation about $X$ and $Z$ are respectively:

$$\begin{array}{lll} X_1' = X_1; & X_2' = X_2; & X_3' = X_3; \\ X_4' = X_4; & X_5' = -X_5; & X_6' = -X_6. \end{array} \tag{4a}$$

$$\begin{array}{ll} X_1' = \tfrac{1}{4}X_1 + \tfrac{3}{4}X_2 - \tfrac{1}{4}\sqrt{3}\,X_6; & X_2' = \tfrac{3}{4}X_1 + \tfrac{1}{4}X_2 + \tfrac{1}{4}\sqrt{3}\,X_6; \\ X_3' = X_3; & X_4' = -\tfrac{1}{2}X_4 - \tfrac{1}{2}\sqrt{3}\,X_5; \\ X_5' = \tfrac{1}{2}\sqrt{3}\,X_4 - \tfrac{1}{2}X_5; & X_6' = \tfrac{1}{4}\sqrt{3}\,(X_1 - X_2) - \tfrac{1}{2}X_6. \end{array} \tag{4b}$$

Substitution of (4a) and (3) in (2) and comparison with (1) show that on account of the digonal symmetry of the $X$ axis that

$$\rho_{15}=\rho_{16}=\rho_{25}=\rho_{26}=\rho_{35}=\rho_{36}=\rho_{45}=\rho_{46}=\rho_{51}=\rho_{52}=\rho_{53}=\rho_{54}=\rho_{61}=\rho_{62}=\rho_{63}=\rho_{64}=0. \quad (5)$$

The rotation about the $Z$ axis together with (5) demands that the relations expressed in the following matrix of 8 separate constants exist:

$$\begin{array}{cccccc} \rho_{11} & \rho_{12} & \rho_{13} & \rho_{14} & 0 & 0 \\ \rho_{12} & \rho_{11} & \rho_{13} & -\rho_{14} & 0 & 0 \\ \rho_{31} & \rho_{31} & \rho_{33} & 0 & 0 & 0 \\ \rho_{41} & -\rho_{41} & 0 & \rho_{44} & 0 & 0 \\ 0 & 0 & 0 & 0 & \rho_{44} & 2\rho_{41} \\ 0 & 0 & 0 & 0 & \rho_{14} & (\rho_{11}-\rho_{12}). \end{array} \quad (6)$$

Eight, then is the minimum number of constants to completely express the piezo-resistive effect in bismuth. Notice that $\rho_{ij}\neq\rho_{ji}$ when $i\pm j$. Therefore in the general or triclinic case 36 constants are needed. The reduction of the constants for any crystal class is to be noted as being exactly the same as that for the piezo-optical effect and the changes of the coefficients of thermal conductivity of a body under stress which have been studied by Pockels, the matrices for which may be found elsewhere.[6, 7]

JOHN W. COOKSON

University of Wisconsin,
Madison, Wisconsin,
December 31, 1934.

[1] M. Allen, Phys. Rev. **42**, 848 (1932).
[2] R. Goranson, *Thermodynamic Relations* (Carnegie Inst. of Washington, 1930), p. 105.
[3] A. E. H. Love, *Math. Theory of Elasticity*, 3rd Ed. p. 148.
[4] Reference 3, p. 78.
[5] P. W. Bridgman, Phys. Rev. **42**, 858 (1932).
[6] F. Pockels, *Lehrbuch der Kristalloptik* (Leipzig, 1906), p. 472.
[7] G. Szivessy, *Handbuch der Physik* (Geiger-Scheel, Berlin) **21**, 840 (1929).

# Proceedings of the American Physical Society

MINUTES OF THE ST. LOUIS MEETING, NOVEMBER 30–DECEMBER 1, 1934

THE 194th regular meeting of the American Physical Society was held at Washington University, St. Louis, Missouri, on Friday, November 30, and Saturday, December 1, 1934. The presiding officers were Professors Henry G. Gale, G. E. M. Jauncey, F. W. Loomis and D. C. Miller. The attendance at the sessions was between one hundred and twenty and one hundred and fifty persons.

This meeting marked the opening of the new Wayman Crow Hall of Physics. On Friday morning at ten o'clock short addresses were given by Chancellor George R. Throop on *Wayman Crow* (founder of the University), and by Professor A. L. Hughes on *Physics at Washington University*. On Saturday morning there was a symposium on *X-Ray Scattering* with Professor Henry G. Gale presiding. The invited papers were as follows: *The Structure of Radicals in Crystals* by W. H. Zachariasen, University of Chicago; *Diffuse Scattering of X-Rays by Crystals* by G. E. M. Jauncey, Washington University; *The Study of the Nature of Liquids by Means of X-Ray Diffraction*, by G. W. Stewart, State University of Iowa; and *The Scattering of X-Rays by Gases*, by E. O. Wollan, Washington University.

The University invited the members of the Physical Society to be its guests at luncheon on Friday, November 30th, in McMillan Hall. The dinner for the members of the Society and their friends was on Friday evening at the Hotel Chase. The after-dinner speakers were Professors Henry G. Gale, D. C. Miller, G. W. Stewart and O. M. Stewart. Professor A. L. Hughes presided. Seventy-seven persons attended the dinner.

*Meeting of the Council.* At its meeting on Friday, November 30, 1934, the Council elected three candidates to fellowship, and eighty-three candidates to membership. *Elected to fellowship:* Alfred Landé, Llewellyn H. Thomas, and Ernst Wilhelmy. *Elected to membership:* Arthur G. Barkow, Sister Mary Cleophas Beck, Maurice E. Bell, Selma H. Blazer, Joseph E. Bliven, C. D. Bradley, Francis P. Bundy, Dean S. Carder, Henry Carroll, John D. Clark, Earl A. Clemans, Robert P. Coleman, Albert P. Crary, Eugene C. Crittenden, Jr., R. Curry, James W. Dunifon, Frank R. Elder, Cecil B. Ellis, Hiram B. Ely, Karl H. Fried, Orin P. Gard, William T. Ham, Jr., S. Hamada, Alvin W. Hanson, John B. Hawkes, Gabriel Heller, Harry Hill, Donald D. Hinman, Leo E. Hudiburg, J. Itoh, G. P. Ittmann, Nathan Janco, M. E. Jefferson, A. J. Klapperich, Julian K. Knipp, Winston E. Kock, Polykarp Kusch, Lawrence M. Langer, Alexander Langsdorf, Jr., Russell R. Law, Edward T. Lessig, Howard C. Lindemann, Harry C. Lipson, John H. Manley, Albert May, Emery Meschter, J. Franklin Meyer, Karl Z. Morgan, George J. Mueller, Edgar J. Murphy, Clarence W. Nelson, Raymond Pepinsky, Thomas J. Pope, Barbara G. Raines, Edward G. Ramberg, Louis N. Ridenour, Jr., A. V. Ritchie, Eric Rodgers, William F. Roeser, Morris E. Rose, Gerald A. Rosselot, George W. Scott, Jr., John F. Senger, Ken'ichi Shinohara, William A. Shurcliff, George Singer, Willard L. Smith, Harold T. Smyth, Herman M. Southworth, Thomas Foster Strong, Masao Sugimoto, Sister Helen Sullivan, S. Takizawa, Vincent E. Thornburg, Albert E. von Doenhoff, Marshall Walker, S. G. Weissberg, W. Emerson Wenger, S. Stewart West, Francis D. Williams, G. M. Wissink, Harold O. Wyckoff, and Lester I. Zimmerman.

The regular scientific program consisted of thirty-seven papers; number nine was read by title. The abstracts of these papers are given in the following pages. An *Author Index* will be found at the end.

W. L. SEVERINGHAUS, *Secretary*

## Abstracts

**1. Wayman Crow, Founder of Washington University.** Chancellor George R. Throop.

**2. Physics at Washington University.** Professor A. L. Hughes.

**3. The Formation of a Potassium Film on Silver.** James J. Brady, *St. Louis University.*—Photoelectric studies were made of potassium films deposited on a freshly evaporated silver surface. The photoelectric cell was of the concentric sphere type used in the study of the energy distribution of photoelectrons. Current-voltage curves were obtained with particular attention being given to the study of the saturation of the photocurrent. It was previously reported (Phys. Rev. **41**, 613 (1932)), that films deposited on a surface at room temperature did not yield a constant photocurrent after deposition. The current decreases with time. Curves were obtained showing the way the photocurrent approaches saturation when the surface is at room temperature. A study was then made of the way these curves change with time after deposition. It was found that the photocurrent approaches saturation at lower voltages when examined immediately after deposition than after the film has been standing for some time. This change in photocurrent is much more pronounced with films less than 3 molecular layers than with thicker films. Similar studies were made with the condensing surface cooled with carbon dioxide snow. In this case the changes are much slower than at room temperature. Likewise, when the surface is cooled with liquid air the changes are very small even for the thinnest films examined. The formation of patches is suggested as a likely explanation for the phenomena.

**4. Electrical Resistance of Cadmium Films.** Edith Townes and Duane Roller, *University of Oklahoma.*—Continued experiments with a molecular beam apparatus in which pure cadmium films were deposited on a glass plate cooled by either liquid air or solid carbon dioxide show that these films first become electrically conducting at a thickness of $2\text{–}7\times10^{-7}$ cm and have a critical thickness of $6\text{–}8\times10^{-7}$ cm. Special precautions were taken to have good contact between the film and the electrodes, lack of which probably accounts for the large critical thickness previously reported [Roller and Wooldridge, Phys. Rev. **45**, 119 (1934)]. The resistivity of cadmium at the critical thickness is about 15 times that of the bulk metal. The relations of these results to photoelectric phenomena in metallic films and to theories of film structure are discussed.

**5. Heat Losses from a Tungsten Wire in Helium.** Walter C. Michels, *Bryn Mawr College*, and Gladys White, *Duke University.*—One of the difficulties which arise in connection with the determination of the accommodation coefficient of a gas against a metal is that correction must be made for the thermal etching of the surface produced by the heat treatment necessary to clean the wire. It is possible to compute the effect of this etching by means of Taylor and Langmuir's data on thermionic emission (Phys. Rev. **44**, 423 (1933)) or by measurement of the total emissivity of the wire used. The two methods check each other satisfactorily, and indicate that a stable condition of the surface can be achieved. The heat losses from a tungsten wire in helium have been studied at room temperature and an accommodation coefficient of 0.092 has been found. When the correction has been made for etching, the value of the coefficient for a smooth, clean surface is 0.069, in good agreement with the lowest values obtained by Roberts (Proc. Roy. Soc. **A129**, 146 (1930)). There is some evidence that the value of 0.17 obtained for a rough surface by both Roberts and Michels is due to a semi-stable condition of the etched surface.

**6. Proton Emission Resulting from Alpha-Ray Bombardment of Boron and Phosphorus.** R. F. Paton, *University of Illinois.*—Protons emitted when boron is bombarded with $\alpha$-particles from Th C′ are found to consist of at least four groups with characteristic velocities and corresponding energies. Phosphorus yields three such groups. On the assumption that the $\alpha$-particles are captured by $B^{10}$ and $P^{31}$ leaving new nuclei of $C^{13}$ and $S^{34}$ respectively the characteristic energies for these groups are for boron: $Q=3.1\times10^{6}$ e.v., $0.35\times10^{6}$ e.v., $-0.78\times10^{6}$ e.v., $-1.86\times10^{6}$ e.v.; and for phosphorus, 0, $-1.47\times10^{6}$ e.v., $-2.96\times10^{6}$ e.v. The values for boron check with those found by other observers who used polonium $\alpha$-particles, three of them having been previously announced. The phosphorus groups are all new and indicate the advantage of using the higher energy $\alpha$-particles to bombard the heavier nuclei. One faint group of protons with a small positive energy previously observed for phosphorus is not definitely observed here but the results do admit the possibility of this group's existence. These experiments were performed at the University of Tübingen, Germany. The protons were observed with a Geiger proportional counter and at right angles to the direction of the impinging $\alpha$-particles, thus avoiding counting of protons produced by collision of $\alpha$-particles with contaminating hydrogen.

**7. The Study of the Electrical Characteristics of Geiger-Müller Tubes using a Cathode-Ray Oscillograph.** J. F. Sears and G. E. Read, *Purdue University.*—Photographic records of the electrical characteristics of an air filled Geiger-Müller counter have been obtained with a Purdue cathode-ray oscillograph. The analysis of the photographs shows that the counting cycle may be divided into three portions: (1) breakdown, (2) conducting period, (3) charging period. The initial breakdown occurs in a time shorter than $10^{-6}$ seconds. The charge flow in this period is a function of the tube pressure and voltage but is not dependent on the capacity and resistance in the circuit. Following the breakdown the potential across the counter drops to a constant value $V$ somewhat below the threshold voltage of the counter. Circuit conditions affect the duration of and charge flow during the conducting period. The threshold

voltage is a function of the pressure and geometrical characteristics. The length of the charging period depends upon the circuit characteristics and usually is the determining factor in the time of the counting cycle. The following recomendations for increasing the resolution of a Geiger-Müller counter follow from this analysis. Decrease the distributed capacity of the counter. Reduce the coupling capacity to about the same value as the grid capacity of the amplifier tube. In some cases it may be advisable to replace the resistance in series with the counter with a constant current device having a low capacity.

**8. Apparatus for Transmitting Cosmic-Ray Data from Stratosphere.** J. M. BENADE AND R. L. DOAN, *University of Chicago.*—Ionization current is measured by a specially constructed electrometer used in connection with an optical system in which a photoelectric cell is energized whenever the charge builds up to a certain point. Flow of current through the photo-cell closes a grounding relay and also the filament circuit of a short wave radio oscillator for a length of time determined by a delayed circuit breaker. While the oscillator filament is on, impulses are sent out from two magnetic vibrators whose frequencies are determined by temperature and pressure, respectively. The transmitting apparatus, weighing approximately ten pounds, is suspended from a small balloon expansible to about 20 feet filled with hydrogen. The data are received on a short wave receiver feeding into an automatic recording mechanism. On a recent trial flight in which the pressure measuring device only was sent up, radio signals were received up to a height of 9½ miles, at which point it was known previously that the device would cease to function. The balloon rose to an estimated height of 17½ miles as observed in telescopes. On future flights it is planned to send up the entire apparatus.

**9. Spectrographic Determination of Calcium in Plant Ashes.** KATHARINE WAY AND JOHN M. ARTHUR, *Boyce Thompson Institute for Plant Research. (Introduced by A. E. Ruark.)*—Standard solutions of nitrates containing 1.75% Sr, Ca in amounts from 0.266% to 0.533%, and other elements in approximately the proportionate amounts found in the ashes under consideration are prepared. Amounts of Sr necessary to make the concentration 1.75% are added to nitrated solutions of plant ashes from which Cl and $SO_4$ have been removed. 0.05 cc of solution is dried under controlled conditions on the lower electrode of a graphite arc. The arc, placed 55 in. from the slit of a Hilger E3 quartz spectrograph without intervening condensing lens, is run at 6 to 4 amp. on 125 volt d.c. mains. Spectra of several standard and ash solutions are taken on each plate and the differences in blackening of the lines 5330A Sr and 5350A Ca in each spectrum are determined with a photoelectric microphotometer whose construction is described. The percentage of Ca in the ash solutions is estimated from a curve made by plotting differences in blackening of the above pair against % Ca, for the standards. Only blackenings which fall on the straight line portion of the characteristic curve of the Cramer Spectrum Process plates employed, are used. Mean spectrographic determinations of Ca in plant ashes agree with mean chemical determinations within 5%.

**10. Fluorescence of the Chlorophyll Series: The Reversible Reduction of Chlorophyll *a* and *b*.** V. M. ALBERS, H. V. KNORR AND PAUL ROTHEMUND, *Kettering Foundation, Antioch College.*—Pure chlorophyll *a* was reduced in pyridine under an atmosphere of $N_2$ and reoxidized in air, according to the method of Pummerer (Ber. **46**, 2368 (1913)) as applied to chlorophyll by Kuhn and Winterstein (Ber. **66**, 1741 (1933)). The fluorescence spectra of the original, reduced and reoxidized chlorophyll solutions were photographed by the method previously described (Phys. Rev. **43**, 379 (1933)). Spectrograms were also obtained when the reduction took place under $CO_2$. The same procedure was followed for chlorophyll *b*. The reduced chlorophyll did not exhibit characteristic absorption in the visible region. The absorption spectra of the original and the reoxidized chlorophyll, in the visible region, were identical. The fluorescence spectra of the reduced and reoxidized chlorophyll are different and both are different from the original chlorophyll. The densitometer curves indicate that the fluorescence is less intense in the reduced and reoxidized chlorophyll than in the original chlorophyll. The positions of the maxima of the fluorescence bands of the original chlorophyll appear at longer wavelengths than those in the reduced and reoxidized chlorophyll. The fluorescence spectra for both the reduced and reoxidized chlorophyll *a* and chlorophyll *b* are different when the reaction is run under $CO_2$ than when it is run under $N_2$.

**11. Behavior of the Absorption Band of Uranine Solution under High Pressure.** W. JAMES LYONS, *St. Louis University. (Introduced by F. E. Poindexter.)*—A dilute aqueous solution (83 mg per liter) of uranine, having an absorption band maximum at 4930A, was studied in the high-pressure spectrometer. Refractive indices for the three principal lines of the mercury arc, and for the wavelength corresponding to the absorption maximum were determined for pressures ranging up to 915 kg per $cm^2$. Due to the dilution of the solution no anomalous dispersion was observed. There are theoretical grounds for expecting that the absorption band maximum should shift under pressure to regions of longer wavelength. In this investigation, however, it was found that the absorption band retained its position, relative to the rest of the spectrum.

**12. Raman Spectra of $N_3^-$, $NCS^-$ and $CO_2$.** A. LANGSETH, *University of Copenhagen,* AND J. RUD NIELSEN, *University of Oklahoma.*—The Raman spectra of $N_3^-$ and $NCS^-$ have been studied further and the results applied to determine the constitution of these ions. With prolonged exposure, the overtone $2\nu_2$ appears in the spectrum of $NCS^-$, although the fundamental $\nu_2$, which is permitted by Placzek's selection rules, is absent; the implications of this peculiar result, which we previously observed in the case of $N_2O$ [Nature **130**, 92 (1932)], are discussed. New measurements have also been made of the depolarizations and relative intensities of the principal Raman bands of $CO_2$.

**13. Evidence from Raman Effect for a Slight Asymmetry of the Carbon Atom.** R. T. DUFFORD, *University of Missouri.*—An examination of the Raman spectra of a large number of simple compounds of carbon shows widespread evidence of two slightly different strengths of bond. This paper discusses this evidence, and points out that similar but more limited evidence exists for oxygen and nitrogen. No such evidence for any elements beyond the first row of the periodic table has yet come to the attention of the writer.

**14. Band Spectrum of Arsenic Oxide and Lead Oxide.** E. N. SHAWHAN AND FRANK MORGAN, *Ohio State University. (Introduced by Alpheus W. Smith.)*—The band spectrum of arsenic oxide (AsO) has been investigated in emission and in absorption, and that of lead oxide (PbO) in absorption. The emission spectrum of arsenic oxide was obtained by passing the vapor of $AsCl_3$ into a flame or by introducing $As_2O_3$ into an arc. To get the absorption spectrum of arsenic oxide, light from an underwater spark was passed through the flame. In the case of lead oxide, pure PbO was vaporized in an electric furnace. Two systems of double double-headed bands have been observed in arsenic oxide. One system is degraded toward the red, the other toward the violet. A vibrational analysis of both systems has been made. In the system degraded toward the red the less refrangible heads are represented by the formula:

$$\nu = \begin{Bmatrix} 31738 \\ 31094 \end{Bmatrix} + [372(v'+\tfrac{1}{2}) - 5.5(v'+\tfrac{1}{2})^2] - [965(v''+\tfrac{1}{2}) - 5(v''+\tfrac{1}{2})^2]$$

and in the system degraded toward the violet, the more refrangible heads by the formula:

$$\nu = \begin{Bmatrix} 39861 \\ 38836 \end{Bmatrix} + [1098(v'+\tfrac{1}{2}) - 6(v'+\tfrac{1}{2})^2] - [965(v''+\tfrac{1}{2}) - 5(v''+\tfrac{1}{2})^2].$$

The *D*-system of PbO observed in emission by Bloomenthal (Phys. Rev. **35**, 34 (1930)) has been extended in absorption and a new system located which is approximately represented by the formula:

$$\nu = 30898 + [427(v'+\tfrac{1}{2}) - 1.5(v'+\tfrac{1}{2})^2] - [721(v''+\tfrac{1}{2}) - 3(v''+\tfrac{1}{2})^2].$$

**15. The Band Spectrum of $OH^+$.** F. W. LOOMIS AND W. H. BRANDT, *University of Illinois.*—Two bands at 3332 and 3565A, discovered by Rodebush and Wahl in the electrodeless discharge in pure water vapor, and two new bands at 3695 and 3893A, are shown to be, respectively, the (1,0), (0,0), (1,1) and (0,1) bands of $OH^+$. Rotational analysis establishes that they correspond to a $^3\Pi \rightarrow {}^3\Sigma$ transition in which the $^3\Pi$ state is inverted, with coupling intermediate between cases *a* and *b*. The lambda type doubling is large and there are exceptionally large perturbations in the 3*b*, 2*a* and 1*b* levels of the $v'=1$ state, with maxima at approximately $K'=18.5$, 14.5 and 10.5, respectively. The nine strong branches to be expected in this type of transition are found, and also enough satellite branches (nine in the 0,0 band) to determine the multiplet intervals in both states.

**16. Emission Spectrum of Diatomic Arsenic.** G. M. ALMY AND G. D. KINZER, *University of Illinois.*—The molecular spectrum of arsenic has been photographed in emission, using as source an end-on discharge tube into which metallic arsenic was driven from a side tube by a flame. The spectrum was greatly enhanced when the tube contained about 20 mm hydrogen. The spectrum consists of two parts, (1) an extensive group of bands between 2250A and 3750A and (2) a weak group near 4200A. Vibrational analysis of the extensive group shows it to consist of two almost completely overlapping band systems having a common lower state and similar upper states. This spectrum is evidently that obtained in absorption by Gibson and MacFarlane (Phys. Rev. **45**, 899 (1934)). The lower state, for which $\omega_e''=431.1$, $x''\omega_e''=1.15$, has been extended to $v''=45$, $G''=17{,}227$ cm$^{-1}$, and extrapolation gives $D_e''=27{,}500$ cm$^{-1}$ (upper limit). The two upper states appear to be nearly coincident, with each state perturbing the other. For each state, $\omega_e'$ is about 265 cm$^{-1}$, and the vibrational intervals are perturbed near $v'=3$ and $v'=8$, though the displacements of the levels differ for the two states. In the stronger system no emission bands appear for values of $v'$ from 10 to 13 although *absorption edges* do appear at the estimated positions of the heads. Bands for which $v'=14$ appear in emission.

**17. Solarization at Low Intensity.** A. J. REARDON AND H. P. GRIGGS, S.J., *Saint Louis University. (Introduced by F. E. Poindexter.)*—Experimental evidence for the existence of reversals higher than the second is put forth in this paper. The solarization curves exhibited herein were obtained by exposing continuously Extra Fast Dry Undyed Hammer photographic plates to light of low intensity (0.00012 and 0.0003 foot-candle). The results obtained show that with a total prolonged exposure of 27,652 minutes eight reversals appear in the solarization curve for each of the above intensities. The numerical value of the density of the first maximum point and the time necessary to attain it depend upon the intensity of the light source. In the case of the lower intensity (0.00012 foot-candle) a curve containing 16 reversals is exhibited, the total exposure-time being 105,532 minutes. This curve closely resembles the damped vibration curve which is found in electricity. Another important point which is brought out is that both the density resulting from the development of the latent image and the solarization effect decrease with the aging of the emulsion. The care with which the experimentation was performed is emphasized in the explanation of a series of checks made on several possible sources of error.

**18. Electrostatic Pendulum.** J. A. VAN DEN AKKER, *Washington University.*—Oscillation of the pendulum is maintained by electrical forces alone. A rectangular bob swings between two vertical, parallel plates placed at the center of oscillation. The pair of plates and the bob are

connected to a condenser of small capacitance $C$, which is permanently connected to a battery or simple rectifier through a high resistance $R$. Thus a central force proportional to the square of the potential difference between the bob and plates acts on the bob at all times. An electrode at the base of the bob sweeps over a mercury cup or fixed electrode in passing through the center of oscillation, hence the condenser is discharged each half oscillation. If the proper time constant $RC$ is chosen, the central force during a return swing is considerably greater than the retarding force during an outward swing. It may be shown that, for moderate amplitudes, the optimum value of the time constant is $RC=0.13T$, where $T$ is the period of the pendulum. Other relations for sustained oscillations are given, and various modifications and applications of the pendulum are suggested.

**19. The Liquefaction of Gases—A Demonstration.** CHARLES T. KNIPP, *University of Illinois.*—This paper presents two simple demonstrations on the liquefaction of gases. No new physical principles are involved. The gas to be liquefied (oxygen in the first) is placed in a 12 liter flask to which is fused a stem about 4 cm in diameter and 40 cm long, the lower end of which terminates in a Dewar flask of about 40 cc capacity. The pressure within the bulb is raised to two atmospheres and sealed off. If now the stem is submerged in liquid air the oxygen within the bulb will condense rapidly and liquid oxygen will trickle down into the Dewar. This condensation will cease in two or three minutes, resulting in about 30 cc of liquid. The thermos bottle is now removed and the Dewar containing the liquid oxygen is defrosted. The liquid oxygen thus condensed will slowly re-evaporate over a period of an hour or more. The pressure within the bulb during the cooling process will fall from about 140 cm to 40 cm of mercury. The second demonstration is to repeat the above with a duplicate container but using *dry air* instead of oxygen. The yield of liquid now is but 2 or 3 cc and comes from the oxygen content of the air which approximates the calculated volume under the conditions of the experiment. The liquids thus condensed may be leisurely studied as regards their colors and magnetic properties.

**20. Elastic Scattering of Electrons in Argon, Krypton and Hydrogen.** G. M. WEBB, *Washington University.*—The distribution-in-angle of electrons scattered elastically in A, Kr and $H_2$ has been determined over the angular range 10°–150° for primary electron energies of 25 to 900 volts. In argon it was found that one maximum and two minima are present up to 300 volts. From 300 to 800 volts one minimum only occurs. Two *different* maxima are exhibited in the scattering by krypton, the first being prominent from 25 to 100 volts, the second appearing at this voltage for large angles. With increasing energies the first maximum changes position progressively to smaller angles and merges with the main body of scattering at about 350 volts. There is a single maximum in the range 350 to 900 volts. In the scattering by $H_2$ a single minimum occurs for low energies. At higher energies (200 to 900 volts) the curves all fall monotonically with angle. The experimental results have been compared with theory At low voltages (for A and Kr) the qualitative agreement is fairly good when Henneberg's phase shifts are used. At higher voltages (500 to 800 volts, in A; and 700 to 900 volts, in Kr) the scattering is given quite accurately by the Born approximate equation for a limited angular range (10° to 60°). In $H_2$, at the higher voltages, fair agreement is obtained with the theoretical scattering predicted by theory.

**21. Intensity Distribution in Electron Diffraction Patterns of ZnO and Atomfactor.** H. J. YEARIAN, *Purdue University.* (*Introduced by K. Lark-Horovitz.*)—As has been shown already (K. Lark-Horovitz and H. J. Yearian, Phys. Rev. **42**, 905 (1932)) the intensity of electron diffraction rings of ZnO differs markedly from the intensity of the corresponding x-ray pattern. It was pointed out previously, that this difference is due to a distortion of the electron cloud around the nucleus. Careful new measurements have made it possible to evaluate this distortion quantitatively. Instead of treating the different electron shells, as calculated by James's and Brindley's methods, as concentric, it has been assumed that the $L$, $M$, $N$ shells are slightly displaced along the $c$-axis. In this way complete agreement between calculated and observed intensities has been obtained. The x-ray $F$-curves are not influenced by this distortion and the calculated values agree with the experimental results.

**22. A Mathematical Modulus Derived from X-Ray Data for Evaluation of Residual Distortion in Crystals.** G. L. CLARK AND M. M. BECKWITH, *University of Illinois.*—From accurate measurement of the peripheral widening of diffraction intensity maxima from a series of silicon steel specimens with a widely varying residual grain distortion or strain, it has been possible to derive a mathematical modulus which enables the numerical evaluation of this distortion in points above a basic value. Comparisons are made in terms of degree of cold work and temperature and time of heat treatment. These values are then correlated with actual measurements of magnetic permeability, and a very close parallel is established.

**23. X-Ray Extinction in Piezoelectric Crystals.** GERALD W. FOX AND WALTER A. FRASER, *Iowa State College.*—The original work of Fox and Carr on the effect of piezoelectric vibrations of quartz crystals on the Laue patterns has been continued and extended to include tourmaline and Rochelle salt crystals. The effect of different surface conditions on the Laue patterns has also been studied. The results obtained for all three types of crystals were similar, all the effects being most pronounced in quartz. Quartz is undoubtedly the best material for the study of x-ray extinction in piezoelectric crystals. It was concluded that this phenomenon may be explained as the effect upon the primary and secondary extinctions due to the warping of the lattice planes in the surface during piezoelectric oscillation. More precise definitions of primary and secondary extinctions are offered.

**24. A Simplification of Prins' Formula for Diffraction of X-Rays by a Perfect Crystal.** FRANKLIN MILLER, JR., *University of Chicago. (Introduced by S. K. Allison.)*—The intensity formula of Prins for diffraction of x-rays from a perfect crystal has been simplified so that $F(l)$ is a real, single-valued, algebraic function of $l$, the deviation of the glancing angle from the corrected Bragg angle. By neglecting absorption in the crystal Darwin's formula is obtained in a new form. By differentiation the maximum ordinate of the diffraction pattern is obtained. To calculate percent reflection (i.e., maximum ordinate of the rocking curve of a double crystal spectrometer in the $1,-1$ position) $\int_{-\infty}^{\infty} F(l)dl$ and $\int_{-\infty}^{\infty} F^2(l)dl$ are needed, and these integrals have been evaluated analytically for Darwin's case of no absorption, leading to a value of 4/5 for $P_0$. To include absorption $F(l)$ has been expanded into a series in powers of $\beta/\delta$ and an approximate formula taking account of polarization has been obtained for $P_0$ in terms of the constants of the crystal. This formula agrees with the graphically determined values of $P_0$ to within a few percent.

**25. The Structure of Liquid Methyl Alcohol.** W. H. ZACHARIASEN, *University of Chicago.*—By use of the method developed by Warren and Gingrich (Phys. Rev. **46**, 369 (1934)) Fourier integral analyses of the liquid x-ray diffraction patterns of alcohols have been made. Stewart and Morrow's experimental data (Phys. Rev. **30**, 232 (1927)) were used. The radial atom distribution found for the long chain alcohols completely confirms the structure model recently proposed by Warren (Phys. Rev. **44**, 969 (1933)). On the basis of the atom distribution curve found for methyl alcohol the structure of the liquid is derived. It is found that the oxygen atom of one molecule is linked to the oxygen atoms of two neighboring molecules through hydrogen binding. The hydrogen atom of the hydroxyl group thus is lying in between two oxygen atoms, although probably nearer to one than to the other. This type of hydrogen binding is responsible for the glass forming tendency of the alcohols.

**26. The Structure of Radicals in Crystals.** W. H. ZACHARIASEN, *University of Chicago.*—During the last years a great number of crystal structure investigations have been made with the object of determining the shape and dimensions of radicals. The results of this extensive and systematic work will be presented in comprehensive form, and discussed in connection with theories of the chemical bond. Especially the oxygenic radicals of boron, carbon, nitrogen, phosphorus, sulphur and chlorine will be taken up for consideration.

**27. Diffuse Scattering of X-Rays by Crystals.** G. E. M. JAUNCEY, *Washington University.*—Early experiments by Jauncey and May showed that Debye's theory of the diffuse scattering of x-rays from single crystals was inadequate at least for rocksalt and calcite. A much more adequate theory was worked out in 1931 by Jauncey and Harvey and independently by Woo, and a formula for $S$ (the ratio of the actual scattered intensity to the intensity on the Thomson theory) was obtained for crystals consisting of atoms of one kind. The theory has since been extended to crystals consisting of atoms of several kinds and so as to include the extra negative term which appears in the incoherent part of $S$ according to the Waller-Hartree quantum-mechanical theory of scattered radiation from a free atom. (This term does not appear in Wentzel's formula.) Experimental $S$ values have been obtained by Claus, Harvey, Williams, Ehrenfest, Pennell and the writer for NaCl, KCl and NaF at various angles and various temperatures. Both monochromatic x-rays and x-rays from the continuous spectrum were used. Theoretical $S$ curves can be calculated from James and Brindley's quantum-mechanical $f$ and $E_r$ values. The most recent experimental $S$ values for KCl agree remarkably well with the theoretical values provided that the $E_r$'s for the various electrons are taken to be different and not all equal as was previously suggested by A. H. Compton. The best agreement for NaF is obtained when the Waller-Hartree negative term is included in the theoretical formula.

**28. The Study of the Nature of Liquids by Means of X-Ray Diffraction.** G. W. STEWART, *State University of Iowa.*—This paper discusses the limitations and attainments in the x-ray diffraction study of liquids, and the usefulness of present and prospective results.

**29. The Scattering of X-Rays by Gases.** E. O. WOLLAN, *Washington University.*—The intensity of scattering of x-rays by gases was given a satisfactory theoretical treatment only after the advent of the new quantum mechanics. Since then, however, practically identical results have been obtained on the basis of classical theory. Measurements of the total intensity of scattering of x-rays by a number of gases have been made and the results have been found to be in good accord with the predictions of the theory. For the case of monatomic gases the theory makes it possible to convert the measured intensities into the corresponding atomic structure factors to a very close approximation. The structure factors calculated in this way correspond to the atom at rest and hence the electron distribution curves derived from these data give an accurate picture of the charge distribution within the atom. A comparison of these curves with corresponding ones obtained by x-ray reflection from crystals in which case the intensity is affected by the thermal agitation of the atoms has given information regarding the existence of zero point energy for the atoms in the crystal. For a more complete test of the theory of scattering by gases, measurements have also been made on the incoherent portion of the scattered radiation which is modified in wavelength by the Compton effect. The results of these experiments are also in accord with the theory.

**30. Index of Refraction of Water and Paraffin at High Frequencies.** LESTER S. SKAGGS AND R. T. DUFFORD, *University of Missouri.*—By use of a special magnetron oscillator, and an interference method, the index of refraction of water and of paraffin has been measured at

wavelengths of approximately 10 cm, extending the observations about 2.5 octaves above any values known to the authors to have been previously reported. The results are in accord with classical electromagnetic theory.

**31. The Effect of Pressure on the Refractive Index of Carbon Disulfide.** FRANKLIN E. POINDEXTER, *St. Louis University.*—The refractive index of $CS_2$ for each of the Hg arc lines, 5790A, 5460A and 4360A, was measured on a high pressure spectrometer at a series of pressures from 1 to 1880 kg per cm². It was found that the dispersion increases over the whole range of pressure, the increase being much more rapid at the lower pressures. The high pressure spectrometer is discussed with reference to sources of error and recent improvements. A table of values obtained is given below, where pressures are in kg per cm², and $n_Y$, $n_G$ and $n_B$ are the indices of the above wavelengths respectively.

| Pressure | $n_Y$ | $n_G$ | $n_B$ |
|---|---|---|---|
| 1 | 1.6526 | 1.6556 | 1.6735 |
| 290 | 1.7005 | 1.7053 | 1.7339 |
| 730 | 1.7119 | 1.7169 | 1.7464 |
| 1070 | 1.7208 | 1.7259 | 1.7556 |
| 1370 | 1.7262 | 1.7342 | 1.7673 |
| 1720 | 1.7347 | 1.7396 | 1.7705 |

**32. On the Comparison with Experiment of the Fermi Theory of Beta-Ray Disintegration.** E. J. KONOPINSKI AND G. E. UHLENBECK, *University of Michigan.*—One can show that in the Fermi theory in most cases the nuclear charge $Z$ has only a slight influence on the probability of emission of an electron (or positron). Putting $Z=0$, the probability of emission of an electron in the impulse range $dp$ becomes (for the neutrino mass $\mu=0$) proportional simply to the squares of the impulses of electron and neutrino. Or one can say that the energy is divided between the electron and the neutrino according to the number of states into which the electron and the neutrino can go. This explains Sargent's law about as accurately as the more exact theory with $Z\neq 0$. It also represents rather well the dependence of the average energy on the maximum energy, which is a test on the form of the $\beta$-ray spectrum. There is, however, a systematic deviation from experiments, which is not removed either by taking $Z\neq 0$ or by introducing a neutrino mass $\mu>0$. The theoretical distribution is not asymmetric enough. Other possible reasons for this discrepancy will be discussed.

**33. The Present State of the Neutrino Hypothesis.** G. BECK, *University of Kansas.* (*Introduced by W. L. Severinghaus.*)—It is now generally recognized that the continuous $\beta$-spectra emitted during the radioactive $\beta$-decay have to be formally treated as a double process in which beside the emerging electron a second particle of unknown properties is emitted. If $E(Z)$ and $E(Z\pm1)$ denote the energy of the initial and the final nucleus, $W$ and $m$ the energy and mass of the emitted electron, $W'$ and $m'$ energy and mass of the hypothetical second particle, the relation holds $E(Z)-E(Z\pm1)=W+W' \geq(m+m')\cdot c^2$. From this equation we deduce the condition for the $\beta$-stability of a nucleus, $E(Z)-E(Z\pm1) <(m+m')\cdot c^2$. Evidence for the validity of this condition is found in the system of known isotopes. A more detailed treatment of the $\beta$-decay requires assumptions on the formally introduced second particle. Two attempts have been made in this respect by Fermi and by Beck and Sitte. Fermi treats the second particle as a neutrino of high penetrating power and has to assume $m'=0$. Beck and Sitte connect the $\beta$-emission with the production of a pair of differently charged electrons, one of which is absorbed by the nucleus without conservation of mechanical integrals. Arguments are given to show that the neutrino hypothesis is not sufficient to remove the difficulties arising from the experimental evidence.

**34. Discussion of Fermi's Theory of the Beta-Decay.** R. L. DOLECEK, *University of Kansas.* (*Introduced by W. L. Severinghaus.*)—The shape of the continuous $\beta$-spectra and the relative decay probabilities of different types of nuclei have been determined according to Fermi's theory and are compared with the experimental data.

**35. A Search for a Photomagnetic Effect.** RICHARD M. EMBERSON AND R. T. DUFFORD, *University of Missouri.*—The magnetic susceptibilities of more than sixty substances were measured by the method of Lord Kelvin. The list of substances includes many of the Grignard solutions which give the photovoltaic effect studied extensively in this laboratory, and the primary substances from which they are made. Most of these susceptibilities have values in the neighborhood of $6\times10^{-7}$ c.g.s. units. The equipment used could measure such values with an error of less than half of one percent. In no case was any change in susceptibility due to illumination detected. Hence, either the magnetic susceptibility is not dependent on the number of free electrons present, or else the photovoltaic effect does not involve the liberation of electrons.

**36. The Surface Tension of Mercury in the Presence of Gases. I. Dry Air.** MARIE KERNAGHAN, RSCJ, *Maryville Corporate College of the Saint Louis University.*—The main section of the apparatus and the method (flat-drop) are those used by the author (Phys. Rev. **37**, 990 (1931)) to find the surface tension of mercury in a vacuum. A combination of drying tubes and pressure gauge has been inserted between the surface tension chamber and the McLeod gauge. The arrangement dispenses with stopcocks and is designed to admit any gas in small quantities and to hold the pressure constant during any length of time. By means of a special attachment nitrogen can be obtained directly from the air. The apparatus has been tested by studying the effect of varying pressure in the presence of dry air. The surface tension, evaluated by application of Worthington's formula, was found to drop rapidly from 464 dynes per cm in a vacuum until an apparently critical pressure of 7 mm was reached. Values for higher pressures remained fairly constant.

**37. Incoherent Scattering and the Concept of Discrete Electrons.** ARTHUR H. COMPTON, *University of Chicago and Oxford University.*—Experiment has shown that scattered x-rays contain both a coherent and an incoherent portion. Classical electron theory provides a formula for scattering closely similar to that based on wave mechanics but includes both coherent and incoherent components only if the atom consists of discrete electrons. From a comparison of the classical and wave mechanics theories of scattering it is concluded that the most accurate classical analog of Schrödinger's $\psi\psi^*$ is the probability of occurrence of discrete electrons, and that a particular electron is associated with each particular function $\psi_n\psi_n^*$.

## AUTHOR INDEX TO ABSTRACTS OF THE ST. LOUIS MEETING

**Albers, V. M., H. V. Knorr and Paul Rothemund**—No. 10
**Almy, G. M. and G. D. Kinzer**—No. 16
**Arthur, John M.**—see Way

**Beck, G.**—No. 33
**Beckwith, M. M.**—see Clark
**Benade, J. M. and R. L. Doan**—No. 8
**Brady, James J.**—No. 3
**Brandt, W. H.**—see Loomis

**Clark, G. L. and M. M. Beckwith**—No. 22
**Compton, Arthur H.**—No. 37

**Doan, R. L.**—see Benade
**Dolecek, R. L.**—No. 34
**Dufford, R. T.**—No. 13
—— see Skaggs
—— see Emberson

**Emberson, Richard M. and R. T. Dufford**—No. 35

**Fox, Gerald W. and Walter A. Fraser**—No. 23
**Fraser, Walter A.**—see Fox

**Griggs, H. P., S.J.**—see Reardon

**Jauncey, G. E. M.**—No. 27

**Kernaghan, Marie, RSCJ.**—No. 36
**Kinzer, G. D.**—see Almy
**Knipp, Charles T.**—No. 19
**Knorr, H. V.**—see Albers
**Konopinski, E. J. and G. E. Uhlenbeck**—No. 32

**Langseth, A. and J. Rud Nielsen**—No. 12
**Loomis, F. W. and W. H. Brandt**—No. 15
**Lyons, W. James**—No. 11

**Michels, Walter C. and Gladys White**—No. 5
**Miller, Franklin, Jr.**—No. 24
**Morgan, Frank**—see Shawhan

**Nielsen, J. Rud**—see Langseth

**Paton, R. F.**—No. 6
**Poindexter, Franklin E.**—No. 31

**Read, G. E.**—see Sears
**Reardon, A. J. and H. P. Griggs, S.J.**—No. 17
**Roller, Duane**—see Townes
**Rothemund, Paul**—see Albers

**Sears, J. F. and G. E. Read**—No. 7
**Shawhan, E. N. and Frank Morgan**—No. 14
**Skaggs, Lester S. and R. T. Dufford**—No. 30
**Stewart, G. W.**—No. 28

**Townes, Edith and Duane Roller**—No. 4

**Uhlenbeck, G. E.**—see Konopinski

**Van den Akker, J. A.**—No. 18

**Way, Katharine and John M. Arthur**—No. 9
**Webb, G. M.**—No. 20
**White, Gladys**—see Michels
**Wollan, E. O.**—No. 29

**Yearian, H. J.**—No. 21

**Zachariasen, W. H.**—Nos. 25, 26

# THE AMERICAN INSTITUTE OF PHYSICS

INCORPORATED


## GOVERNING BOARD

*For The American Physical Society:*

KARL T. COMPTON, *Chairman*
Massachusetts Institute of Technology

GEORGE B. PEGRAM, *Secretary*
Columbia University

JOHN T. TATE
University of Minnesota

*For The Optical Society of America:*

E. C. CRITTENDEN
Bureau of Standards

PAUL D. FOOTE
The Gulf Companies

F. K. RICHTMYER
Cornell University

*For The Acoustical Society of America:*

HARVEY FLETCHER
Bell Telephone Laboratories

VERN O. KNUDSEN
University of California at Los Angeles

WALLACE WATERFALL
The Celotex Company

*For The Society of Rheology:*

E. C. BINGHAM
Lafayette College

A. STUART HUNTER
du Pont Rayon Company

S. E. SHEPPARD
Eastman Kodak Company

*For The American Association of Physics Teachers:*

HOBART L. DODGE
University of Oklahoma

PAUL E. KLOPSTEG
Central Scientific Company

FREDERIC PALMER
Haverford College



## ADMINISTRATIVE STAFF

HERBERT A. BARTON, *Director* JOHN T. TATE, *Adviser on Publications*

MADELINE M. MITCHELL, *Editorial Secretary*

*Office:* 11 East 38th Street, New York, New York


---

## JOURNALS

THE PHYSICAL REVIEW

REVIEWS OF MODERN PHYSICS

PHYSICS
JOHN T. TATE, *Editor*
J. W. BUCHTA, *Assistant Editor*
E. C. BINGHAM, *Rheology Editor*

THE JOURNAL OF THE OPTICAL SOCIETY OF AMERICA

THE REVIEW OF SCIENTIFIC INSTRUMENTS
WITH PHYSICS NEWS AND VIEWS
F. K. RICHTMYER, *Editor*

JOURNAL OF THE ACOUSTICAL SOCIETY OF AMERICA
F. R. WATSON, *Editor*

THE JOURNAL OF CHEMICAL PHYSICS
HAROLD C. UREY, *Editor*

THE AMERICAN PHYSICS TEACHER
DUANE ROLLER, *Editor*

The American Institute of Physics is a membership corporation of which five societies are the founding members. These five societies are the principal national societies devoted to pure and applied physics in America. Their names, and those of their representatives who form the Governing Board of the Institute, are given above. The principal work of the Institute is the publication of journals sponsored by the societies or by itself. The names and the editors of the journals are also listed above.

The broad purpose of the Institute is to represent, in all matters of wide or common interest, the five thousand or more members and subscribers associated with the Founder Societies and the journals. It aims to advance the science and profession of physics, and to promote cooperation between pure research, the applied sciences and the industries. To achieve these aims, it is greatly in need of an endowment and is empowered by law to administer grants and funds of any kind.

# CONTENTS


[illegible] Rev. 67 (1945) January 15

[illegible]gation of Nitrogen by Neutrons . . . . Frank N. D. Kurie 97

[illegible] Levels of Radioactive Elements with Applications to Beta and Gamma-[illegible]ray Spectra . Arthur Edward Ruark and Frederick A. Mavfield 107

[illegible]tation of the First Spark Spectrum of Lead: Pb II . . . . . Lester T. Earls and Ralph A. Sawyer 115

[illegible] Structure of Singly Ionized Lead . . . . . John L. Rose 122

[illegible] Absorption of Benzene . . . . . R. Bowling Barnes, W. S. Benedict and C. M. Lewis 129

[illegible] Effect of the Spectra of Arsenic . . . . . J. R. Greer and W. M. Barrows, Jr. 131

[illegible] of AsO . . . . . F. A. Jenkins and L. A. Strait 136

[illegible] Type of Separation in Radiation Problems . . . . W. W. Hansen 139

[illegible] Charge and Field Distributions . . . . J. R. Oppenheimer 144

[illegible] the Production of Pairs by Charged Particles . J. R. Oppenheimer 146

[illegible]-Shield Field Theory of the Electron . . . Eugene Feenberg 148

[illegible] of Dimensional Changes in Magnetization in Monocrystal Bars and Blades of Silicon-Iron . . R. F. Clash, Jr. and F. J. Beck, Jr. 159

[illegible] of Dislocation in Crystals of Rochelle Salt . . . . . R. D. Schelwas-Sorokin and M. V. Posnov 166

[illegible] of Rochelle Salt . . . . . Hans Mueller 175

[illegible] the Editor:

[illegible] Spectrum of Arsenic Oxide (AsO) . Frank Morgan and E. N. Shawhan 192

[illegible] of Fall of Meteoric Material on the Earth . . . . . C. C. Wylie 192

[illegible] of the Night Sky . . . . . Joseph Kaplan 193

[illegible]ption and Scattering of Neutrons . . W. F. Libby and W. M. Latimer 193

[illegible]duction of Induced Radioactivity by the Cosmic Radiation . J. R. L. Carlisle 194

[illegible]ory of the Nuclear Electron . . . . . John W. Coleman 194

[illegible]ings of the American Physical Society:

[illegible], St. Louis Meeting, November 30-December 1, 1945; Minutes and Abstracts: [illegible] 1-37; Author Index . . . . . 195



Lancaster Press, Inc., Lancaster, Pa.